The Role of Sensory Experience in Intrinsic Biophysical Diversity of Glomerular Interneurons of the Olfactory Bulb

Anja Kerstin Schmaltz

PhD Supervisor: Troy Margrie

A thesis submitted for the degree of
Doctor of Philosophy

University College London

December 2016

Declaration

I, Anja Schmaltz, confirm that the work presented in this thesis is my own. Where information has been derived from other sources, I confirm that this has been indicated in the thesis.

Anja Schmaltz, 14. May 2017

Abstract

Investigating the adaptive properties of neuronal circuits is central to understanding the operations of the brain. The mouse olfactory bulb is a structure well suited for studying these processes, since it is composed of relatively simple excitatory and inhibitory networks. Recently, it has been shown that principal neurons (mitral cells) of the olfactory bulb that participate in the same glomerular circuit exhibit similar biophysical properties based on their I_h-mediated membrane potential sag. In many cell types, including mitral cells, I_h is known to profoundly influence excitability and thus impact the input/output function of individual neurons and networks.

Like principal cells, inhibitory neurons are known to exhibit I_h that influences their integrative properties. In the olfactory bulb, interneurons of the glomerular layer can receive input from one or more glomerular networks and are thought to mediate lateral or centre-surround inhibition. The regulation of I_h in these cells could thus be used as a gain-control mechanism to facilitate contrast enhancement.

During my project, I therefore investigated the diversity of I_h in $GAD65^+$ and TH^+ juxtaglomerular cells belonging to the same or different glomeruli to determine the diversity of I_h-mediated membrane potential sag within and across different inhibitory circuits.

I found that the two juxtaglomerular populations differed substantially in their levels of membrane potential sag. Contrary to TH^+ juxtaglomerular cells, the similarity in the amount of sag recorded in $GAD65^+$ juxtaglomerular cells was high when two neurons were found to participate in the same glomerular circuit. Furthermore, the sag amplitude of interneurons affiliated to a specific glomerular circuit was upregulated when mice were exposed to odour stimuli. This indicates that, at least for $GAD65^+$ juxtaglomerular cells, the amount of I_h membrane sag reflects local network processing of odour information.

Acknowledgements

I would like to thank my supervisor Troy Margrie for his patience, support and scientific guidance. He helped me all the way from my first day in his lab to the writing of this thesis, giving me advice when needed, but also the freedom to develop my own ideas. I am very grateful for that.

I am thankful to Christian Niedworok, who helped me with data organisation by customising a Filemaker database for my electrophysiological recordings. Christian Niedworok and Alexander Brown helped me by designing a data analysis framework in Matlab. Charly Rousseau customised the SpAcAn plugin for coincident event detection and gave me advice regarding data acquisition and analysis. All three never gave up encouraging me to improve my programming skills. I really appreciate your patience, thank you.

I would like to thank Molly Strom for establishing and maintaining my mouse lines, Zara Allardyce and Danielle Carmignac for doing immunohistochemical stainings, Edward Bracey for the $ZnSO_4$-treatments, Martyn Stopps and Nicholas Burczyk for designing and building the channelrhodopsin stimulation device.

Christian, Zara, Sepi, Alex, Ed and Janine, thank you so much for proof reading this thesis.

I would also like to thank everyone in the Margrie Lab, as well as the former Division of Neurophysiology at the National Institute for Medical Research for numerous scientific discussions and constructive feedback. Working with enthusiastic and reliable people is invaluable and I very much like to thank all of you for your kind support.

I am also thankful for significant input and guidance I received from my thesis committee, Andreas Schäfer, Iris Salecker and Vassilis Pachnis.

I would like to thank the MRC and the Wellcome Trust, for funding my work.

My family and friends provided me with great support throughout my PhD. I am incredibly grateful to all of you. Thank you.

Table of Contents

Table of Figures

List of Tables

Abbreviations

2D	Two-dimensional
3D	Three-dimensional
2-HAP	2'-hydroxyacetophenone
AIS	Axon initial segment
cAMP	Cyclic adenosine 3',5'- monophosphate
ChR2	Channelrhodopsin-2
DAB	3,3'-diaminobenzidine
D-AP5	D-2-amino-5-phosphonovalerate
DAPI	4',6-diamidino-2-phenylindole
EPL	External plexiform layer
EPSP	Excitatory post-synaptic potential
ET cell	External tufted cell
EYFP	Enhanced yellow fluorescent protein
GABA	γ−aminobutyrate
GAD	Glutamic acid decarboxylase
GFP	Green fluorescent protein
HCN channel	Hyperpolarisation-activated cyclic nucleotide-gated channel
I_h	Hyperpolarisation-activated current
JG cell	Juxtaglomerular cell
MC	Mitral cell
n.s.	Not significant
NBQX	2,3-Dioxo-6-nitro-1,2,3,4-tetrahydrobenzo[*f*]quinoxaline-7-sulfonamide disodium salt
OB	Olfactory bulb
OR	Odour receptor
OSN	Olfactory sensory neuron
PB	Phosphate buffer
PBS	Phosphate-buffered saline

PFA	Paraformaldehyde
PG cell	Periglomerular cell
RFP	Red fluorescent protein
RMP	Resting membrane potential
RT	Room temperature
SA cell	Short axon cell
SPA	Sag potential amplitude
TC	Tufted cell
TEA-Cl	Tetraethylammonium chloride hydrate
TH	Tyrosine hydroxylase
TTX	Tetrodotoxin
YFP	Yellow fluorescent protein

Chapter 1. Introduction

1.1 Information Processing in the Brain

Neurons are the fundamental elements for information processing in the central nervous system. They are electrically excitable cells that communicate largely via chemical transmission. Most classes of neuron receive the vast majority of input onto their dendritic tree, and send the resultant output via the axon, although there are exceptions to this rule. The kind of computations performed by a neuron is dictated by the combination of its intrinsic and synaptic properties (Turrigiano 2011), which in turn are defined by morphological and biophysical properties and the synaptic connectivity and strength, respectively.

1.1.1 Heterogeneity Between Cell Types

To achieve a comprehensive understanding of the nervous system, it is essential to explore its cellular composition and biophysical diversity to relate that to connectivity and ultimately network function. The general aim of cell classification is to define a group of cells that serve a distinct function. Traditionally, neurons have been grouped in classes or types based on their location, morphology, expression of proteins, firing profiles and the make-up of the synaptic connections they receive (Markram et al. 2004; Toledo-Rodriguez et al. 2004; Petilla Interneuron Nomenclature et al. 2008). Classification of neurons is an ongoing field of research, in which new classification methods are continuously being developed. For example, two groups recently began to link the diversity of cell types based on electrophysiological properties with differential gene expression (Cadwell et al. 2016; Fuzik et al. 2016).

Decades of research have identified many different types of neurons in the nervous system and in some cases have demonstrated the functional importance of such heterogeneity. For instance, various types of neocortical interneurons, differentiated by molecular markers, have been suggested to have distinctly different functional roles (Moore et al. 2010; Lee et al. 2012; Wilson et al. 2012).

It is generally thought that such diversity either reflects biological noise or the functional complexity of a neuronal system, whereby normal network operation

requires large numbers of highly specialised neurons (Fishell and Heintz 2013). The mammalian retina provides a good example for a highly complex neuronal network, where more than 60 discrete cell types have been identified so far (Masland 2012). Although the functional contribution of each of these cell types in not yet fully understood, highly specialised cell types have been found to serve distinct functions within visual perception, such as JamB cells responding to upward motion (Kim et al. 2008).

1.1.2 Heterogeneity Within Cell Types

Differences between cell types co-exist with molecular, epigenetic, morphological and physiological heterogeneity within a given class of neurons. The functional role of these within-class cell-to-cell differences has attracted increasing interest in many areas of biology including developmental biology, genetics, cancer biology and infectious disease research (Altschuler and Wu 2010; Paszek et al. 2010; Pelkmans 2012).

In many cases, cell-to-cell heterogeneity can probably be ascribed to the imperfection of nature and may be ignored as functionally irrelevant (Altschuler and Wu 2010). However, in several brain areas in which neurons were thought to be highly homogeneous or even clonally identical, differences in properties from one neuron to the next have been found to play a critical functional role. For instance, diversity in biophysical properties within neuronal types has been observed to be functionally relevant for principal cells of the cortex (Mason and Larkman 1990; Kumar and Ohana 2008), cerebellum (Kim et al. 2012) and olfactory bulb (Padmanabhan and Urban 2010; Angelo and Margrie 2011).

It is thought that heterogeneity within cell types is, like the diversity between cell types, a feature of complex neuronal systems. In neurons, the composition and localisation of non-synaptic ion channels in the membrane significantly contribute to the unique biophysical properties of each neuron (Zhang and Linden 2003), and in turn contribute to within-class heterogeneity (Nusser 2009). This biophysical diversity can result in a diverse firing pattern of neurons belonging to the same type (Padmanabhan and Urban 2010), which has been shown to substantially contribute to signal decorrelation (Padmanabhan and Urban 2010) and reduction of signal redundancy (Marsat and Maler 2010). Therefore, biophysical diversity is becoming increasingly more recognised as

crucial for robust encoding of stimuli on a complex circuit level (Tripathy et al. 2013). Population-based heterogeneity in the olfactory system can arise from differences between local, functionally distinct networks of neurons (Angelo et al. 2012). In this study, paired whole-cell recordings were conducted from mitral cells (MCs) affiliated either to the same glomerulus or to two different glomeruli. MCs can be highly diverse in their levels of membrane potential sag (Angelo and Margrie 2011), however the amplitude of this sag was significantly more similar in sister-MCs innervating the same glomerulus compared to MCs innervating different glomeruli. When repeating these experiments in a "monoclonal nose" mouse model, in which the same odour receptor is expressed in more than 95% of olfactory sensory neurons (OSNs), the MC population exhibited a more homogenous distribution of sag amplitudes and were also more homogeneous in their HCN2 expression levels. These findings clearly indicate that a regulatory mechanism can underlie the diversity of intrinsic cellular properties, like I_h levels. If such properties depend on local network membership, it follows that the plasticity of these properties is not only regulated on a single-cell level, but could be functionally relevant for the operation of neuronal microcircuits.

1.2 Mechanisms of Homeostatic Plasticity

Many different excitatory and inhibitory cell types with heterogeneous biophysical properties are organised in neuronal microcircuits that functionally contribute to the computations of a brain area. Homeostatic plasticity refers to all mechanisms in a circuit that stabilise the excitability of neurons to keep them responsive in the context of widely varying levels of synaptic input (Marder and Goaillard 2006; Turrigiano 2008; Feldman 2009; Turrigiano 2011). Neuronal circuits rely on various, mostly slow acting biophysical mechanisms to maintain the mean firing of their neurons at a stable level and these mechanisms are thought to operate as a negative feedback loop, counteracting Hebbian synaptic plasticity (Turrigiano 2011). These mechanisms can either homeostatically regulate the synaptic strength (Burrone et al. 2002; Sammons and Keck 2015) or adapt the intrinsic excitability (Zhang and Linden 2003) of a neuron according to synaptic input.

1.2.1 Homeostatic Synaptic Plasticity

In the brain, neurons communicate information mostly by specialised connections, termed synapses. At synapses, the activity of a presynaptically connected neuron can cause the release of neurotransmitters from the presynaptic terminal, which diffuse through the synaptic cleft to the postsynaptic membrane and activate neurotransmitter receptors, causing postsynaptic current flow. Synapses can be excitatory or inhibitory and there is evidence for tight regulation of excitation versus inhibition in local neuronal networks (Shu et al. 2003; Xue et al. 2014).

The main excitatory neurotransmitter is glutamate, which activates metabotropic and ionotropic glutamate receptors. Metabotropic receptors are coupled to G-proteins and act on a much slower time scale than ionotropic receptors, as they initiate an intracellular signalling cascade upon activation. Such second messenger systems have been shown to impact on synaptic plasticity and neuronal excitability (Bashir et al. 1993; Gereau and Conn 1995; Pin and Duvoisin 1995; Anwyl 1999; Benquet et al. 2002). Ionotropic glutamate receptors (AMPA, kainite, NMDA) are cation channels, gating Na^+, K^+ and Ca^{2+} ions. In the presence of glutamate, AMPA and kainate receptors exhibit fast gating properties and therefore mediate fast currents. NMDA receptors activate upon binding to glutamate, their activation is voltage-dependent and they exhibit slower gating properties. NMDA receptors are known to be important in the induction of long-term plasticity (Coan et al. 1987; Collingridge and Bliss 1987). The opening of these ionotropic glutamate receptors generates an excitatory postsynaptic current (EPSC), usually with a fast exponentially rising phase (predominately shaped by AMPA and kainate receptors) and a slow decaying phase (predominately shaped by NMDA receptors). EPSCs cause a depolarisation of the membrane potential in the form of an excitatory postsynaptic potential (EPSP; Hille 2001).

The main inhibitory neurotransmitters are γ−aminobutyrate (GABA) and glycine, however fast synaptic inhibition in the brain is primarily mediated by ionotropic $GABA_A$ receptors (Hille 2001). These GABA-gated ion channels are permeable to anions and the ion flow through these channels (inhibitory postsynaptic current; IPSC) significantly contributes to the hyperpolarisation of the membrane potential (inhibitory postsynaptic potential; IPSP) in a postsynaptically connected neuron. When the

depolarisation of a neuron through excitatory synapses exceeds the hyperpolarisation of inhibitory synapses, the membrane potential can be driven over the firing threshold of a neuron, resulting in an action potential.

Depending on the strength or pattern of activation, the efficacy of transmission at excitatory and inhibitory synapses can be up- or downregulated, a mechanism referred to as synaptic plasticity. According to the timescale on which synaptic plasticity occurs, it can be divided into short-term and long-term plasticity. Homeostatic synaptic plasticity is seen as a form of long-term synaptic plasticity that keeps a neuron within a target firing rate range, for instance by counteracting changes in synaptic strength through mechanisms like long-term potentiation or long term depression (O'Brien et al. 1998; Turrigiano et al. 1998; Burrone et al. 2002; Desai et al. 2002; Turrigiano and Nelson 2004). Homeostatic plasticity can scale all synapses of a neuron (Turrigiano 2008) or only affect a subset of synapses (Rabinowitch and Segev 2008; Yu and Goda 2009; Wefelmeyer et al. 2016) and it can occur presynaptically and postsynaptically (Davis and Bezprozvanny 2001). Interestingly, these activity-dependent scaling processes appear to be initiated intrinsically and can be seen as a form of self-tuning (Turrigiano 2008; Turrigiano 2011).

Initially, homeostatic synaptic plasticity was observed in cultured cortical neurons that have been pharmacologically blocked or activated over 48 hours (Turrigiano et al. 1998). This long-term block or activation resulted in a neuron-wide increase or decrease of EPSC amplitudes; a negative feedback mechanism termed ‘synaptic scaling’. As a result, homeostatic synaptic plasticity was first described as a multiplicative up- or downregulation of the strength of all excitatory synapses upon reduction or increase of network activity and was thought to preserve the ratios between synaptic weights in a neuron (Thiagarajan et al. 2005; Ibata et al. 2008; Turrigiano 2008). Today, synaptic scaling is among the best studied homeostatic plasticity mechanisms and has been observed not only in cortical structures (Turrigiano et al. 1998), but also in spinal neurons (O'Brien et al. 1998) and in the hippocampus (Lissin et al. 1998; Burrone et al. 2002; Thiagarajan et al. 2005).

However, homeostatic synaptic plasticity mechanisms do not necessarily affect neurons as a whole, but can also be restricted to subcellular structures, or even single synapses (Thiagarajan et al. 2005; Sutton et al. 2006; Hou et al. 2008). For example, Thiagarajan

et al. (2005) showed that an activity blockade in hippocampal culture not only altered the magnitude, but also the distribution of EPSCs, leading to a shift of the relative weights of synapses. Furthermore, prolonged depolarisation of hippocampal pyramidal cells has been shown to cause inactivation of only a subset of synapses (Moulder et al. 2006). Also, the AMPA receptor subunit GluR1 can be synthesised locally in dendrites in an activity-dependent manner (Ju et al. 2004; Sutton et al. 2006) and upon chronic inhibition of single synapses, AMPA receptors accumulate selectively at these synapses (Hou et al. 2008).

Regarding the mechanisms underlying homeostatic synaptic plasticity evidence for both changes in postsynaptic AMPA (Lissin et al. 1998; O'Brien et al. 1998; Turrigiano et al. 1998; Wierenga et al. 2005) and NMDA receptors (Rao and Craig 1997; Watt et al. 2000; Mu et al. 2003) exists. An increase in network activity can result postsynaptically in a calcium-dependent reduction of AMPA receptors and thereby decrease the strength of a synapse (O'Brien et al. 1998). Accordingly, the decrease of network activity can result in reduced calcium influx, which leads to an increase in postsynaptic AMPA receptors and thereby larger quantal transmission (Lissin et al. 1998; O'Brien et al. 1998; Thiagarajan et al. 2005; Wierenga et al. 2005; Ibata et al. 2008). The efficacy of presynaptic transmitter release can also be affected by changes in postsynaptic excitability, whereby presynaptic transmitter release is more efficient upon decreased network activity (Petersen et al. 1997; Burrone et al. 2002; Desai et al. 2002; Thiagarajan et al. 2005). Interestingly, a very recent publication showed that presynaptically located HCN1 channels restrict the release of synaptic vesicles in pyramidal neurons of layer III in the entorhinal cortex (Huang et al. 2017). Since the gating probability and occurrence of HCN channels heavily depend on a neuron's activity (Biel et al. 2009), such a presynaptic mechanism might homeostatically regulate the synaptic strength of these neurons.

Homeostatic scaling mechanisms in inhibitory synapses are less well studied, but appear to work in an inverted way, with weakening of synapses upon chronically reduced network activity (Rutherford et al. 1997; Hartman et al. 2006; Swanwick et al. 2006). In cultured hippocampal neurons, a prolonged depolarisation increases the expression of postsynaptic $GABA_A$ receptors, which correlates with an increased IPSC amplitude and frequency and therefore an increased synaptic strength (Rannals and Kapur 2011).

Inversely, a reduced visual input leads to a decreased expression of $GABA_A$ receptors in primary visual cortex (Hendry et al. 1994). Presynaptically, neuronal activity has been shown to regulate the amount of GABA released by individual vesicles (Hartman et al. 2006).

While the homeostatic regulation of neurons via changes in synaptic strength is a large field of research, it is not the focus of this thesis. Rather, this project focuses on a much less studied area of neuronal plasticity that occurs via regulation of a neuron's intrinsic biophysical properties.

1.2.2 Homeostatic Intrinsic Plasticity

Most efforts to understand network plasticity have focussed on synaptic mechanisms (Turrigiano 2008; Feldman 2009; Turrigiano 2011; Wefelmeyer et al. 2016). However, neurons respond to fluctuating input not only with a change in synaptic efficacy, but also by adapting their intrinsic input/output curve and therefore altering how they integrate the synaptic signals. More specifically, homeostasis of a neuron and network stability is heavily influenced by the interplay of synaptic strength and various intrinsic voltage-dependent currents (Marder and Goaillard 2006). The strength of a voltage-dependent macroscopic current is defined by the number and location of the underlying membrane channels (Desai et al. 1999; Schulz et al. 2006) as well as the gating properties of these channels (Li et al. 1992) and can be sensitive to activity-dependent intracellular signalling (Turrigiano et al. 1994; Bito et al. 1996). Such an activity-dependent regulation of ion channels can occur by modulation of ion channel density through changes in transcription and translation (Aptowicz et al. 2004; Campanac et al. 2013), channel endocytosis or channel trafficking along the membrane (Misonou et al. 2004; Kim et al. 2007), as well as changes of ion channel function by altered posttranslational mechanisms such as phosphorylation (Gasparini and Magee 2002; Frick et al. 2004; Misonou et al. 2004; Park et al. 2006) or binding of secondary messengers (Baines 2003; Wang et al. 2007).

Activity-dependent regulation of intrinsic properties has been demonstrated in many brain areas, including neocortex (Desai et al. 1999; Gibson et al. 2006; Bartley et al. 2008), hippocampus (Aptowicz et al. 2004; van Welie et al. 2004; O'Leary et al. 2010), striatum (Azdad et al. 2009), and brainstem (Nelson et al. 2003). It has been observed in

principal neurons (Desai et al. 1999; Aptowicz et al. 2004; van Welie et al. 2004; Azdad et al. 2009; O'Leary et al. 2010) as well as in interneurons (Gibson et al. 2006; Bartley et al. 2008). This type of plasticity depends on the plastic strength of several different non-synaptic ion currents, including Na^+, K^+ and Ca^{2+} currents (Desai 2003; Sun 2009; Campanac et al. 2013), as well as the hyperpolarisation-activated current (I_h; van Welie et al. 2004; Gibson et al. 2006). These currents are crucial for integration of synaptic inputs and neuronal computations, since they determine the firing threshold and shape of the action potential. Action potentials are the fundamental basis of signal transmission and are predominately generated by the interplay of voltage-gated Na^+, K^+ and Ca^{2+} channels (Hille 2001). These voltage-gated ion channels open according to changes in membrane potential. Most fast action potentials are the result of a Na^+ influx through voltage-gated Na^+ channels (but can also be generated by voltage-gated Ca^{2+} channels), which activate upon synaptic depolarisation. However, voltage-gated Na^+ channels exhibit an inactivating mechanism, causing a voltage-independent, rapid closing of these channels. This state persists for several milliseconds even when the membrane potential has returned to its resting state. Action potentials are shaped by the interplay of these voltage-gated Na^+ channels with another type of ion channel, the voltage-gated K^+ channels. Voltage-gated K^+ channels also activate upon depolarisation of the membrane potential, but exhibit slower activation kinetics. The outward K^+ ion flow gated by these channels counteracts the Na^+ ion flow through voltage-gated Na^+ channels with a delay, thereby terminating the rapid depolarisation of the membrane potential and repolarising the potential back to the resting state. Depending on the timing of the interplay between voltage-gated Na^+ and K^+ channels, many neurons exhibit an afterhyperpolarisation, which refers to a hyperpolarisation of the membrane potential directly after an action potential (Hille 2001). Afterhyperpolarisation is caused by the persistent inactivation of Na^+ channels and delayed inactivation of K^+ channels and can be characteristic for a cell type, because its occurrence and shape depend on the ion channel composition of a neuron (Saar et al. 2002). Depending on the cell type, this afterhyperpolarisation can open hyperpolarisation-activated ion channels, like hyperpolarisation-activated cyclic nucleotide-gated (HCN) channels, that gate a cation current (I_h) and thereby promote the repolarisation of the neuron (Robinson and Siegelbaum 2003).

It has been demonstrated in pyramidal cells that a prolonged up- or downregulation of spontaneous firing resulted in decreased or increased intrinsic excitability, respectively (Desai et al. 1999). Interestingly, the increased excitability in these neurons resulted not from a homotypic, but diverging regulation of voltage-gated ion channels. Abolishing spontaneous activity increased the voltage-dependent Na^+ currents whereas persistent K^+ currents were reduced, in sum causing more rapid firing and lower spiking threshold in these neurons. It appears that many neurons use intracellular Ca^{2+} levels to regulate synaptic efficacy and the density of non-synaptic ion channels in an activity-dependent way (LeMasson et al. 1993; Liu et al. 1998; Desai 2003; Fan et al. 2005). Several studies demonstrated an inhibition of homeostatic intrinsic plasticity by blocking voltage-dependent calcium channels or calcium-related pathways (Fan et al. 2005; Frick and Johnston 2005; O'Leary et al. 2010), however the precise mechanisms are not yet fully understood.

I_h, mediated by HCN channels, has long been postulated to impact on homeostasis of neuronal activity (van Welie et al. 2004). In hippocampal CA1 neurons, a prolonged increase in activity causes an upregulation of I_h in the soma and dendrites (Fan et al. 2005; Campanac et al. 2008), which is mediated by an activity-dependent increase in Ca^{2+} entry, that activates CaMKII (Fan et al. 2005). Also, induction of long-term depression in CA1 neurons, results in long-lasting downregulation of I_h, which ultimately leads to an increased neuronal excitability (Brager and Johnston 2007). The activity-dependent decrease of I_h is mediated by activation of group 1 metabotropic glutamate receptors, through the activation of protein kinase C and the release of Ca^{2+} from internal storages (Brager and Johnston 2007). Interestingly, HCN channels can be actively trafficked along the membrane by binding to TPR-containing Rab8b interacting protein (TRIP8b; Santoro et al. 2004). TRIP8b appears to have a strong effect on I_h density, whereby different TRIP8b isoforms can up- or downregulate surface expression of HCN channels, and all isoforms negatively impact the channel's gating probability (Santoro et al. 2009). TRIP8b itself could be dynamically regulated through phosphorylation according to neuronal activity (Shin et al. 2008). Thus, one could imagine a homeostatic regulation of neuronal excitability through activity-dependent, TRIP8b-mediated HCN channel trafficking, however a detailed mechanism remains to be shown.

Activity-dependent plasticity has also been shown to occur at the axon initial segment (AIS). The AIS is located close to the soma and consists of a dense population of voltage-gated cation channels. The density of these ion channels combined with passive axonal properties leads to a low action potential threshold at the AIS. As a result, action potentials are usually initiated at the AIS (Bender and Trussell 2012). The precise location of the AIS (Grubb and Burrone 2010) as well as the length of the AIS and the distribution of voltage-gated Na^+ channels (Kuba et al. 2010) depend on the history of a particular neuron's electric activity, and in turn impacts on the input/output function.

To summarise, voltage-dependent ion channels form the basis of intrinsic excitability, however these channels exhibit a rather rapid turn-over rate of hours to days (Marder and Goaillard 2006). Additionally, neurons, even of the same class, do not have identical ion channel composition and therefore exhibit different electrical properties, resulting in considerable heterogeneity (see section 1.1.1; Schulz et al. 2006). In this context, the robustness of neuronal excitability and global activity levels throughout the lifetime of an animal is remarkable and mechanisms must be in place to tightly regulate the complex interplay between fluctuating synaptic strength and the levels of ion channels (LeMasson et al. 1993; Liu et al. 1998).

In accordance with existing literature (Angelo et al. 2012), this thesis proposes that the diversity of I_h in glomerular layer interneurons of the olfactory bulb may serve as a network-based gain control mechanism. We hypothesise that the levels of I_h depend on the history of activation, not only in a single neuron, but also in the local network, which in turn tune the excitability of neurons. The following chapter summarises how HCN channels, the voltage-gated ion channels underlying I_h, work mechanistically and gives an overview over the functional impact I_h is known to have in several different brain regions and cell types.

1.3 The Role of I_h in Neuronal Integration

1.3.1 Hyperpolarisation-Activated Cyclic Nucleotide-Gated Channels

A well-studied neuronal membrane ion channel, known to impact on neuronal excitability and synaptic integration, is the HCN channel. In mammals, HCN channels are encoded by at least four different genes (Santoro et al. 1997; Ludwig et al. 1998; Santoro et al. 1998) and the four different protein isoforms (HCN 1 - 4) can form homo- or heterotetramers around a central pore (Figure 1.1a; Chen et al. 2001; Ulens and Tytgat 2001; Much et al. 2003; Zagotta et al. 2003). All four isoforms contain both a core transmembrane segment domain and a carboxy-terminal cyclic nucleotide-binding domain motif (Figure 1.1b). Each of the four subunits is thought to be independently regulated by membrane voltage, and the opening probability of the channel as a whole increases with the activation of each subunit (Altomare et al. 2001).

The channel structure is similar to that of the voltage-gated potassium channel, including a number of positively charged residues on the fourth transmembrane domain and the "GYG" motif of a K^+-channel selectivity filter (Figure 1.1b), but lacks other K^+-channel specific sequences. As a result, HCN channels gate cations rather non-specifically (Yanagihara and Irisawa 1980) with a preference for K^+ but also a significant permeability for Na^+ (Pape 1996).

HCN channels exhibit the phenomenon of "dual channel activation", whereby the gating of the ion channels is regulated not only by voltage, but also the direct binding of cyclic nucleotides (summarised by Wahl-Schott and Biel 2009). The channel's activity is modulated by direct binding of the second messenger cyclic adenosine 3',5'-monophosphate (cAMP) at the cytoplasmic cyclic nucleotide-binding domain (Figure 1.1a and b; DiFrancesco and Tortora 1991; Zagotta et al. 2003). The binding of cAMP shifts the voltage relation of HCN channel gating, so that the channel opens at less negative membrane potentials (DiFrancesco and Tortora 1991). The four channel isoforms differ in their activation kinetics and sensitivity to the nucleotide cAMP (Chen et al. 2001; Kaupp and Seifert 2001; Stieber et al. 2005). HCN1 has the fastest activation kinetics, followed by HCN2 and HCN3, whereas activation of HCN4 is distinctively slower (Santoro et al. 2000; Chen et al. 2001; Stieber et al. 2005).

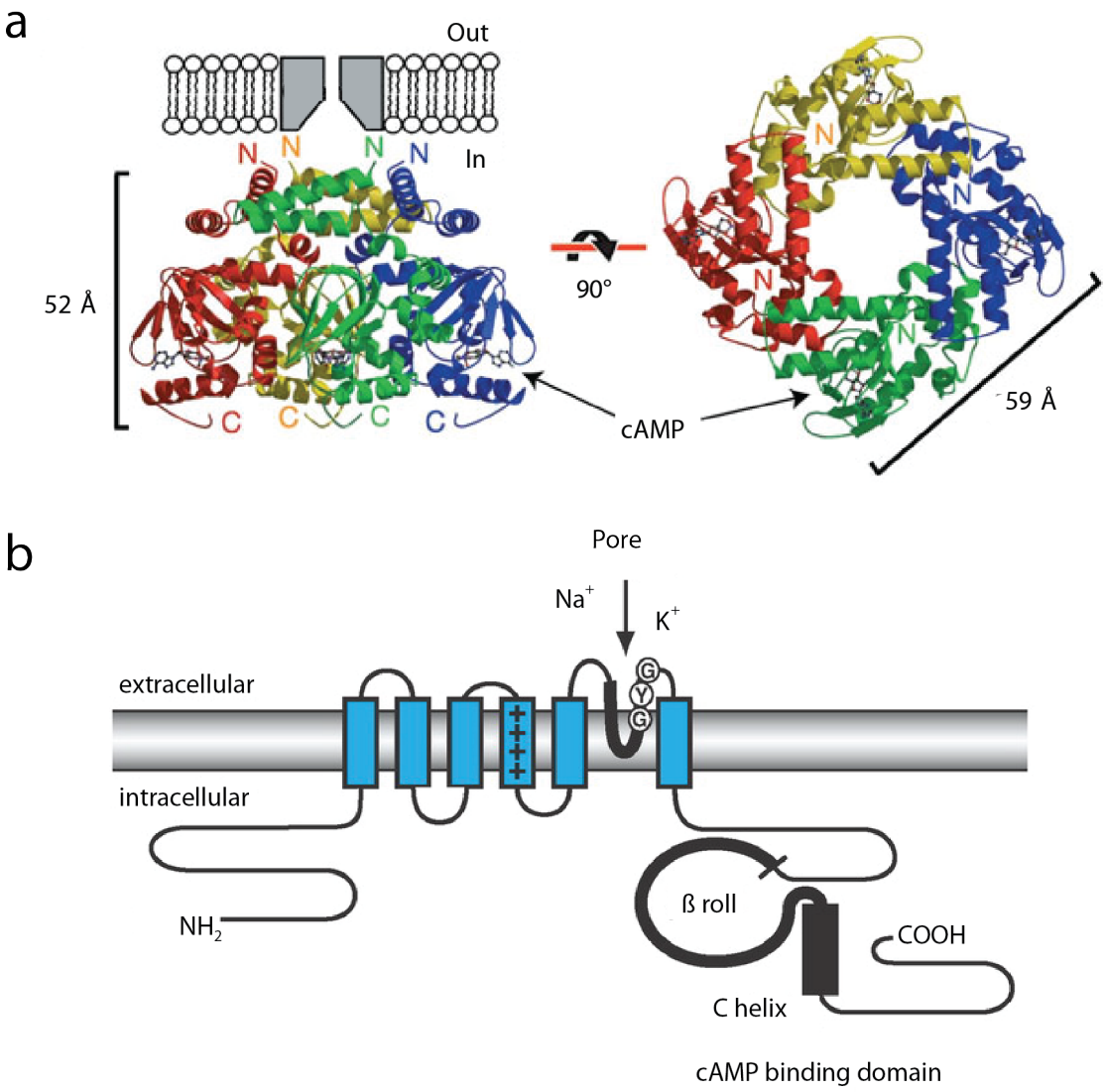

Figure 1.1 Molecular Structure of HCN Channels

(a) Crystal structure of four C-linker and CNBD constructs in a HCN2 homotetramer. Each of the four subunits is labelled in a different colour and has a cAMP molecule bound to the CNBD (modified from Zagotta et al. 2003).

(b) Schematic of a single HCN channel subunit transmembrane conformation with six transmembrane regions *(blue)*. Voltage sensing domains (indicated with +) are located within the fourth transmembrane segment and the pore region is between the fifth and sixth segment. A P-loop forms the pore and contains the "GYG" motif of a K^+-channel selectivity filter. On the intracellular C-terminal side is a cyclic nucleotide-binding domain consisting of three α-helices (A-C) with a β-roll between the A- and B-helix (modified from Robinson and Siegelbaum 2003).

Furthermore, HCN channel gating properties, and therefore the time course of I_h, are sensitive to the balance of a large variety of molecular and external factors, including phosophatidylinositol-4,5-bisphosphate (PIP_2; Zolles et al. 2006), phosphorylation (Zong et al. 2005), chloride concentration (Wahl-Schott et al. 2005), pH (Zong et al. 2001) and temperature (Pignatelli et al. 2013). It is still unclear whether HCN channels form heteromers *in vivo.* Several groups suggested that heteromers might contribute to functional diversity of HCN channels (Chen et al. 2001; Ulens and Tytgat 2001; Much et al. 2003), but HCN channel isoforms may also co-localise without forming heteromers (Muller et al. 2003). In the brain, HCN channels show a rather ubiquitous expression, occurring in nearly every principal neuron type (Pape 1996; Williams and Stuart 2000; Berger et al. 2001; Nolan et al. 2003; Angelo et al. 2007; Nolan et al. 2007; Angelo and Margrie 2011) and also in some interneurons (Aponte et al. 2006; Pignatelli et al. 2013). The subcellular localisation of HCN channels can vary between different types of neurons, including somatic, dendritic and axonal compartments and contributes to the functional diversity of the ion channel across different brain areas (Nusser 2009). For instance, somatic HCN channel expression is prominent in GABAergic interneurons of the olfactory bulb, cerebellum and hippocampus, where the activity of HCN channels influences the membrane properties of neurons (Notomi and Shigemoto 2004; Brewster et al. 2007b; Bender and Baram 2008; Pignatelli et al. 2013). HCN channels have also been localised in the axonal regions of some interneurons (Notomi and Shigemoto 2004; Aponte et al. 2006; Brewster et al. 2007a), where they may regulate the release of neurotransmitters (Beaumont and Zucker 2000; Mellor et al. 2002). The dendritic distribution of HCN channels can vary greatly between pyramidal neurons of different brain areas. In hippocampal, subicular and neocortical layer 5 pyramidal neurons, HCN channels exhibit a graded distribution with a 60-fold increase in HCN channels from the soma to the apical dendrite (Lorincz et al. 2002; Poolos et al. 2002). HCN channels in distal dendrites can heavily influence the dendritic excitability as well as temporal integration of synaptic input (Williams and Stuart 2000; Berger et al. 2001). In contrast, cerebellar purkinje cells regulate temporal summation of EPSPs along their dendrites through a uniform distribution of HCN channels (Angelo et al. 2007).

1.3.2 Properties of the Hyperpolarisation-Activated Cation Current

The membrane current mediated by HCN channels is referred to as I_h and has been shown to significantly impact the computational properties of a number of different cells types (Robinson and Siegelbaum 2003; Wahl-Schott and Biel 2009). In the brain the current was first observed in rod photoreceptors and pyramidal neurons of the hippocampus (Bader et al. 1979; Halliwell and Adams 1982). As the name implies, I_h activates at negative membrane potentials and inactivates at positive potentials, causing neurons with hyperpolarised membrane potentials to slowly depolarise, driving their membrane potential closer to the firing threshold (Yanagihara and Irisawa 1980). Depending on the cell type, the activation range can be between -50 mV and -100 mV, which is why in some cells, the channel can be open at resting membrane potential. The half maximum of activation is around -80 mV. I_h is an inward current, with a sigmoidal activation and deactivation time course (DiFrancesco et al. 1986; Spain et al. 1987). It exhibits a nearly linear current-voltage relation and has a reversal potential around -30 mV (Yanagihara and Irisawa 1980; Mayer and Westbrook 1983; Pape 1996).

1.3.3 Physiological Functions of Hyperpolarisation-Activated Cation Current

Several groups have shown that I_h is involved in modulating the neuronal input/output function as well as regulating various network properties (Magee et al. 1998; Williams and Stuart 2000; Hu et al. 2002; Aponte et al. 2006; Angelo et al. 2007; Nolan et al. 2007; Giocomo and Hasselmo 2009) via mechanisms including the regulation of excitability (Poolos et al. 2002; van Welie et al. 2004; Fan et al. 2005; Nolan et al. 2007), synaptic integration (Williams and Stuart 2000; Berger et al. 2001; Angelo et al. 2007) and generation of intrinsic oscillations and resonance (Pape 1996; Luthi and McCormick 1998; Dickson et al. 2000; Santoro et al. 2000; Giocomo and Hasselmo 2007; Liu and Shipley 2008b).

For instance, I_h can be activated at voltages close to the resting membrane potential (RMP), resulting in the depolarisation of a neuron, which has been shown to enhance auditory coincidence detection (Yamada et al. 2005). Also, HCN channels characteristically exhibit both voltage-dependant activation and deactivation. This

mechanism actively opposes any changes away from the RMP, thereby stabilising the RMP (Mayer and Westbrook 1983; Pape 1996; Hu et al. 2002; Nolan et al. 2003; Nolan et al. 2007). I_h-mediated stabilisation of the RMP has been associated with limiting long-term potentiation in CA1 pyramidal neurons (Tsay et al. 2007).

In the dendrites of in CA1 pyramidal neurons and layer V pyramidal neurons HCN channels are expressed in a gradient, with sparse HCN channel occurrence at the soma and a high density at the distal end of the apical dendrite (Williams and Stuart 2000; Berger et al. 2001; Lorincz et al. 2002; Poolos et al. 2002). This gradient is thought to counterbalance dendritic filtering of EPSPs and therefore spatially normalises the temporal integration of synaptic input along the dendrite. The mechanism underlying this effect is the active opposition of deviation from the RMP, as described in section 1.3.1. When a dendrite is locally depolarised through an EPSP, HCN channels (that are partly open during RMP) deactivate and cause a faster repolarisation of the membrane potential and thereby reduce EPSP duration (Magee 1999; Williams and Stuart 2000). Since HCN channels have rather slow gating properties, this deactivation of HCN channels even causes membrane hyperpolarisation following the EPSP. Conversely, an IPSP-dependent activation of HCN channels actively opposes the hyperpolarisation of the membrane potential and shortens the IPSP duration, as well as causing a small depolarisation directly after the IPSP (Williams and Stuart 2003). However, the described dendritic HCN channel gradient does not seem to be a general feature of pyramidal neurons. Purkinje cells generate location independence of EPSP summation despite a uniform distribution of HCN channels along their dendrites (Angelo et al. 2007) and pyramidal-like principal neurons in the stratum radiatum of the hippocampus exhibit a reverse HCN gradient with higher expression in the soma than in dendrites (Bullis et al. 2007).

Additionally, the slow activation kinetics of HCN channels act as a high-pass filter, supressing low frequency changes in the membrane potential. Such filter functions are crucial for tuning neuronal activity to preferred frequencies ("membrane resonance", Hutcheon and Yarom 2000; Ulrich 2002; Wang et al. 2006). For instance, in rod photoreceptors the interplay of I_h with other ionic conductances creates a band pass filter effect, thereby tuning the response in the retina to certain frequencies (Barrow and Wu 2009). Finally, I_h can be involved in the generation of intrinsic neuronal oscillations

like in the thalamus (Pape 1996) or entorhinal cortex (Dickson et al. 2000), where an interplay of I_h and a low threshold Ca^{2+} current causes repetitive bursts of action potentials. Intrinsic oscillations function as pacemakers and can thereby synchronise neuronal circuits (Dickson et al. 2000).

Interestingly, expression levels of I_h have been shown to be behaviourally relevant: Along the dorso-ventral axis of the medial entorhinal cortex, neurons systematically vary in their frequency of subthreshold membrane potential oscillations and membrane resonance (Giocomo and Hasselmo 2007). Dorsal–ventral changes in neuronal firing depend on HCN1 channel expression (Giocomo and Hasselmo 2009) and in large areas of medial entorhinal cortex the magnitude of I_h can be up- or downregulated by chemically targeting the neuromodulatory systems which regulate I_h (upregulation of cAMP or muscarinic acetylcholine receptors; Heys and Hasselmo 2012). The I_h-mediated topographic organisation in the cellular properties not only corresponds to the gradient changes in the size and spacing of grid-cell firing fields (Giocomo and Hasselmo 2007), but has recently been shown to alter grid field spacing and grid field size (Giocomo et al. 2011). A similar I_h-mediated gradient in the distribution of intrinsic biophysical properties has also been shown to exist in spiral ganglion neurons, the sensory afferents in the cochlea (Liu et al. 2014).

In the olfactory bulb, expression levels of I_h have been shown to be more similar in principal neurons participating in the same microcircuit and processing similar odour-related information. Therefore I_h expression has been proposed to function as a network based gain control mechanism (Angelo et al. 2012).

In addition to its significant impact on intrinsic properties of individual neurons and on network regulation, I_h is an ideal membrane property to study for practical reasons. When recording from intracellular using whole-cell patch clamp in current-clamp mode, a hyperpolarisation-evoked membrane sag potential can be observed, the amplitude of which strongly correlates with the amplitude of pharmacologically isolated I_h recorded in voltage-clamp mode (Robinson and Siegelbaum 2003; Wahl-Schott and Biel 2009; Angelo and Margrie 2011). Therefore, the amount of sag in a recorded neuron can be determined and plotted against other parameters, such as firing profile and synaptic strength, under physiological conditions either in a slice preparation (without requiring synaptic receptor channel blockers) or in vivo (Angelo and Margrie 2011).

1.4 The Olfactory System

The anatomical structures for odour detection are highly conserved between different species (Ache and Young 2005). In mammals, odour sampling occurs by nasal inhalation, causing odour molecules to be conveyed from the environment to receptor cells in the epithelium of the nasal cavity. Odour information is processed by two parallel pathways, namely the main olfactory system and the accessory olfactory system. The main olfactory system, located at the roof of the nasal cavity, detects volatile odours, while the vomeronasal organ of the accessory olfactory system at the base of the nasal septum senses both, volatile and non-volatile stimuli, mostly pheromones (Wysocki 1979). This thesis exclusively focuses on the main olfactory system. Information about odour stimuli detected in the main olfactory epithelium is relayed to the primary sensory area, the olfactory bulb (OB), where it is processed and afterwards projected to higher brain areas belonging to the primary olfactory cortex, like amygdala, piriform cortex or entorhinal cortex (Haberly and Price 1977; Nagayama et al. 2010; Igarashi et al. 2012).

One advantage of studying the OB lies in the possibility to easily access, modulate and observe functionally discrete and anatomically well-delineated neuronal networks *in vitro* and *in vivo*. The OB, which is the first brain area to process olfactory information, can be stimulated using naturalistic stimuli and activity can be recorded electrically or visually (e.g. via calcium imaging methods; Wachowiak et al. 2004). The exposed anatomical position of the OB facilitates physical manipulations without the risk of damaging other brain areas. Furthermore, well-established olfactory training paradigms exist (Slotnick and Katz 1974; Cleland et al. 2002; Abraham et al. 2004; Mandairon et al. 2006b), which can be used to assess the relevance of these changes in the olfactory circuit on behaviour.

1.4.1 Anatomy

1.4.1.1 Olfactory Epithelium

In the olfactory epithelium, odour molecules are detected by specialised neurons, the olfactory sensory neurons (OSN), which transduce olfactory stimuli into electrical activity, and transmit this information to the OB (Figure 1.2a). In the cilia of OSNs,

odour molecules bind to specialised olfactory receptors (OR). To be able to detect the nearly infinite amount of odour molecules, more than a thousand different types of ORs exist in rodents (Zhang and Firestein 2002; Zhang et al. 2004). However, the molecular receptive range of each OSN is determined by the expression of usually one OR gene in each OSN (Vassar et al. 1993; Serizawa et al. 2000). Ors have a broad odour-quality tuning, with one OR being able to bind to multiple odour molecules and one odour molecule being recognised by several Ors (Duchamp-Viret et al. 1999; Malnic et al. 1999). This rather unspecific odour–receptor interaction enables each odour to activate several different OSN types.

1.4.1.2 Olfactory Bulb

Sensory information from the OE is relayed to the OB, which consists of six layers: Most superficially is the olfactory nerve layer, followed by glomerular layer, external plexiform layer, mitral cell layer, internal plexiform layer and, as a core, the granule cell layer.

Axons of OSNs project to glomeruli in the glomerular layer (Figure 1.2a, Mori and Sakano 2011). A glomerulus is a synaptically dense, 30-100µm neuropil encapsulated structure, in which the axons of OSNs form synapses with dendrites of principal and interneurons. It therefore acts as an information hub by processing and transmitting the odour-related input. In general, each glomerulus receives input from a homogeneous population of several thousand OSNs (Shepherd 2003) which all express the same OR (Figure 1.2a; Mombaerts et al. 1996). Usually, all OSNs expressing the same OR project to two glomeruli, one located more laterally in the OB and the other one more medial (Mombaerts et al. 1996). Within each glomerulus, one individual OSN axon branches multiple times (Klenoff and Greer 1998) and forms synapses onto the OB principal neurons and JG interneurons (Figure 1.2b; Pinching and Powell 1971a; Pinching and Powell 1971b; Kasowski et al. 1999). The bulbar neurons receiving and processing OSN input are described in the following sections.

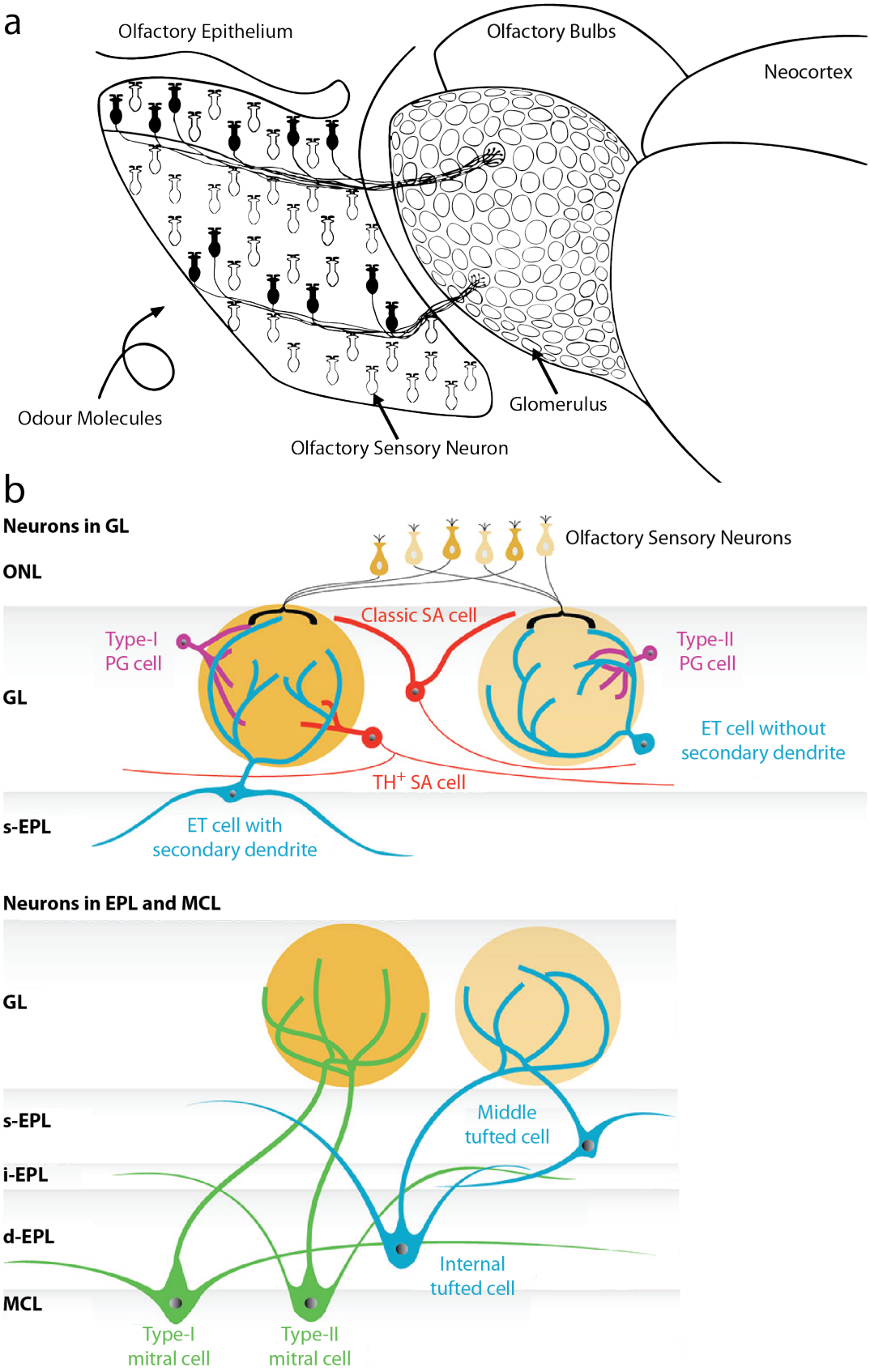

Figure 1.2 Projections of the Olfactory Epithelium to the Olfactory Bulb and Major Cell Types of the Olfactory Bulb

Figure 1.2 Projections of the Olfactory Epithelium to the Olfactory Bulb and Major Cell Types of the Olfactory Bulb (cont.)

(a) Schematic illustrating the pattern of axonal projections from OSNs in the olfactory epithelium to the two Obs. All OSNs expressing the same OR *(black)* converge onto the same one or two glomeruli in each OB. Therefore each glomerulus represents the cumulated input of one OR type (modified from Mori et al. 2006).
(b) Schematic showing the location and innervation pattern of selected OB neurons. *top:* Sub-classes of JG cells and principal neurons in the OB. PG cells are considered part of the JG cell population and can be divided into two types. Type-I is monosynaptically connected to OSNs and type-II only receives indirect OSN input through ET cells. SA cells are also JG cells and two types of SA cells have been described. The classic superficial SA cell does not innervate glomeruli, whereas the TH^+ superficial SA cells can innervate several glomeruli. The last group of JG cells are ET cells. They can be divided based on the occurrence of secondary dendrites. *bottom:* Principal neurons typically innervate large areas of a single glomerulus with their apical tuft. TCs can be found in the external plexiform layer and are subdivided by their soma location into middle TCs and internal TCs. Subtypes of MCs are classified based on the innervation pattern of their basal dendrites, with type-I MCs extending their basal dendrites into deeper layers of the external plexiform layer than type-II MCs (modified from Nagayama et al. 2014). ET cell = external tufted cell, GL = glomerular layer, s-EPL/i-EPL/d-EPL = superficial/intermediate/deep external plexiform layer, JG = juxtaglomerular cell, MC = mitral cell, MCL = mitral cell layer, ONL = olfactory nerve layer, PG cell = periglomerular cell, SA cell = short axon cell, TC = tufted cell.

1.4.1.3 Cell Types of the Olfactory Bulb

Principal Neurons

In mammals, the principal output neurons of the OB are referred to as mitral cells (MCs) and tufted cells (TCs) and they transmit olfactory information into higher brain areas via the lateral olfactory tract. Approximately 60 MC and TC ramify an apical dendritic tuft within one glomerulus (Figure 1.2b, bottom; Royet et al. 1998), whereby the number of affiliated principal neurons depend on the activation history of the glomerular network (Liu et al. 2016).

The somata of MCs (15 – 30 µm in diameter) are located in the mitral cell layer and their dendritic tuft ramifies throughout most of the targeted glomerulus (Figure 1.2b, bottom). Within the glomerulus, MCs receive excitatory input from OSNs (Berkowicz et al. 1994; Ennis et al. 1996) and ETs (De Saint Jan et al. 2009). They have reciprocal dendro-dendritic synapses with inhibitory interneurons (Pinching and Powell 1971b), perform recurrent self-excitation (Friedman and Strowbridge 2000; Margrie et al. 2001; Salin et al. 2001) and lateral excitation of neighbour MCs via gap junctions (Christie

and Westbrook 2006) as well as chemical transmission (Urban and Sakmann 2002; Pimentel and Margrie 2008). MCs also possess lateral dendrites and can be subdivided into type-I and type-II depending on their location in the external plexiform layer (Orona et al. 1984). With these basal dendrites they may perform additional recurrent self-excitation (Salin et al. 2001) and form extensive dendro-dendritic synapses with granule cells, a type of inhibitory interneuron (Rall et al. 1966). Several studies revealed that the axons of MCs target nearly all regions of the olfactory cortex (Haberly and Price 1977; Nagayama et al. 2010; Igarashi et al. 2012).

The morphology of TCs is similar to MCs, with a smaller soma (15 – 20 μm) usually located in the external plexiform layer. Already in early studies from Cajal (1909), TCs have been distinguished into three types, based on their soma position within the OB: internal-, middle- and external tufted cell (Figure 1.2b). External tufted cells morphologically differ from middle and internal tufted cells and since they are considered to be part of the juxtaglomerular (JG) cell population, they will be discussed later in further detail. The apical dendritic tuft of middle- and internal tufted cells innervates a slightly smaller area of a single glomerulus than the tuft of MCs and they extend lateral dendrites within the superficial external plexiform layer (Figure 1.2b, bottom; Haberly and Price 1977; Orona et al. 1984). The axonal projections of TCs are much more restricted to anterior and rostral parts of the olfactory cortex than MC projections (Nagayama et al. 2010; Igarashi et al. 2012). Several studies indicate that even if MCs and TCs have similar morphologies and receive similar sensory input, they process odour information differently and relay it to different brain areas (Nagayama et al. 2010; Fukunaga et al. 2012; Manabe and Mori 2013).

Granule Cells

Granule cells are the major inhibitory interneurons in the OB (Mori 1987). Their small somata are located in the granule cell layer and their dendrites innervate the external plexiform layer. Here they form dendro-dendritic synapses with the lateral dendrites of MCs and TCs. Since granule cells lack axons (Golgi 1886), they only receive local input and send output via dendro-dendritic synapses. At these synapses, MCs excite granule cells by releasing glutamate onto AMPA and NMDA receptors located on granule cell dendrites (Wellis and Kauer 1993), which can evoke a recurrent GABA release from the granule cells back onto the MC dendrite (Ribak et al. 1977). Since

several MCs can converge onto the same granule cell, MCs can inhibit each other via granule cell-mediated lateral inhibition (Isaacson and Strowbridge 1998).

Juxtaglomerular Cells

A less well-studied group of OB interneurons are the inhibitory JG cells, located in the glomerular layer. Each glomerulus is innervated by as many as 1500–2000 inhibitory and excitatory JG cells (Shipley et al. 1996). Despite JG cells being morphologically heterogeneous, they are classically divided into three morphologically identified types (Pinching and Powell 1971a): excitatory external tufted (ET) cells, inhibitory periglomerular (PG) cells and inhibitory short axon (SA) cells (Figure 1.2b).

External Tufted Cells

In contrast to the other TCs, the ET cell somata lie in the periglomerular region and not in the external plexiform layer (Pinching and Powell 1971a). Because of their location in proximity to the glomeruli, they can be considered a class of JG cells together with inhibitory glomerular interneurons. ET cells exhibit several properties making them distinctly different from MCs and other TC subclasses. They have a rather small soma (around 15 μm in diameter) and a primary dendrite with an elaborate arborisation, ramifying throughout the whole area of a single glomerulus (Figure 1.2b, top; Hayar et al. 2004b). Interestingly, they do not seem to form dendro-dendritic synapses with granule cells in the external plexiform layer (Wachowiak and Shipley 2006). All ET cells appear to receive monosynaptic excitatory input from OSNs within a single glomerulus (Hayar et al. 2004a). ET cells in turn excite inhibitory interneurons of the same glomerulus (Hayar et al. 2004a; Shao et al. 2009; Kiyokage et al. 2010). They also excite local MCs and other TCs (Hayar et al. 2004a; De Saint Jan et al. 2009; Gire et al. 2012), potentially via gap junctions or glutamatergic spillover, as has been observed between MCs. ET cells might form dendro-dendritic synapses with MCs (De Saint Jan et al. 2009). Most prominently, ET cells possess intrinsic membrane properties, generating spontaneous rhythmical bursts of action potentials (Hayar et al. 2004b). Like MC and other TC axons, the ET cell axon appears to project out of the OB to higher brain areas, although the downstream target of this projection remains unknown (Wachowiak and Shipley 2006).

Periglomerular Cells

The two classes of inhibitory interneurons in the glomerular network can be clearly distinguished from the excitatory ET cells. The most abundant type of neuron in the glomerular network is the PG cell (70-85%, Wachowiak and Shipley 2006; Parrish-Aungst et al. 2007). With a soma of only 5-8 μm in diameter, they are among the smallest neurons in the brain (Pinching and Powell 1971a; Hayar et al. 2004a). The innervation pattern of a PG cell dendrite is typically restricted to only one or two glomeruli and the dendrites cover a much smaller volume of a glomerulus than the dendrites of principal neurons or ET cells (Figure 1.2b, top; Pinching and Powell 1971a; Pinching and Powell 1971b). Therefore, these neurons are generally thought to mediate inhibition within single glomerular networks. PG cells form inhibitory synapses onto OSNs (Aroniadou-Anderjaska et al. 2000; Murphy et al. 2005; Shao et al. 2009) and other PG cells in close proximity (Murphy et al. 2005; Panzanelli et al. 2007). They are also known to form reciprocal dendro-dendritic synapses with MCs (Pinching and Powell 1971b; Ribak et al. 1977) and ET cells (Hayar et al. 2005; Shao et al. 2012). If a PG cell has an axon, it projects laterally and extends over several glomeruli (around 600 μm; Pinching and Powell 1971a; Pinching and Powell 1971b; Kosaka and Kosaka 2011).

Glomeruli have been anatomically divided into two areas, one innervated by OSNs and one which is exclusively targeted by the processes of secondary sensory neurons (Kasowski et al. 1999). Based on their glomerulus innervation pattern, PG cells can be classified into two sub-populations. Dendrites of type-I PG cells innervate all areas of a glomerulus, whereas dendrites of type-II PG cells do not project to the glomerular zone containing OSNs (Figure 1.2b, top; Kosaka et al. 1998). Furthermore, 70-80 % of PG cells receive indirect OSN input via ET cells (Hayar et al. 2004a; Shao et al. 2009; Kiyokage et al. 2010), a population that could theoretically relate to type-II PG cells. Only 20-30 % of PG cells receive monosynaptic excitatory input from OSNs, however it remains to be shown how this synaptic organisation relates to the subtypes defined by glomerular innervation patterns.

Short Axon Cells

The second class of inhibitory interneurons participating in glomerular circuits are superficial short axon cells, which will from now on be referred to as SA cells (Figure 1.2b, top). SA cells have a slightly larger soma than PG cells (around 10µm in diameter, Hayar et al. 2004a). Initially they were reported to extend their dendritic tree exclusively within the interglomerular space and possess a short axon, terminating 1-2 glomeruli away from the soma (Figure 1.2b, top; Pinching and Powell 1971a; Pinching and Powell 1971b). However in this thesis the focus lies on a more recently described type of SA cell, which ramifies with its dendritic tree in several closely located glomeruli and exhibits an axon that can project up to 1 mm away from the soma (Figure 1.2b, top; Aungst et al. 2003; Kiyokage et al. 2010; Banerjee et al. 2015). These SA cells receive monosynaptic input from ET cells (Hayar et al. 2004a; Kiyokage et al. 2010) and OSNs (Kiyokage et al. 2010). In their axonal target glomeruli they form inhibitory synapses onto ET cells and potentially PG cells (Aungst et al. 2003; Liu et al. 2013; Whitesell et al. 2013) and are therefore considered to provide inter-glomerular inhibition. They may mediate dopaminergic inhibition onto D2 receptors of OSN terminals, but no direct connection has thus far been demonstrated (Maher and Westbrook 2008) and a potential mechanism for such a presynaptic inhibition remains unclear (as discussed in McGann 2013).

Neuronal connections within a glomerulus are fundamental for the work in this thesis and will be discussed in detail in the following section.

1.4.2 The Glomerular Microcircuits

1.4.2.1 Intra-Glomerular Connections

The most studied connection within the glomerulus is the excitatory input from OSNs onto MCs and TCs (Figure 1.3a, arrows 1). This input can be monosynaptic or polysynaptic, which results in a biphasic excitatory-inhibitory response in principal neurons (Najac et al. 2011; Gire et al. 2012). In a monosynaptic connection, axonal glutamate release from the OSN nerve terminals activates AMPA and NMDA receptors in the apical dendrites of MCs and TCs, leading to a short latency and a delayed excitatory response in these postsynaptic neurons (Berkowicz et al. 1994; Ennis et al. 1996; Najac et al. 2011; Gire et al. 2012). OSN synapses generally have a high release

probability that rapidly depresses with increasing number of OSN action potentials (Murphy et al. 2004).

Within the glomerulus, chemical transmission between dendrites of MC – MC, MC – TC and TC – TC pairs mediate lateral excitation (Figure 1.3a, arrows 2; Urban and Sakmann 2002; Hayar et al. 2005; Christie and Westbrook 2006; Pimentel and Margrie 2008). Glutamate released at these dendrites activates both AMPA and NMDA receptors and excitation can be unidirectional or bidirectional (Aroniadou-Anderjaska et al. 1999; Schoppa and Westbrook 2002; Urban and Sakmann 2002; Pimentel and Margrie 2008). Glutamate release from the primary MC and TC dendrites has also been shown to cause recurrent self-excitation, again mediated by AMPA and NMDA receptors (Figure 1.3a, arrow 3; Aroniadou-Anderjaska et al. 1999; Friedman and Strowbridge 2000; Salin et al. 2001).

More recent studies provide evidence that ET cells, rather than MCs, are the primary target of monosynaptic OSN input, providing an intraglomerular feedforward pathway that prominently shapes the response of principal neurons (Hayar et al. 2004a; Najac et al. 2011; Gire et al. 2012). Biphasic excitation of MCs is composed of fast monosynaptic OSN input as well as a slower polysynaptic response that is thought to be mediated by dendritic release from ET cells and other MCs (De Saint Jan et al. 2009; Najac et al. 2011; Gire et al. 2012). Supporting this hypothesis, all ET cells are thought to receive monosynaptic input from OSNs (Hayar et al. 2004a) and ET cell activity can unidirectionally excite MCs (De Saint Jan et al. 2009), suggesting ET cells might play a key role in the amplification and coordination of sensory integration in the glomerulus.

In addition to chemical transmission, MCs and TCs sharing the same glomerulus are known to be coupled via gap junctions (Figure 1.3a, connection 4; Christie and Westbrook 2006; Pimentel and Margrie 2008; Ma and Lowe 2010). Paired recordings from MCs indicated that all MCs within a glomerular circuit might be electrically coupled (Schoppa and Westbrook 2002; Christie and Westbrook 2006; Pimentel and Margrie 2008) and therefore laterally excite and inhibit each other. This property of intraglomerular electrical transmission likely facilitates synchronisation of principal neuron activity.

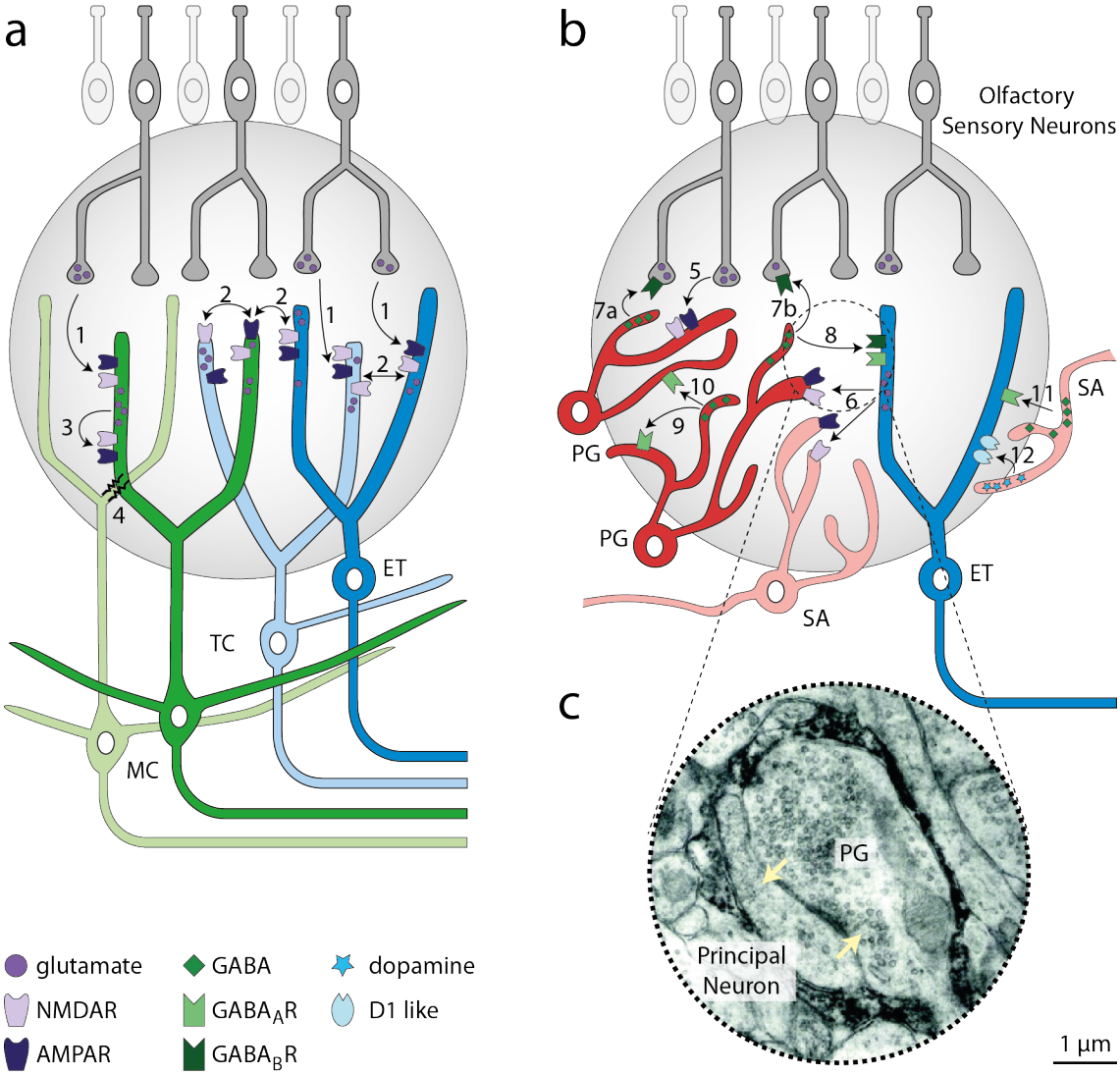

Figure 1.3 Intra- and Interglomerular Connections in the Glomerular Microcircuit

(a) 1. Glutamatergic axo-dendritic transmission onto dendrites of principal neurons. 2. Lateral glutamatergic transmission between principal neuron dendrites. 3. Self-excitation of principal neurons via AMPA and NMDA receptors. 4. Electrical gap junctions between principal neuron apical dendrites.
(b) 5. Glutamatergic axo-dendritic transmission onto interneuron dendrites. 6. Lateral glutamatergic transmission onto interneuron dendrites. 7. Presynaptic GABAergic inhibition of OSN terminals. 8. Lateral GABAergic inhibition of principal neurons. 9. Self-inhibition of interneurons via $GABA_A$ receptors. 10. Lateral GABAergic inhibition between interneurons. 11. Interglomerular GABAergic inhibition of principal cells. 12. Interglomerular dopaminergic transmission from interneurons onto principal cells.
(c) Electron-microscopy picture of a dendro-dendritic synapse between a principal neuron and a PG cell. Arrows indicate direction of transmitter release (adapted from Higashi et al. 2001). AMPAR = AMPA receptor, ET = external tufted cell, GABAR = GABA receptor, MC = mitral cell, NMDAR = NMDA receptor, OSN = olfactory sensory neurons, PG = periglomerular cell, SA = short axon cell, TC = tufted cell.

In general, MCs and TCs exhibit long lasting depolarisations after OSN stimulation (Carlson et al. 2000) that is attenuated by intraglomerular inhibition (Shao et al. 2012).
Both MCs and TCs provide excitatory input to inhibitory interneurons via glutamate release onto AMPA and NMDA receptors at symmetrical, dendro-dendritic synapses with interneurons (Figure 1.3c; Pinching and Powell 1971b; Ribak et al. 1977; Hayar et al. 2005). In close proximity to these glutamatergic synapses, the local inhibitory interneurons release GABA onto $GABA_A$ receptors of MCs and $GABA_A$ and $GABA_B$ receptors of TCs (Aroniadou-Anderjaska et al. 1997; Shepherd 2003; Hayar et al. 2005; Shao et al. 2012), thereby providing the first level of inhibition to the principal neurons.
Only 20-30% of PG cells are thought to receive monosynaptic input from OSNs (Figure 1.3b, arrow 5), but 70-80% receive indirect input via excitatory synapses from ET cells in the same glomerulus (Figure 1.3b, arrows 6; Hayar et al. 2004a; Shao et al. 2009), providing additional evidence for ET cells being the major gatekeepers of glomerular output. Based on their spontaneous and OSN-evoked activity, PG cells can also be physiologically divided into two groups. PG cells receiving input from ET cells exhibit characteristic rhythmical bursts of EPSPs and EPSCs, whereas PG cells monosynaptically connected to OSNs receive invariant, short latency post synaptic potentials following OSN stimulation (Hayar et al. 2004a; Shao et al. 2009).
PG cells have been shown to play a key role in the presynaptic inhibition of OSN terminals, as well as the interglomerular inhibition of principal neurons (Wachowiak and Shipley 2006). In general, PG cells form dendro-axonic synapses back onto OSN terminals (Figure 1.3b, arrow 7a and 7b). At these synapses, monosynaptically or polysynaptically excited PG cells release GABA back onto presynaptic $GABA_B$ receptors located on the OSN terminal (Bonino et al. 1999; Panzanelli et al. 2004), mediating presynaptic inhibition of OSN glutamate release (Aroniadou-Anderjaska et al. 2000; Murphy et al. 2005; Wachowiak et al. 2005; Pirez and Wachowiak 2008).
Furthermore, GABA-mediated presynaptic OSN inhibition by PG cells consists of a feedback and a tonic component (Shao et al. 2009). It has been proposed that feedback inhibition of OSNs is specifically mediated by PG cells receiving monosynaptic OSN input (Figure 1.3b, arrow 7a; Shao et al. 2009). In contrast, the tonic OSN inhibition potentially arises from the spontaneously bursting ET cells, causing enough GABA release at the PG cell dendrites to tonically inhibit OSN terminals within one

glomerulus (Figure 1.3b, arrows 6 and 7b). Potentially, PG cells belonging to both functional groups also form inhibitory connections with MCs, TCs and other PG cells of the same glomerulus (Figure 1.3b, arrow 8; Aungst et al. 2003; Hayar et al. 2005; Murphy et al. 2005; Panzanelli et al. 2007). However, monosynaptically driven PGs might provide inhibition that is more tightly coupled to the sensory input than polysynaptically driven PG cells (Shao et al. 2009).

PG cells also express $GABA_A$ receptors (Laurie et al. 1992) that potentially mediate self-inhibition (Figure 1.3b, arrow 9) as well as lateral inhibition from neighbouring PG cells (Figure 1.3b, arrow 10; Puopolo and Belluzzi 1998b; Smith and Jahr 2002). Since the synapses between dendrites of PG cells and MCs are reciprocal, PG cells are likely to provide GABA-mediated recurrent inhibition onto the MCs that activated them (Aroniadou-Anderjaska et al. 1997; Shepherd 2003). Furthermore, interposed PG cells mediate disynaptic lateral inhibition between MCs (Urban and Sakmann 2002). Similar inhibitory mechanisms have been found between PG cells and ET cells, whereby a single ET cell can excite numerous PG cells within the same glomerulus and PG cells in turn release GABA on the presynaptic ET cell, other ET cells and MCs (Hayar et al. 2005; Shao et al. 2012).

1.4.2.2 Inter-Glomerular Connections

Since SA cell dendrites ramify in three to four glomeruli, they potentially integrate inputs from OSNs expressing different ORs (Aungst et al. 2003; Cleland et al. 2007). Although some SA cells might not be monosynaptically driven by OSNs (Hayar et al. 2004a; Kiyokage et al. 2010), they can receive sensory information via ET cell mediated pathways (Figure 1.3b, arrow 6; Aungst et al. 2003; Hayar et al. 2004a; Cleland et al. 2007; Banerjee et al. 2015). The extensive inter-glomerular projections of SA cell axons can target ET cells and PG cells in glomeruli up to several hundred micrometres away (Aungst et al. 2003; Kiyokage et al. 2010; Liu et al. 2013; Whitesell et al. 2013; Banerjee et al. 2015). This suggests that SA cells, in contrast to PG cells, mediate long-range interglomerular interactions (Kiyokage et al. 2010; Banerjee et al. 2015). The nature and purpose of those interactions is still not entirely clear, but a potential role in centre-surround inhibition (Aungst et al. 2003) and gain control (Banerjee et al. 2015) has been proposed. At least a subpopulation of SA cells co-

expresses tyrosine hydroxylase (TH) and GAD67, but not GAD65 (Aungst et al. 2003; Maher and Westbrook 2008; Kiyokage et al. 2010; Whitesell et al. 2013). A recent study showed the co-release of both GABA and dopamine from SA cells onto $GABA_A$ and D1-like receptors located on ET cells in other glomeruli (Figure 1.3b, arrows 11 and 12; Maher and Westbrook 2008; Liu et al. 2013). Interestingly, the release of the inhibitory transmitters GABA and dopamine can cause a net excitation of ET cells (Liu et al. 2013). High levels of I_h in ET cells can explain ET cell excitation, because I_h causes rebound excitation after GABA-mediated hyperpolarisation (Hayar et al. 2004b; Liu and Shipley 2008a). The rebound depolarisation can trigger bursts of action potentials in ET cells (Liu and Shipley 2008a), which in turn are thought to activate local PG cells mediating intraglomerular inhibition onto OSN terminals, MCs and TCs. Furthermore, it has been shown that the dopamine release from SA cells enhances I_h in ET cells by targeting D1-like receptors, which increases depolarisation and leads to a stronger rebound spike burst (Liu et al. 2013). Thus, while SA cells initially inhibit ET cells using GABA, dopamine-enhanced I_h can mediate a delayed but dominant excitation. Such a bi-phasic, inhibitory-excitatory connection onto ET cells likely impacts the processing in the target glomerular network, but the effect of this phenomenon remains to be fully characterised.

1.4.3 Odour Coding in the Olfactory Bulb

As described above, a single type of odour molecule can bind to several ORs with varying affinity, leading to differential activation of OSN types (Duchamp-Viret et al. 1999; Malnic et al. 1999). Since OSNs that express the same OR subtype converge onto the same glomerulus (Mombaerts et al. 1996), one odour molecule activates several glomeruli (Meister and Bonhoeffer 2001; Wachowiak and Cohen 2003). This produces an odour specific spatial pattern of glomerular activity in the OB (Guthrie and Gall 1995; Johnson et al. 1998; Rubin and Katz 1999; Johnson and Leon 2000; Belluscio and Katz 2001).

Glomeruli activated by structurally similar odours tend to cluster in the OB (Uchida et al. 2000; Mori et al. 2006). Therefore, odour binding often causes activation of co-localised glomeruli, resulting in a chemotopic map of odour representation (Johnson et al. 1998; Rubin and Katz 1999; Belluscio and Katz 2001; Mori et al. 2006). Compared

to other sensory maps, this chemotopy seems to be rather loosely organised with a robust coarse chemotopic layout (Wachowiak and Cohen 2001; Takahashi et al. 2004), but variability in precise glomerulus placement across animals and rodent species (Soucy et al. 2009). Increasing concentrations of an odour molecule also recruit ORs with lower affinities to the particular odour (Malnic et al. 1999; Hamana et al. 2003), leading to widespread glomerular activation and thus concentration-dependent changes in the pattern of glomerular activity (Duchamp-Viret et al. 1999; Meister and Bonhoeffer 2001; Fried et al. 2002; Spors and Grinvald 2002; Vincis et al. 2012). Also, glomeruli that only activate at high odour concentrations tend to be less spatially clustered (Wachowiak and Cohen 2001; Bozza et al. 2004).

OB activity is modulated by the animal's rhythm of breathing (Spors and Grinvald 2002; Buonviso et al. 2003; Cang and Isaacson 2003; Margrie and Schaefer 2003). Rodents sniff at frequencies between 2 and 12 Hz (Welker 1964), odour sampling occurs between 6 and 9 Hz (Kepecs et al. 2007) and glomerular activity maps evolve over time within a single "sniff" cycle (Schaefer and Margrie 2007; Wachowiak 2011). Increasing evidence suggests that odour identity may actually be encoded by the relative timing of spikes within a sniff-cycle (Buonviso et al. 2003; Margrie and Schaefer 2003; Shusterman et al. 2011). Taken together, odour stimuli are most likely represented as spatiotemporal patterns of glomerular activity maps in the OB (Schaefer and Margrie 2007).

This activity map is not only determined by quality, quantity and timing of odour stimuli, but also modulated by the excitatory and inhibitory interconnections of principal neurons and interneurons within the OB (section 1.4.2). The first level of sensory processing in the olfactory system occurs in the glomeruli. Glomerular mono- and polysynaptic microcircuits were proposed to perform fundamental information processing in the form of odour pattern decorrelation (Arevian et al. 2008; Wiechert et al. 2010; Cleland and Linster 2012), stimulus synchronisation (Kashiwadani et al. 1999; Dhawale et al. 2010) and response normalisation (Cleland et al. 2007; Banerjee et al. 2015).

In rodents, olfactory processing in the OB is fast and can occur within less than 200ms (Abraham et al. 2004; Kepecs et al. 2006). Discrimination times are independent of similarity in glomerular representation (Uchida and Mainen 2003). However, for

accurate discrimination of highly similar binary odour mixtures, animals require more time (Abraham et al. 2004). Furthermore, due to OB processing, the initial chemotopic activity pattern caused by an odour stimulus becomes more sparse and odour-specific over time (Yaksi et al. 2007). A potential mechanism for the slightly delayed discrimination of similar odours is pattern decorrelation (Yaksi et al. 2007). Pattern decorrelation is a mechanism occurring in multiple sensory systems to reduce the overlap in neuronal representation in similar sensory stimuli, by inhibitory interconnections between neighbour neurons processing topographically organised sensory information (Wick et al. 2010; Cleland and Linster 2012). Inhibition between neighbouring glomeruli could result in decorrelation of odour representation in the OB, a mechanism potentially mediated by interglomerular connections of SA cells as described in section 1.4.2.2 (Arevian et al. 2008; Wiechert et al. 2010; Banerjee et al. 2015). However, the loose topographic organisation of sensory input in the glomerular layer (Soucy et al. 2009) may require a more complex inhibition mechanism than just lateral inhibition between neighbouring neurons and glomeruli. Pattern decorrelation in the OB might also be a result of intraglomerular non-topographical contrast enhancement (Cleland and Sethupathy 2006) or a selective, non-random interglomerular inhibition, as recently demonstrated across glomeruli of the dorsal OB (Economo et al. 2016).

A notable feature of MCs and TCs is the intra- and interglomerular synchrony of their firing pattern (Kashiwadani et al. 1999; Dhawale et al. 2010). A substantial amount of firing pattern synchronisation in MCs and TCs is caused by the tight coupling of OB activity to the respiration cycle (Margrie and Schaefer 2003; Fukunaga et al. 2012; Gerkin et al. 2013). However, neighbouring MCs and TCs exhibit stronger synchrony in their firing patterns, indicating stimulus correlation must occur on a local scale (Gerkin et al. 2013). This might be due to common synaptic input, but also due to the previously described local connections (section 1.4.2.1): On the level of glomeruli, principal neurons receive feedforward, feedback and lateral excitation from other principal neurons, mediated via gap junctions and dendro-dendritic synapses. Additionally, similar inhibitory mechanisms can be mediated locally via PG cells and, more globally, via SA cells. Furthermore, the spontaneous rhythmic activity of ET cells has been shown to synchronise spontaneous activity of MCs (De Saint Jan et al. 2009). Therefore,

ET cells have been proposed to locally synchronise principal neurons (Hayar et al. 2004b) and to act as a pacemaker within the OB circuit (De Saint Jan et al. 2009).
Normalisation in the OB refers to the equalisation of responses to variable concentrations of sensory stimuli in order to preserve the information about odour identity. The continuous adjustment of sensitivity to input is crucial in order to maintain stable concentration-independent odour-evoked activity (Cleland et al. 2007). The activity of neurons mediating lateral inhibition and lateral excitation between glomeruli as well as the spread of activity have been shown to scale with odour concentration (Banerjee et al. 2015) and therefore been proposed to implement gain control (Zhu et al. 2013; Banerjee et al. 2015).

1.4.4 Plasticity in the Olfactory Bulb

Most brain areas exhibit substantial plasticity during early developmental stages, however the OB appears to maintain plasticity of its neuronal circuits throughout adulthood at nearly all stages of processing, from OSNs to cortex (Mouly and Sullivan 2009; Lledo and Valley 2016). Various early behavioural plasticity studies have already suggested that olfactory learning and memory does occur within the olfactory bulb (Bruce and Parrott 1960; Rosser and Keverne 1985; Wilson et al. 1985; Levy et al. 1990; Kendrick et al. 1992; Brennan and Keverne 1997; Sullivan et al. 2000). Today we know that that olfactory learning and memory via neurons of the olfactory system highly depends on the intrinsic state of these neurons as well as the context of the task and the animal's experience. To perform this task, the olfactory system employs a wide range of plasticity mechanisms, including classic mechanisms affecting the synaptic efficacy, such as long- and short term plasticity, but also adult neurogenesis and experience-dependent apoptosis (Wilson et al. 2004).

1.4.4.1 Hebbian Plasticity Mechanisms in the Olfactory Bulb

Already at the first synapse of the olfactory system, the OSN – MC synapse, paired-pulse depression has been demonstrated, whereby the reduced glutamate release from OSN terminals is mostly caused by $GABA_B$ receptor-mediated inhibition of voltage-gated Ca^{2+} channels (Delaney et al. 2009). The same form of short-term plasticity has been shown at the OSN – PG cell and OSN – TC synapse (Murphy et al. 2004). The

OSN terminals express dopamine D2 receptors and the activation of these receptors can result in reduced transmitter release from the OSN terminals (Wachowiak and Cohen 2001). The level of D2 receptors at the OSNs is dynamically regulated and stimulus depression (for instance through naris occlusion) induces a fast, NMDA receptor-dependent decrease of dopamine receptors, which ultimately increases the gain of this synapse (Wilson and Sullivan 1995; Puche and Shipley 1999). Dopaminergic juxtaglomerular cells may also mediate feedback inhibition onto OSNs through D2 receptors (Shipley and Ennis 1996), however no functional connection has thus far been demonstrated (Maher and Westbrook 2008; McGann 2013). In juxtaglomerular neurons, $GABA_A$ receptor-mediated IPSCs exhibit several patterns of short-term plasticity, including depressing and combined facilitating/depressing patterns (Nusser 2002). Further downstream, the reciprocal MC – GC synapse also exhibits heterogeneous short-term plasticity. Paired-pulse stimulation of the excitatory MC – GC synapse resulted in moderate paired-pulse facilitation, whereas a strong paired-pulse depression can be observed at the inhibitory GC – MC synapse (Dietz and Murthy 2005). This constellation might weaken the auto-inhibition of MCs during strong sensory stimulation. Finally, synapses of the MC axons show short-term depression upon prolonged odour stimulation, a form of plasticity mediated by presynaptic metabotropic glutamate receptors (Best and Wilson 2004). Short-term plasticity occurs in the OB and is thought to be necessary for a quick adaptation to altered odour stimulation, but also for optimisation of sensory processing during the fast odour sampling of animals (Wilson et al. 2004).

The OSN – MC synapse has also been the focus of several long-term plasticity studies. Long-term potentiation of NMDA receptor-dependent spiking after high frequency stimulation of OSNs has been shown at this synapse (Ennis et al. 1998), as well as metabotropic glutamate receptor-dependent long-term depression after brief low-frequency stimulation (Mutoh et al. 2005). It has been suggested that long-term plasticity at this synapse might act as a gain mechanism by shifting the excitation/inhibition homeostasis of the glomerulus, and potentially make previously strongly activated MCs more sensitive to incoming stimuli (Wilson et al. 2004). Interestingly, lateral excitation between MC dendrites has also been shown to be plastic,

with theta burst stimulations causing enhanced or depressed lateral excitation through a unknown presynaptic mechanism (Pimentel and Margrie 2008).

The MC – GC synapse is seen as a key synapse for long-term potentiation and olfactory memory (Satou et al. 2005). In rodents, theta-burst stimulation of the glomerular network mimicking olfactory input at a respiratory rhythm has been demonstrated to elicit long-term depression in the MC – GC synapse (Ma et al. 2012; Chatterjee et al. 2016). However, stimulation with single bursts mimicking a single sniff can cause either long-term potentiation or depression, indicating that long-term potentiation of this synapse requires short bursts of activity (Chatterjee et al. 2016). This very recent study also suggests a NMDA receptor-dependent change in presynaptic release sites underlying this form of long-term plasticity. Since short bursts of activity presumably correspond to new, physiologically relevant sensory inputs, it is conceivable that long-term potentiation at this synapse results in sensitivity for new, weak or distant odours, while at the same time a desensitization occurs for repeatedly presented odours. Also, a study by Brennan et al. (1998) showed that after olfactory learning through a conditioning protocol, rodents exhibit a decrease in the ratio of glutamate to GABA in the OB when presented with the conditioned odour, but not when presented with a novel odour. These experiments show that olfactory learning and memory is at least partly due to a gain function of reciprocal synapses between principal neurons (like MCs) and interneurons (like GCs). To summarise, it appears that a fine balance of short and long-term plasticity at the MC – GC synapse (based on the history of MC activation) is a key determent of the OB output and olfactory memory formation.

1.4.4.2 Adult-Born Interneurons in Local Networks of the Olfactory Bulb

A remarkable plasticity feature of the olfactory system is the continuous renewal of neurons throughout the lifetime of an individual, also termed adult neurogenesis. This form of neurogenesis exists only in two areas of the adult brain, the OB and the dentate gyrus (Lledo et al. 2006). Because of this continuous neurogenesis, OB glomeruli are composed of processes forming some of the most plastic synapses in the brain. Presynaptically, OSNs undergo a continuous activity-dependent turnover and are, on average, replaced every 30 - 60 days (Watt et al. 2004; Lledo and Valley 2016). Postsynaptically, PG cells, SA cells and GCs are generated predominately in the

postnatal period (Altman 1969; Baker et al. 2001; Belluzzi et al. 2003; Carleton et al. 2003; Whitman and Greer 2007). Throughout adulthood, a continuous supply of newly generated interneurons migrate from the subventricular zone through the rostral migratory stream to the OB (Coskun and Luskin 2002), where they differentiate and synaptically integrate into the OB circuitry (Belluzzi et al. 2003; Carleton et al. 2003; Ming and Song 2005; Livneh et al. 2014). This constant circuit remodelling might underpin experience-induced, structural plasticity, which enables the olfactory system to adapt to changing odour environments (Livneh et al. 2014). Most of the newly generated OB interneurons become granule cells (94%) and a small subset develops into JG cells (Altman 1969; Lledo and Valley 2016).

One interesting subpopulation of these adult-born JG cells are TH-expressing interneurons. TH^+ JG cells can be divided into two subpopulations, based on soma size (Halasz et al. 1981; McLean and Shipley 1988), prenatal development (McLean and Shipley 1988) and occurrence of an axon (Chand et al. 2015). Only the smaller, axon-less type of TH^+ JG cells appears to undergo the lifelong continuous turnover (Kosaka and Kosaka 2009). TH expression in these migrating neuroblasts is attenuated by histone deacetylase until the interneurons fully mature in their target layer (Akiba et al. 2010; Banerjee et al. 2013). The integration of these neurons into local glomerular microcircuits has recently been shown to be activity-dependent (Sawada et al. 2011; Bonzano et al. 2014) and sensory input appears to be crucial for the survival of adult-born JG cells (Baker et al. 1983; Bovetti et al. 2009; Sawada et al. 2011). Even in mature neurons (pre-existing and adult-born) the TH expression levels depend on the strength of sensory input and therefore exhibit significant activity-dependent plasticity (Baker et al. 1983; Cigola et al. 1998; Parrish-Aungst et al. 2011; Banerjee et al. 2013).

It has also been shown that GABAergic inhibitory interneurons (PG cells and granule cells) are continuously renewed throughout adult life (De Marchis et al. 2004; Lledo et al. 2008). In contrast to TH, glutamate decarboxylase is already expressed in migrating neuroblasts, and in mature neurons the expression levels of *Gad1* (encoded by the GAD_{67} gene), but not *Gad2* (encoded by the GAD_{65} gene) are regulated via an activity-dependent mechanism (Parrish-Aungst et al. 2011). These differences between TH^+ and $GAD65^+$ neurons strongly suggest that the network of TH^+ neurons, which mediates interglomerular inhibition, might be more plastic and underlies stronger adaptive

regulation by sensory input than the network of $GAD65^+$ interneurons, which mediates intraglomerular inhibition.

1.4.4.3 Homeostatic Plasticity and Hyperpolarisation-Activated Cation Current in the Olfactory Bulb

Homeostatic plasticity is a less well-studied form of plasticity in the OB. The activity-dependent integration and survival of newly born TH^+ (Baker et al. 1983; Bovetti et al. 2009; Sawada et al. 2011; Bonzano et al. 2014) and $GAD65^+$ neurons (Parrish-Aungst et al. 2011), as well as activity-dependent TH expression (Baker et al. 1983; Cigola et al. 1998; Parrish-Aungst et al. 2011; Banerjee et al. 2013), as described in the previous section, can be seen as a form of homeostatic plasticity. Furthermore, naris occlusion experiments in adult rodents have demonstrated homeostatic plasticity mechanisms exist already at the first synapse in the olfactory system. In a study from Tyler et al. (2007), odour deprivation triggered plastic regulation of synaptic strength by increased release probability of glutamate from OSN terminals, as well as increase of glutamate receptors in the glomerular layer. Additionally, the study demonstrated a deprivation-dependent increase in the amplitude of AMPA- and NMDA-dependent quantal synaptic currents. Taken together, homeostatic modulations at the OSN synapse occur pre - and postsynaptically and are at least one mechanism underlying the increased odour sensitivity reported under these experimental conditions (Guthrie et al. 1990; Wilson and Sullivan 1995; Leon 1998).

A recent study from Chand et al. (2015) described homeostatic plasticity of the AIS in a subset of cultured dopaminergic interneurons. Action potentials are usually initiated at the AIS and location and size of the AIS on the axon can have an impact on neuronal excitability (Bender and Trussell 2012). Interestingly, after depolarising the dopaminergic OB interneurons for 24 hours, the AIS were longer and closer to the soma. This effect is unusual in a way since the reverse can be observed in non-GABAergic neurons of the OB and in excitatory neurons of the hippocampus, here the AIS gets shorter and located further distal on the axon after prolonged depolarisation (Grubb and Burrone 2010; Chand et al. 2015). However, since the depolarised dopaminergic interneurons in the study from Chand et al. (2015) only exhibited a trend towards

decreased excitability, the functional implications of this effect are not entirely clear and need further investigation.

As stated above, I_h, mediated by HCN channels, has repeatedly been shown to impact on homeostasis of neuronal activity in various brain areas (section 1.3.3). In the OB, neurons express the HCN channel isoforms HCN1, HCN2 and HCN4, with high expression levels of HCN2 in the glomerular layer (Moosmang et al. 1999; Santoro et al. 2000; Angelo et al. 2012) and high variability of HCN1 expression between juxtaglomerular cells. However, most studies investigating I_h in the olfactory system do not research on potential homeostatic properties of this channel in the OB.

A tonically active I_h has been found in principal and interneurons of the OB (Cadetti and Belluzzi 2001; Hayar et al. 2004b; Angelo and Margrie 2011). ET cells exhibit substantial hyperpolarisation-evoked sag and therefore I_h (Hayar et al. 2004b; Liu and Shipley 2008a; Liu and Shipley 2008b). I_h plays a key role in pacemaking in many auto-rhythmic neurons (Wahl-Schott and Biel 2009) and also contributes to the intrinsic neuronal oscillations of ET cells (Liu and Shipley 2008b) and the generation of spontaneous rhythmical bursts of action potentials (Hayar et al. 2004b). Furthermore, the current has been proposed to play a key role in synchronising ET cells and shaping interglomerular inhibition of postsynaptic principal neurons by reducing EPSP durations in ET cells (Liu and Shipley 2008a). Little is known about the functional relevance of I_h in inhibitory glomerular interneurons. In visually identified PG cells, a small I_h (around 10pA) has been described and is suspected to influence slow oscillatory network rhythms (Cadetti and Belluzzi 2001). The same group also identified a small, tonically active I_h in TH^+ interneurons, which had an influence on their RMP, but could not be shown to impact on any pacemaking activity (Pignatelli et al. 2013). Except for these two specific interneuron types, the expression levels of the I_h across different classes of glomerular interneurons have not yet been systematically described and the underlying function of the small I_h levels in these cells remains elusive. Since PG and SA cells can have high input resistances (Puopolo and Belluzzi 1998a; Hayar et al. 2004a; Shao et al. 2009), even a modest amount of the I_h could have a substantial impact on the neuron's integrative properties (Cadetti and Belluzzi 2001).

Interestingly, in MCs I_h has been shown to substantially influence the cells' computational properties (Angelo and Margrie 2011). Furthermore, the level of I_h has

been shown to depend on a MC's affiliation to a glomerular network and this dependence has been proposed to function as an activity-dependent gain control mechanism, specific for each glomerular micro-circuit (Angelo et al. 2012). Such a homeostatic mechanism might also serve to homogenise the output of principal neurons receiving the same sensory stimuli.

Based on these results from experiments in MCs, this thesis aims to quantify I_h-mediated sag in at least two types of JG cells with a view to understanding its cellular function and its relation (if any) to the history of activity within neurons affiliated to a microcircuit of the glomerular layer. By combining morphological reconstructions with simultaneous recordings, the extent to which I_h-mediated sag relates to glomerular membership and synaptic activity will be assessed.

1.5 Hypothesis and Aim of My Project

Several recent papers have highlighted the importance of within-class biophysical heterogeneity to brain function (Altschuler and Wu 2010; Paszek et al. 2010; Pelkmans 2012). These studies suggest that analysis of the bulk or average properties of large populations of cells may mask the complexity of real cell populations or tissues and may lead to difficulty in addressing complex functional questions concerning the modulation of biophysical properties.

My project focuses on understanding the diversity in expression of I_h in interneuronal circuits in the glomerular layer. Specifically, I aimed to:

1: Quantify the diversity of membrane potential sag (I_h) expression within and between two chemically defined classes of JG cells.

2: Establish whether the amount of membrane potential sag (I_h) within specific inhibitory types of JG cells is dependent on the affiliation of individual neurons to local microcircuits.

3: Assess the extent to which membrane potential sag (I_h) in different classes of JG cells is dependent on odour experience.

Chapter 2. Materials & Methods

2.1 Mouse Lines

All animals were maintained on 12h:12h light/dark cycle with free access to food and water. All experiments were carried out on acute brain slices of transgenic male and female mice (three to seven weeks old), expressing a red fluorescent protein under the control of the promoter for either glutamic acid decarboxylase (Gad2-IRES-Cre-tdTomato) or tyrosine hydroxylase (TH(9.0)tagRFP; Table 2-1). Fluorescent neurons recorded in these two mouse lines are from now on referred to as $GAD65^+$ and TH^+ neurons. $GAD65^+$ and TH^+ neurons exhibited morphologies (section 3.2.3) and electrophysiological properties (section 3.2.4) similar to previously published data.

Table 2-1 List of Genetically Modified Mouse Lines

Name	Type	Promoter	Fluorophore	Source
Gad2-IRES-Cre-tdTomato	Targeted knock-in	Gad2	tdTomato	Cross of lines from Jackson Laboratory
TH(9.0)tagRFP	Random insertion transgenic	TH(9.0kb)	tagRFP	Molly Strom, SWC
M72-IRES-ChR2-YFP	Targeted knock-in	Olfr160	EYFP	Jackson Laboratory

2.1.1 Gad2-IRES-Cre-tdTomato

For fluorescent labelling of a subset of GABAergic neurons, a cross between a Gad2-IRES-Cre knock-in mouse line ($Gad2^{tm2(cre)Zjh}$/J, stock no.: 010802, The Jackson Laboratory) and the tdTomato reporter line Ai14 (B6.Cg-Gt(ROSA)26Sor$^{tm14(CAG-tdTomato)Hze}$/J, stock no: 007914, The Jackson Laboratory) was established.

The neurotransmitter γ−aminobutyrate (GABA) is synthesised from L-glutamic acid by two isoforms of the enzyme glutamic acid decarboxylase (GAD), GAD_{67} and GAD_{65}, encoded by two genes, Gad1 and Gad2 respectively. The Gad2-IRES-Cre line, targets GABAergic neurons via the Cre/loxP binary gene expression system (Sternberg and Hamilton 1981; Dymecki and Kim 2007) and was initially produced and published by Taniguchi et al. (2011). The co-expression of Cre with Gad2, has a 92.2 % specificity in

the neocortex and the line targets "most or all GABA neurons" in the olfactory bulb (OB), based on visual observation (Taniguchi et al. 2011). GABAergic interneurons in the OB are known to undergo continuous turnover throughout development and adult life (De Marchis et al. 2004; Lledo et al. 2008) and migrating neuroblasts express GAD_{65} protein before reaching their destination (De Marchis et al. 2004).

On average, Gad2-IRES-Cre animals discriminated two odours in a go/no go operant conditioning task equally well compared to wild type animals. They reached criterion (first block when an animal reaches at least 80% discrimination accuracy for five blocks consecutively) on average after 11.4 ± 6.5 blocks (n = 5), with each block being ten S+ and ten S- presentations. This learning duration was not significantly different from wild type animals (8.9 ± 3.6, n = 9, p = 0.363, t-test; unpublished data, Edward Bracey).

2.1.2 TH(9.0)tagRFP

Transgenic mice were generated according to a previously published protocol (Min et al. 1994) resulting in the expression of tagRFP under the control of rat tyrosine hydroxylase (TH) promoter (9.0kb). Transgenic animals crossed to C57BL/6 animals exhibited normal breeding behaviour, with 51% of the offspring being transgenic ($n_{transgenic}$ = 99 vs. $n_{non\text{-}transgenic}$ = 97) and a normal male/female ratio (n_{male} = 92 vs. n_{female} = 104).

TH is the rate-limiting enzyme in the biosynthesis of the catecholamine neurotransmitters dopamine, norepinephrine, and epinephrine. The expression of a fluorescent marker molecule from the TH promoter results in the labelling of dopaminergic cells in the OB, which are nearly exclusively located in the glomerular layer (Jaffe and Cuello 1980; Nadi et al. 1981). TH expression has been shown to be activity-dependent, decreasing with sensory deprivation (Baker et al. 1983; Cigola et al. 1998; Parrish-Aungst et al. 2011; Banerjee et al. 2013) and is attenuated by histone deacetylase enzymes in migrating neuroblasts until the interneurons fully mature in their target layer (Akiba et al. 2010).

2.1.3 M72-IRES-ChR2-YFP

M72-IRES-ChR2-YFP knock-in mice ($Olfr160^{tm1.1(COP4*/EYFP)Tboz}$/J, stock no: 021206, The Jackson Laboratory) express a ChR2(H134R)-EYFP fusion gene from the locus of the olfactory receptor 160. The H134R substitution is a gain-of-function mutation,

which enhances the photocurrent. The axons of each olfactory sensory neuron (OSN) expressing the odour receptor 160 (OR160) project onto one of the two M72 glomeruli, which are located medial and lateral on the dorsal surface of both OBs. Since the ChR2-YFP expression is specific to OSNs projecting to the M72 glomeruli, it is possible to evoke activity in neurons connected to a single glomerular network by stimulation with blue light (450-490 nm). To identify and record from GABAergic and dopaminergic neurons affiliated to the M72 network, M72-IRES-ChR2-YFP mice were crossed with animals from either the TH(9.0)tagRFP or the Gad2-IRES-Cre-tdTomato mouse line. In these crosses, the M72 glomerulus is fluorescently labelled with enhanced yellow fluorescent protein (EYFP) and a subset of interneurons express either tdTomato or tagRFP (Figure 2.1).

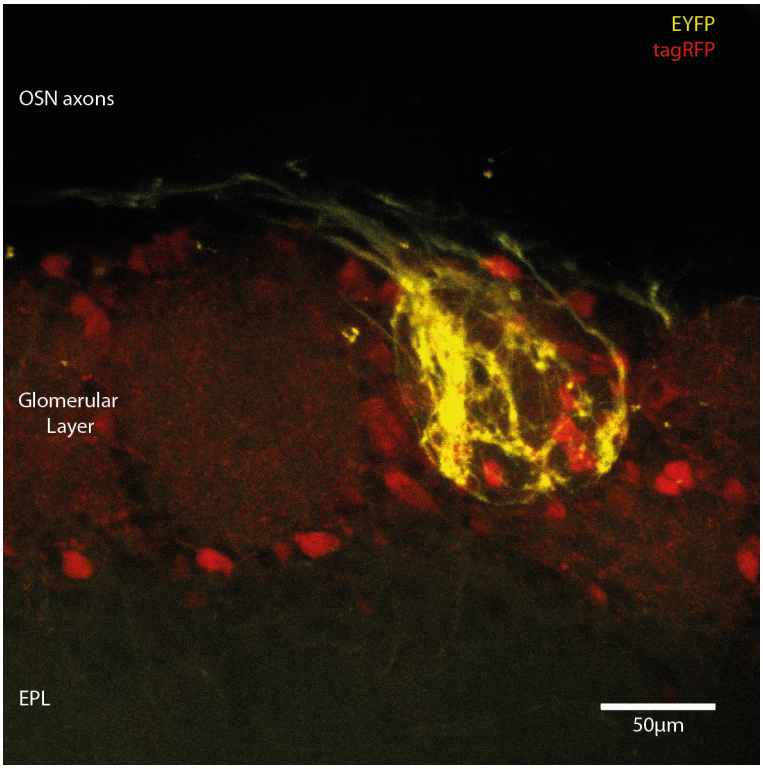

Figure 2.1 Confocal Image of an M72 Glomerulus in a TH(9.0)tagRFP Animal

A cross between M72-IRES-ChR2-YFP and TH(9.0)tagRFP animals result in fluorescent labelling of the M72 glomerulus and dopaminergic interneurons in the glomerular layer. *Yellow channel:* Axons of OSNs expressing a ChR2-EYFP fusion gene converge onto the M72 glomerulus. *Red channel:* tagRFP labelled TH^{+} interneurons, surrounding the glomeruli in the glomerular layer. Maximum projection, 40x objective. EPL = external plexiform layer, OSN = olfactory sensory neurons.

2.2 Quantification of Genetic Labelling Specificity Using Immunohistochemistry

For assessing the specificity of genetic labelling in TH(9.0)tagRFP mice, animals were terminally anesthetised via intraperitoneal application of ketamine (200-300 mg/kg; Vetalar®, Zoetis) and xylazine (20-30 mg/kg; Rompun® 2 %, Bayer) and transcardially perfused with phosphate-buffered saline (PBS), followed by 4 % paraformaldehyde (PFA) in ddH_2O. The dissected brains were post-fixed in 4 % PFA overnight at 4°C and embedded in 3 % Agarose. The OBs were cut in serial horizontal sections of 50 µm thickness using a vibratome (HM 650 V, Microm International GmbH). After two hours of permeabilization with 0.1 % Triton X-100 and 5 % normal goat serum in PBS, the sections were stained with anti-TH antibody (1:1000 dilution with 0.1 % Triton X-100 and 0.5 % normal goat serum, overnight at room temperature (RT), rabbit anti-tyrosine hydroxylase, Pelfreez) or anti-Gad2 antibody (1:50 dilution, overnight at 4°C, GAD2 (D5G2) XP® Rabbit mAb, Cell Signalling) as primary and goat anti rabbit 488 (1:500 dilution, for two hours at RT, Goat anti-Rabbit IgG (H+L) Alexa Fluor® 488, Life Technologies) as secondary antibody. For easier identification of cells and cell layers, all sections were additionally stained with 4',6-diamidino-2-phenylindole (DAPI; 1:10000 dilution, 10 min at RT, Santa Cruz Biotechnology). Sections were mounted in Mowiol and imaged with a Leica SP5 microscope (Leica Microsystems) and a 40x/1.25 oil objective (HCX PL APO lambda blue, Leica Microsystems).
To analyse the specificity of cell labelling, red and green fluorescent cells were counted in subregions of the glomerular layer with the Cell Counter Image J plugin (https://imagej.nih.gov/ij/plugins/cell-counter.html, Kurt De Vos, University of Sheffield).

2.3 *In vitro* Electrophysiological Recordings

2.3.1 Solutions for Electrophysiological Recordings

2.3.1.1 External Solutions

All extracellular solutions were prepared from a stock solution on the day of the experiment. The stock solution was freshly made every week and kept at 4°C. External solutions had a final osmolality of 305-310 mOsm, which was measured with a vapour

osmometer (Vapro 5520, Wecor). All solutions were perfused with 95 % O_2 and 5 % CO_2 and contained (in mM):

- *Slicing solution* (high $MgCl_2$, low $CaCl_2$): 125 NaCl, 26 $NaHCO_3$, 25 D-glucose, 2.5 KCl, 2 $MgCl_2$, 1.5 NaH_2PO_4, 1 $CaCl_2$ and 0.5 ascorbic acid
- *External recording solution* (low $MgCl_2$, high $CaCl_2$): 125 NaCl, 26 $NaHCO_3$, 25 D-glucose, 2.5 KCl, 2 $CaCl_2$, 1.25 NaH_2PO_4, 1 $MgCl_2$ and 0.5 ascorbic acid
- *Synaptic blocker cocktail* 125 NaCl, 26 $NaHCO_3$, 25 D-glucose, 2.5 KCl, 2 $MgCl_2$, 1.25 NaH_2PO_4, 1 $CaCl_2$ and 0.5 ascorbic acid, 0.05 D-AP5, 0.05 picrotoxin and 0.01 NBQX
- S*ynaptic and ion channel blocker cocktail* for voltage-clamp recordings (without NaH_2PO_4 and $CaCl_2$): 105 NaCl, 26 $NaHCO_3$, 20 D-glucose, 12.5 KCl, 10 TEA-Cl, 5 4-AP, 1 $MgCl_2$, 1 $CoCl_2$, 1 $BaCl_2$, 0.05 D-AP5, 0.05 picrotoxin, 0.01 NBQX and 0.001 TTX
- S*ynaptic and ion channel blocker cocktail + ZD7288*: *Synaptic and ion channel blocker cocktail* (see above) + 0.04 ZD7288

2.3.1.2 Internal Solution

A double concentrated internal solution was prepared, adjusted with KOH to pH 7.28 ± 0.1 and filtered with a 0.2 µm syringe filter. This stock solution was split into 200 µl aliquots and frozen at -20°C. Similarly, a 1 % (w/v) biocytin stock solution in ddH_2O and a 2 mM Alexa Fluor® 488 stock solution in ddH_2O were prepared, filtered and frozen in aliquots at -20°C.
On the day of the experiment the internal stock solution was diluted with the biocytin and Alexa Fluor® 488 stock solution to an *internal solution* containing (in mM):

- 10 KMeSO3, 6 NaCl, 3 MgCl2, 40 HEPES, 2 Na2-ATP, 2 Mg-ATP, 0.5 Na2-GTP, 0.05 EGTA, 0.02 CaCl2, 0.05 Alexa Fluor® 488 and 0.5% biocytin

The solution was filtered with a 0.2 µm centrifugal filter and had a final osmolality of 286 ± 4 mOsm.

2.3.2 Preparation of Acute Olfactory Bulb Brain Slices

All procedures were performed in compliance with Home Office regulations and in accordance with the project and personal license. Animals were killed via cervical dislocation and decapitation; the skin was cut from neck to nose and pulled to both sides to expose the skull. The occipital, interparietal and parietal parts of the skull were carefully cut with scissors (Iris scissors ToughCut, F.S.T.) up to the coronal suture. In most cases this resulted in a cracking of the skull along the midline of the frontal area up to the nasal bone without any damage of the OBs underneath. Next, the skull was cut laterally along both sides from posterior to anterior up to the eye socket. To avoid any damage to the OBs, the skull was not cut in the area of the eye socket, but a spring scissor (Student Vannas Spring Scissors, F.S.T.) was carefully inserted into the optic canal. Then a final cut was made towards the front of the nasal bone allowing removal of the dorsal part of the skull with a fine pair of forceps. The brain was then cut with a scalpel blade inside the remaining skull along the medial-lateral axis, leaving roughly 2 mm of the forebrain attached to the OBs. After removing the posterior parts of cortex and the cerebellum, the OBs were transferred into ice cold *slicing solution*. The OBs were then removed from the *slicing solution*, dried with a filter paper and glued on a metal tissue holder using cyanoacrylate. 350 µm thick horizontal or coronal (for M72 glomerulus experiments) sections of mouse OB were obtained in ice-cold *slicing solution* using a vibratome (Leica VT1200 S, Leica Biosystems, 0.16 mm/s, 1.0 mm amplitude). All brains were cut from anterior to posterior (horizontal sections) or dorsal to ventral (coronal sections). Subsequently, the OB slices were separated with a scalpel blade into the two individual OBs, incubated in continuously perfused *slicing solution* for 30 - 35 minutes at 36°C and then left to equilibrate at RT in the same solution. The process from cervical dislocation to incubation of the slices at 36°C was normally completed within 8 to 12 minutes.

2.3.3 Visualisation of Genetically Labelled Neurons

For electrophysiological recordings, individual slices were transferred to a custom-made chamber which was continuously perfused with *external recording solution* at a flow rate of 2.5 - 3 ml/min at 35 ± 1.5°C (heater with integrated temperature sensor, Sigmann Elektronik GmbH). To provide mechanical stability for electrophysiological recordings,

brain slices were fixed in the chamber with a custom made platinum harp. A Zeiss Axio Examiner microscope with a 10x (W N-Achroplan 10x/0.3, Zeiss) and 40x water immersion objective (W Plan-Apochromat 40x/1.0 DIC, Zeiss) was used in infrared differential interference contrast mode to visualise the slices. For electrophysiological recordings, $GAD65^+$ and TH^+ neurons were chosen based on the location of their soma within the glomerular layer and the expression of red fluorescent protein (RFP), visualised with a RFP filter set (Zeiss filter set 64 HE; excitation: BP 587/25; emission: BP 647/70, beam splitter: FT 605).

In order to confirm the successful targeting of a neuron, all cells were filled with Alexa Fluor® 488 during the recording and were visualised with a GFP filter set (Zeiss filter set 38 HE, Zeiss; excitation: BP 470/40; emission: BP 525/50, beam splitter: FT 495) or, in channelrhodopsin experiments, a YFP filter set (excitation: 510/10; emission: 542/27, beam splitter: HP 520).

2.3.4 Whole-Cell Recordings and Data Acquisition

Whole-cell recordings were carried out under controlled temperature conditions at 35 ± 1.5°C. Electrodes were prepared from borosilicate glass capillaries (outer diameter: 2.0 mm, inner diameter 1.5 mm, Hilgenberg) using a DMZ-Universal-Puller (Zeitz Instruments). Pipettes were pulled to a tip diameter of 1 - 2 µm with a resistance of 4-8 MΩ when filled with *internal solution* while dipped in recording solution. Pipettes were mounted in pipette holders (DB-S Electrode Holder, G23 Instruments UCL) attached to headstages (CV-7B Cat I, Channel A and B, Axon Instruments), which could be moved independently via two manipulators (LN Junior RE/LE (3 axes), Luigs & Neumann).

Recordings were performed using a dual channel Multiclamp 700B amplifier (Axon Instruments) and visualised online with an analog/digital oscilloscope (HM507, Hameg Instruments). Starting in voltage-clamp mode, a test square pulse of 10 mV (at 100 Hz and 0 mV holding potential) was applied and the pipettes were lowered into the bath and visualised under the 40x objective. Both pipettes were placed above the OB slice and then moved towards their target cells one pipette at a time while applying strong positive pressure. Several µm before reaching the target neuron with the first pipette the pressure on this pipette was reduced and the process was repeated with the second pipette. Once both pipettes were placed closely above their target neurons the pipette

offsets were adjusted and each pipette was positioned next to the target neuron, so that the positive pressure created a dimple in the membrane of the neurons. Rapid release of positive pressure and gentle application of negative pressure resulted in formation of a gigaseal (series resistance > 1 GΩ).

At a holding potential of -75 mV, the test square pulse was increased to -40 mV at 100 Hz and the fast capacitive current transients of the pipette were compensated with the automatic pipette capacitance compensation mode. Electrical access to the neurons was gained one cell at a time by application of an increasing negative pressure until the neuron's membrane ruptured, as indicated by a sudden, slow capacitive transient. Shortly after breaking into a neuron, gentle positive pressure was applied and the pipette was slowly pulled back by 1 - 2 µm, which often improved the access resistance to the neuron.

Current-clamp recordings were filtered at 6 kHz using a low pass Bessel filter. For adjusting the pipette capacitance compensation and bridge balance, a tuning pulse of -100 pA at 100 Hz was briefly injected into the neuron. Series resistance and resting membrane potential (RMP) were regularly monitored throughout the recording. All recordings with a series resistance larger than 20 MΩ, a RMP outside the range of -48 mV to -75 mV or a RMP change bigger than 10 mV were not used for any analysis.

For voltage-clamp recordings, currents were filtered at 2 kHz and series resistance errors were compensated online by 40 - 50 %. The membrane voltage was not corrected for the liquid junction potential.

Data was digitised at 20 kHz using an ITC-18 A-D interface (InstruTECH, Heka Elektronik). A 'HumBug' line noise eliminator (Quest Scientific) was interposed to filter 50Hz electrical noise. For data acquisition, the Neuromatic package (v2.00, J. Rothman, http://www.neuromatic.thinkrandom.com/) was used with Igor Pro 6.34A software (Wavemetrics).

2.3.5 Pharmacology

In all experiments using the *synaptic blocker cocktail* or the *synaptic and ion channel blocker cocktail*, whole-cell access was established as described in Section 2.3.4 while the slice was perfused with normal *external recording solution*. If more than one blocker cocktail was applied during an experiment (for example *synaptic and ion channel blocker cocktail* followed by *synaptic and ion channel blocker cocktail* +

ZD7288), each cocktail was introduced through separate tubing, which were joined together in a Teflon manifold (MP-3 chamber manifold, Warner Instruments) directly before the heater element. In order to guarantee a similar flow rate (2.5 - 3 ml/min), all solutions were perfused using the same peristaltic pump (Minipulse 2, Gilson). The bath was perfused with each pharmacological solution for a minimum of five minutes before any recordings of the sag potential amplitude (SPA) or I_h were made. Between two different recordings the empty recording chamber was washed for at least 15 minutes with external recording solution.

2.3.6 Stimulus Protocols

2.3.6.1 Current-Clamp

Dependent on the current-clamp experiment, each cell was subjected to one or several different stimulus protocols. The parameters of the stimulus protocols are listed in Table 2-2. When two neurons were recorded simultaneously, current injections were alternated between the two cells and never applied simultaneously. Generally, the *I-V protocol* was applied shortly after breaking into a neuron, followed by varying numbers of repetitions of the *hyperpolarisation step protocol* (Figure 2.2). Due to the dilution of second messengers in the whole-cell configuration and the sensitivity of hyperpolarisation-activated cyclic nucleotide-gated (HCN) channels to these second messengers, the SPA of neurons decreases over the time course of a recording (DiFrancesco et al. 1986; Wahl-Schott and Biel 2009). It was therefore the aim to complete any SPA recording within five minutes after establishing whole-cell access to a neuron. The *hyperpolarisation step protocol* was followed by a brief passive recording of the membrane potential without any current injection and, depending on the experiment, either a *depolarisation step* (to test for gap junctions) or *ChR2 stim protocol* (to test for connectivity to the M72 glomerulus).

2.3.6.2 Voltage-Clamp

A single *VC-I_h protocol* was used in all voltage-clamp experiments. During the protocol the neurons were held at -55 mV and hyperpolarised to -105 mV for 2000 ms (Figure 2.3a). The hyperpolarisation was repeated five times with an inter-stimulus-interval of 1000 ms. The *VC-I_h protocol* was first applied to a neuron perfused with normal

Table 2-2 Properties of Stimulus Protocols

Protocol / Property	*I-V*	*Hyperpolarisation step*	*Depolarisation step*	*ChR2 stim*
Target membrane potential [mV]	-	53.5 ± 4.5	-70 ± 2	-70 ± 2
Start current step [pA]	-70	variable	variable	-
End current step [pA]	+130	variable	variable	-
No. of steps	20	3	1	-
Step increments [pA]	10	5	-	-
Stimulus length [ms]	250	500	2	2
Inter stim interval [ms]	750	800	1125	1000
Stimulus repeats	1	5	40	20 or 50

extracellular solution, followed by one or several recordings in *synaptic and ion channel blocker cocktail* and *synaptic and ion channel blocker cocktail + ZD7288* (see section 2.3.1.1).

2.4 Analysis of Electrophysiological Data

Data analysis was performed in MATLAB (Version R2015b, MathWorks).

2.4.1 Quantification of Sag Potential Amplitude

In current-clamp recordings the SPA was determined by maintaining the membrane potential with constant current injection at 53.5 ± 4.5 mV and repeatedly hyperpolarising the neuron for 500 ms with three negative current steps at -5 mV increments (see *hyperpolarisation step protocol* Table 2-2 and Figure 2.2). The amplitudes of the injected current steps were adjusted for each neuron to reach a steady-state membrane potential of -95 ± 5 mV (Figure 2.2, lower grey dashed box). All recordings with an initial membrane potential or steady-state membrane potential outside the given ranges were discarded. The SPA was quantified as the difference between the minimum peak membrane potential recorded at the first 250 ms of the hyperpolarisation step and the average steady-state voltage recorded during the last 100 ms of the current step injection (Figure 2.2, blue bars and black arrow).

For simultaneous whole-cell current-clamp recordings of two neurons, SPAs were recorded separately in each neuron. Otherwise, stimulation protocol and analysis criteria were identical to those used in single whole-cell current-clamp recordings.

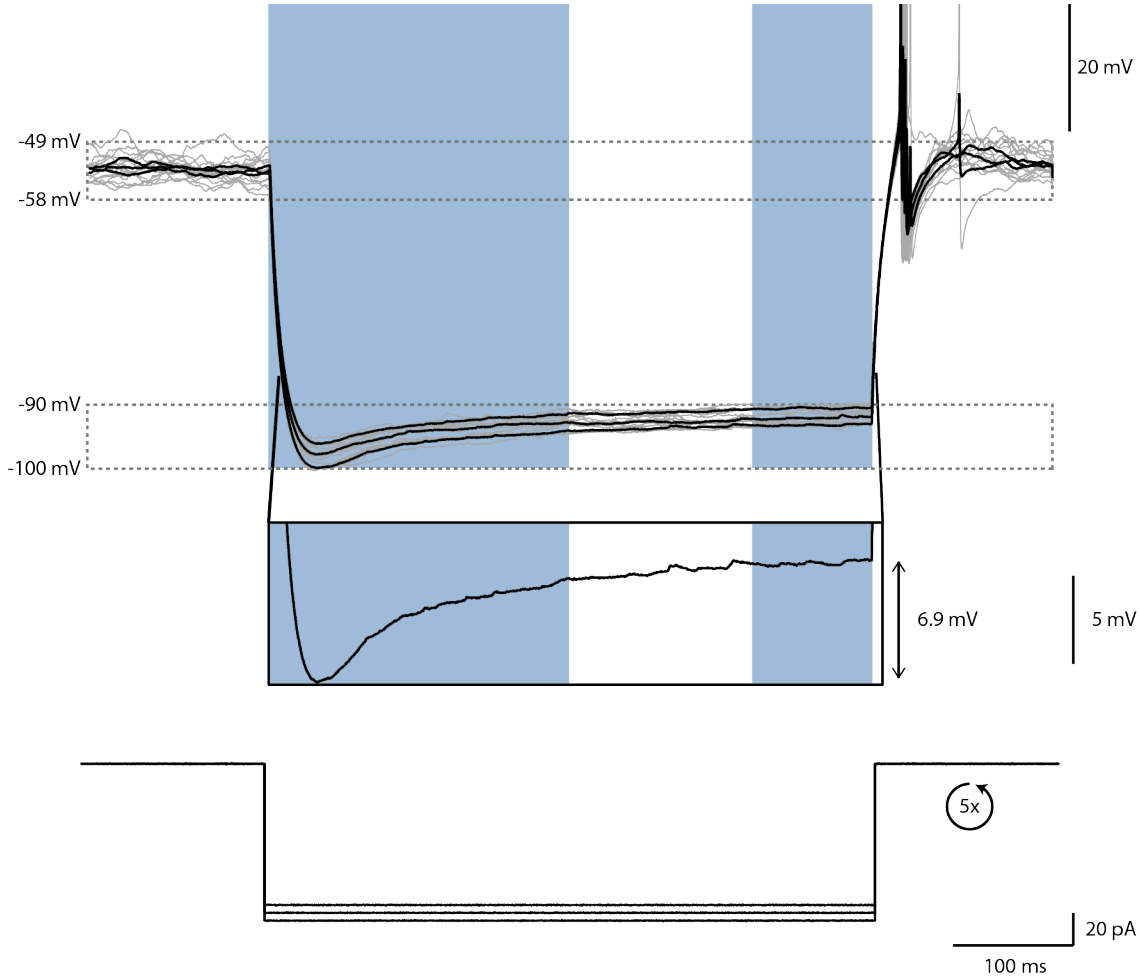

Figure 2.2 Recording and Calculation of Sag Potential Amplitude

Example of hyperpolarisation-induced SPA in a GAD65^{+} neuron. The neuron was hyperpolarised five times with three different current steps (5 pA increment, *bottom*). Black membrane voltage traces displayed *(top)* are the average of five repetitions *(grey traces)*. The membrane potential was held at -53.5 ± 4.5 mV *(upper grey dashed box*) and the injected current steps were adjusted for the neuron to reach a steady-state membrane potential at the end of the current step of -95 ± 5 mV *(lower grey dashed box)*. Only recording traces within these ranges were used to calculate the SPA. Insert shows a magnification of the neurons membrane potential in response to the most hyperpolarising current injection. The SPA *(black arrow)* was calculated as the difference between the minimum peak voltage potential in the first 250 ms of the hyperpolarisation step *(left blue box)* and the average steady-state voltage recorded during the last 100 ms of the current step *(right blue box)*.

2.4.2 Quantification of Hyperpolarisation-Activated Cation Current

To quantify the amplitude of the hyperpolarisation-activated current (I_h) in voltage-clamp recordings, a hyperpolarising voltage step from -55 mV to -105 mV was applied five times for 2000 ms in the presence of *synaptic and ion channel blocker cocktail* (*VC-I_h protocol*; Figure 2.3a, black trace). Afterwards the *VC-I_h protocol* was repeated in the presence of *synaptic and ion channel blocker cocktail + ZD7288* (Figure 2.3a, blue trace). ZD7288 acts as a selective blocker of HCN channels, whereby the block is time and concentration dependent with a half maximum blocking concentration of 0.02 mM (Harris and Constanti 1995). It has been suggested to allow for a perfusion time of 10 - 15 minutes before any electrophysiological recording (Harris and Constanti 1995). However, with a concentration of 0.04 mM no further change in the I_h block was observed after five minutes of perfusion. As the *synaptic and ion channel blocker* solution had a detrimental impact on recording quality, recordings of I_h or SPA were started after five minutes of blocker perfusion. The I_h amplitude was determined by post-hoc digital subtraction of the mean currents at -105 mV, recorded in the absence and presence of ZD7288 (Figure 2.3b). In the resulting trace the difference between the last 140 ms of the hyperpolarising step and the last 300 ms after the end of the current step was defined as the I_h amplitude.

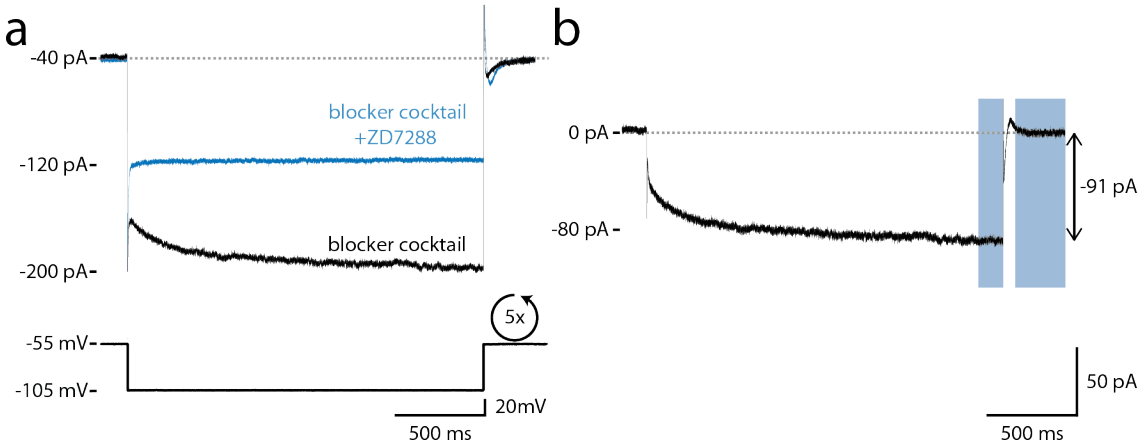

Figure 2.3 Pharmacological Isolation and Determination of I_h Amplitude

(a) Voltage-clamp recordings of a neuron perfused with *synaptic and ion channel blocker solution* in black and the recording of the same neuron perfused with *synaptic and ion channel blocker solution+ZD7288* in blue. Current traces *(top)* are the average response to five consecutive hyperpolarising (55mV to -105 mV) current steps *(bottom)*. **(b)** I_h amplitude of the neuron in (a), determined by subtracting the blue current trace under ZD7288 block from the black trace recorded in *synaptic and ion channel blocker* isolation cocktail. The amplitude *(black arrow)* was calculated as the mean difference

between the last 140 ms during the hyperpolarising step and the last 300 ms after the end of the hyperpolarising step *(blue bars)*.

2.4.3 Quantification of Other Biophysical Properties

By analysing the responses of each neuron to the *I-V protocol* (Table 2-2), biophysical parameters could be compared between $GAD65^+$ and TH^+ neurons.

Action Potential Detection and Action Potential Clipping

The action potential detection algorithm was written by Alexander Brown in MATLAB. This algorithm detects local peaks in the first derivative of a voltage trace, whereby a peak is defined as a change larger than five times the standard deviation of a baseline measure. For the baseline, the 10^{th} to 90^{th} percentile of the first 100ms of a recording were averaged. For the analysis of input resistance and RMP all action potentials in the recording traces were clipped by deleting the data points in a range of 1 ms before to 10 ms after the detected event and interpolating between the remaining points.

The spiking threshold was defined as the membrane potential at the peak of the second derivative in a 4 ms window before the detected spike. The spiking threshold was measured and averaged from all action potentials, occurring during the step of the *I-V protocol* (Table 2-2) where the first action potential was detected.

Detection of Excitatory Post-Synaptic Potentials

All single and coincident excitatory post-synaptic potential (EPSP) detection was conducted with the Igor Pro plugin "SpAcAn" (http://www.spacan.net/). The plugin uses a modified threshold-crossing detection algorithm (Vincent and Marty 1993; Dugue et al. 2005). The algorithm detects when the difference between two rolling averages exceeds a set threshold. EPSPs were considered to occur coincidentally when the onset of two events was less than 2ms apart.

Input Resistance

Input resistance was calculated by fitting a linear function to the mean voltage responses of a neuron to current injections of 0 pA, -10pA and -20pA during the last 50 ms of the hyperpolarising steps in the *I-V protocol* (Table 2-2).

Resting Membrane Potential

The RMP was determined from the mean membrane potential of a neuron during the zero current step condition (*I-V protocol*, Table 2-2).

2.4.4 Analysis of Membrane Voltage in Simultaneous Recordings

Simultaneous recordings were performed in neurons with somata located directly next to each other if possible, but never more than the equivalent of one glomerulus apart (approximately 50 μm). For correlating the spontaneous synaptic activity in simultaneously recorded neurons, the membrane potential in each neuron was kept at -70 ± 2 mV using constant current injection. The spontaneous synaptic activity was recorded and a continuous cross-correlation with a ± 1000 ms lag was performed ("xCorr" function, MATLAB). This algorithm normalises the trace before correlation. The peak value was calculated in the resulting cross-correlogram as the difference between the highest point at 0 ± 5 ms and a baseline measure. The baseline measure was taken between -1000 ms to -500 ms and 500 ms to 1000 ms. The significance of the correlated activity was tested by comparing simultaneously recorded neurons to 'pseudo pairs'. Pseudo pairs were generated by systematically assigning two neurons from the dataset of simultaneous recordings such that all possible combinations (except for the original simultaneously recorded 'pairs') were represented. A simultaneously recorded pair of neurons was considered to be 'synchronised' when its cross-correlation value was larger than the highest pseudo pair cross-correlation value of each chemotype. A nonparametric test was performed to determine whether SPAs were more similar in synchronised simultaneously recorded neurons versus pseudo pairs from the same dataset.

2.4.5 Identification and Exclusion of External Tufted Cells

As shown by Tatti et al. 2014, the population of GABAergic interneurons in the glomerular layer not only consists of inhibitory interneurons, but also contains a small population of excitatory, glutamatergic external tufted (ET) cells, that co-express GABA. ET cells have comparably low input resistances (161 MΩ (55-490), n = 59), RMPs at -56.8 ± 6.2 mV (n = 59) and large SPAs (23.2 ± 10.6 mV, n = 59; Hayar et al. 2004a), as well as characteristic intrinsic bursting (McQuiston and Katz 2001; Hayar et al. 2004a). An intrinsic burst is composed of a characteristic cluster of two or more action potentials on top of a slow depolarising envelope. In order to exclude the ET cell population from the $GAD65^{+}$ dataset, neurons that exhibited intrinsic bursting were removed from the analysis.

2.5 Light Stimulation in M72-IRES-ChR2-YFP Mice

For all channelrhodopsin experiments the M72-IRES-ChR2-YFP mouse line, described in section 2.1.3. was used (Smear et al. 2013). In this line, a ChR2-EYFP protein is selectively expressed under the odour receptor 160 (OR160) promoter, resulting in a restriction of channelrhodopsin-2 (ChR2) to all OR160 OSNs. These OSNs converge onto only two, bilaterally symmetrical M72 glomeruli per OB. A cross between this line and either Gad2-IRES-Cre-tdtomato or TH(9.0)tagRFP provides a way of targeting distinct subpopulations of juxtaglomerular interneurons that can be tested for their affiliation to the M72 network via ChR2 activation (Figure 2.4).

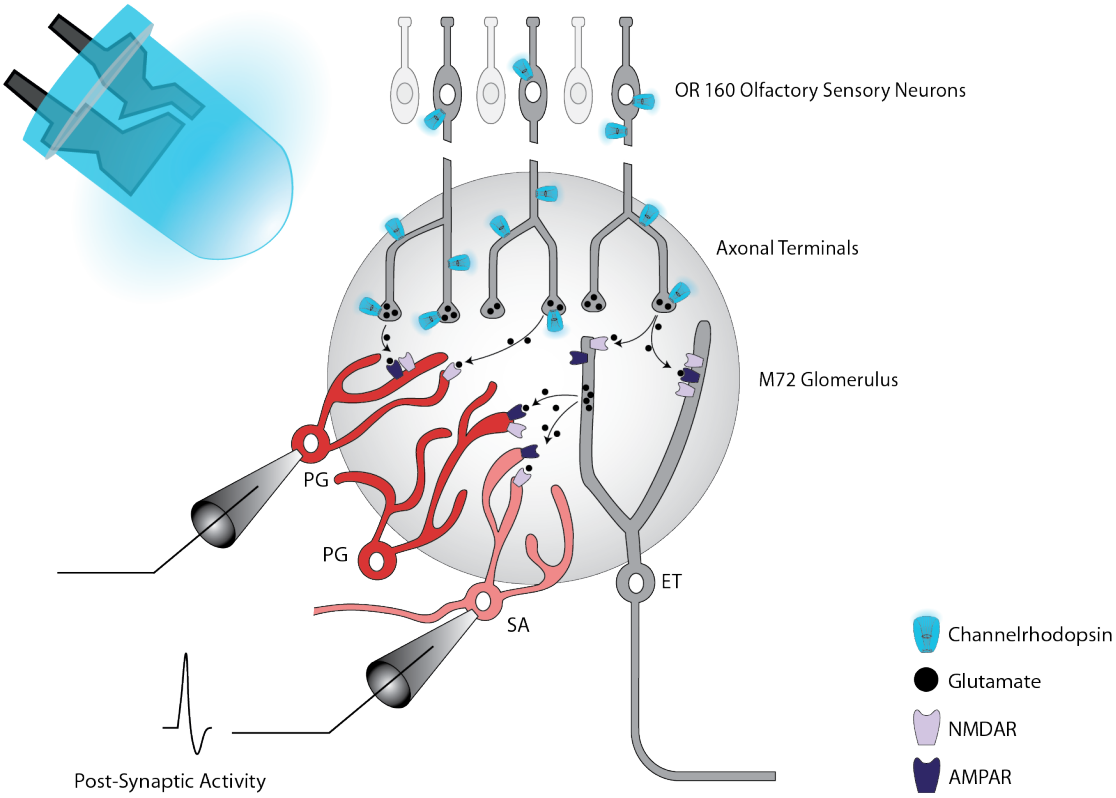

Figure 2.4 M72-IRES-ChR2-YFP Mice as a Model to Test Local Network Affiliation

In the M72-IRES-ChR2-YFP line ChR2 *(bright blue)* is specifically expressed in OR160 OSNs that converge onto the M72 glomeruli *(grey)*. After slice preparation, the ChR2 in the remaining OSN axons is activated by focussing a blue LED light (476 nm) onto the area around the M72 glomerulus. The light activates ChR2, which depolarises OSN axons, triggers release of the synaptic transmitter glutamate *(black)* from the OSN terminals and excites neurons, postsynaptically connected to the M72 OSNs. This light-evoked, postsynaptic activity was used as evidence for affiliation of the recorded neuron to the M72 glomerulus. AMPAR = AMPA receptor, ET = external tufted cell, NMDAR = NMDA receptor, PG = periglomerular cell, SA = short axon cell.

2.5.1 Properties of the ChR2(H134R) Ion Channel

ChR2(H134R) expressed in the M72-IRES-ChR2-YFP line is a light-driven cation channel and the first published gain-of-function mutation of the original ChR2 (Nagel et al. 2005). ChR2(H134R), like other ChR2 variants, is non-selectively permeable to cations and exhibits a reversal potential around 0 mV. The channel is activated by targeted illumination with blue light, but in contrast to the original ChR2, the peak response is shifted slightly towards lower wavelengths (450 nm instead of 470 nm) and the channel exhibits reduced desensitisation to steady-state photocurrent (Nagel et al. 2005; Lin et al. 2009).

A feature of ChR2(H134R) is a YFP protein fused to the C-terminus, enabling easier visualisation of expression levels. Evoked activity in M72-affiliated interneurons could reliably be observed with the GFP filter set (Figure 2.5, green trace), but not with the YFP filter set or the RFP filter set (Figure 2.5, yellow and red trace). Therefore, the YFP filter set was used instead of the GFP filter set for visualisation of Alexa Fluor® 488 filled neurons and the M72 glomerulus in channelrhodopsin experiments.

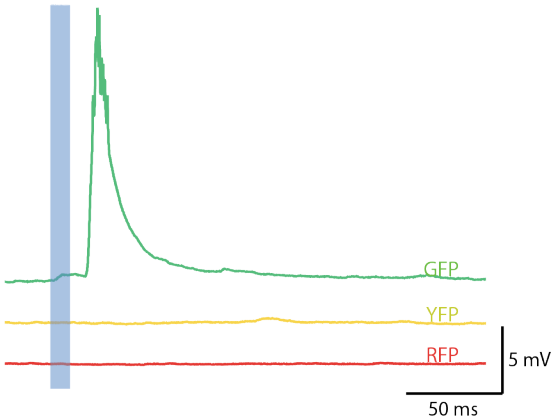

Figure 2.5 Light-Evoked Responses of M72-Affiliated Neurons Dependent on Wavelength

Current-clamp recording of a TH^+ neuron anatomically shown to be affiliated to the M72 glomerulus. The neuron responded to a 10 ms GFP light stimulation (*green trace*; excitation: BP 470/40; emission: BP 525/50, beam splitter: FT 495), but not to light stimulation with the YFP (*yellow trace*; excitation: BP 510/10; emission: BP 542/27, beam splitter: HP 520) or RFP filter set (*red trace*; excitation: BP 587/25; emission: BP 647/70, beam splitter: FT 605). Displayed are the average voltage traces in response to 20 consecutive 10ms light stimulations.

2.5.2 Photostimulation

In order to achieve reliable and comparable light stimulation across experiments, an LED-based light stimulation device, called “Rhodolight”, was developed by Martyn Stopps and Nicholas Burczyk as an addition for the Zeiss Axio Examiner microscope (Figure 2.6). The device replaces the eyepieces of the microscope and emits a light pulse into the microscope chamber through the optical path of the microscope (Figure 2.6a).

Rhodolight has a bright, blue LED (OSRAM LBW5AM-GYHY-25, High Brightness LED, Golden DRAGON Plus Series, 476 nm, 170°) as a light source with a reflector at the back. It is encased by a 3D printed polymer shell (printer: Objet 30, resin: VeroGray) and connected to the microscope via a rotatable flange (Igubal®, flange bearing KFSM-GT) and a 3D printed adapter (Figure 2.6b).

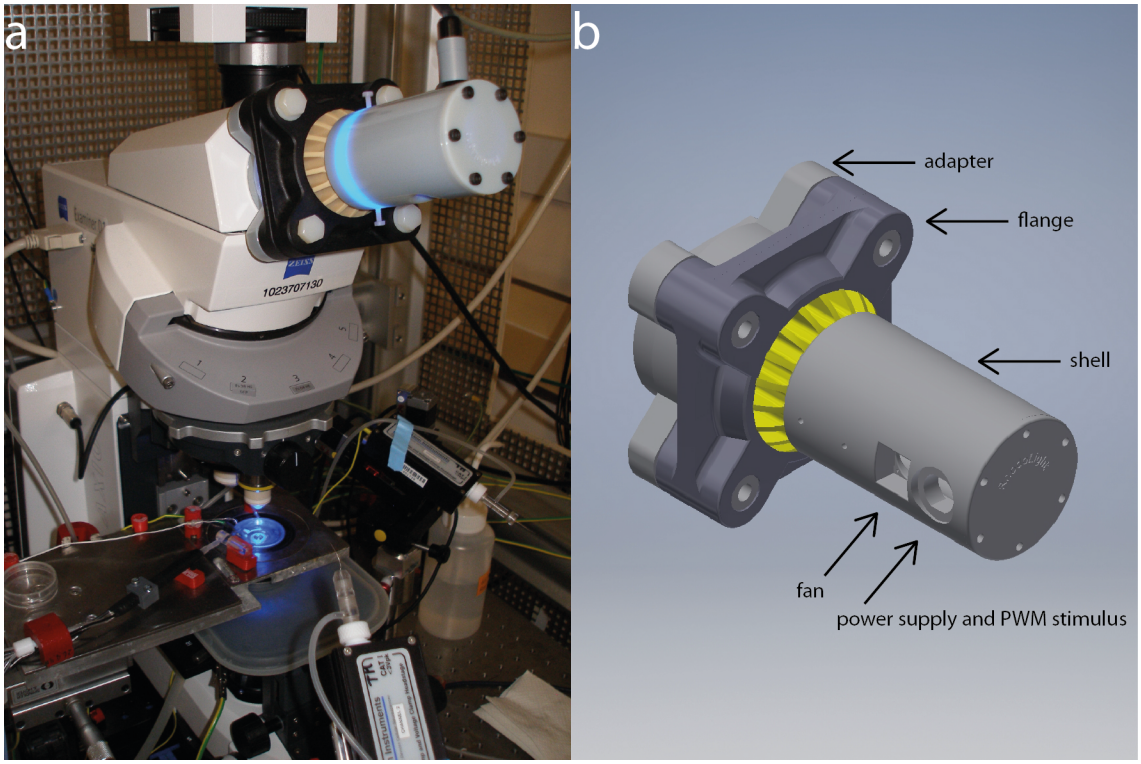

Figure 2.6 Light Stimulation Device "Rhodolight"

(a) The light stimulation device replaced the eyepieces of the Zeiss Axio Examiner microscope and emitted light pulses up to a light density of 21 mW/mm^2, which were focussed on the specimen using the optical pathway of the microscope.
(b) The 3D printed shell contains a blue LED (476 nm, 170° radiation angle), aligned to the centre hole of the rotatable flange and a reflector at the back of the LED. It was driven by a pulse width modulator and cooled with a fan. PWM = pulse width modulator.

The blue LED is actively cooled with a fan, built into the shell, and pulse width modulation is used to control the intensity of the LED. The brightness of the LED can be regulated by the strength of the voltage input to an external control box (0.3-1.2 V), triggered and modulated via a stimulus protocol created in Neuromatic (section 2.3.6.1., *ChR2 stim protocol*). A calibration curve (Figure 2.7) was established at the focal point of the 40x objective (in air) using an optical power measurement system (X-Cite®, Excelitas Technologies). The diameter of the objectives focal point can be calculated as

$$\emptyset\, focal\, point = \frac{field\ of\ view}{magnification}$$

The focal point was calculated as 0.785 mm^2 based on a 20mm with a field of view and a 40x magnification. When the LED was driven with the maximal stimulus intensity (1.2 V), a light density of 21 mW/mm^2 was estimated for the focal point area (Figure 2.7).

The linear relation between the output light intensity and the voltage of the control stimulus allows to accurately evaluate different light densities for ChR2. Unless stated otherwise, all ChR2 experiments were conducted with a 2 ms long light pulse, 20 ms after onset of the recording, with a 1.2 V input to the LED and repeated 20 or 50 times at a frequency of 1Hz (section 2.3.6.1., *ChR2 stim protocol*).

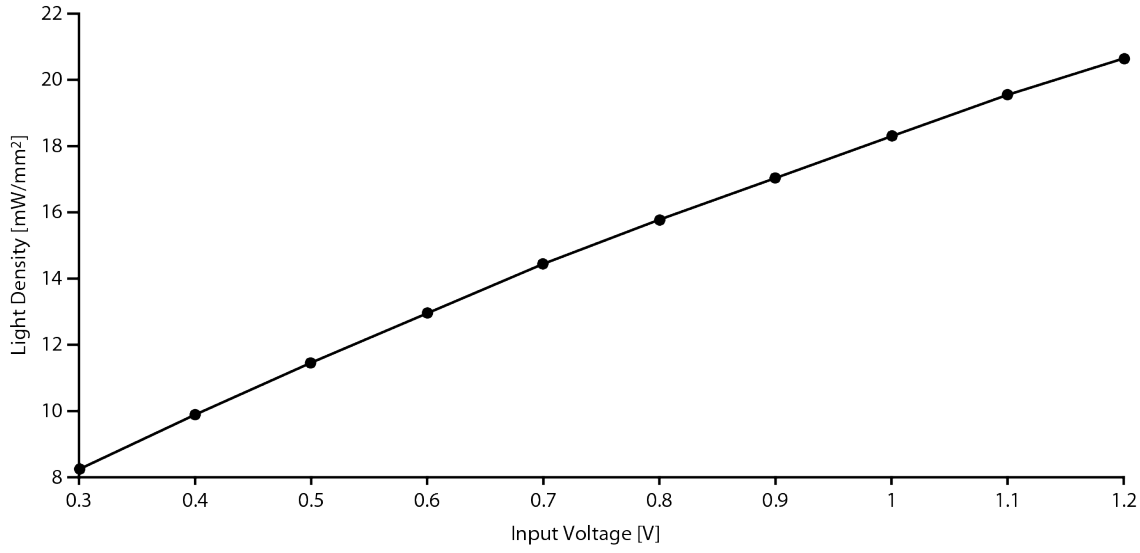

Figure 2.7 Output Light Densities of "Rhodolight" Linearly Depend on Input Voltage

Calibration curve established with an optical power meter measuring at 480 nm. The light beam of a 40x objective was focused on the $1cm^2$ large sensor. The command voltage was increased in increments of 0.1 V over the working range of the pulse width modulator (0.3 - 1.2 V) and plotted against the detected light power.

2.5.3 Event Detection for M72 Glomerulus Connectivity Analysis

In order to assess whether an interneuron responding to a light stimulus was monosynaptically connected to the M72 OSNs, the latency between onset of the light stimulus and onset of light-evoked events was calculated. Therefore, an average response waveform was generated by aligning all light-evoked events to the onset of the light stimulus. The baseline was calculated as the average of all trials during the 20 ms before the light stimulus onset. The onset of the light-evoked event was defined as the time at which membrane potential deviated by more than 2.5 times the standard deviation (SD) of the baseline after the light stimulus onset. In order to only consider high frequency noise for the SD calculation, the SD of the baseline was calculated via a rolling SD with a window of 1 ms.

2.6 Sensory Deprivation and Enrichment

2.6.1 Sensory Stimulation of Mice with 2'-Hydroxyacetophenone

Animals were exposed for seven to ten days to 2'-hydroxyacetophenone (2-HAP), a known ligand for M72 odour receptors (Feinstein et al. 2004). The odour was diluted in mineral oil to a final concentration of 5 % and 1 ml of the 5 % 2-HAP solution was dispersed on a clean paper tissue. The tissue was loosely rolled and inserted into a tube in front of the air inlet of the animal cage, so air could flow through tube and tissue and distribute the odour throughout the cage. The odour-soaked tissue was replaced every 12 hours. Mice were housed in groups of three to five animals in individually ventilated cages with the odour source out of reach for the animals.

2.6.2 Sensory Deprivation via Chemical Lesion of the Olfactory Epithelium

Chemical lesions of OSNs with $ZnSO_4$ were performed according to a previously published protocol (Bracey et al. 2013). Briefly, animals were anaesthetised in the morning with a subcutaneous injection of fentanyl (0.05 mg/kg, Fentanyl citrate, Antigen Pharmaceuticals), midazolam (5 mg/kg, Hypnovel®, Roche) and medetomidin (0.5 mg/kg, Domitor®, Pfizer). Depending on the weight of the animal, each naris was irrigated three times with 1 - 3 µl of 8.4 % w/v $ZnSO_4$ in ddH_2O solution (293 mOsm).

In the five minutes interval between each irrigation the animals were placed supine in a 30°C warm recovery chamber. After the last irrigation, the animals were placed in the recovery chamber for 10 minutes before inducing the recovery from anaesthesia by subcutaneous injection of naloxone (1.2 mg/kg, Naloxone, CP Pharmaceuticals), flumazenil (0.5 mg/kg, Anexate, Roche) and atipamezol (2.5 mg/kg, Antisedan®, Pfizer). After regaining consciousness, the animals, were left to recover in the warm recovery chamber for a maximum time period of 2 hours. In all but two animals, the treatment was repeated in the afternoon of the same day. After recovery a phenotype in the behaviour of all treated animals could be observed. The animals exhibited less exploring behaviour, their nose was often lowered to the ground and they did not retract the head from the experimenter's hand. This protocol is known to result in a lack of glomerular response to odour and anosmia as tested using go – no go olfaction discrimination task (Bracey et al. 2013).

Since the intent was to chemically lesion OSNs in the olfactory epithelium while still preserving ChR2 expression in axons of M72 OSNs, all electrophysiological experiments were conducted one day post chemical lesion.

2.7 Visualisation and Anatomical Analysis of Biocytin-Filled Recorded Neurons

2.7.1 Tissue Processing and Histology

For post-hoc morphological reconstruction, all neurons were filled with 0.5 % biocytin (w/v) during the electrophysiological recording. After the recording, brain slices were fixed in a 4 % PFA solution for at least two hours at RT and subsequently transferred to phosphate buffer (PB).

For 3,3'-diaminobenzidine (DAB) staining (Vectastain ABC kit, Vector Laboratories Inc.), endogenous peroxidase activity was blocked with 3 % (w/v) H_2O_2 for 20 to 30 minutes, followed by incubation overnight in 1 % (v/v) avidin-biotinylated HRP complex (ABC) solution. To amplify the DAB signal, DAB solution (0.66 mg/ml) was added and the staining was developed with 3 % (w/v) H_2O_2 afterwards. For an easier reconstruction of cell layers, DAPI counterstaining (1:10000 dilution, 10 min at RT) was performed on all brain slices.

2.7.2 Morphological Reconstruction

The stained neurons, their position and projections within the OB were manually reconstructed with Neurolucida 11 (MicroBrightField Inc.) and a wide-field, inverted microscope (Olympus BX61). For 2D reconstruction of the brain outlines, cell layers and glomerular outlines, a 10x/0.25 air objective (Plan N 10x, Olympus) was used, whereas soma (2D) and cell processes (3D) were reconstructed using a 100/1.25 oil objective (Plan N 100x, Olympus).

2.7.3 Morphological Analysis

For a comparative morphological analysis between $GAD65^+$ and TH^+ neurons, all parameters were calculated with the Neurolucida Explorer software.

Sholl Analysis

To assess the dendritic trees in $GAD65^+$ and TH^+ neurons, the maximum radius of each neuron in a Sholl analysis was calculated and compared. In a Sholl analysis concentric spheres with an increasing radius are drawn around the centre of a soma. For the present analysis an increment of 10 µm per sphere was chosen. The result of the analysis is the smallest sphere that encompasses the whole dendritic tree.

Convex Hull Analysis

A Convex Hull analysis was performed on all reconstructions. Here, the algorithm constructs a 3D convex polygon that connects the endings of all dendrites and calculates the volume of the polygon, providing an estimate of the area innervated by the dendrites of a neuron.

Crossing of Glomeruli by Dendritic Processes

Consistent with the morphological analyses in Kiyokage et al. 2010, the innervation pattern of a neuron was assessed by quantification of the intersections between dendrites and reconstructed glomerular spheres. Only reconstructions with full recovery of all glomeruli in the area of interest were used for this analysis. The percentage of dendritic tree intersecting the glomeruli was calculated, as well as how many glomeruli were crossed by > 6 µm of dendritic process.

Dendritic Proximity Analysis

To determine the average distance between dendrites of two simultaneously recorded neurons, a proximity analysis was performed using Neurolucida Explorer. Here, the dendritic tree of one neuron was divided into segments of 1 µm and for each segment the algorithm tested whether dendrites of the second neuron were within a vicinity of 5 µm. This calculation was performed in both directions (neuron A in vicinity of B and vice versa) and averaged. The percentage of dendritic segments where the two neurons' dendrites were closer than 5 µm was used to quantify the degree of dendritic overlap.

Identifying Axons

An axon could only be identified for a limited number of $GAD65^+$ and TH^+ neurons. Some juxtaglomerular cells do not have axons or their axons can depart from a dendrite instead of the soma and some of their dendritic processes can resemble axons (Pinching and Powell 1971a; Kiyokage et al. 2010; Kosaka and Kosaka 2011). Therefore, it was challenging to clearly identify an axon in some reconstructions. Axonal characteristics considered for axon identification were (1) long, lateral extension of the process within the OB, (2) slender diameter at the origin of the process, (3) no tapering in the process' diameter and volume, (4) little branching (5) natural terminals outside the glomerular space.

2.8 Statistical Analyses

All statistical analyses were performed in MATLAB. All data groups were tested for normality with a Lilliefors test (MATLAB function "lillietest"), and parametric tests were used when appropriate in form of a two-sample t-test ("ttest2") or two-sample F-test ("vartest2"). Otherwise, a Wilcoxon rank sum test ("ranksum") was used to compare medians and a Brown-Forsythe test ("vartestn") to compare variances. Anova tests were used where appropriate to test for interaction effects and post-hoc tests were corrected using the Holm-Bonferroni method. Significance values of $p < 0.05$ were labelled with a single asterisk, values of $p < 0.01$ with two asterisks and values of $p < 0.001$ with three asterisks. According to the parametric or non-parametric nature of the applied statistical test, results are presented as mean ± standard deviation or median (range). In all boxplots, the central mark indicates the median, the outline of the box extend to the 25th and 75th percentiles and the whiskers indicate the most extreme data

points not considered outliers. Outliers, denoted with '+', are data points outside 1.5 times the interpercentile range.

Chapter 3. Recordings in Molecularly Identified Subpopulations of Juxtaglomerular Neurons

3.1 Introduction

This chapter classifies and describes the neuronal populations under investigation in this thesis, in the context of already described subpopulations of inhibitory interneurons in the glomerular layer. With roughly 100 GABAergic interneurons per excitatory neuron (Shepherd 2004), the olfactory bulb (OB) has a considerably higher ratio of interneurons than most other areas of the brain. This suggests that these cells are central to computations performed in the OB. The interneuron population of the OB is known to be highly heterogeneous and many attempts have been made to subdivide this population based on location, expression of molecular markers, morphology or biophysical properties. Some subclasses of OB interneurons have been researched intensively and the functional contributions of distinct interneuron populations to the computations of the OB network are beginning to be understood (Hayar et al. 2004a; Shao et al. 2009; Liu et al. 2013). Despite this, a more complete understanding of functional integration of most interneuron populations remains elusive.

Depending on the classification approach, subpopulations of bulbar interneurons can be highly overlapping, resembling a continuum rather than discrete classes. This results in controversial and on-going classification with publications regularly describing newly discovered interneuron populations (Merkle et al. 2014). Furthermore, glomerular interneurons are continuously generated, resulting in turnover throughout juvenile and adult life (Belluzzi et al. 2003; Carleton et al. 2003; Ming and Song 2005; Livneh et al. 2014). Adult-born interneurons migrating from the subventricular zone through the rostral migratory stream to the OB, where they mature and integrate into already operating local OB networks. During migration, the neurons not only change their location, but also develop morphological features, molecular expression profiles and biophysical properties.

This chapter aims to provide a description of the molecular, morphological and electrophysiological properties of the $GAD65^+$ and TH^+ interneuron populations, in

order to facilitate the interpretation of the computational properties of these neurons, which are described and discussed in later chapters.

3.1.1 Molecular Characterisation of Juxtaglomerular Cells

Classic Golgi staining reveals few morphologically defined neuronal classes within distinct OB layers, with only two major types of inhibitory glomerular interneurons (Pinching and Powell 1971a). However, immunohistochemical stainings against marker molecules suggest the OB has a highly heterogeneous neuronal population, particularly in the glomerular layer. In this layer, juxtaglomerular (JG) neurons have been shown to express one or several molecular markers, including glutamic acid decarboxylase (GAD), an enzyme catalysing the synthesis of the synaptic transmitters γ−aminobutyrate (GABA; Kosaka et al. 1995; Panzanelli et al. 2007; Parrish-Aungst et al. 2007), dopamine (enzyme TH; Halasz et al. 1985; McLean and Shipley 1988; Parrish-Aungst et al. 2007), and the calcium-binding proteins calretinin (Resibois and Rogers 1992; Rogers and Resibois 1992; Kosaka et al. 1995), calbindin-D28k (Halasz et al. 1985; Brinon et al. 1992; Rogers and Resibois 1992; Kosaka et al. 1995), neurocalcin (Brinon et al. 1998; Brinon et al. 1999) and parvalbumin (Kosaka et al. 1994; Brinon et al. 1999) as well as peptides, like enkephalin and thyrotropin-releasing hormone (Kosaka et al. 1995) and the $GABA_A$ receptor α5 subunit (Panzanelli et al. 2007).

Additionally, two isoforms of the GAD enzyme (GAD_{65} and GAD_{67}) are expressed in only partly overlapping subpopulations of glomerular interneurons, in roughly equal proportions in the OB (Parrish-Aungst et al. 2007). Both isoforms are known to actively catalyse the synthesis of GABA from L-gutamic acid, but it has been suggested that they vary in their distribution within a neuron and are involved differently in information processing (Soghomonian and Martin 1998).

The ratios of molecular markers expressed in the JG cell population vary between studies, most likely due to different estimations of the total number of cells in the glomerular layer. One of the most comprehensive studies in mouse OB (Parrish-Aungst et al. 2007) estimated the total number of glomerular neurons by combining the number of histochemically labelled neurons in their experiments with numbers from previously published stainings for different molecular markers. They concluded the following

expression profiles: The largest proportion of JG cells in the glomerular layer is GABAergic, with 37 % being GAD65$^+$ and 31 % being GAD67$^+$, whereby 52 % of GAD67$^+$ cells co-express the GAD65 isoform. Nearly a third of all JG cells expressed

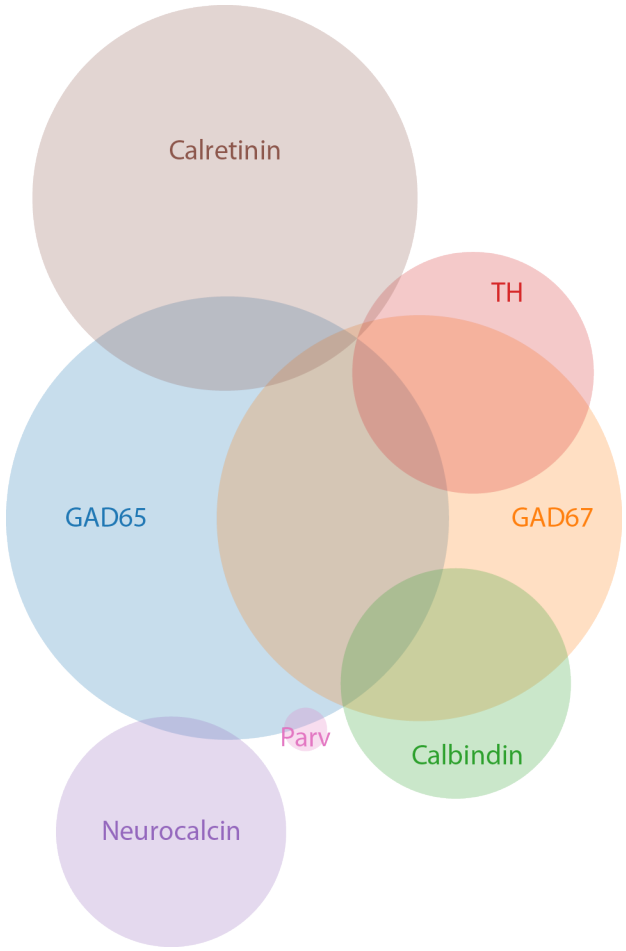

Figure 3.1 Expressional Overlap of Molecular Markers in the Glomerular Layer

Venn diagram visualising the overlap of marker molecules in neurons of the glomerular layer. Around 53 % of all glomerular neurons are GABAergic (37 % GAD65$^+$, 31 % GAD67$^+$), 28 % are positive for calretinin, 11 % for TH, 10 % for calbindin, 10 % for neurocalcin and less than 1 % for parvalbumin. Less than 20 % of TH$^+$ neurons co-express GAD_{65}, but at least 70 % co-express GAD_{67}. Less than 15 % of all calretinin$^+$ neurons are also GABAergic, and virtually all co-express the GAD_{65} isoform. Calbindin$^+$ neurons exhibit a substantial overlap with the GABAergic population (65 %), around 60 % co-express GAD_{67} and 17 % GAD_{65}. The neurocalcin$^+$ population only has a small (3 %) overlap with the GAD65$^+$ population and 38% of all parvalbumin$^+$ neurons were GAD65$^+$. The expression profiles of the marker proteins TH, calretinin, calbindin, neurocalcin and parvalbumin are mutually exclusive in the glomerular layer. Parv = parvalbumin. (Diagram generated based on data from Parrish-Aungst et al. 2007).

calretinin (28 %) and a significantly smaller fraction of neurons are dopaminergic (11 %) or positive for the calcium-binding proteins calbindin (10 %), neurocalcin (10 %) and parvalbumin (0.35 %). TH and the four calcium-binding proteins have diverse co-expression levels of the GAD isoforms GAD_{65} and GAD_{67} (Figure 3.1), but exhibit only infrequent expressional overlap among one another (Kosaka et al. 1995; Brinon et al. 1999; Parrish-Aungst et al. 2007).

Neurochemical classification could potentially define functional subpopulations within the morphologically defined types of glomerular interneurons. However, several publications indicate that neurons being positive for one of the calcium-binding proteins lack a set of common morphological features, resulting in at least some periglomerular (PG), short axon (SA) and external tufted (ET) cells expressing the same calcium-binding molecules (*calretinin*: Kosaka et al. 1998; *calbindin*: Brinon et al. 1992, Philpot et al. 1997; *parvalbumin*: Kosaka et al. 1994; *neurocalcin*: Brinon et al. 1998).

In contrast, it has been suggested that targeting inhibitory interneurons by their expression profile of the neurotransmitter marker molecules GAD_{65} and GAD_{67}/TH results in morphologically distinct groups, whereby the $GAD65^+$ class morphologically resembles PG cells (Shao et al. 2009; Kiyokage et al. 2010) and the $GAD67^+/TH^+$ population exhibits the morphology of SA cells (Kiyokage et al. 2010; Liu et al. 2013). Initially, TH^+ neurons were classified based on their soma size and location as either small PG cells or large ET cells (Halasz et al. 1981; Baker et al. 1983; McLean and Shipley 1988). However, more recent studies investigated the innervation pattern of these neurons and found that TH^+ neurons more likely resemble the morphology of SA cells, with processes targeting multiple glomeruli across large areas (Kosaka and Kosaka 2008; Kiyokage et al. 2010). The assignment of the two molecular classes to the morphologically discrete PG and SA cell population is still controversial and these molecularly defined groups likely only comprise subpopulations of the PG and SA cells (Nagayama et al. 2014).

Regardless, most if not all TH^+ neurons co-express GAD_{67} and only relatively few are also $GAD65^+$ (Parrish-Aungst et al. 2007). Therefore, the marker proteins GAD_{65} and TH provide a way of reliably targeting two distinctly different interneuron populations, potentially exhibiting specific morphological and functional features.

3.1.2 Morphological Characterisation of Juxtaglomerular Cells

Based on morphology, the heterogeneous population of glomerular neurons can be distinguished into three major types of neurons: ET cells, PG cells and SA cells (Pinching and Powell 1971a; Pinching and Powell 1971b). However, since ET cells have been shown to provide feed-forward excitation onto principal neurons via glutamatergic synaptic transmission (De Saint Jan et al. 2009; Najac et al. 2011; Gire et al. 2012), they are not typically considered to be part of the inhibitory interneuron network and were therefore excluded from all results in this thesis (see Material and Methods, section 2.4.5).

Although the morphologies of PG and SA cells have been exhaustively described since the seventies (see section 1.4.1.3), many of their features such as soma size, innervation pattern, axonal projections, at least partly overlap within the parameter space and so a classification purely based on morphological outlines can be error-prone. Also, the distinction between axons and dendrites can be problematic in both populations, since some neurons seem to completely lack an axon (Pinching and Powell 1971a) or can have thin dendrites that resemble axons when using bright field microscopy (Kiyokage et al. 2010).

3.1.3 Biophysical Characterisation of Juxtaglomerular Cells

In contrast to ET cells, which exhibit a distinct physiological profile (see Material and Methods, section 2.4.5), the intrinsic physiological properties of SA and PG cells appear generally similar, hampering a classification of these two cell types purely based on biophysical properties.

PG cells exhibit a resting membrane potential (RMP) around -57 to -65 mV, a relatively high input resistance around 600-1000 MΩ and a small hyperpolarisation-activated current (I_h; Puopolo and Belluzzi 1998a; McQuiston and Katz 2001; Hayar et al. 2004a; Shao et al. 2009). Although SA cells have consistently been reported to exhibit a slightly more hyperpolarised RMP and lower input resistance (Hayar et al. 2004a; Liu et al. 2013), these intrinsic biophysical properties are highly overlapping in both populations, making unambiguous classification of individual neurons impossible. When depolarised, both PG cells and SA cells tend to discharge single action potentials,

with further depolarisation resulting in regular firing and finally spike inactivation, but in contrast to ET cells they never exhibit intrinsic bursting behaviour (Hayar et al. 2004a; Shao et al. 2009). At least some neurons in both populations exhibit infrequent spontaneous spiking at RMP (Hayar et al. 2004a).

PG cells can be further divided into two populations, based on diverging firing patterns, which are the result of diverging pre-synaptic connectivity. Around 70 % of PG cells receive direct input from ET cells and therefore exhibit bursts of activity driven by bursting ET cells. In contrast, around 30 % of PGs cells are monosynaptically connected to OSNs and only display single invariant postsynaptic potentials (Hayar et al. 2004b; Shao et al. 2009). A similar difference in firing profiles has been shown for SA cells (Kiyokage et al. 2010).

3.1.4 Classification Based on Multiple Approaches

Research over several decades has transformed our initial picture of the glomerular layer as a simple structure for information relay from sensory neurons onto principal neurons into a highly complex lateral and recurrent inhibitory network, performing significant computation on sensory information as early as the first synapse (Kosaka et al. 1998; Wachowiak and Shipley 2006; Lledo et al. 2008; Nagayama et al. 2014).

Despite the ongoing classification of new OB cell populations and the still fragmentary links between morphological, electrophysiological, biochemical and functional properties of the cell types in the glomerular layer, some populations have been widely acknowledged to exhibit distinct features across several classification methods, making them ideal candidates for targeted experimental investigation. Among these populations are $GAD65^+$ cells and TH^+ cells. $GAD65^+$ neurons have small somata (6-11µm; Parrish-Aungst et al. 2007; Shao et al. 2009) and mostly (> 90 %) project to a single glomerulus (Aungst et al. 2003; Shao et al. 2009). Both morphological attributes have previously been assigned to PG cells (Pinching and Powell 1971a). $GAD65^+$ neurons resemble PG cells not only morphologically, but also in their intrinsic properties (compare Shao et al. 2009 with Hayar et al. 2004a and Murphy et al. 2005). Some $GAD65^+$ neurons exhibit bursts of spontaneous EPSCs whereas others only exhibit single, isolated EPSCs. It has been proposed that the $GAD65^+$ population includes both PG cells with input from OSNs and PG cells with input from ET cells. $GAD65^+$ may therefore be involved in two

separate regulation mechanisms of presynaptic glutamate release from OSN terminals (Shao et al. 2009). A recent study found a subpopulation of glutamatergic ET cells co-expressing GABA (Tatti et al. 2014), however ET and PG cells can be reliably distinguished based on their physiological profile (section 2.4.5, Hayar et al. 2004a).

Like SA cells, TH^+ neurons generally have larger somata than typical PG cells (> 10 µm; Parrish-Aungst et al. 2007) and exhibit SA cell–like dendritic and axonal morphology and innervation pattern (Kiyokage et al. 2010), as well as SA cell-like intrinsic biophysics (compare Liu et al. 2013 with Hayar et al. 2004a). As in the $GAD65^+$ population, around 70 % of $GAD67^+/TH^+$ neurons receive bursts of EPSCs and 30 % exhibit only single EPSCs, which is why these neurons have also been suggested to have diverging presynaptic connectivity (Kiyokage et al. 2010).

In summary, accumulating evidence suggests that neurons featuring the marker proteins GAD_{65} and TH correspond to the morphologically well-defined PG and SA cell populations (Nagayama et al. 2014) and several researchers have used these molecular markers to specifically target PG- and SA-cell-like populations in order to explore their functional qualities (Aungst et al. 2003; Shao et al. 2009; Liu et al. 2013).

3.1.5 Hyperpolarisation-Evoked Sag Potentials in $GAD65^+$ and TH^+ Neurons

Glomerular interneurons potentially mediate many of the integrative processes underlying the computations performed by the OB (section 1.4) and the output of these neurons is influenced by their passive and active membrane properties.

I_h-mediated membrane potential sag has been found in principal and glomerular interneurons in the OB (Cadetti and Belluzzi 2001; Hayar et al. 2004b; Angelo and Margrie 2011), but while the impact of the current on excitatory OB neurons has been well-described (Liu and Shipley 2008b; Angelo and Margrie 2011; Angelo et al. 2012; Liu et al. 2013), little is known about its functional relevance in inhibitory glomerular interneurons. In visually identified PG cells, a small I_h (around 10 pA) has been described and was suggested to influence slow oscillatory network rhythms (Cadetti and Belluzzi 2001). The same research group also identified a small, tonically active I_h in TH_+ neurons, which had an influence on RMP, but could not be shown to impact on any pacemaking activity (Pignatelli et al. 2013). Except for these two interneuron types, the

expression levels of the I_h across different classes of inhibitory glomerular interneurons have not yet been systematically described and the underlying function of the consistent, but small I_h levels in these neurons remains elusive.

This chapter describes the quantification of I_h and the I_h-mediated sag in $GAD65^+$ and TH^+ interneurons, in order to explore underlying cellular functions. In later chapters, the relationship between I_h-mediated sag and glomerular innervation, as well as synaptic activity, is established with the aim of determining whether I_h in glomerular interneurons reflects local network activity, as has been shown for mitral cells (MCs; Angelo et al. 2012).

3.2 Results

3.2.1 Quantitative Analysis of the Specificity of Genetic Labelling in the TH(9.0)tagRFP Mouse Line

To validate the TH(9.0)tagRFP line, the specificity of the fluorescent labelling was assessed using antibody stainings in four mice. 50 µm thick horizontal sections were cut from different areas of the OB and stained with anti-TH as primary and Alexa Fluor® 488 as secondary antibody (Figure 3.2 a-c, Material and Methods 2.2). Because the OB exhibits substantial non-specific auto-fluorescence, an additional nucleus staining was performed with 4',6-diamidino-2-phenylindole (DAPI), enabling easier identification of cells (not shown). In both the genetic labelling and the TH-antibody staining, the strength of fluorophore expression was heterogeneous in different neurons. Classification of weakly labelled neurons can be subjective, therefore two raters analysed all stainings independently and the results from over 2000 counted neurons were averaged. Overall, 76 % of $tagRFP^+$ neurons were immuno-reactive to the anti-TH antibody (Figure 3.2c, white arrowheads). Conversely, 31 % of all immuno-reactive neurons did not show tagRFP expression in the TH(9.0)tagRFP mouse line.

3.2.2 Overlap between $GAD65^+$ and TH^+ Neurons in the Glomerular Layer

Although it has been shown that GAD_{65} and TH marker proteins exhibit little expressional overlap in the OB (Kiyokage et al. 2010; Parrish-Aungst et al. 2011), the overlap between these markers was determined as a control: OBs of two Gad2-IRES-Cre-tdTomato animals were sliced into 50 µm sections, stained with anti-TH and Alexa Fluor® 488 antibody (Figure 3.2 d-f), as well as DAPI, and all images were analysed independently by two raters, as described above (see 3.2.1). With only 15 % of all $GAD65^+$ neurons and 16 % of all immunoreactive TH^+ neurons exhibiting double labelling, a reasonably clear separation of the two interneuron populations could be confirmed. Distinctly different soma sizes were observed between $GAD65^+$ and TH^+ neurons, with $GAD65^+$ neurons generally having smaller somata than TH^+ neurons (Figure 3.2 a-f, bottom magnifications), however no further quantifications were conducted.

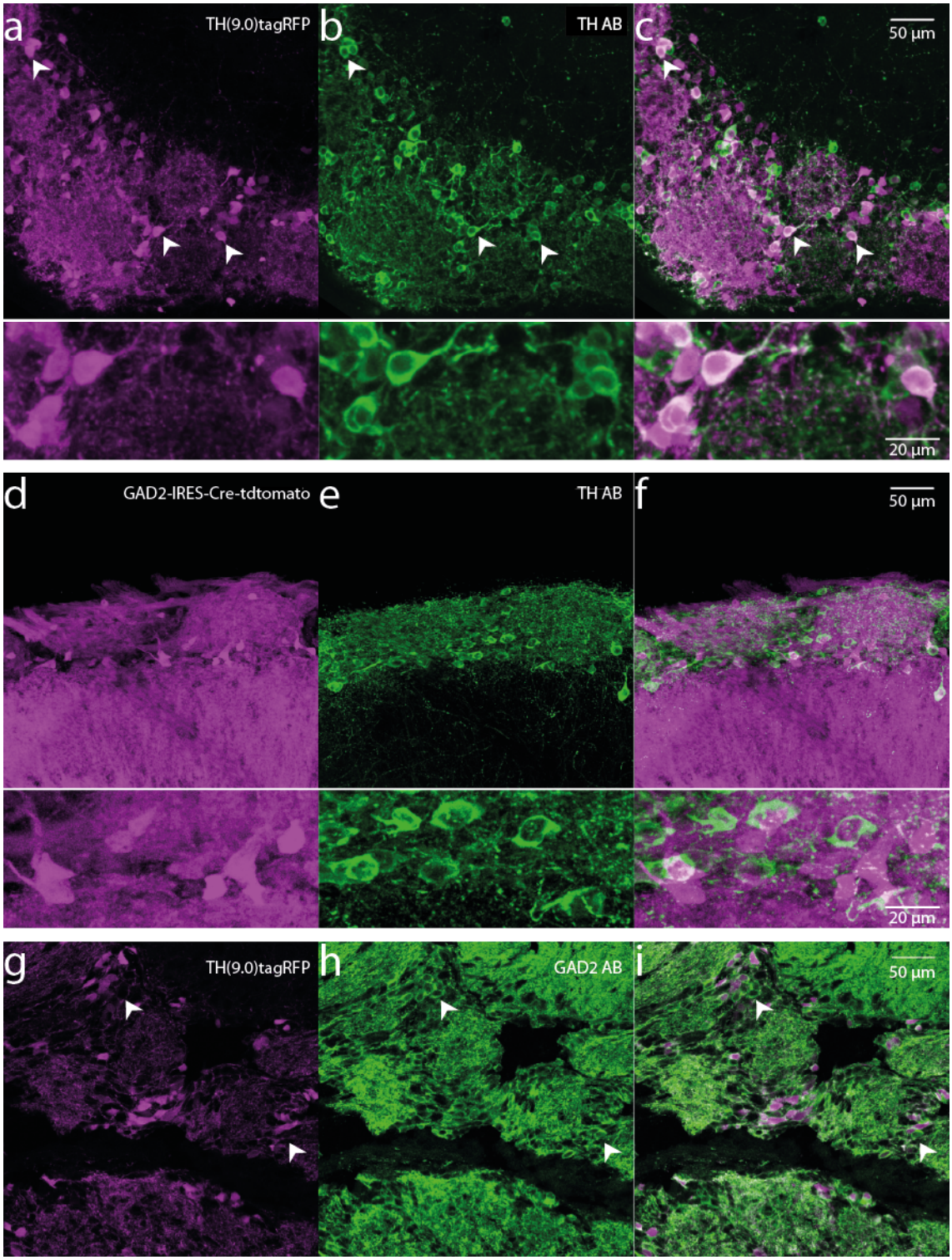

Figure 3.2 TH Antibody Staining in the Glomerular Layer of TH(9.0)tagRFP and Gad2-IRES-Cre-tdTomato Animals

(a-c) *top:* Example anti-TH antibody staining in a TH(9.0)tagRFP animal, showing a large overlap between antibody staining and RFP labelling in the transgenic animal. White arrowheads indicate examples of double-labelled cells. *Bottom:* Magnification of the area in the white box visualising soma sizes of fluorescent TH^+ neurons.

(d-f) *Top:* Example anti-TH antibody staining in Gad2-IRES-Cre-tdTomato animal, validating the distinct labelling of two different interneuron subpopulations by the genetic markers TH and GAD_{65}. *Bottom:* Magnification of the area in the white box visualising soma sizes of fluorescent TH^+ and $GAD65^+$ neurons.
(g-h) Anti-GAD2 antibody staining in 10 µm thick cryosections of a TH(9.0)tagRFP animal. Visual observation suggests little overlap between RFP expression and antibody staining, but no quantitative analysis was performed. Arrowheads indicate clearly identified antibody-stained $GAD65^+$ neurons. *All rows from left to right:* Intrinsic fluorescence of genetic mouse line, antibody staining, composite image.
Images a-f: Maximum projections of 17 confocal images with a z-spacing of 1.5 µm. *Images g-i:* Single confocal image. All images were taken using a 40x objective.

For assessing the reverse overlap, an anti-GAD2-antibody staining was performed in the TH(9.0)tagRFP mouse line. However, since the staining resulted in a rather diffuse labelling of cytosolic GAD2 protein and also strongly labelled the processes of GABAergic neurons, the reliable identification of immunoreactive neurons was difficult, even when the tissue was cut in 10 µm thin cryosections. Visual inspection of the stained tissue revealed little fluorescent overlap (Figure 3.2 g-i), but due to the diffuse staining, no reliable counting or further analysis could be performed to assess the number of double labelled neurons.

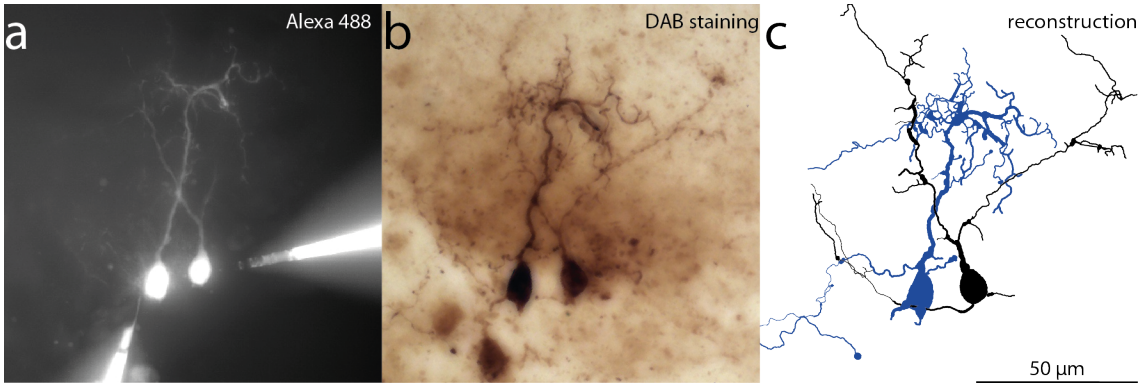

Figure 3.3 Example Process of Morphological Reconstruction for Two Simultaneously Recorded $GAD65^+$ Neurons

(a) Simultaneous whole-cell recording of two $GAD65^+$ neurons. During recording, neurons were filled with internal solution, containing biocytin and Alexa Fluor® 488 (Maximum projection, GFP filter set, 40x objective).
(b) Post-recording the brain slice was fixed in 4 % paraformaldehyde and stained with a DAB staining (Minimum projection, brightfield illumination, 40x objective).
(c) Morphological reconstruction of both neurons was conducted with Neurolucida software. The axon of the blue neuron has been cropped for display purposes.

3.2.3 Morphological Quantification of GAD65$^+$ and TH$^+$ Neurons

As noted in the introduction to this chapter, GABAergic and dopaminergic neurons of the OB can have diverse morphologies, potentially contributing to distinctly different functions of these two neuronal populations. This section aims to give insight into the morphological differences between GAD65$^+$ and TH$^+$ interneurons, providing a foundation for explaining the physiological differences described and analysed in subsequent sections of this thesis. In order to obtain morphological reconstructions, neurons were filled with 0.5 % biocytin during whole-cell recording, enabling a post-recording recovery of their morphology following 3,3'-diaminobenzidine (DAB) staining (Figure 3.3, Materials and Methods 2.7). The quality and completeness of the staining depended heavily on the quality of the recording and the pull-off from the cell. The dendritic tree and soma of only a fraction of all recorded neurons could be fully reconstructed and analysed (Figure 3.4 and Figure 3.5). Only neurons with a strong, high contrast staining, a complete soma and the majority of dendritic endings within the brain section were considered to be complete and were reconstructed. As it was only possible to sufficiently recover the axons of few neurons (Figure 3.4 and Figure 3.5, black traces), no further analysis was performed on the occurrence and shape of axons.

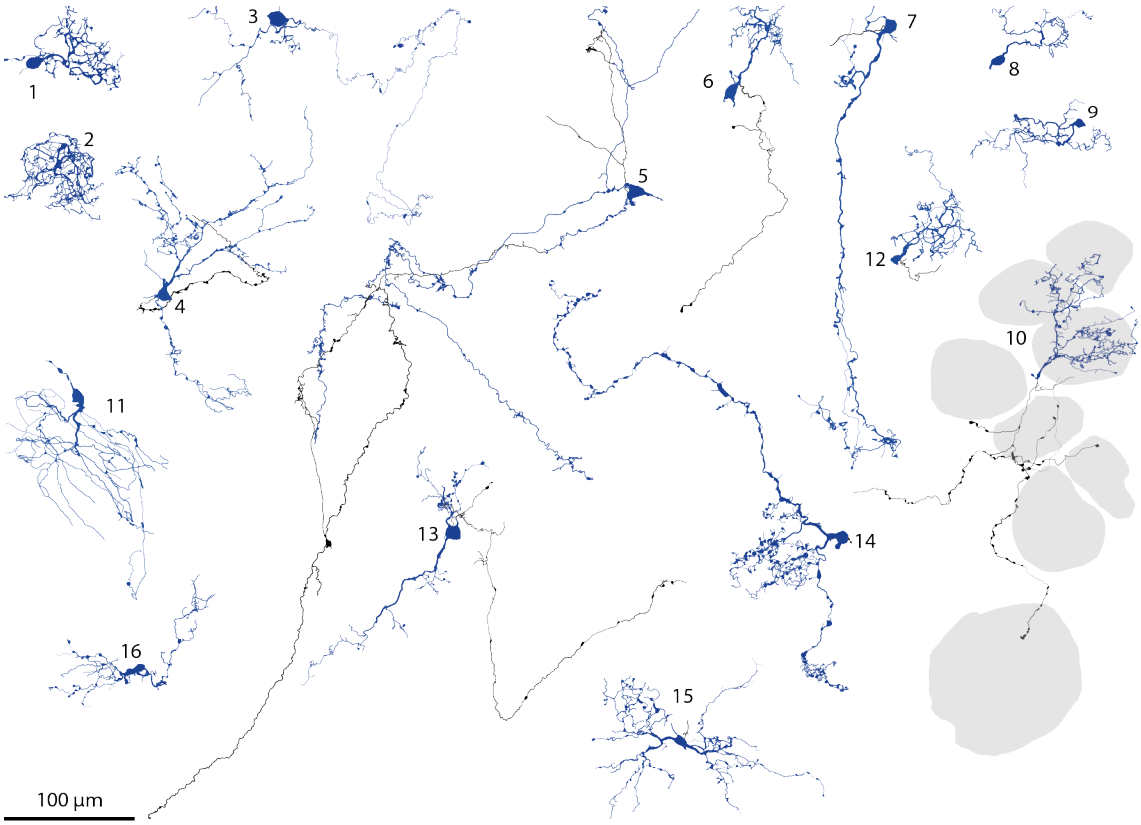

Figure 3.4 Reconstructions of Recorded GAD65$^+$ Neurons Used for Morphological Analysis

Example tracings from 3D morphological reconstructions of 16 GAD65$^+$ neurons. Whole-cell recordings of all neurons were performed in Gad2-IRES-Cre-tdTomato animals and GAD65$^+$ neurons were identified by fluorescent labelling. Soma and dendritic tree displayed in blue, axons displayed in black. An additional DAPI staining of the fixed tissue was used to determine the outlines of glomeruli *(grey)* innervated by the reconstructed neurons.

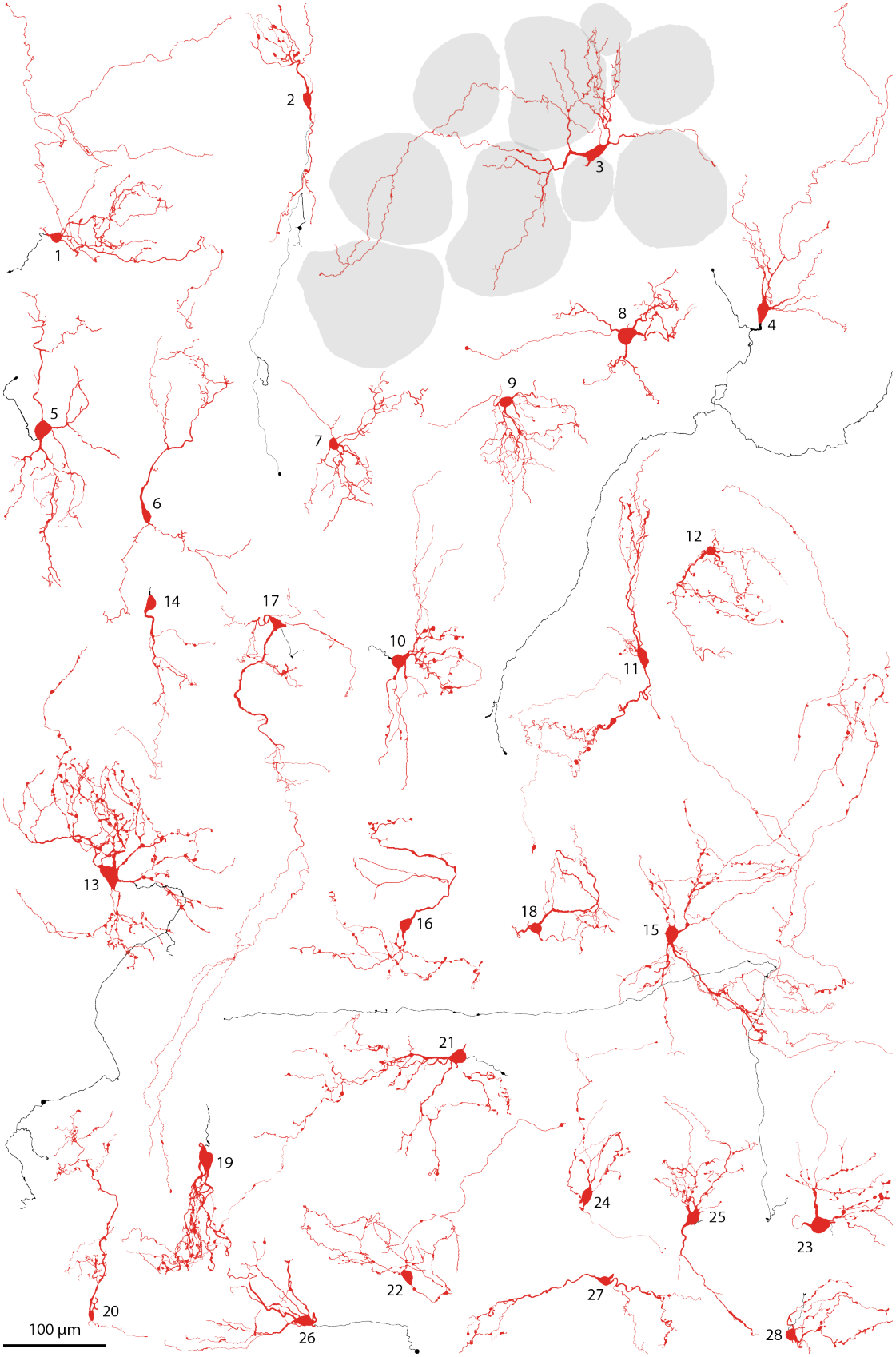

Figure 3.5 Reconstructions of Recorded TH$^+$ Neurons Used for Morphological Analysis

Figure 3.5 Reconstructions of Recorded TH$^+$ Neurons Used for Morphological Analysis (cont.)
Example tracings from 3D morphological reconstructions of 28 TH$^+$ neurons. Whole-cell recordings of all neurons were performed in TH(9.0)tagRFP animals and TH$^+$ neurons were identified by fluorescent labelling. Soma and dendritic tree displayed in red, axons displayed in black. An additional DAPI staining of the fixed tissue was used to determine the outlines of glomeruli *(grey)* innervated by the reconstructed neurons.

As expected, GAD65$^+$ neurons had a significantly smaller soma perimeter than TH$^+$ neurons ($soma_{GAD65}$ = 30.35 ± 6.48 µm vs. $soma_{TH}$ = 42.57 ± 10.85 µm, p_{mean} = 0.0002, Figure 3.6a). Soma size was assessed using the soma perimeter instead of the soma diameter, because TH$^+$ neurons in particular exhibited elongated, pear shaped soma outlines (Figure 3.5, for instance neuron number 3). TH$^+$ neurons also had slightly more primary dendrites than GAD65$^+$ neurons (primary $dendrites_{GAD65}$ = 2 (1-3) vs. primary $dendrites_{TH}$ = 3 (1-6), p_{median} = 0.0003, Figure 3.6b), however GAD65$^+$ neurons exhibited more branching points in their dendritic tree ($nodes_{GAD65}$ = 57 (21-195) vs. $nodes_{TH}$ = 37 (15-123), p_{median} = 0.017, Figure 3.6c) and therefore more dendritic terminals ($terminals_{GAD65}$ = 61 (25-210) vs. $terminals_{TH}$ = 39 (18-134), p_{median} = 0.011, Figure 3.6d). When comparing the dendritic trees, the overall length of the dendrites were similar in both genotypes (dendritic $length_{GAD65}$ = 1534 µm (485-3147) vs. dendritic $length_{TH}$ = 1619 µm (721-5835), p_{median} = 0.267, Figure 3.6e), but TH$^+$ neurons exhibited thicker dendrites (dendritic $volume_{GAD65}$ = 480 µm^3 (201-1837) vs. dendritic $volume_{TH}$ = 900 µm^3 (414-3387), p_{median} = 0.002, Figure 3.6f).

Figure 3.6 Morphological Differences Between GAD65$^+$ and TH$^+$ Neurons (next page)
Comparative boxplots, illustrating the morphological differences and similarities of GAD65$^+$ neurons (*blue*, n = 16) and TH$^+$ neurons (*red*, n = 28) based on
(a) soma perimeter,
(b) number of primary dendrites,
(c) number of branching points at dendritic tree,
(d) number of endings at dendritic tree,
(e) total length of dendritic tree and
(f) total volume of dendritic tree.
Numbered filled circles correspond to the numbered reconstructions in Figure 3.4 and Figure 3.5. Black horizontal bars indicate the median for each group. Significance was determined with a t-test for soma perimeter and with a Wilcoxon rank sum test for all other properties; n.s.: no significant, *: p-value < 0.05, **: p-value < 0.01, ***: p < 0.001).

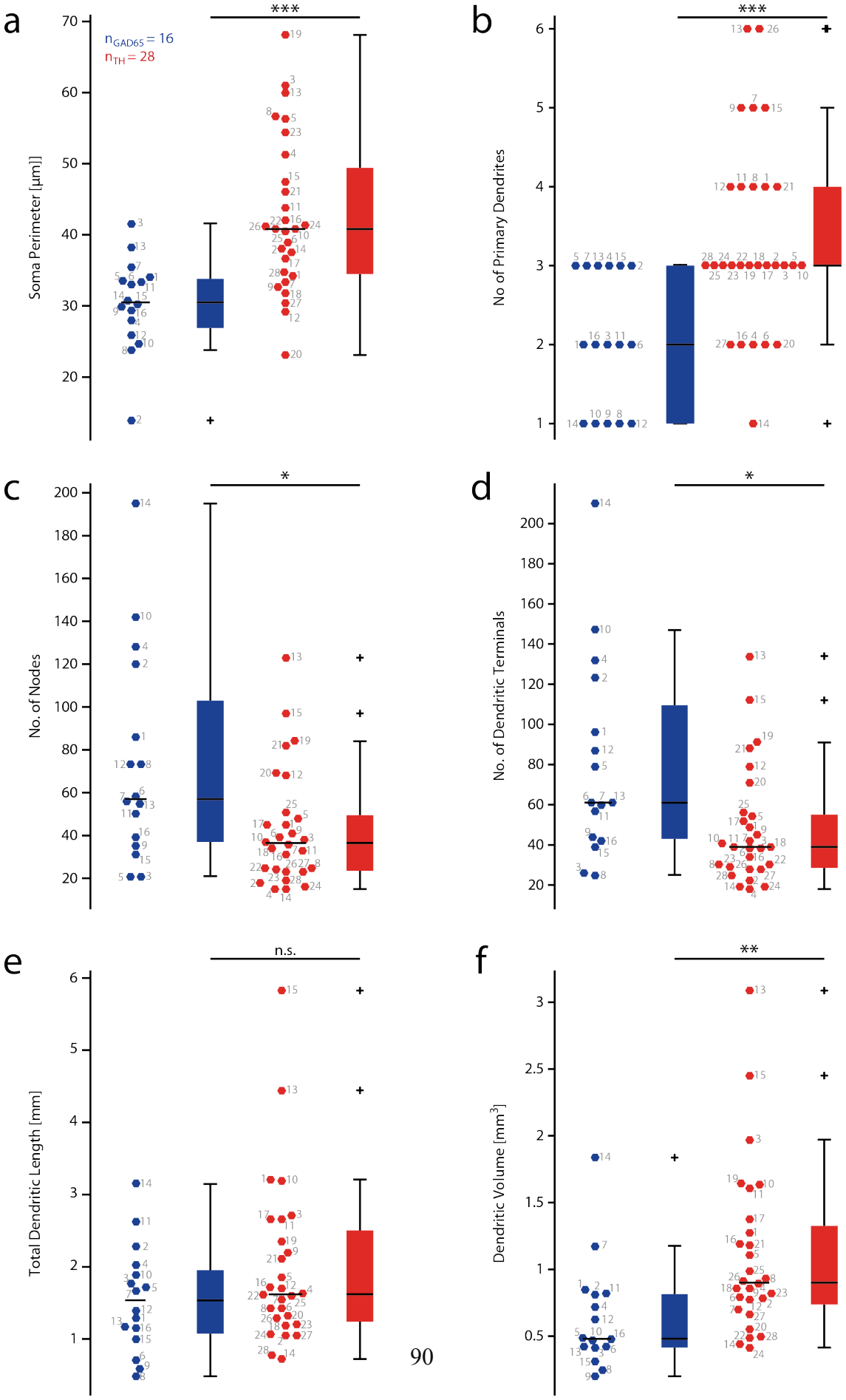
a
b
c
d
e
f
n_{GAD65} = 16
n_{TH} = 28
Soma Perimeter [µm]
No of Primary Dendrites
No. of Nodes
No. of Dendritic Terminals
Total Dendritic Length [mm]
Dendritic Volume [mm^3]
***
*
n.s.
**

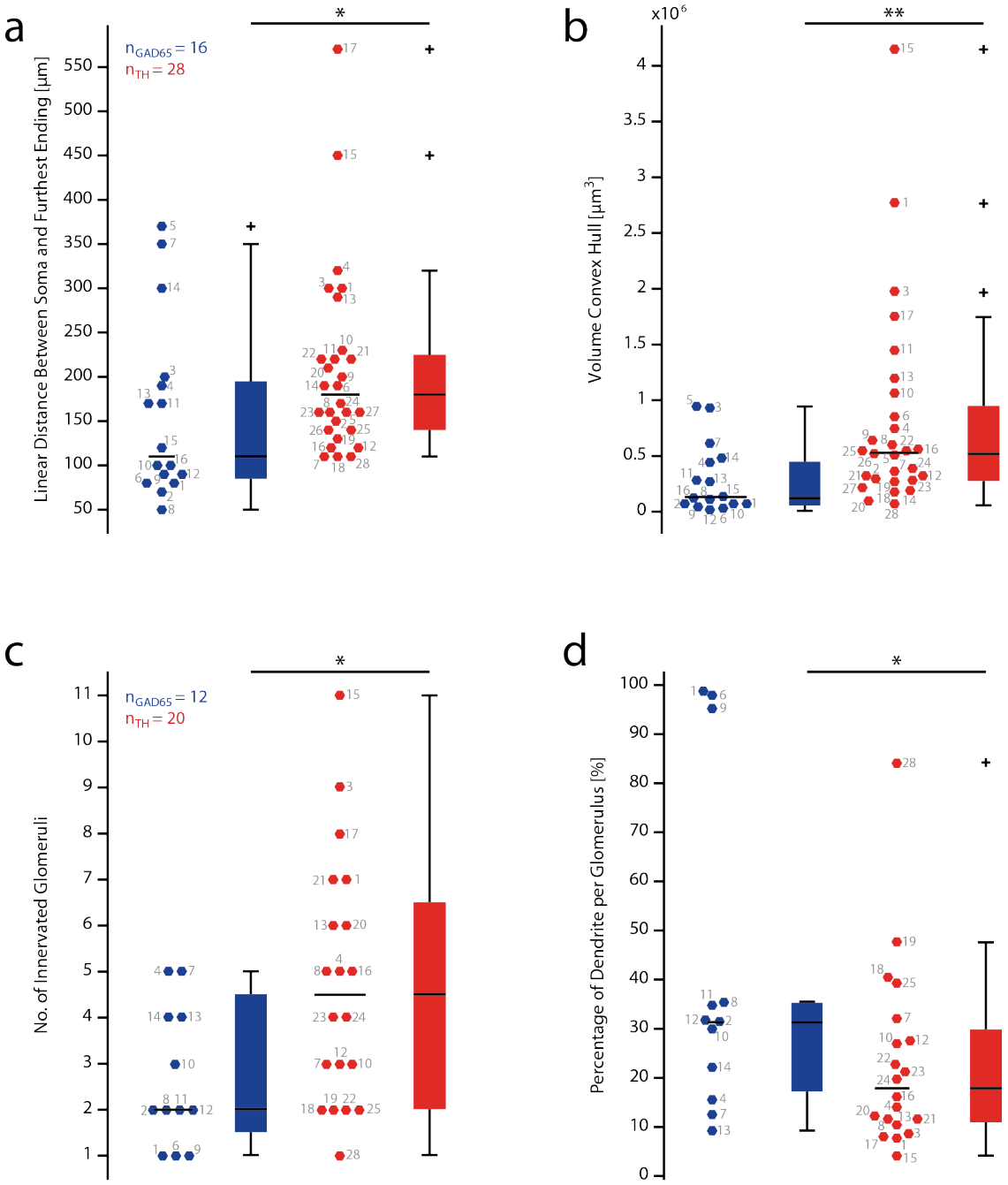

Figure 3.7 Differences in Dendritic Distance, Volume and Glomerular Innervation Between GAD65$^+$ and TH$^+$ Neurons

Comparative boxplots illustrating the differences in glomerular innervation between dendrites of GAD65$^+$ neurons (*blue*, n = 16 or n = 12) and TH$^+$ neurons (*red*, n = 28 or n = 20). Parameters plotted are **(a)** largest radius of a Sholl analysis, **(b)** innervated volume determined using Convex-Hull analysis, **(c)** number of innervated glomeruli and **(d)** average percentage of dendritic tree intersecting a single glomerulus. Numbered dots correspond to the numbered reconstructions in Figure 3.4 and Figure 3.5. Black horizontal bars indicate the median for each group. Significance levels of all properties were calculated with a Wilcoxon rank sum test; *: p-value < 0.05, **: p-value < 0.01.

On visual inspection, TH^+ neurons appeared to innervate larger areas of the glomerular layer (Figure 3.4 vs. Figure 3.5) and the similarity of both populations in overall dendritic length was therefore unintuitive. Hence, further analysis on complexity, spread and innervation pattern of dendritic trees was performed. When using the largest radius of a Sholl analysis as a measure for the linear distance between soma and the most distal dendritic ending, the dendrites of TH^+ neurons extended over a larger area than the dendrites of $GAD65^+$ neurons (linear $distance_{GAD65}$ = 110 µm (50-370) vs. linear $distance_{TH}$ = 180 µm (110-570), p_{median} = 0.038, Figure 3.7a).

A Convex-Hull analysis confirmed that TH^+ neurons innervated a significantly larger volume of the glomerular layer than $GAD65^+$ neurons ($volume_{GAD65}$ = 132 mm^3 (20-952) vs. $volume_{TH}$ = 529 mm^3 (68-4148), p_{median} = 0.004, Figure 3.7). This result indicated that individual TH^+ neurons innervated more glomeruli than individual $GAD65^+$ neurons.

Analysis of tracings containing a reconstruction of glomeruli surrounding a neuron of interest (n_{GAD65} = 12, n_{TH} = 20), confirmed a significant difference between the number of glomeruli innervated by the dendrites of $GAD65^+$ and TH^+ neurons ($glomeruli_{GAD65}$ = 2 (1 to 5) vs. $glomeruli_{TH}$ = 4.5 (1 to 11), p_{median} = 0.044, Figure 3.7c). Consistently, $GAD65^+$ neurons exhibited a higher percentage of their dendritic tree innervating a given glomerulus (dendrite per $glomerulus_{GAD65}$= 31% (9 to 98) vs. dendrite per $glomerulus_{TH}$ = 18% (4 to 84), p_{median} = 0.025, Figure 3.7d). Together with the larger number of terminals, these results illustrate that $GAD65^+$ neurons innervate fewer glomeruli than TH^+ neurons, but that those innervations are more dense and complex than TH^+ neurons.

3.2.4 Biophysical Characterisation of GAD65$^+$ and TH$^+$ Interneurons

Neuronal populations can have characteristic intrinsic biophysical properties, which can be used for classification purposes. To physiologically characterise the GAD65$^+$ and TH$^+$ population, an *I-V protocol* (Materials and Methods, section 2.3.6.1) was applied to each recorded neuron and RMP, input resistance and spiking threshold were determined (Figure 3.8). On a population level, significant differences in all three properties were found between GAD65$^+$ and TH$^+$ neurons, however the two populations were found to be overlapping in all three properties (Figure 3.9). TH$^+$ neurons exhibited a significantly lower and less variable RMP (RMP_{GAD65} = -66.4 mV (-80.6 to -45.6) vs. RMP_{TH} = -68.6 mV (-83.1 to -47.8), p_{median} = 0.0006, p_{var} = 0.0008, Figure 3.9a). On average, GAD65$^+$ neurons had a higher spiking threshold ($threshold_{GAD65}$ = -33.6 mV (-55.4 to -25.2) vs. $threshold_{TH}$ = -36.0 mV (-47.2 to -27.6), p_{median} = 6.62x10^{-5}, Figure 3.9b), distributed over a similar range in both populations (p_{var} = 0.519). In accordance with the literature, the smaller GAD65$^+$ neurons had significantly higher input resistances than TH$^+$ neurons (R_{GAD65} = 550 MΩ (207 to 1401) vs. R_{TH} = 333 MΩ (100 to 1087), p_{median} = 5.8x10^{-14}, p_{var} = 0.010, Figure 3.9c), but again, both populations showed overlap.

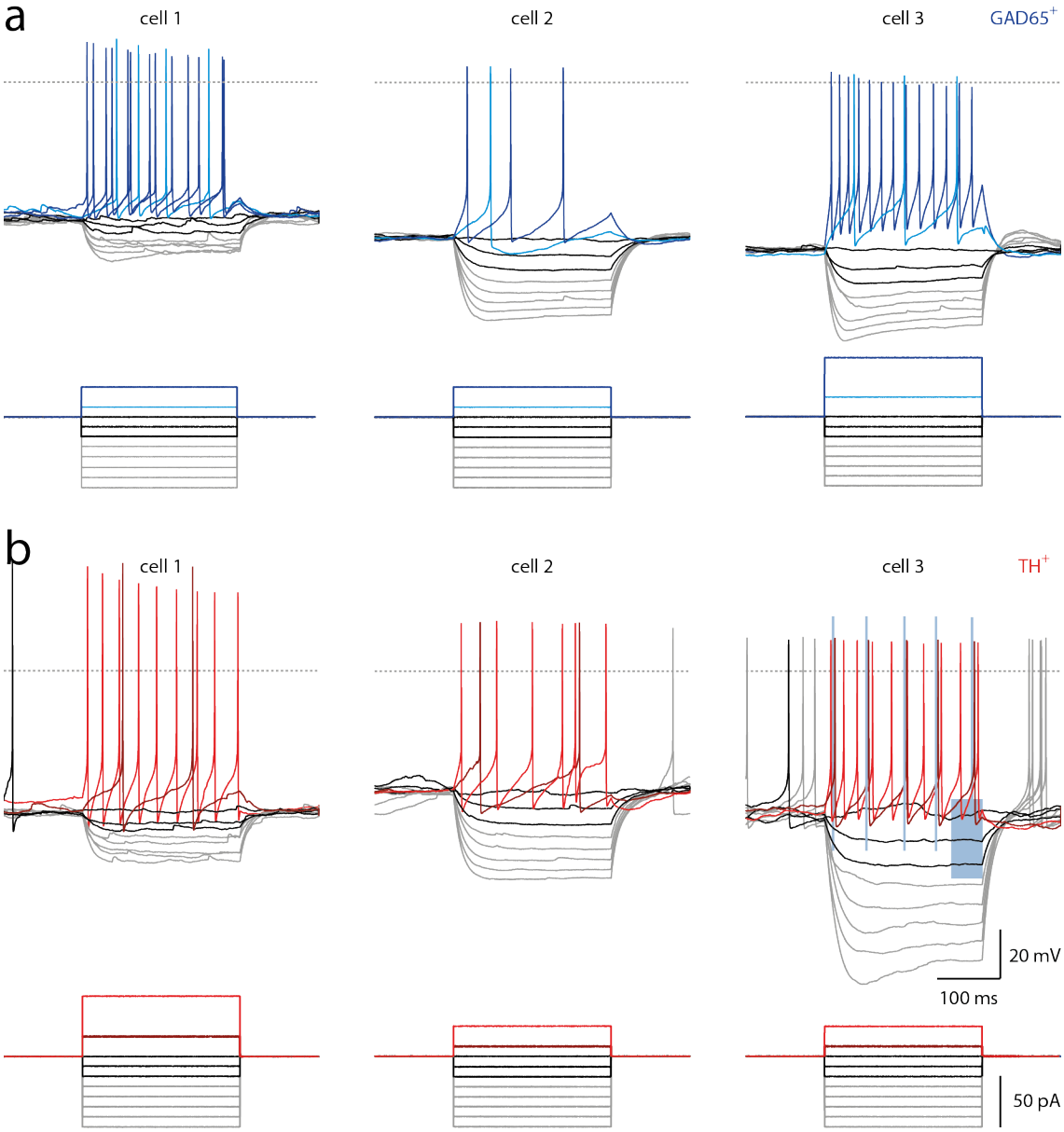

Figure 3.8 Example Current-Voltage Relations in GAD65$^+$ and TH$^+$ Neurons

(a) Membrane potential responses of three GAD65$^+$ neurons *(blue)* and **(b)** three TH$^+$ neurons *(red)* to current injections (*I-V protocol*), displayed under each current-clamp recording.
Both: Displayed are the responses to the first two hyperpolarising current steps and the step without any current injection *(black traces,)* the five most hyperpolarising current steps (*grey traces*;), the rheobase step *(dark read or light blue traces)* and the 300 % rheobase step *(blue or red traces)*. Grey dotted lines denote 0 mV. As indicated on the rightmost example trace of a TH$^+$ neuron, the input resistance was calculated from the average of the last 50 ms in the first two hyperpolarising current steps *(blue box)*. The RMP was determined by taking the average membrane potential at the no-current step *(black trace)* and the spike threshold was determined at rheobase in a 4 ms window before the detected spike *(vertical blue lines)*.

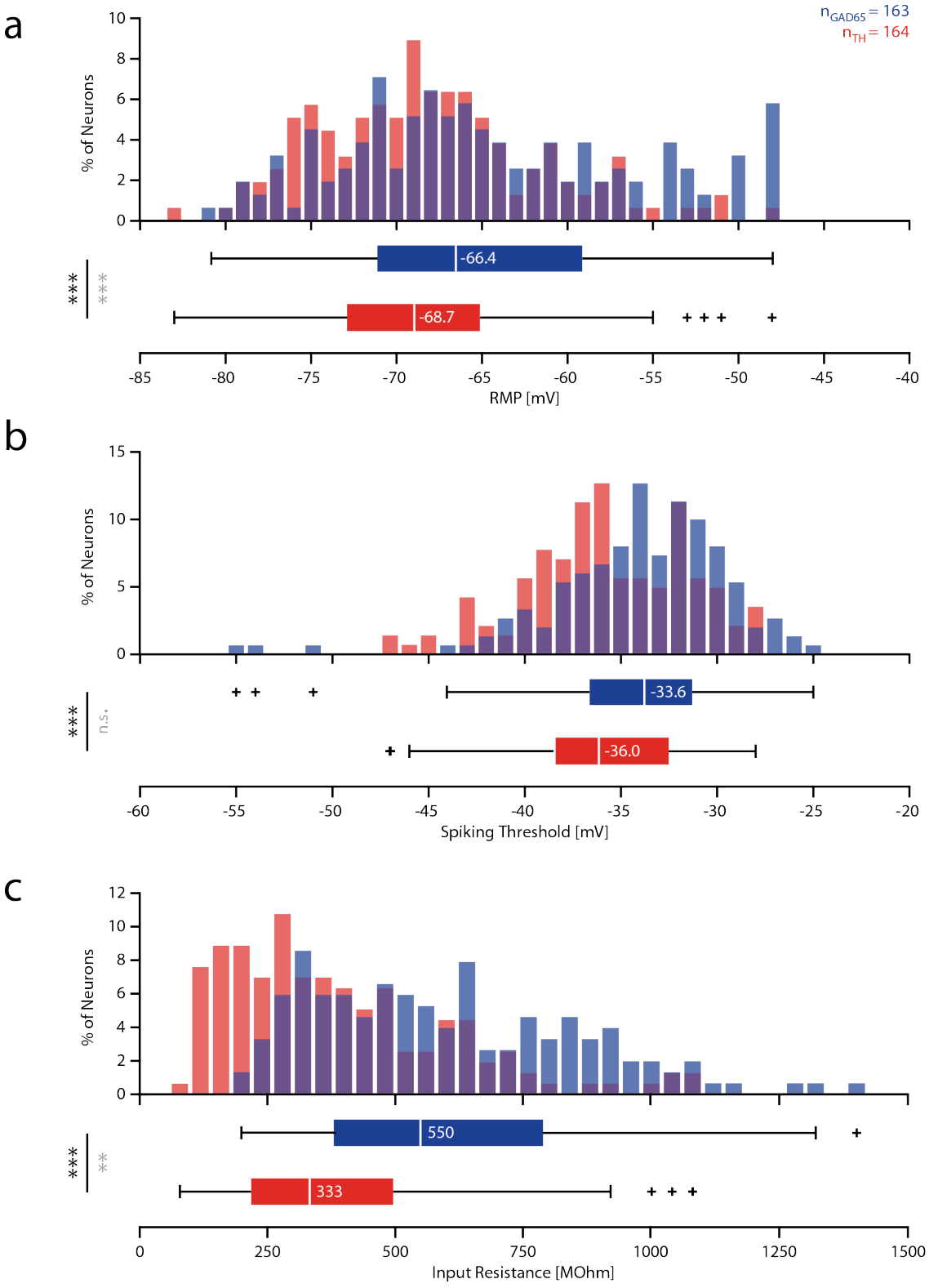

Figure 3.9 Physiological Properties of GAD65$^+$ and TH$^+$ Neurons

(a) Histogram and boxplot describing the distribution of RMP in GAD65$^+$ neurons (*blue*, n = 163) and TH$^+$ neurons (*red*, n = 164), recorded directly after gaining electrical access to the cell, without any holding current.

(b) Histogram and boxplot illustrating the significantly lower spiking threshold of $GAD65^+$ neurons compared to TH^+ neurons. Data points were calculated from the same recordings as in (a).
(c) Histogram and boxplot showing input resistance of $GAD65^+$ and TH^+ neurons.
RMP = resting membrane potential. Significance levels were determined by a Wilcoxon rank sum test for median *(black)* and a Brown–Forsythe test for variance *(grey)*; n.s. = not significant, ***: $p < 0.001$.

3.2.5 Occurrence and Physiological Relevance of Hyperpolarisation-Activated Cation Current in $GAD65^+$ and TH^+ Neurons

Hyperpolarisation-activated cyclic nucleotide-gated (HCN) channels occur in most principal neurons and many interneurons of the brain, and I_h has been shown to impact on neuronal information processing in many different brain areas (McCormick and Pape 1990; Hutcheon and Yarom 2000; Giocomo and Hasselmo 2009; Wahl-Schott and Biel 2009). Following hyperpolarisation, the voltage-gated opening of HCN channels causes influx of cations (I_h) into the neuron, which actively opposes the hyperpolarisation and drives the membrane potential back towards the resting value (Wahl-Schott and Biel 2009). This phenomenon can be observed in current-clamp mode as a sag in the membrane potential during depolarisation (Figure 3.10a). It has been shown for various different neuronal types that the amplitude of this sag correlates well with the amplitude of I_h.

3.2.5.1 The Sag Potential as a Proxy for Hyperpolarisation-Activated Cation Current

To confirm the correlation of I_h and sag potential amplitude (SPA) in $GAD65^+$ and TH^+ neurons, a 2-step experiment was conducted, in which the I_h was pharmacologically isolated with a cocktail of *synaptic and ion channel blockers* (Material and Methods, section 2.3.5) and subsequently blocked by additional application of 0.4 mM ZD7288. Subtraction of the currents recorded under these two conditions revealed the amplitude of I_h, which could be compared to the SPA, measured earlier under control conditions (Figure 3.10a, also see Material and Methods, sections 2.4.1 and 2.4.2).
Although $GAD65^+$ (n = 12) and TH^+ (n = 9) neurons exhibited a similar range of I_h amplitudes ($median_{GAD65}$ = -28.1 pA (-10.8 to -101.1) vs. $median_{TH}$ = -45.3 pA (-16.2 to -75.2); $p_{median} = 0.21$, $p_{variance} = 0.74$, Figure 3.10b left), the SPAs recorded in

the $GAD65^+$ population were on average larger and more variable than the SPAs recorded in the TH^+ population ($median_{GAD65}$ = 4.6 mV (0.0 to 22.0) vs. $median_{TH}$ = 1.1 mV (0.3 to 4.1); p_{median}= 0.02, $p_{variance}$= 0.0002, Figure 3.10b right). In both populations, the amplitudes of I_h and the membrane potential sag correlated well (R=-0.73, $p_{GAD65} < 0.01$ and $p_{TH} < 0.05$, Figure 3.10c), indicating that the SPA recorded in current-clamp mode can be used to estimate the I_h amplitude in these cell types.

Figure 3.10 Correspondences of I_h and Membrane Potential Sag (next page)

(a) Example voltage-clamp recordings of pharmacologically isolated ZD7288-sensitive current in a $GAD65^+$ *(blue)* and TH^+ *(red)* neuron (*top*, average of five traces) and the corresponding SPAs recorded in current-clamp mode (*bottom*, average of three traces). **(b)** Boxplots visualising the distribution of I_h *(left)* and SPA *(right)* in $GAD65^+$ (*blue*, n = 12) and TH^+ (*red*, n = 9) neurons. While the I_h is similar in both neuronal populations, the SPA is significantly bigger and more diverse in $GAD65^+$ neurons.
(c) Correlation between the amplitude of I_h and SPA in the $GAD65^+$ and TH^+ population. Open circles correspond to the example traces in (a). Significance levels were determined by a Wilcoxon rank sum test for median *(black)* and a Brown–Forsythe test for variance *(grey)*; n.s. = not significant, *: p-value < 0.05, ***: p < 0.001.

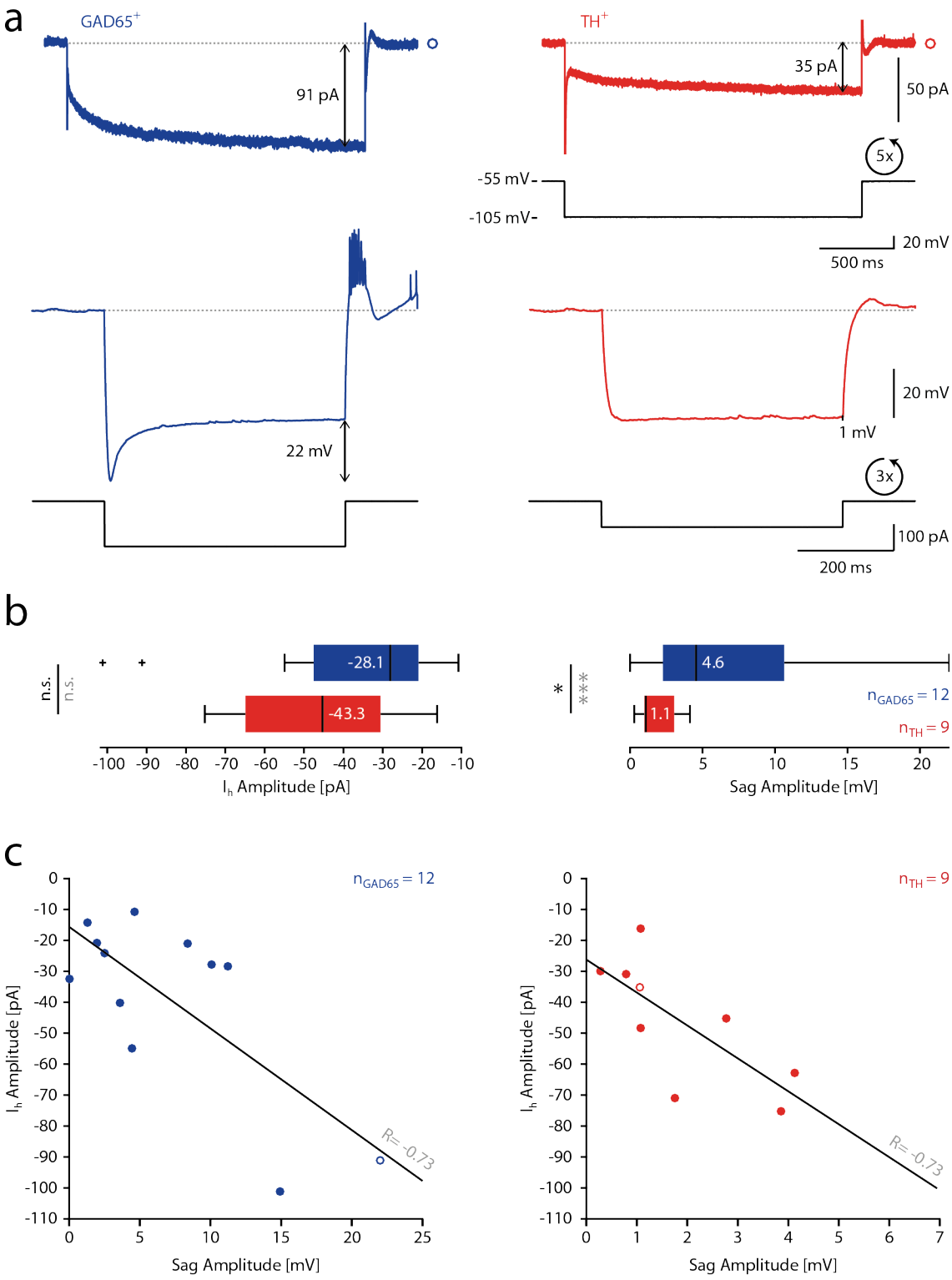

Figure 3.10 Correspondences of I_h and Membrane Potential Sag

3.2.5.2 The Impact of ZD7288 Application on Input Resistance and Firing Properties of GAD65$^+$ and TH$^+$ Neurons

To investigate the potential physiological significance of I_h in GAD65$^+$ and TH$^+$ neurons, whole-cell recordings in current-clamp mode (*I-V protocol*, see Table 2-2 and section 2.3.6) were performed in the absence and presence of ZD7288.

Five minutes after perfusion of the tissue with ZD7288 the I_h-mediated SPA was completely abolished (Figure 3.11a and b), resulting in a more linear relationship between hyperpolarisation peak and steady-state potential in GAD65$^+$ neurons (Figure 3.11b, blue vs. black trace). Therefore, all measurements under the influence of the ion channel blocker were made at least five minutes after initiation of perfusion with ZD7288. In the presence of ZD7288, GAD65$^+$ neurons exhibited a significant increase in input resistance ($R_{control}$ = 525 ± 105 MΩ vs. R_{ZD7288} = 779 ± 101 MΩ, p_{median} = 0.011, Figure 3.11c). In TH$^+$ neurons, only a small trend towards increased input resistance was observed ($R_{control}$ = 261 ± 105 MΩ vs. R_{ZD7288} = 336 ± 168 MΩ, p_{median} = 0.301, Figure 3.11c). When analysing recordings in GAD65$^+$ neurons, which exhibited rebound spiking in control conditions after the end of a hyperpolarisation (n = 7), a significant impact of ZD7288 on the probability of generating rebound action potentials could be observed (rebound $spike_{control}$ = 60 ± 26 % vs. rebound $spike_{ZD7288}$ = 22 ± 26 %, p_{median} = 0.018, Figure 3.11d). Because only two TH$^+$ neurons exhibited rebound spiking under control conditions, no analysis of rebound spiking probability was conducted in this chemotype. Furthermore, when GAD65$^+$ neurons under ZD7288 blockade were depolarised with increasingly positive current injections, they failed to reliably fire action potentials at current injections higher than 30 pA. However, under control conditions they could increase their firing frequency in response to increasingly depolarising current injections up to 110 pA and this difference between control condition and ZD7288 blockade was overall significant (repeated measures ANOVA, p_{GAD65} = 2.6 x 10^{-6}, Figure 3.11e, left). In TH$^+$ neurons the F-I curve was not significantly different under ZD7288 blockade compared to normal condition, (repeated measures ANOVA, p_{TH} = 0.31, Figure 3.11e, right). However, the difference between the GAD65$^+$ and TH$^+$ population in regards to ZD7288 influence on average firing rate was not significant (two-way repeated measures ANOVA, p = 0.12). All p-values were Greenhouse-Geisser adjusted to correct for lack of compound symmetry.

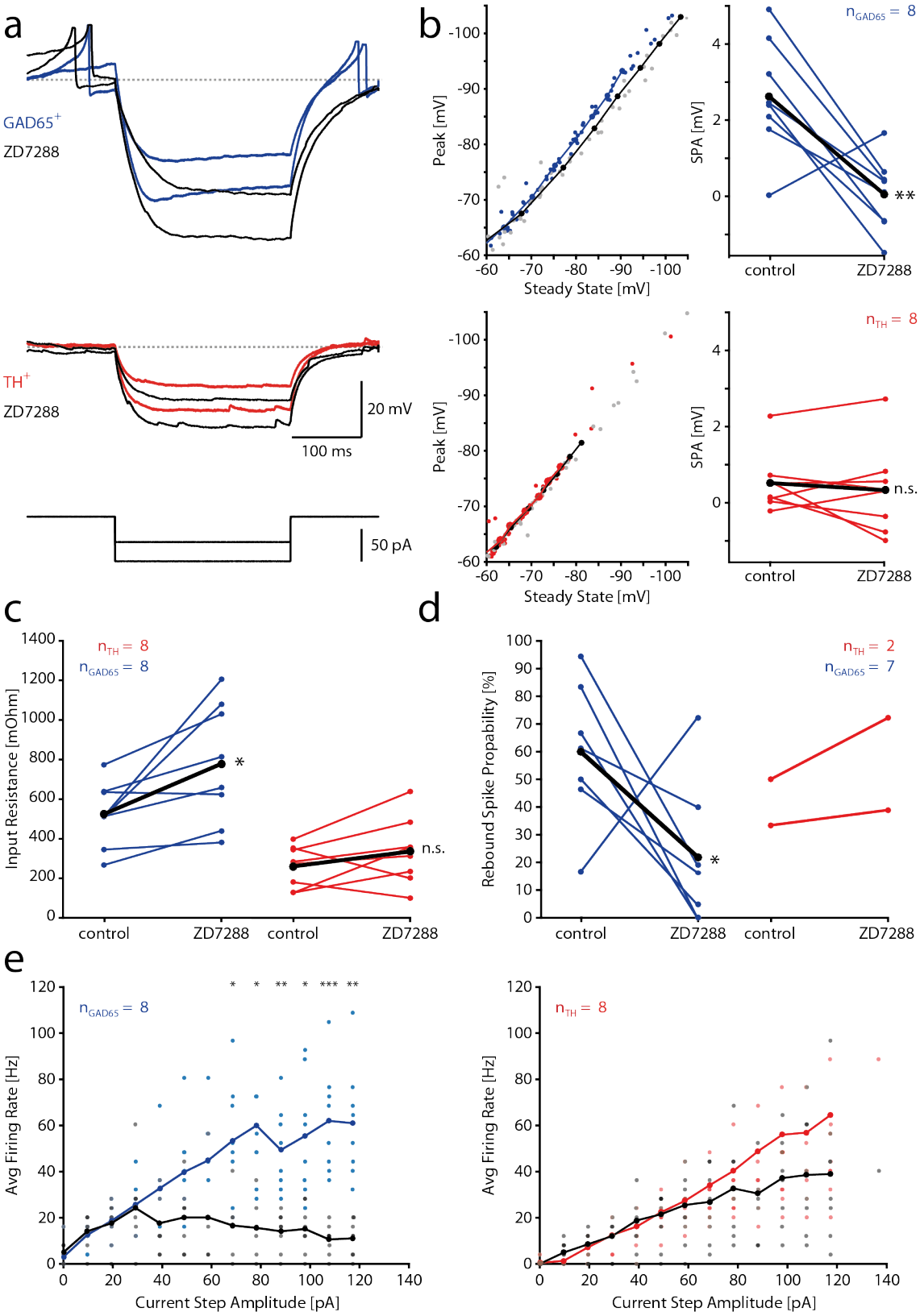

Figure 3.11 The Physiological Impact of ZD7288 Application on GAD65$^+$ and TH$^+$ Neurons

Figure 3.11 The Physiological Impact of ZD7288 Application on GAD65$^+$ and TH$^+$ Neurons (cont.)
(a) Example membrane voltage traces of a GAD65$^+$ *(blue)* and a TH$^+$ *(red)* neuron, recorded under control conditions and after bath application of HCN channel blocker ZD7288 *(black traces)*. Action potentials were clipped for visualisation. Neurons were held at a membrane potential of 53.5 ± 4.5 mV and test current steps were applied (example current steps of -40 pA and -70 pA, *black traces at bottom*).
(b) *left:* Plots showing the relation between peak and steady-state voltage during a hyperpolarising step in GAD65$^+$ *(blue)* and TH$^+$ *(red)* neurons. In GAD65$^+$ neurons, the SPA appeared to be voltage-dependent, with sag amplitudes increasing upon stronger hyperpolarisation. *right:* SPA of GAD65$^+$ *(blue)* and TH$^+$ *(red)* neurons, recorded under control conditions and after bath application of HCN channel blocker ZD7288 *(black traces)*. The mean is shown with a black line.
(c) Input resistance before and after bath application of ZD7288 in the same eight GAD65$^+$ and TH$^+$ neurons as in (b). Mean is illustrated with a black line.
(d) Spike occurrence in GAD65$^+$ neurons with and without ZD7288, 0 - 125 ms after the end of the hyperpolarising step. Mean of GAD65$^+$ neurons is illustrated with a black line. Only two TH$^+$ neurons exhibited rebound spiking under control conditions, and no statistical analysis was performed on this dataset.
(e) Relationship of average firing rate and current step amplitude in the same GAD65$^+$ and TH$^+$ neurons as in (b) and (c), without *(blue and red trace)* and with *(black trace)* pharmacological block of I_h via ZD7288; Significance was determined by repeated measures ANOVA and post-hoc test (t-test, Holm-Bonferroni corrected); n.s. = not significant, *: p-value < 0.05, **: p-value < 0.01, ***: p-value < 0.001.

3.2.5.3 The Dependency of I_h-mediated Sag Potential on Experimental Conditions and Input Resistance

The amplitude of I_h, and therefore membrane potential sag, depends heavily on factors like second messengers, temperature, pH and strength of hyperpolarisation (see section 1.3.1). The SPA was therefore measured under controlled recording conditions, including a bath temperature of 35 ± 1.5 °C, an internal solution with a pH of 7.28 ± 0.1, a holding potential at 53.5 ± 4.5 mV, hyperpolarisation to a steady-state potential of 95 ± 5 mV and a time window of no more than five minutes for determining the SPA (see Materials and Methods, section 2.3.6.1). In addition to the strict adherence to recording conditions for measuring the SPA, several analyses were conducted to validate the independence of the SPA from experimental parameters within the predefined recording conditions. No correlations were found for the GAD65$^+$ and TH$^+$ populations individually or for the pooled dataset: No effect of the age of the animal (three to seven weeks) on the SPA could be determined (R_{GAD65} = -0.112, p_{GAD65} = 0.156 and R_{TH} = 0.079, p_{TH} = 0.317; Figure 3.12a). Furthermore, the SPA was not

dependent on the bath temperature (R_{GAD65} = 0.035, p_{GAD65} = 0.658 and R_{TH} = -0.029, p_{TH} = 0.107; Figure 3.12b) and no correlation was found between input resistance and the SPA under these defined recording conditions (R_{GAD65} = -0.211, p_{GAD65} = 0.009 and R_{TH} = -0.147, p_{TH} = 0.065; Figure 3.12c). Finally, the SPA did not change systematically in consecutive recordings from different neurons over the time course of a day (R_{GAD65} = 0.124, p_{GAD65} = 0.156 and R_{TH} = -0.034, p_{TH} = 0.680; Figure 3.12d).

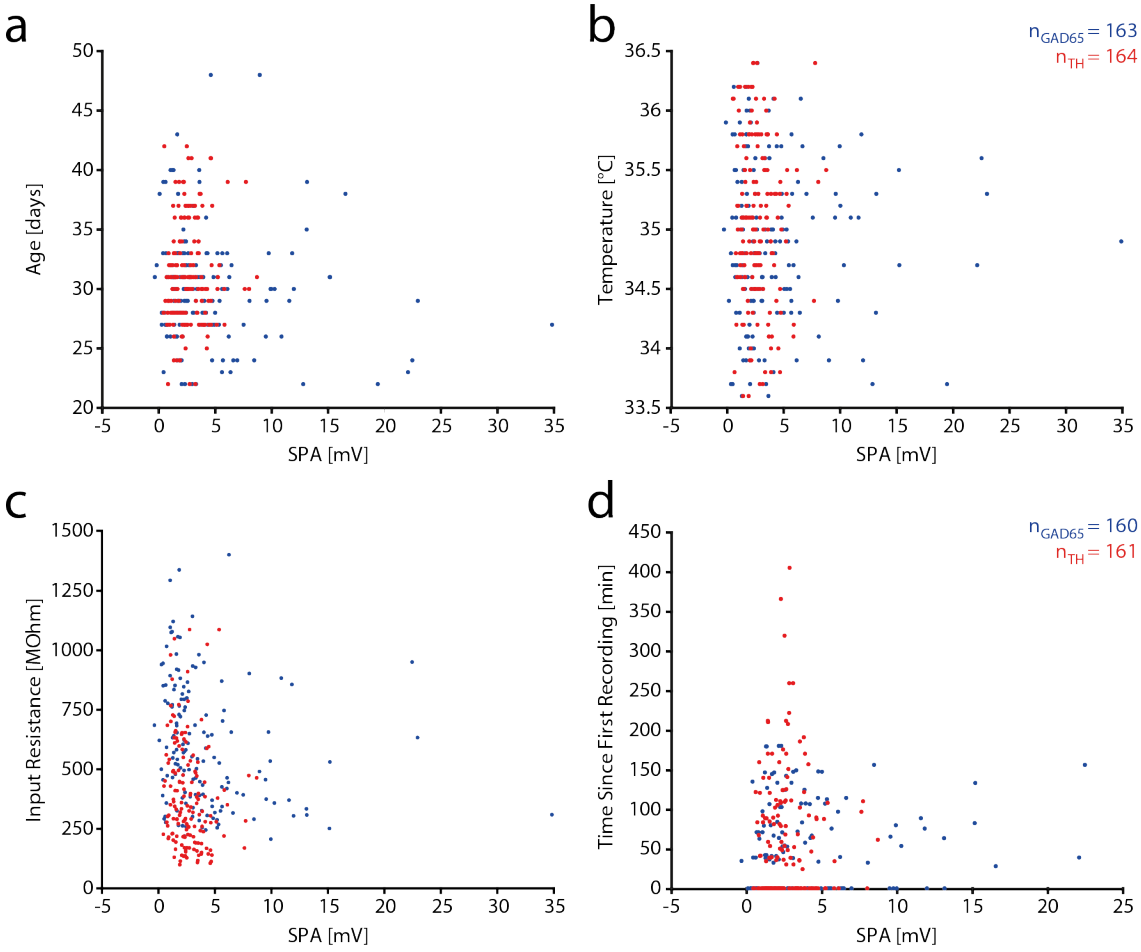

Figure 3.12 The SPA Measured Across a Range of Experimental Parameters

Scatter plots illustrating in both GAD65$^+$ *(blue)* and TH$^+$ *(red)* neurons the relationship between SPA and

(a) the age of animals (three to seven weeks).

(b) the bath temperature (within the used range of 33.5 to 36.5 °C).

(c) the input resistance.

(d) the age of the prepared tissue. Within each experiment, the beginning of the first recording was used as time point zero.

3.2.5.4 The Distribution of Sag Potential Amplitude in the GAD65$^+$ and TH$^+$ Population

To quantify the distribution of SPA in the GAD65$^+$ and TH$^+$ populations, a *hyperpolarisation step protocol* (Table 2-2 and Figure 2.2) with three negative current steps in increments of -5 mV was repeatedly applied to each neuron, whereby the amplitudes of the current steps were adjusted to hyperpolarise each neuron to a steady state membrane potential within the given range of 95 ± 5 mV (Figure 3.13a, top right). The difference between the peak of the hyperpolarisation during the first 250 ms of the step and the steady-state membrane potential during the last 100 ms of the step was used to determine the SPA of each neuron (Figure 3.13a, blue bars and black arrow). These current-clamp recordings of GAD65$^+$ and TH$^+$ neurons revealed a broad range of SPAs in GAD65$^+$ neurons, but a narrow distribution in TH$^+$ neurons (Figure 3.13b). On average, the SPA of GAD65$^+$ neurons was significantly greater than that recorded in TH$^+$ neurons and the GAD65$^+$ population exhibited a significantly larger variance in SPAs than the TH$^+$ population (median$_{GAD65}$ = 2.7 mV (-0.4 to 34.8) vs. median$_{TH}$ = 2.4 mV (-0.4 to 8.7), p_{median} = 0.03, $p_{variance}$ = 4.24x10^{-7}, Figure 3.13b). Both populations were not normally distributed (Lilliefors test, $p_{GAD65} < 0.001$ and $p_{TH} < 0.01$), with a skewed extension towards bigger SPAs (Figure 3.13b).

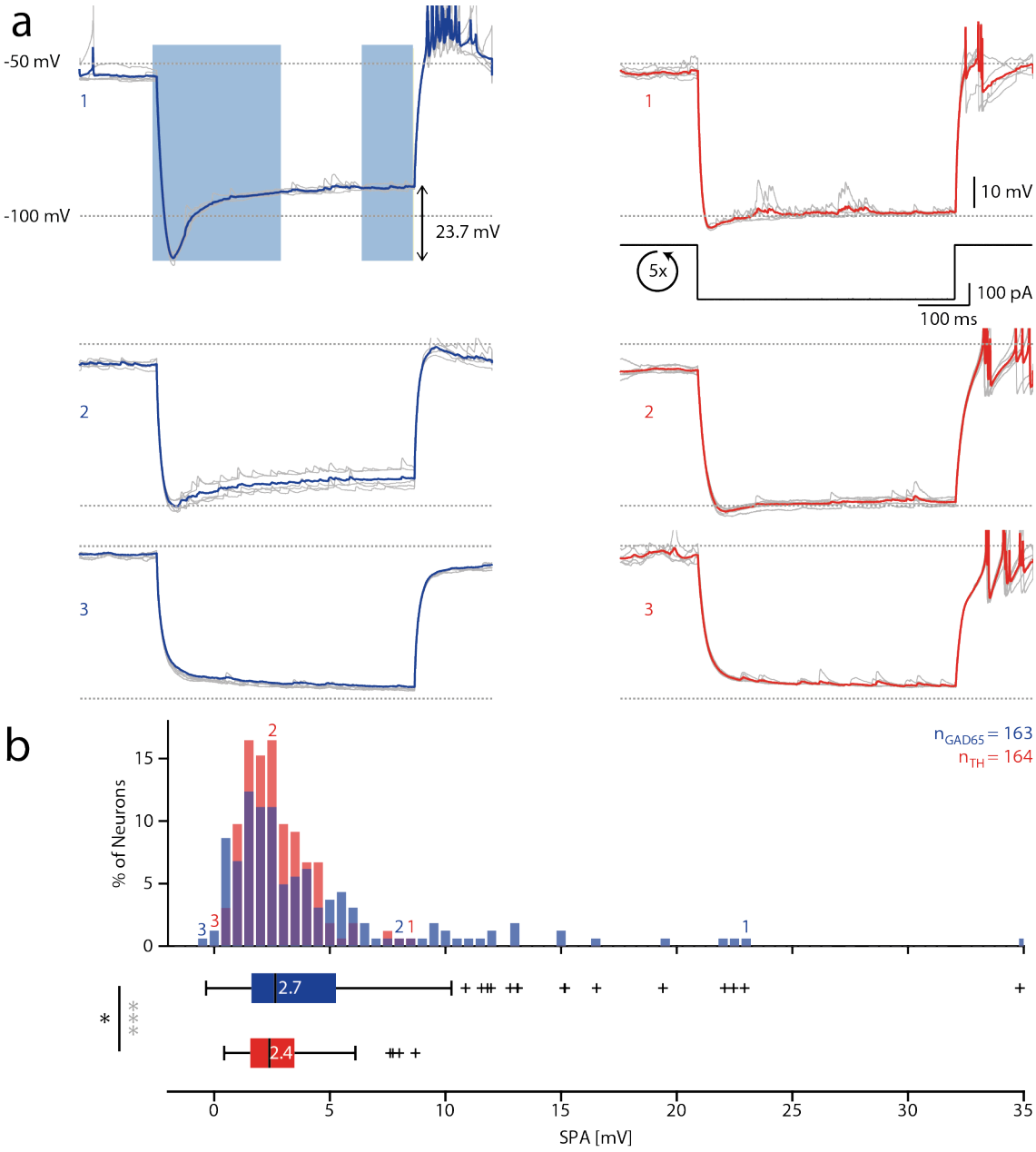

Figure 3.13 Diversity of Membrane Potential Sag in GAD65$^+$ and TH$^+$ Neurons

(a) Representative current-clamp recordings from three GAD65$^+$ *(blue)* and TH$^+$ *(red)* neurons. Blue and red traces are the average of five hyperpolarising steps from a neuron's holding potential at 53.5 ± 4.5 mV to a hyperpolarised steady-state potential of 95 ± 5 mV *(dashed grey lines)*. Numbers correspond to the numbered bins in (b). SPA *(black arrow in first GAD65$^+$ neuron)* was calculated as the voltage difference between the peak hyperpolarisation in the first 250 ms after the current step onset *(left blue box)* and the average steady-state membrane potential at the last 100 ms of the current step *(right blue box)*. Action potentials have been clipped for display clarity.
(b) Histogram and boxplot showing the distribution of SPA in GAD65$^+$ *(blue)* and TH$^+$ *(red)* neurons. Significance levels were determined by a Wilcoxon rank sum test for median *(black)* and a Brown–Forsythe test for variance *(grey)*; *: p-value < 0.05, ***: p < 0.001.

3.3 Discussion

Classification of the glomerular interneuron population is an ongoing endeavour, with a wide range of morphological, molecular and electrophysiological classification approaches being applied (Nagayama et al. 2014). To explore the functional relevance of glomerular circuits, it is important to understand the diversity of the population of neurons conventionally classified as JG cells. This chapter provides a characterisation of the two molecularly defined interneuron populations, $GAD65^+$ and TH^+ that include a comparative analysis of their morphological and physiological features. Furthermore, the results presented here suggest that targeting subsets of GABAergic and dopaminergic interneurons using transgenic mice expressing tdTomato and tagRFP under the control of the GAD_{65} and TH promoter, provides a reliable way of targeting morphological and physiological subclasses of OB interneurons. These classes may correspond to a certain extent to PG and SA cells and are likely functionally different.

3.3.1 Cell Classification

3.3.1.1 Immunohistochemistry

Using neurochemical markers seems the most reliable way of targeting subpopulations of heterogeneous JG interneurons across different animals and experiment types.
Because the transgenic mouse line labelling TH-expressing neurons (TH(9.0)tagRFP) was produced within the laboratory, a validation was performed by counterstaining with TH-antibody, to address the specificity of fluorescent labelling. With a conservative counting, in which only cells with an unambiguous fluorescence were considered as positively stained, 76 % of the genetically labelled neurons in the TH(9.0)tagRFP line were identified as immuno-reactive to the TH antibody. Unfortunately, this result could not be directly compared to the original protocol (Min et al. 1994), since the authors did not quantify their false positive and negative labelling. It is important to acknowledge that TH expression has been shown to be activity-dependent, with stronger TH expression in highly active neurons (Baker et al. 1983; Cigola et al. 1998; Parrish-Aungst et al. 2011; Banerjee et al. 2013). The ongoing fluctuation of TH expression likely impacts these data, making it difficult to quantify overall TH expression levels at a single time point. However this result, together with the fact that 31 % of the immuno-

reactive cells were not genetically labelled, indicates that fluorescent labelling in the TH(9.0)tagRFP mouse line is potentially not comprehensive, but may be restricted to a subpopulation of TH-expressing neurons. Also, it is important to note that since the expression of tagRFP is driven by the promoter for TH, the 24% of genetically labelled neurons in the TH(9.0)tagRFP line, which did not exhibit immuno-reactivity to the TH antibody, could be due ectopic tagRFP expression.

The 15 % overlap of fluorescent labelling between TH^+ neurons identified via antibody staining and $GAD65^+$ neurons in a Gad2-IRES-Cre-tdTomato animal was similar to previously reported overlap between these two populations of neurons (Parrish-Aungst et al. 2007; Kiyokage et al. 2010), confirming that it is possible to target two mostly distinct populations of glomerular interneurons by using these two chemotypes.

It is worth noting that the molecular identity of $GAD65^+$ neurons in particular may still be heterogeneous, because this population has been shown to co-express several other molecular markers, including a variety of calcium-binding proteins. To my knowledge, no publications further subdivided the group of $GAD65^+$ interneurons and so far no functional differences were established between subtypes of $GAD65^+$ JG cells.

Although other molecular markers have been reported to label non-overlapping populations of JG cells (for instance TH, Calbindin, calretinin and parvalbumin; Parrish-Aungst et al. 2007), the chemotypes GAD_{65} and TH were selected for their abundant occurrence in the glomerular layer and their described overlap with the morphologically defined PG cell and SA cell populations.

3.3.1.2 Morphometry

Several publications (Aungst et al. 2003; Shao et al. 2009; Kiyokage et al. 2010) suggest that the morphology of $GAD65^+$ neurons resembles the morphology of classic PG cells, which was initially described by Pinching and Powell 1971a. TH^+ neurons appear to have a more diverse morphology, with at least two morphologically distinct subtypes (Halasz et al. 1981; Kosaka and Kosaka 2009; Kosaka and Kosaka 2011; Chand et al. 2015), however the morphology of both types has been suggested to resemble SA cell morphology (Kiyokage et al. 2010).

In this chapter, reconstructions performed on $GAD65^+$ and TH^+ neurons after whole-cell recordings were used to further characterise the population. For all measured

morphological parameters, some overlap between the $GAD65^+$ and TH^+ populations could be seen, but the two populations exhibited significant differences in their median parameter values.

The soma sizes of all reconstructed neurons were estimated using the perimeter of the soma instead of the soma diameter, because TH^+ neurons in particular often exhibited rather elongated somata. When converting the soma perimeter to diameter ($GAD65^+$ neurons: 30.35 µm (perimenter) = 9.7 µm (diameter); TH^+ neurons: 42.57 µm (perimeter) = 13.6 µm (diameter); assuming circularity), the calculated average diameters of both chemotypes match previously published soma diameters of $GAD65^+$ and TH^+ neurons ($soma_{GAD65}$ = 7-11 µm and $soma_{TH}$= 6-14 µm; Parrish-Aungst et al. 2007; Kosaka and Kosaka 2009; Shao et al. 2009), as well as morphologically identified PG and SA cells ($soma_{PG}$: 5-8 µm and $soma_A$: 8-12 µm; Pinching and Powell 1971a; Hayar et al. 2004a). Surprisingly, no bimodal distribution in the soma sizes of TH^+ neurons was observed, but rather a continuum from small and large somata. Several publications distinguish TH^+ neurons into two distinct subpopulations based on their soma sizes (Halasz et al. 1981; Baker et al. 1983; McLean and Shipley 1988). These subpopulations differ in their development (McLean and Shipley 1988), turn-over (Kosaka and Kosaka 2009) and occurrence of an axon (Chand et al. 2015), however no further classification could be performed based on the dataset described in this chapter.

Axons were identified based on morphological appearance, as described in Materials and Methods (sections 2.7.3). It can be challenging to unambiguously identify a JG axon without immunohistochemical stainings, because not all JG cells have axons (Pinching and Powell 1971a) and if they do have an axon, it can branch from a dendrite instead of the soma (Kosaka and Kosaka 2011). It has also been reported that the morphology of some dendrites can resemble that of axons (Kiyokage et al. 2010; Kosaka and Kosaka 2011). Therefore, whenever an axon could be identified based on morphological criteria, it was excluded from the quantification, resulting in morphological analysis of the dendritic tree. The processes of all reconstructed neurons were located within the glomerular layer and did not project to higher brain areas, a defining characteristic for local interneurons.

The median number of primary dendrites significantly varied between the two chemotypes, as reported previously (Hayar et al. 2004a; Shao et al. 2009; Kiyokage et

al. 2010). Despite the smaller number of primary dendrites, $GAD65^+$ cells exhibited more branching points and more terminals while having the same average dendritic length, indicating a more convoluted innervation pattern compared to TH^+ neurons. It is worth noting that some dendritic terminals are likely not natural endings, but artefacts caused by brain slicing. However, the dendrites of $GAD65^+$ neurons extended on average over shorter distances and ramified in significantly smaller volumes than the dendrites of TH^+ neurons, a pattern that has been previously observed and that supports the idea of $GAD65^+$ neurons receiving the bulk of their input from only one or two local glomerular networks (Shao et al. 2009; Kiyokage et al. 2010).

When quantifying the number of innervated glomeruli, a clear difference between $GAD65^+$ (average of two glomeruli) and TH^+ neurons (average of five glomeruli) was discovered, which resembles previous descriptions of the mostly uniglomerular innervation pattern of PG cells and the innervation of three to four glomeruli by SA cells (Aungst et al. 2003; Hayar et al. 2004a). Also, in $GAD65^+$ neurons significantly larger parts of the dendritic tree ramified within a single glomerulus compared to TH^+ neurons (32 % vs. 17 %). For a more detailed analysis of innervated areas within the glomeruli, for example to correlate the $GAD65^+$ population to type-I and type-II PG cells or to investigate whether similarly diverging innervation patterns exist for SA cells, a more precise 3D-reconstruction of the glomerular structures will be necessary.

Surprisingly, the largest number of glomeruli innervated by a TH^+ neuron was 12. This is a much more restricted innervation pattern than what has been described for polyglomerular $TH^+/GAD67^+$ SA-like cells (Kiyokage et al. 2010), which innervate on average 40 glomeruli. One reason might be the inevitable truncation of some processes during the tissue preparation into 350 µm thick slices. More extensive dendritic ramifications are more likely to be truncated and therefore removed from the dataset, because of incomplete reconstruction. However, the publication describing extensive processes of $TH^+/GAD67^+$ neurons explicitly includes both dendrites and axons in their analysis. Therefore, an alternative explanation might be that these far-spreading connections are actually made by the axons of $TH^+/GAD67^+$ neurons and not their dendrites. Further experiments, including post-fixation staining for axonal markers would be necessary to reveal the precise glomerular innervation pattern of dendrites and axons in TH^+ neurons, but these were beyond the scope of this thesis.

Unfortunately, it was not possible to subdivide the TH^+ population into the two clear morphological subtypes suggested by several publications (Baker et al. 2001; Kosaka and Kosaka 2009; Kiyokage et al. 2010; Chand et al. 2015). Using the same classification parameters (soma size, dendritic length and spread) did not reveal a bimodal distribution, but rather a single widespread, continuous range. However, all named publications used additional parameters, such as co-expression of other marker molecules (Baker et al. 2001), occurrence of an AIS (Chand et al. 2015), time of origin (Kosaka and Kosaka 2009) or arbitrary thresholds (Kiyokage et al. 2010) to distinguish TH subpopulations. It is therefore possible that soma size and dimensions of dendritic arborisation are continuously distributed within the TH population, but tend to correlate with certain features of TH subpopulations and can therefore only used in combination with these features (which were not given in the presented experiments) to sub-classify the TH population.

To summarise, the $GAD65^+$ and TH^+ chemotypes overlap in their morphology and innervation patterns, but are on average significantly different. $GAD65^+$ neurons exhibited a rather dense and complex dendritic tree, potentially receiving and processing sensory information predominately from only one or two glomeruli. In contrast, TH^+ neurons seem to average information from several different glomeruli from a larger area of the glomerular layer, potentially distributing the computed information to widely spread target neurons, participating in different local networks.

3.3.1.3 Passive Biophysical Properties

Intrinsic biophysical properties have a critical impact on the computations a neuron performs (Marder and Goaillard 2006). The composition of ion channels underlying these properties is unique for each neuron and it has been shown that chemically and morphologically homogeneous populations of neurons can exhibit substantial biophysical diversity (Mason and Larkman 1990; Padmanabhan and Urban 2010; Angelo and Margrie 2011). Both, $GAD65^+$ and TH^+ neurons exhibited rather heterogeneous passive physiological properties. Consistent with the literature, $GAD65^+$ neurons have a more depolarised average RMP and spike threshold than TH^+ neurons, but the range of both properties overlapped strongly between neurons of the two chemotypes (Puopolo and Belluzzi 1998a; Smith and Jahr 2002; Hayar et al. 2004a;

Puopolo et al. 2005; Pignatelli et al. 2013; Parsa et al. 2015). PG cells have been reported to feature higher input resistances than SA cells, which was consistent with the data from $GAD65^+$ and TH^+ neurons (Figure 3.9c). However, the absolute input resistances measured here were slightly lower than literature values for both PG and $GAD65^+$ cells, which have been reported to be between 600 MΩ and 1 GΩ (Puopolo and Belluzzi 1998a; McQuiston and Katz 2001; Hayar et al. 2004a; Hayar et al. 2004b; Murphy et al. 2005; Shao et al. 2009; Pignatelli et al. 2013). The discrepancy between the present results and literature values might be caused by different analysis approaches or experimental conditions, such as the composition of internal solution and use of pharmacological blockers. It is rather difficult to compare the methods for calculating input resistances, since most publications did not specify how they calculated this parameter. However it is worth noting, that several publications used pharmacological ion channel blockers in their internal or external solutions (Puopolo and Belluzzi 1998a; Murphy et al. 2005; Parsa et al. 2015), which very likely caused an increase in input resistance. Nevertheless, input resistances in interneurons were still significantly higher than typical input resistances obtained for OB principal neurons (Hayar et al. 2004a; Liu and Shipley 2008a; Angelo and Margrie 2011; Tatti et al. 2014). Some extreme values, like a SPA larger than 10 mV or input resistance larger than 1 GΩ, could be used as a signature for $GAD65^+$ neurons, but without further context these properties are insufficient to reliably classify glomerular interneurons, because both populations largely overlap in these measured biophysical properties.

3.3.2 Sag as a Proxy for Hyperpolarisation-Activated Cation Current

It is commonly accepted that the SPA is a signature of the functional expression of HCN channels (Robinson and Siegelbaum 2003; Wahl-Schott and Biel 2009). The correlation between SPA and amplitude of I_h was confirmed by changing from current-clamp mode to voltage-clamp mode during the same recording after perfusion of the bath with an I_h isolating cocktail. Interestingly, similar ranges of I_h elicited significantly bigger SPAs in $GAD65^+$ neurons than TH^+ neurons. Also, when compared to recordings from MCs (Angelo and Margrie 2011), the I_h in interneurons was an order of magnitude smaller than I_h measured in principal neurons. However, potentially because of the high

input resistance of GAD65$^+$ neurons these small currents resulted in membrane potential sag amplitudes comparable to those of MCs.

3.3.3 Potential Significance of Hyperpolarisation-Activated Cation Current in GAD65$^+$ and TH$^+$ Neurons

Although it is well established that in response to hyperpolarisation I_h causes a rebound sag in a neuron's membrane potential (Robinson and Siegelbaum 2003; Wahl-Schott and Biel 2009), it is important to explore whether I_h exerts an effect on other aspects of cell function. Therefore, the HCN channel blocker ZD7288 was used to block I_h (Figure 3.11a).

During whole-cell current-clamp recordings from GAD65$^+$ neurons, ZD7288 resulted in a significant increase in input resistance as well as a decrease in the probability of a rebound spike after the end of a hyperpolarisation. These changes indicate the substantial impact I_h might have on the excitability of GAD65$^+$ neurons. Firstly, the sensitivity of a neuron to synaptic input can be regulated through changes in the input resistance, whereby a higher input resistance increases the impact of small currents on a neuron's membrane potential and generally increases its excitability. Secondly, HCN channels are slow gated ion channels that can exhibit opening and closing times of over several hundreds of milliseconds (Wahl-Schott and Biel 2009). When the hyperpolarising drive that initially activates HCN channels terminates, HCN channels close with a delay and their depolarising current can drive the membrane potential over the spiking threshold, resulting in rebound action potentials. Through this mechanism, action potentials and therefore output signals, can be triggered by inhibitory input. Since expression levels and gating properties of HCN channels can be activity-dependent (Wang et al. 2002; Zha et al. 2008), such a mechanism could potentially provide a way for the neuron to shut down ongoing network activity.

When analysing the distribution of SPAs in interneuron populations, it is worth noting that, in contrast to the MC population, inhibitory interneurons rarely exhibited a negative SPA. TH$^+$ neurons had a homogeneous distribution of rather small SPAs. In contrast, GAD65$^+$ neurons exhibited on average larger SPAs (similar to the average

amplitude measured in MCs by Angelo et al. 2012) and had an extremely wide range of SPAs across the whole population.

The heterogeneity of SPAs in the $GAD65^+$ population on one side and the homogeneity of SPAs in the TH^+ populations on the other side, makes these two chemotypes ideally suited to exploring whether I_h is involved in network-based gain control mechanisms, as proposed for MCs (Angelo et al. 2012). In addition to morphological and functional differences, these populations appear to differ greatly in this particular intrinsic property, which raises the possibility that it might be modulated in different ways or to a different extent in these two classes of neurons. As a next step I therefore investigated the extend to which differences in SPA from one neuron to the next might reflect local network processing.

Chapter 4. The Sag Potential Amplitude and Its Relation to Local Glomerular Networks

4.1 Introduction

Each glomerulus receives sensory information from a population of olfactory sensory neurons (OSN) that expresses a single type of odour receptor (OR). Odour information is integrated on an intra- and interglomerular level by several hundred local glomerular interneurons. Since the functional organisation and processing of odour information in the glomerular layer is structurally well-defined, this brain area provides an ideal model system to investigate the extent to which intrinsic properties, such as the hyperpolarisation-activated current (I_h), influence information processing within local sensory networks.

Mitral cells (MCs) exhibit a remarkable diversity in their amplitude of I_h-mediated membrane potential sag and this diversity has been shown not only to reflect odour-specific information processing (Angelo and Margrie 2011), but also act as a signature of glomerulus affiliation (Angelo et al. 2012). These data demonstrate that the diversity of I_h in principal neurons within a single morphological class can reflect a functional organisation within local networks.

Based on the results presented in the previous chapter, I investigated whether processing of common odour information within the local network influences the sag potential amplitude (SPA) of interneurons in the glomerular layer. To address this question, paired whole-cell recordings from $GAD65^+$ and TH^+ interneurons were performed, with the aim to determine if the SPA of two interneurons was more similar in cases where they received similar sensory input.

However, in contrast to MCs, inhibitory interneurons in the glomerular layer exhibit a diverse morphology and glomerular innervation pattern. While periglomerular (PG) cells are thought to innervate only one or two local networks, short axon (SA) cells have sometimes been reported to innervate tens of glomeruli. Furthermore, the dendritic trees of both cell types ramify only in a small area of each glomerulus (Kiyokage et al. 2010). Affiliation of recorded neurons was therefore verified not only by visual inspection of the glomerular innervation pattern, but also by coincident spontaneous synaptic input in

simultaneously recorded cells, under the assumption that coincident synaptic input is most likely to originate from a common glomerular network.

4.2 Results

4.2.1 Synchrony of Spontaneous Sub-Threshold Activity as a Proxy for Affiliation to the Same Local Network

Since the unambiguous determination of a neuron's affiliation to a specific glomerulus using morphological reconstructions is challenging (Figure 4.1), electrophysiological recordings were used to explore whether two simultaneously recorded neurons were affiliated to the same local networks. Simultaneous current-clamp recordings, with both neurons held at a hyperpolarised membrane potential (-70 ± 2 mV; see Materials & Methods, section 2.4.4), were performed and spontaneous synaptic activity was recorded. In both the $GAD65^+$ and TH^+ population, some paired recordings revealed spontaneous synchronous sub-threshold activity in the membrane potential that qualitatively suggested coincident synaptic events (Figure 4.1a, b and c). Therefore, the degree of synchrony between membrane potential fluctuations of two neurons was determined by performing a cross-correlation of simultaneously recorded membrane voltage traces. The peak value calculated from each cross-correlogram was used to quantify how strongly the events in two neurons were synchronised (see Materials & Methods, section 2.4.4 and Figure 4.1).

A small number of experiments (n = 3) were conducted using pharmacological blockade of putative receptors mediating fast synaptic transmission to determine if synchronous sub-threshold events were mediated synaptically rather than by auto-rhythmicity. As shown in Figure 4.2, the block of synaptic glutamate receptors (AMPA and NMDA) and $GABA_A$ receptors by bath application of 0.01 mM NBQX, 0.05 mM AP-5 and 0.05 mM picrotoxin abolished the membrane potential fluctuations and synchrony in sub-threshold events, suggesting that membrane potential synchrony in these neurons was caused by local network activity.

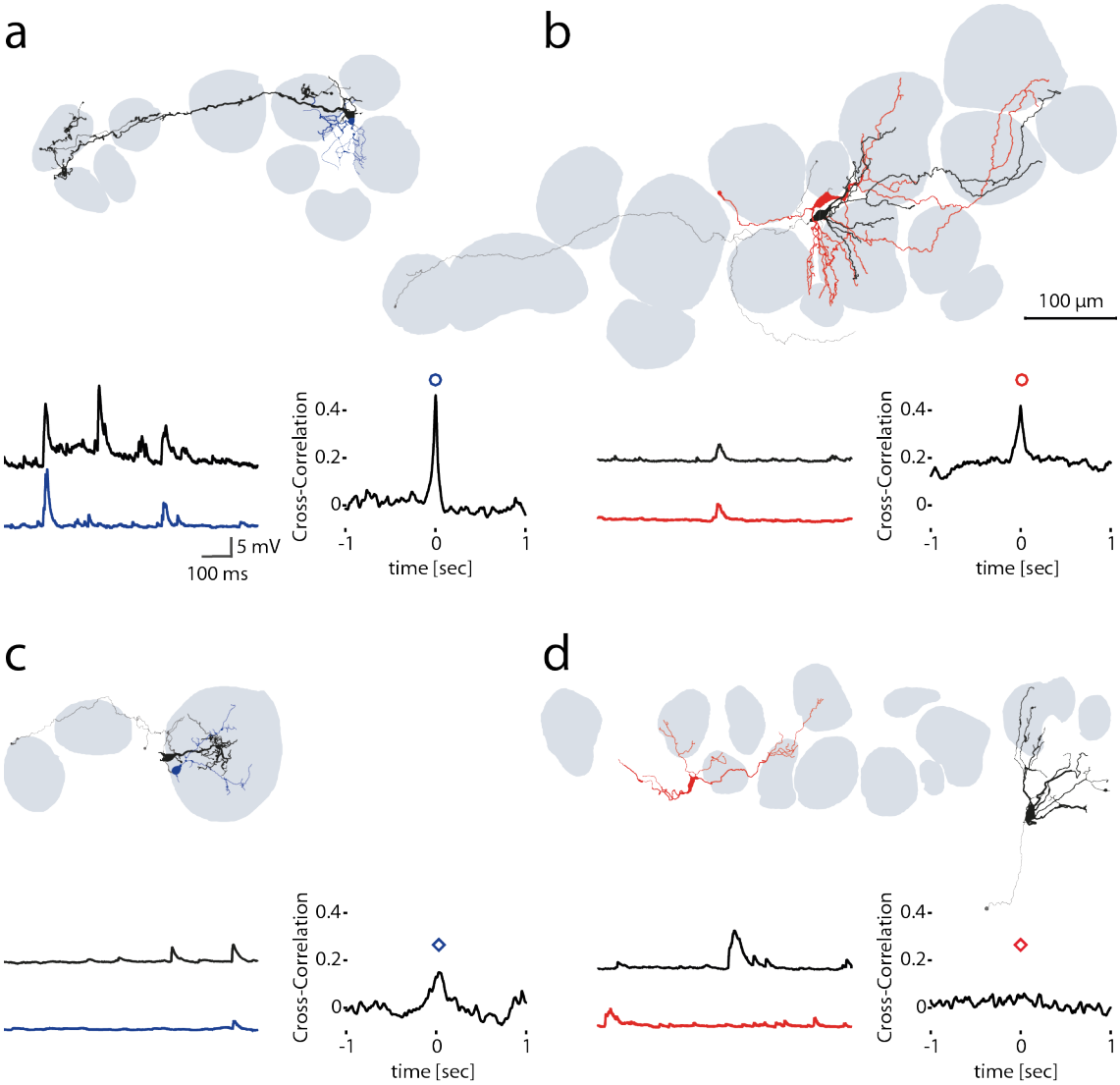

Figure 4.1 Morphological Reconstructions of Simultaneously Recorded Neurons and Quantification of Their Synchronised Sub-Threshold Activity

(a-b) Example reconstructions of simultaneously recorded GAD65$^+$ *(blue and black)* or TH$^+$ *(red and black)* neurons (*top*), displayed with an example trace of spontaneous activity recorded at -70 ± 2 mV (*bottom left*). Colours of reconstructed neurons correspond to colours of membrane potential traces. For each pair a cross-correlogram was performed on the simultaneously recorded membrane potentials to quantify the coincident occurrence of sub-threshold activity (*bottom right*). Both pairs exhibited strong coincident occurrence of sub-threshold activity, resulting in large cross-correlogram peak values.
(c-d) Example reconstructions (*top*), membrane potential recordings (*bottom left*) and cross-correlograms (*bottom right*) of simultaneously recorded GAD65$^+$ *(blue and black)* or TH$^+$ *(red and black)* neurons with little or no coincident activity.
Open circles and diamonds are used to highlight these pairs in Figure 4.3.

If the coincident events were indeed caused by common glomerular input, then the dendrites of any two simultaneously recorded neurons showing high cross-correlation scores should share at least one glomerulus and likely have dendritic overlap. To test this hypothesis, 3,3'-diaminobenzidine (DAB) stainings and morphological reconstructions were conducted for all paired recordings. Reconstructions with a complete recovery of dendritic morphology of both neurons were used to determine the amount of overlap of their innervation pattern. Since glomeruli have a diameter of 50 – 150 µm, close proximity (< 5 µm) of dendrites in the glomerular layer likely indicates innervation of the same glomerulus.

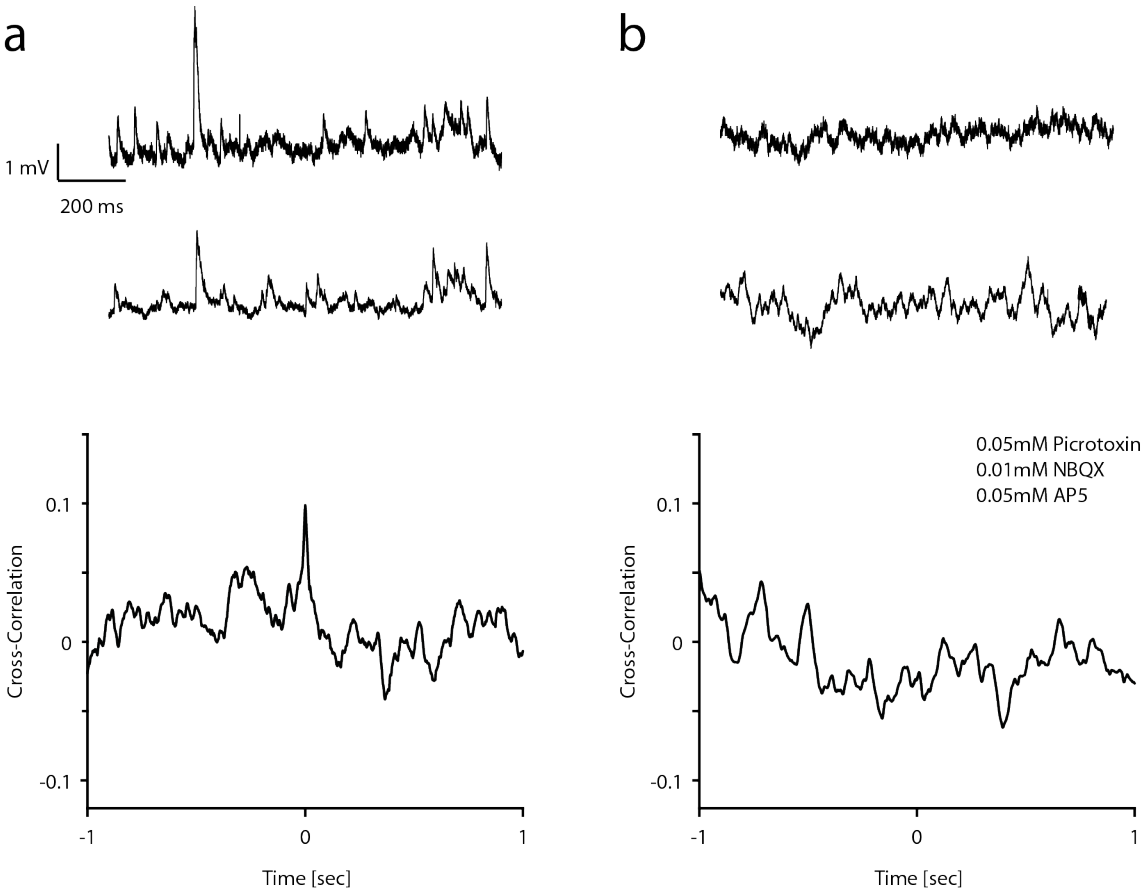

Figure 4.2 Synaptic Ion Channel Blockers Abolish Synchrony in Sub-Threshold Activity

(a) *top:* Membrane potential of two simultaneously recorded TH^+ neurons, exhibiting synchrony in some sub-threshold events. *bottom:* Corresponding cross-correlogram quantifying the strength of synchrony in sub-threshold activity.
(b) Recording from the same neuron as in (a) after block of synaptic glutamate and $GABA_A$ receptors with NBQX, AP-5 and picrotoxin. The synaptic blockers completely abolished the synchrony in sub-threshold events.

The dendritic overlap of both neurons was quantified from morphological reconstructions using the proximity analysis in Neurolucida Explorer (see Materials & Methods, section 2.7.3). The percentage of one neuron's dendritic tree that was located within 5µm of the dendrites of the other neuron correlated well with the strength of membrane potential synchrony between them ($R = 0.68$, $p < 0.05$; Figure 4.3).

Additionally, the synaptic events of $GAD65^+$ and TH^+ pairs showing high cross-correlation scores were detected and analysed (n = 11 pairs). In general, at -70 ± 2 mV spontaneous excitatory postsynaptic potentials (EPSPs) occurred at similar frequencies in both chemotypes ($GAD65^+$ = 14.00 Hz, TH^+ = 20.59 Hz). However, pairs of $GAD65^+$ neurons exhibited coincident EPSPs more than four times less frequent than pairs of TH^+ neurons ($GAD65^+$ = 0.15 Hz, TH^+ = 0.64 Hz). When analysing all EPSPs, the median event amplitude was slightly larger in $GAD65^+$ pairs than in TH^+ pairs ($median_{GAD65} = 0.84$, $median_{TH} = 0.74$, $p = 7.0 \times 10^{-10}$, Figure 4.4a).

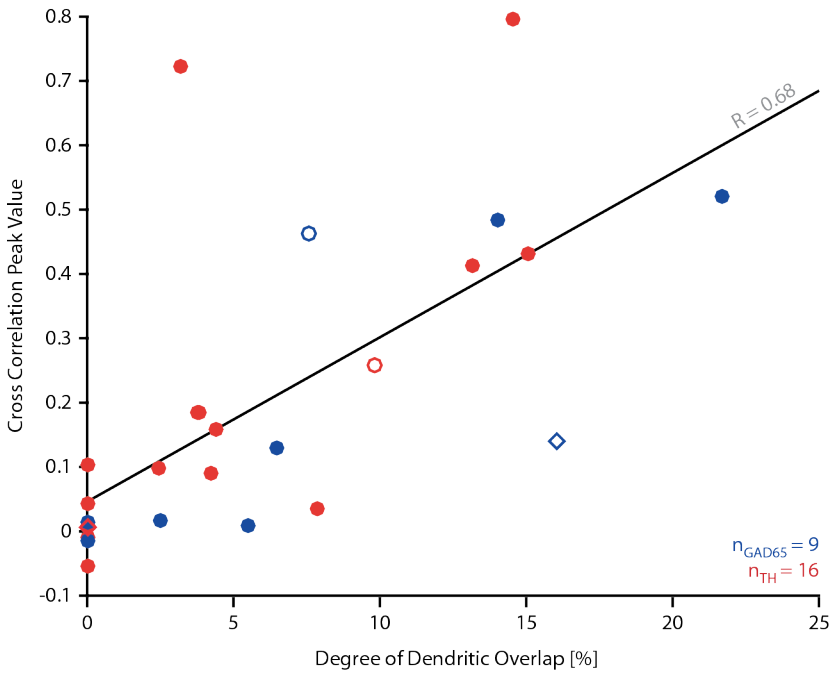

Figure 4.3 Correlation Between Synchronised Sub-Threshold Activity and Dendritic Overlap in $GAD65^+$ and TH^+ Neurons

Scatter plot showing correlation between cross-correlogram peak values, calculated from membrane potentials of two simultaneously recorded $GAD65^+$ *(blue)* or TH^+ *(red)* neurons, and the degree of dendritic overlap in each pair. Dendritic overlap was defined as the mean percentage of one neuron's dendrite in 5 µm vicinity to the other neurons dendrite. Open circles and diamonds correspond to the four example neurons in Figure 4.1.

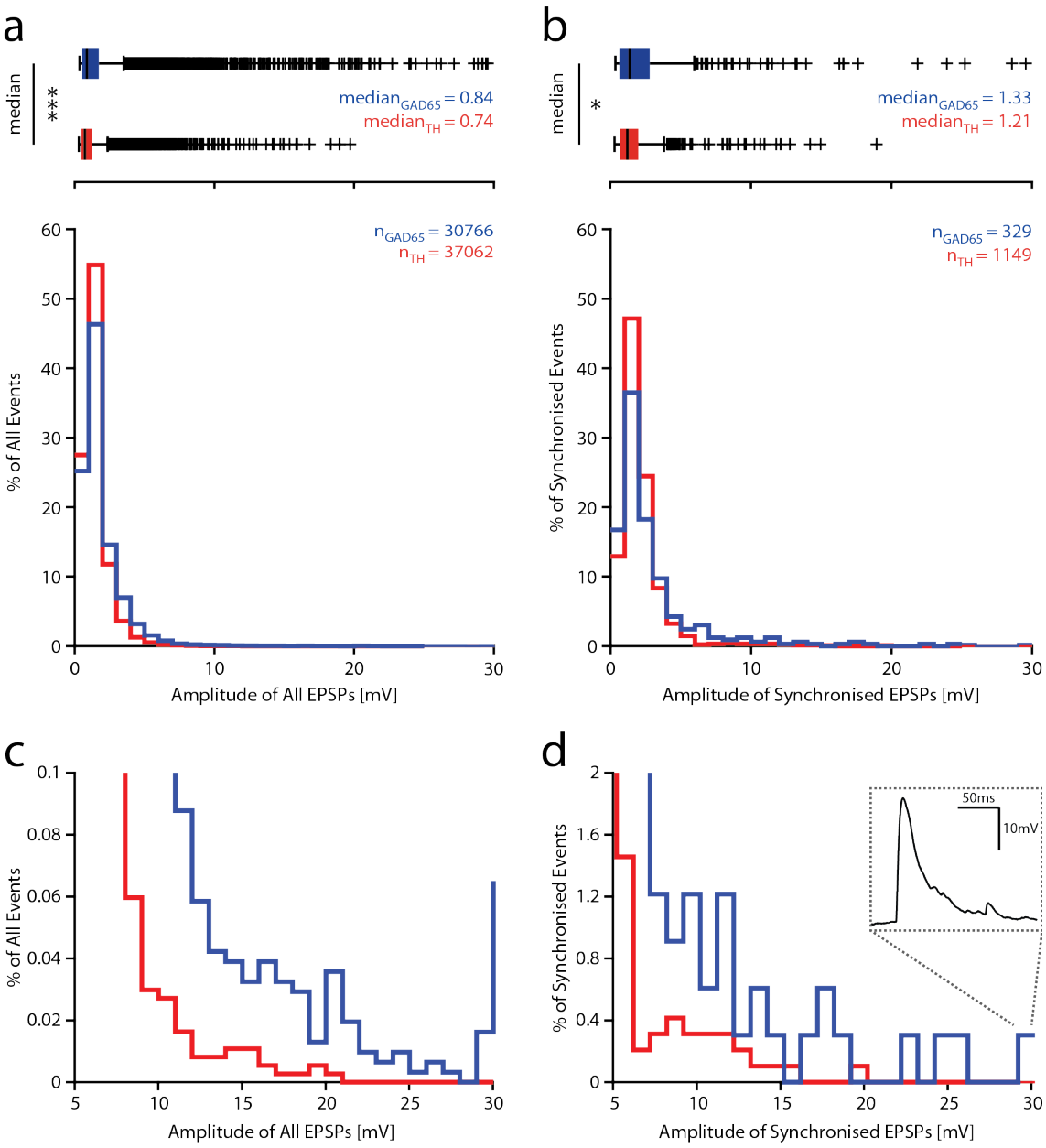

Figure 4.4 Quantitative Analysis of Event Amplitudes in Pairs of GAD65$^+$ or TH$^+$ Neurons

(a) Boxplot (*top*) and histogram (*bottom*) displaying amplitudes of all events in simultaneously recorded GAD65$^+$ *(blue)* or TH$^+$ *(red)* neurons. Median event amplitude was significantly larger in GAD65$^+$ neurons compared to TH$^+$ neurons.
(b) Boxplot (*top*) and histogram (*bottom*) displaying amplitudes of coincidentally occurring events recorded GAD65$^+$ *(blue)* or TH$^+$ *(red)* neurons. GAD65$^+$ and TH$^+$ neurons exhibited a small difference in their median coincident event amplitude.
(c) Magnification of histogram in (a), displaying amplitudes of large (> 5 mV) events in GAD65$^+$ and TH$^+$ neurons.
(d) Magnification of histogram in (b), displaying amplitudes of large (> 5 mV) synchronised events in GAD65$^+$ and TH$^+$ neurons. Insert, single EPSP with large (30 mV) amplitude. Significance levels were determined by a Wilcoxon rank sum test; *: p-value < 0.05, ***: p < 0.001.

Also, when isolating coincidentally occurring EPSPs, only a small difference in median event amplitude became apparent ($median_{GAD65}$ = 1.21, $median_{TH}$ = 1.33, p = 0.050, Figure 4.4b). Interestingly, the median amplitude of coincidentally occurring events was significantly greater than the median amplitude of all events in both $GAD65^+$ ($median_{average}$ = 0.84, $median_{coincident}$ = 1.21, p = $5.5x10^{-13}$) and TH^+ neurons ($median_{average}$ = 0.74, $median_{coincident}$ = 1.33, p = $1.0x10^{-65}$). Inspection of the skewed end of the amplitude histograms (Figure 4.4a and b) revealed that $GAD65^+$ neurons exhibited several large events (> 21 mV) that were not present in the TH^+ population (Figure 4.4c and d).

Since all recordings were conducted at hyperpolarised membrane potentials (-70 ± 2 mV), around half of the cells in the $GAD65^+$ and TH^+ population did not exhibit action potential firing during passive recording of the membrane voltage. The remaining neurons exhibited sporadic action potential firing, which was more common in synchronised $GAD65^+$ pairs compared to TH^+ pairs (10 vs. 1, Figure 4.5). However, no statistical analysis was conducted due to the small size of the dataset.

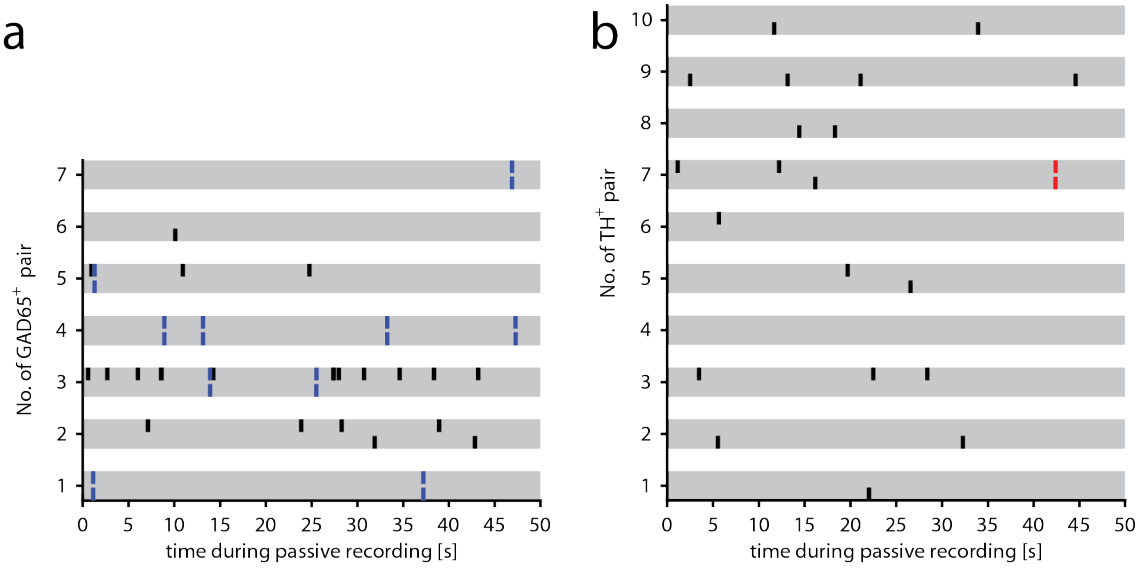

Figure 4.5 Qualitative Analysis of Synchronised Action Potential Firing in $GAD65^+$ and TH^+ Neurons

(a) Raster plot illustrating action potential firing in seven simultaneously recorded $GAD65^+$ pairs. *Grey horizontal bars* indicate a pair of neurons and *vertical black bars* the occurrence of a single action potential. Coincident action potentials shown in *blue*.
(b) Raster plot illustrating action potential firing in ten simultaneously recorded TH^+ pairs. *Grey horizontal bars* indicate a pair of neurons and *vertical black bars* the occurrence of a single action potential. Coincident action potentials shown in *red*.

4.2.2 SPA Diversity of GAD65$^+$ and TH$^+$ Interneurons Within Local Networks

Once the cross-correlation analysis was validated, a method was established to identify pairs of neurons with high levels of event synchrony. Since the range of cross-correlation peak values describing coincident events was continuous rather than bimodal, a threshold value was used to identify pairs of neurons receiving substantial input from a common local network. To determine a cross-correlation peak threshold, all neurons recorded in GAD65$^+$ and TH$^+$ populations were systematically paired with neurons of the same chemotype that had not been recorded simultaneously to form a dataset referred to as pseudo pairs (see Materials & Methods, section 2.4.4).

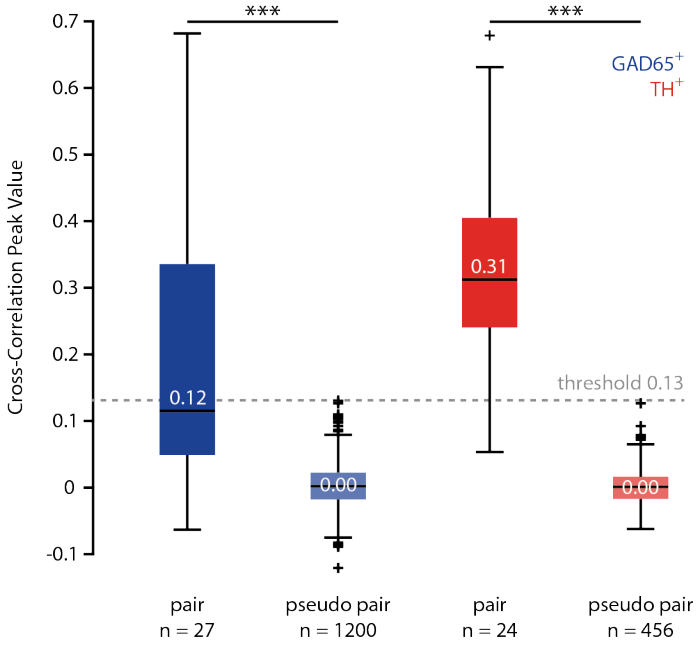

Figure 4.6 Cross-Correlation Peak Scores of GAD65$^+$ and TH$^+$ Pairs

Boxplot comparing cross-correlation peak values of simultaneously recorded GAD65$^+$ *(dark blue)* and TH$^+$ *(dark red)* neurons with cross-correlation peak values of pseudo pairs, generated from the same GAD65$^+$ *(light blue)* and TH$^+$ *(light red)* dataset. The highest cross-correlation score of a pseudo pair (0.13, *grey dashed line*) was used as a threshold to sort simultaneously recorded neurons in groups of strongly and weakly synchronised pairs. Significance levels were determined by two-way ANOVA and post-hoc test (Wilcoxon rank sum test); ***: $p < 0.001$.

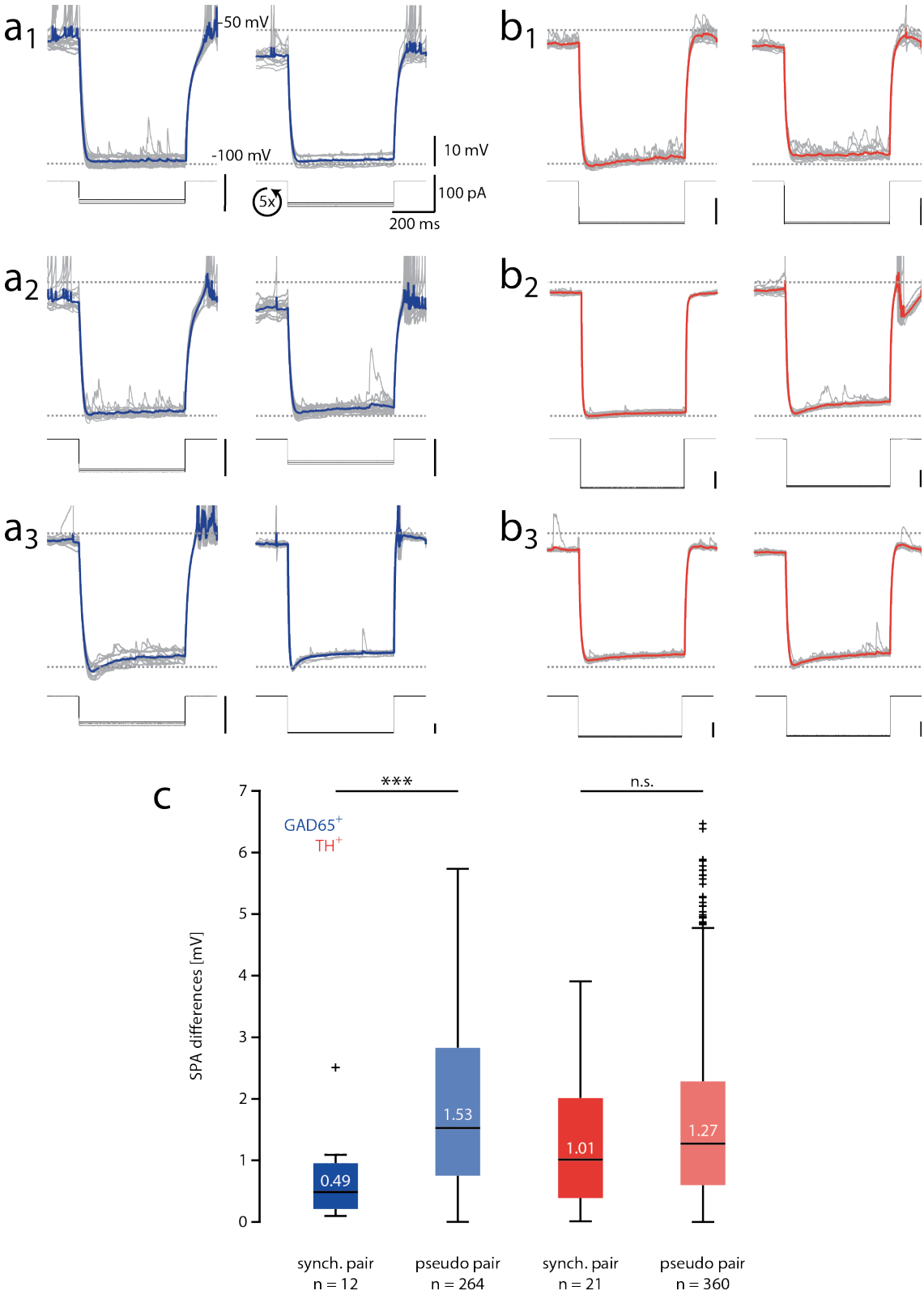

Figure 4.7 SPA Similarity in Synchronised Pairs of GAD65$^+$ and TH$^+$ Neurons

Figure 4.7 SPA Similarity in Synchronised Pairs of GAD65$^+$ and TH$^+$ Neurons (cont.)

(a) Example voltage traces of three simultaneously recorded GAD65$^+$ pairs with corresponding injected hyperpolarising current steps (*underneath*). Average membrane potentials are displayed in blue and individual voltage traces in grey.
(b) Example voltage traces of three simultaneously recorded TH$^+$ pairs with corresponding injected hyperpolarising current steps (*underneath*). Average membrane potential displayed in red and individual voltage traces in grey.
(c) Boxplot of SPA similarity in synchronised pairs of GAD65$^+$ *(dark blue)* and TH$^+$ *(dark red)* neurons and the corresponding pseudo pairs *(light blue and light red)*. Significance levels were determined by two-way ANOVA and post-hoc test (Wilcoxon rank sum test); n.s. = not significant; **: p-value < 0.01.

A cross-correlation analysis was then performed on all GAD65$^+$ and TH$^+$ pseudo pairs. A Wilcoxon rank sum test between simultaneously recorded neurons and pseudo pairs revealed on average significantly higher cross-correlation peak values in the simultaneous recordings than in pseudo paired neurons ($pair_{GAD65}$= 0.12 vs. pseudo $pair_{GAD65}$=0.00, $pair_{TH}$= 0.31 vs. pseudo $pair_{TH}$=0.00; p_{GAD65} = 7.9x10^{-16} and p_{GAD65} = 1.5x10^{-12}; Figure 4.6). The highest cross-correlation peak value found for the pseudo pair groups was then used as a threshold for separating moderately and highly synchronised pairs from weakly or non-synchronised pairs (threshold value = 0.13, Figure 4.6).

Next, the SPA similarity in synchronised pairs (Figure 4.7a and b) was investigated. The simultaneously recorded pairs of neurons were again compared to pseudo pairs assigned from the same dataset (Figure 4.7c). In the GAD65$^+$ population, the SPA was significantly more similar in pairs ($median_{pairs}$ = 0.49 mV, n_{GAD65} = 12) compared to pseudo pairs ($median_{pseudo}$ = 1.53 mV, p_{GAD65} = 0.0007), whereas no significant difference could be observed in the TH$^+$ population ($median_{pairs}$= 1.01 mV, n_{TH} = 21; $median_{pseudo}$ = 1.27 mV, p_{TH} = 0.23034), despite sampling from a larger population of pairs. However, the interaction between genotype and synchronisation was not significant (two-way ANOVA, p = 0.511) and therefore the SPA difference between pairs and pseudo pairs was not significantly larger in the GAD65$^+$ population than in TH$^+$ population.

The SPA similarity in synchronised GAD65$^+$ was highly reliably, and significant over a large range of cross-correlation thresholds (0 – 0.26). Furthermore, the threshold set to define a highly synchronised pair did not affect the lack of significance simultaneously recorded TH$^+$ neurons (Appendix B).

4.3 Discussion

In MCs, where glomerular membership is anatomically unambiguous, it has been shown that the level of I_h is tightly correlated to the affiliation of a neuron to a local glomerular network (Angelo et al. 2012). However, because morphological confirmation of glomerular affiliation can be challenging in interneurons, an alternate method to determine common local network affiliation was introduced and verified. The coincident occurrence of synaptic input was validated as a proxy for the affiliation of simultaneously recorded neurons to the same glomerular network. Here, the peak values of cross-correlograms calculated from the membrane potentials of simultaneously recorded pairs correlated well with the dendritic overlap of these neurons. Furthermore, recordings without dendritic overlap (e.g. Figure 4.1d) did not exhibit notable cross-correlation. In accordance with these results, the dependence of the synchronised events on glutamatergic transmissions indicated a common synaptic origin. Whether these events stem from monosynaptic input from OSNs or polysynaptic input through other principal neurons remains to be demonstrated.

Interestingly, the $GAD65^+$ and TH^+ population exhibited a wide range of cross-correlation peak values, with TH^+ neurons having on average larger values than $GAD65^+$ neurons. A high cross-correlation peak value indicates a strong synchrony between a pair of neurons, but does not reveal the origin of this synchrony, as high cross-correlation values are either the result of synchronised, large amplitude events or a high number of smaller synchronous events. A more detailed analysis of EPSPs in $GAD65^+$ and TH^+ neurons was performed to address this question, which revealed that in TH^+ neurons synchronised EPSPs occurred at a higher frequency than in $GAD65^+$ neurons, consistent with higher cross-correlation peak values (Figure 4.6).

The median amplitude of synchronised EPSPs was nearly identical in $GAD65^+$ and TH^+ neurons. However, the $GAD65^+$ population exhibited a small number of very large (> 21 mV) EPSPs, which were absent in TH^+ neurons. Furthermore, when comparing the spontaneous action potentials recorded in both chemotypes, the $GAD65^+$ population exhibited more action potentials in total and more action potentials that were synchronised. Since it has been demonstrated that the amount of I_h can depend on both the strength of glutamatergic synaptic input (van Welie et al. 2004) and action potential

firing of the post-synaptic cell (Fan et al. 2005), this could provide a possible explanation for the differences in SPA amplitude and diversity between $GAD65^+$ and TH^+ neurons (as shown in Chapter 3).

A low cross-correlation value in a simultaneously recorded pair could result from several different scenarios. Firstly, two neurons might not share common input. Secondly, two neurons might be affiliated to the same local network, but the relevant dendrites may have been truncated in one or both neurons during the slicing process. Thirdly, the network innervated by both cells could be damaged or silent.

Since a number of possible explanations for a lack of observed synchrony may be proposed, it is difficult to interpret the similarity of SPAs in pairs with low synchrony, hence data from these pairs were not analysed further. Instead, pseudo pairs were generated by systematically pairing neurons from the pair dataset that were not recorded simultaneously. By definition, any coincident event detected in pseudo pairs must be noise. Therefore, pseudo pairs provided a more suitable comparison than for example simultaneously recorded neurons with soma locations far apart.

The final aim of this chapter was to explore whether the amplitude of membrane potential sag reflects local network affiliation and similar activity. The experiments demonstrated that SPA was significantly more similar in $GAD65^+$ neurons that exhibited a strong synchrony in their subthreshold activity than in randomly assigned $GAD65^+$ neurons. No such effect could be shown for the TH^+ population. Since the SPAs of two fundamentally different types of neurons – MCs and $GAD65^+$ interneurons – were dependent on network affiliation, these results suggest that I_h may be regulated in a similar way in both principal cells and interneurons. However, the functional relevance of the regulatory mechanism underlying I_h might vary between cell types. It is possible that the excitability of neurons predominantly innervating a single local network (for instance MCs, PG cells and ET cells) is much more tightly regulated by the network activity than the excitability of neurons averaging input from several different networks (for instance SA cells). The activity dependence underlying such regulatory mechanisms will be investigated in the next chapter.

Chapter 5. Experience-Dependence of Sag Potential Amplitude is Glomerulus Specific

5.1 Introduction

Hyperpolarisation-activated cyclic nucleotide-gated (HCN) channels can be regulated on a short time scale via conformational changes caused by cellular metabolites and phosphorylation, and on a longer time scale by changes in protein expression levels and intracellular relocation of HCN isoforms (as summarised by Biel et al. 2009). The dependence of SPA levels on the affiliation to a specific glomerulus in $GAD65^+$ neurons could theoretically be a hard-wired, predetermined process that is stereotypical across animals. However, because expression levels and gating properties of HCN channels can be activity-dependent (Wang et al. 2002; Zha et al. 2008), the SPA in these cells might be the result of the activation history of the glomerular network. If this was the case, it would be reasonable to speculate that SPA in $GAD65^+$ neurons is sensitive to olfactory signalling and that odour processing might be involved in its regulation.

To address this question, a M72-IRES-ChR2-YFP mouse line was used (Smear et al. 2013), whereby a ChR2-EYFP protein is selectively expressed under the promoter of odour receptor 160 (OR160). This results in channelrhodopsin-2 (ChR2) expression restricted to OR160 olfactory sensory neurons (OSNs). The axons of OR160 OSNs converge onto two bilaterally symmetrical M72 glomeruli, one lateral and one dorsal on the surface of each olfactory bulb (OB). These light-sensitive M72 OSNs appear functionally and anatomically normal: they have been shown to express the intact OR160 and exhibit a typical axonal innervation pattern (Smear et al. 2013). Furthermore, the M72 glomerulus is anatomically and developmentally well-described (Zheng et al. 2000; Potter et al. 2001; Feinstein and Mombaerts 2004), with known odour-response curves to several different ligands (Zhang et al. 2012).

The YFP expression in M72 OSNs of the M72-IRES-ChR2-YFP line enables identification of the same glomerular network across animals and experiments. A cross between this line and either Gad2-IRES-Cre-tdtomato or TH(9.0)tagRFP provides a

way of targeting distinct subpopulations of juxtaglomerular (JG) interneurons that can be tested for their affiliation to the M72 glomerular network using ChR2 stimulation.

To assess the extent to which olfactory stimulation might influence the SPAs of $GAD65^+$ and TH^+ neurons, two experiments were set up in which mice were either exposed to an odour or deprived of olfactory input. To ensure M72-OSNs were stimulated, animals were exposed to the odour 2'-hydroxyacetophenone (2-HAP), a ligand known to strongly activate OSNs expressing OR160 (Zhang et al. 2012). By exposing animals to the odour for several days, the aim was to impose a close to natural stimulation of the M72 network. Odour concentration was adjusted to generate neither attractive nor aversive responses from the animals, and animals were otherwise kept in conditions identical to littermates that were not exposed. Odour exposure had no observable effect on their development or behaviour.

Olfactory deprivation was carried out by rinsing the nasal cavity of the animals with $ZnSO_4$, an established method for causing anosmia by degeneration of OSNs (Smith 1938; Harding et al. 1978; Mayer and Rosenblatt 1993; Ducray et al. 2002; McBride et al. 2003; Bracey et al. 2013). Animals were treated with a well-established protocol (Bracey et al. 2013) and are generally considered anosmic one to four days after $ZnSO_4$ treatment (Ducray et al. 2002; McBride et al. 2003; Bracey et al. 2013). However, since the axons of the OSNs expressing ChR2-YFP are required to be intact to locate and stimulate the M72 glomerulus, slices were obtained one day after the treatment.

5.2 Results

5.2.1 Confirming Functionality of the M72-IRES-ChR2-YFP Mouse Model

The YFP-labelled axons of all OR160 OSNs converge onto two M72 glomeruli (Figure 5.1a). It was expected that interneurons receiving synaptic input from the M72 glomerulus (Figure 5.1b) should reliably respond to light activation of ChR2. Several control experiments were conducted to confirm that the responsiveness of an interneuron to light stimulation could be used as a proxy for affiliation to the M72 glomeruli. During all recordings in M72-IRES-ChR2-YFP animals, neurons were filled with biocytin and their morphology was subsequently visualised by DAB staining. Recovered and analysed morphologies indicated that only neurons innervating the M72 glomerulus reliably respond to stimulation of OR160 axons (n = 8; Figure 5.2a). Furthermore, light-evoked responses in neurons innervating the M72 glomerulus could be completely abolished by blocking glutamatergic and GABAergic synaptic transmission (0.05 mM Picrotoxin, 0.05 mM DL-AP5 and 0.01 mM NBQX, Figure 5.2b).

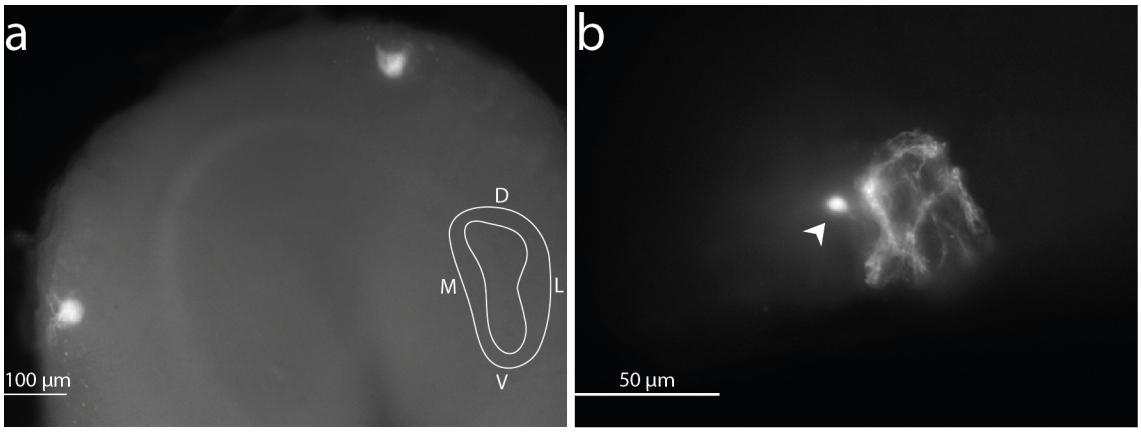

Figure 5.1 Location and Anatomy of the M72 Glomeruli in the M72-IRES-ChR2-YFP Mouse Model

(a) Fluorescent image of YFP-expressing OSN axons exhibiting a typical innervation pattern by converging onto one medial and one lateral M72 glomerulus per OB (5x objective).
(b) Neuron *(white arrowhead)* innervating an M72 glomerulus. The neuron was filled with Alexa Fluor® 488 after whole-cell recording and successful pull-off (40x objective).
Both pictures are overlays of two images taken with a YFP filter set at different optical section within the same brain slice. D= dorsal, L= lateral, M= medial, V= ventral.

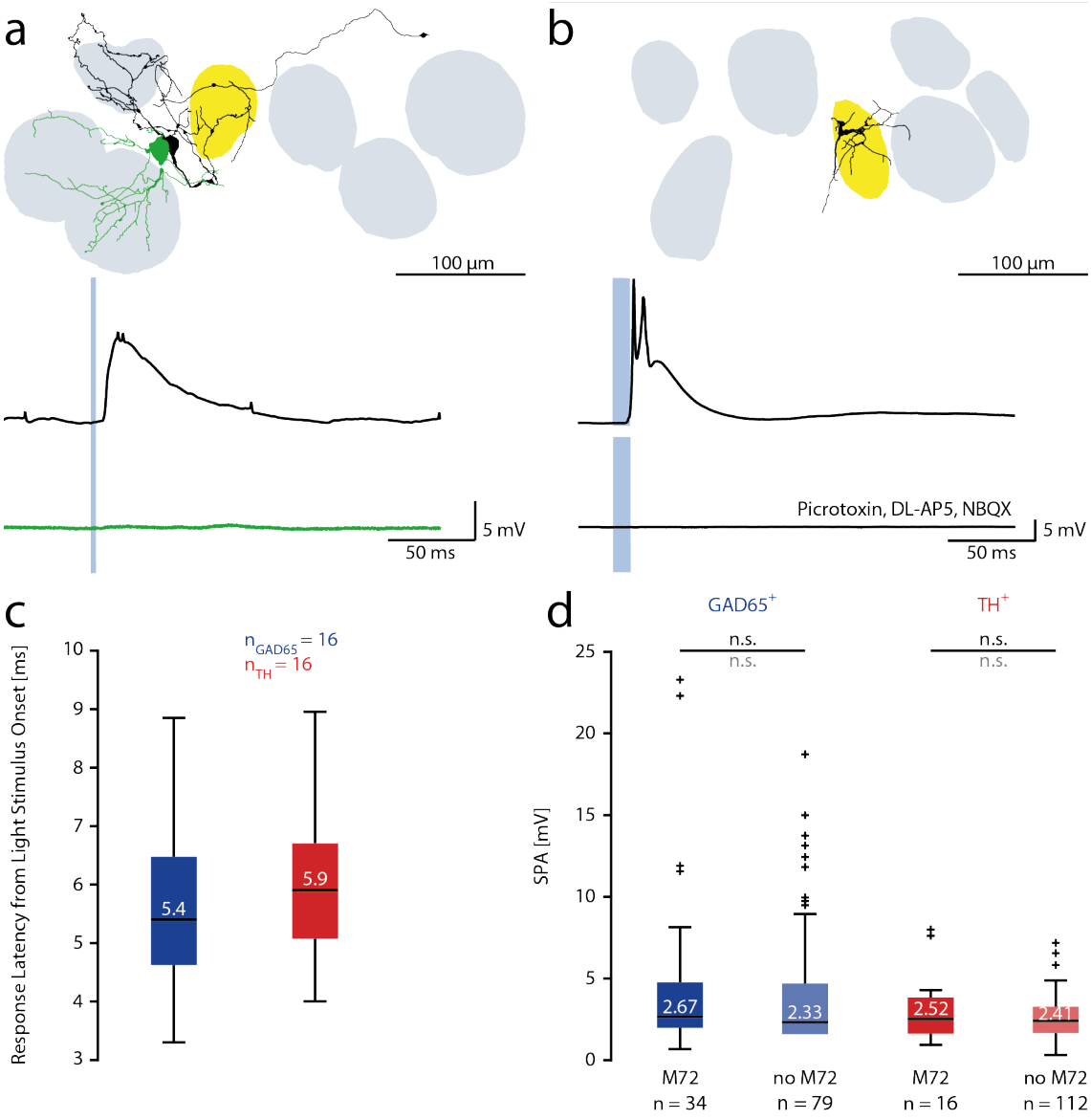

Figure 5.2 Only Neurons Innervating M72 Respond to ChR2 Stimulation

(a) Morphological reconstruction of two simultaneously recorded neurons, one neuron innervating the M72 glomerulus (yellow circle) and responding to a 2 ms light stimulation *(black reconstruction and recording trace)* and the other neuron neither innervating M72 nor responding to the light stimulation *(green reconstruction and recording trace)*. Both recording traces are averages of 20 repeats. **(b)** Morphological reconstruction of a neuron innervating an M72 glomerulus *(yellow circle)*, showing an excitatory response to repeated 10 ms light stimulation *(upper trace)*. The response was completely abolished by bath application of the synaptic blockers 0.05 mM Picrotoxin, 0.05 mM DL-AP5 and 0.01 mM NBQX *(lower trace)*. Both recording traces are averages of 20 repeats. **(c)** Boxplot of response latencies in 16 M72-affiliated GAD65$^+$ and TH$^+$ neurons to the onset of a 2 ms long blue light stimulus. **(d)** Boxplot comparing SPAs in M72-GAD65$^+$ *(dark blue)* and M72-TH$^+$ *(dark red)* neurons to SPAs in GAD65$^+$ and TH$^+$ neurons innervating other glomeruli *(light blue and light red)*. Significance levels were determined by a Wilcoxon rank sum test *(black)* and a Brown–Forsythe test *(grey)*; n.s.= not significant.

In 16 randomly selected M72-affiliated GAD65$^+$ and TH$^+$ neurons, 20 to 50 light-evoked events were analysed to determine the reliability of postsynaptic response and response latency to the stimulus onset. At a frequency of 1 Hz, 98% of 2 ms light stimuli triggered an excitatory post-synaptic potential (EPSP) larger than 0.3 mV in the postsynaptic interneuron and sometimes evoked spiking. The average response latency in these neurons was 5.4 ms for GAD65$^+$ neurons and 5.9 ms for TH$^+$ neurons (Figure 5.2c).

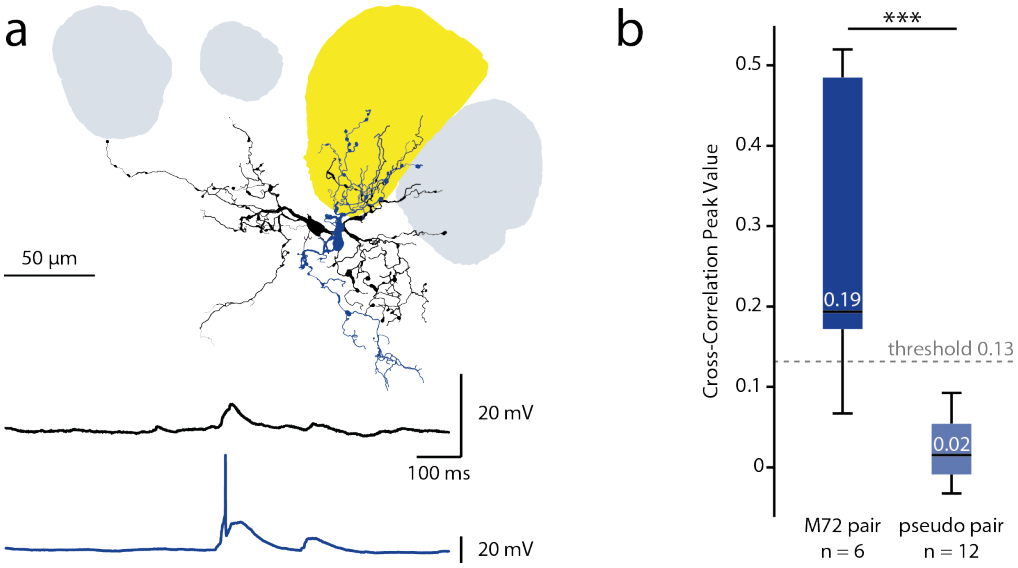

Figure 5.3 Pairs of GAD65$^+$ Neurons Affiliated to the Same M72 Exhibit High Cross-Correlation Values

(a) *top:* Example reconstruction of two simultaneously recorded GAD65$^+$ neurons that exhibited a small cross-correlation peak value (0.07). Both neurons are affiliated to the M72 glomerulus *(yellow)* and respond reliably to light stimulation. *Bottom:* Example voltage traces from the reconstructed pair showing synchronised events. Colours of the traces match colours of the reconstructions.
(b) Boxplot of cross-correlation peak values from six pairs of M72-affiliated GAD65$^+$ neurons and the corresponding pseudo pairs. The same cross-correlation score *(grey dashed line)* as for non-M72-affiliated pairs (Figure 4.6) was chosen to define five out of the six pairs as synchronised in their spontaneous sub-threshold activity. Significance levels were determined by a Wilcoxon rank sum test (***: $p < 0.001$).

The SPA was quantified in 32 $GAD65^+$ and 16 TH^+ neurons receiving input from the M72 glomerulus. The SPAs of these neurons were compared to those of neurons not affiliated with M72, which were selected based on a large anatomical distance between their somata and the M72 glomerulus (> 500 μm). In both chemotypes no significant differences in median SPA (p_{GAD65} = 0.318, p_{TH} = 0.596) or SPA variance (p_{GAD65} = 0.131, p_{TH} = 0.373) were observed between M72-affiliated and non-M72-affiliated neurons (Figure 5.2d).

Next, paired recordings of $GAD65^+$ neurons were conducted in the vicinity of the M72 glomerulus (Figure 5.3a). In total, six pairs of $GAD65^+$ neurons were recorded in which both neurons responded reliably to light stimulation of M72. These six M72-affiliated $GAD65^+$ pairs were analysed using the cross-correlation method previously described for $GAD65^+$ and TH^+ pairs (Chapter 4.2.2). Five out of six pairs exhibited a cross-correlation peak value above the previously set threshold of 0.13 and were therefore considered to exhibit strong synchrony in their sub-threshold activity (Figure 5.3b). The cross-correlation peak values of all six pairs were on average significantly higher than the cross-correlation peak values of pseudo pairs generated from the same dataset (Figure 5.3b). When analysing the reconstruction of the least synchronised pair, it became apparent that the two neurons both innervated the M72 glomerulus (Figure 5.3a, top), but one neuron to a smaller extent (black neuron), which is also reflected in the difference of synchronised event amplitudes in both cells (Figure 5.3a, bottom).

5.2.2 Sensory Stimulation and Deprivation of the M72 Network

To assess the dependence of SPAs on history of glomerular activation, M72-IRES-ChR2-YFP mice were either exposed to 2-AHP or deprived of odour input. After mice received either of these treatments, coronal slices were prepared and the SPA was measured in neurons that were either affiliated to the M72 (confirmed with light stimulation of ChR2) or not affiliated to M72. To ensure lack of affiliation to the M72 networks, only neurons that did not respond to light stimulation and that had somata a large distance from the M72 glomerulus (> 500 μm) were analysed. Results from whole-cell recordings under both experimental conditions were then compared to recordings obtained from control animals that did not receive any treatment.

Analysis of the SPAs of M72-affiliated and non-M72-affiliated neurons within each of the three experimental conditions (odour-exposed, control, odour-deprived) revealed no significant differences in median and variance in any comparison in both chemotypes (GAD65$^+$: $p_{odour} = 0.709$, $p_{control} = 0.318$, $p_{Zn} = 0.779$; TH$^+$: $p_{odour} = 0.107$, $p_{control} = 0.596$, $p_{Zn} = 0.283$; Figure 5.4a and b).

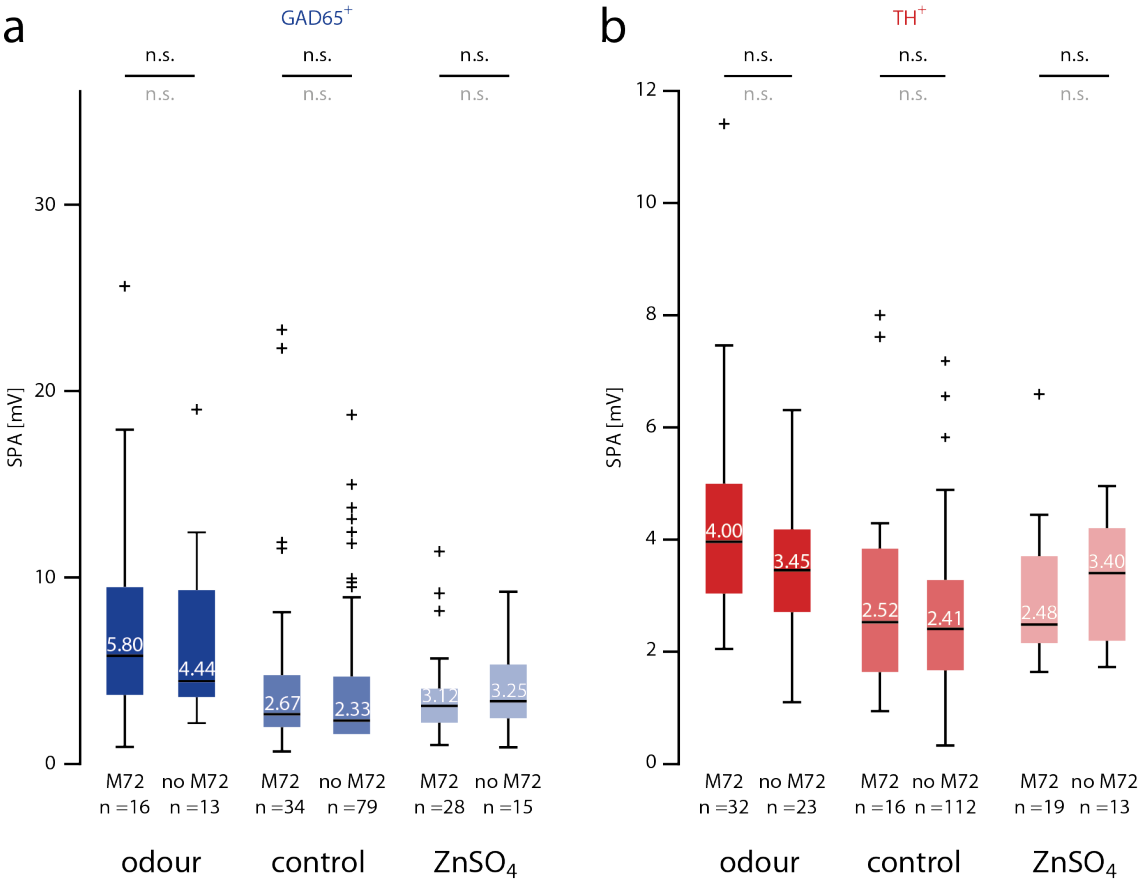

Figure 5.4 SPAs in M72-Affiliated GAD65$^+$ and TH$^+$ Neurons are Similar to Neurons Innervating Other Glomeruli

(a) Boxplot comparing the SPAs of GAD65$^+$ neurons innervating M72 glomeruli to GAD65$^+$ neurons innervating other glomeruli. Recordings from GAD65$^+$ neurons were divided according to the three experimental conditions the cells were recorded in: Seven day exposure to 5 % 2-AHP, untreated control and treatment with $ZnSO_4$. **(b)** Boxplot comparing the SPAs of TH$^+$ neurons innervating M72 glomeruli to TH$^+$ neurons innervating other glomeruli under the same three experimental conditions. Significance levels were determined by a Wilcoxon rank sum test for median *(black)* and a Brown–Forsythe test for variance *(grey)*; n.s.= not significant.

In both GAD65$^+$ and TH$^+$ neurons the SPA in M72-affiliated neurons from odour-exposed animals was significantly larger than the SPA in M72-affiliated neurons from control animals and odour-deprived animals (odour vs. control: p_{GAD65} = 0.026, p_{TH} = 0.012; odour vs. $ZnSO_4$: p_{GAD65} = 0.016, p_{TH} = 0.007; Figure 5.5). Moreover, in both chemotypes the SPAs of odour-deprived animals were not significantly different from

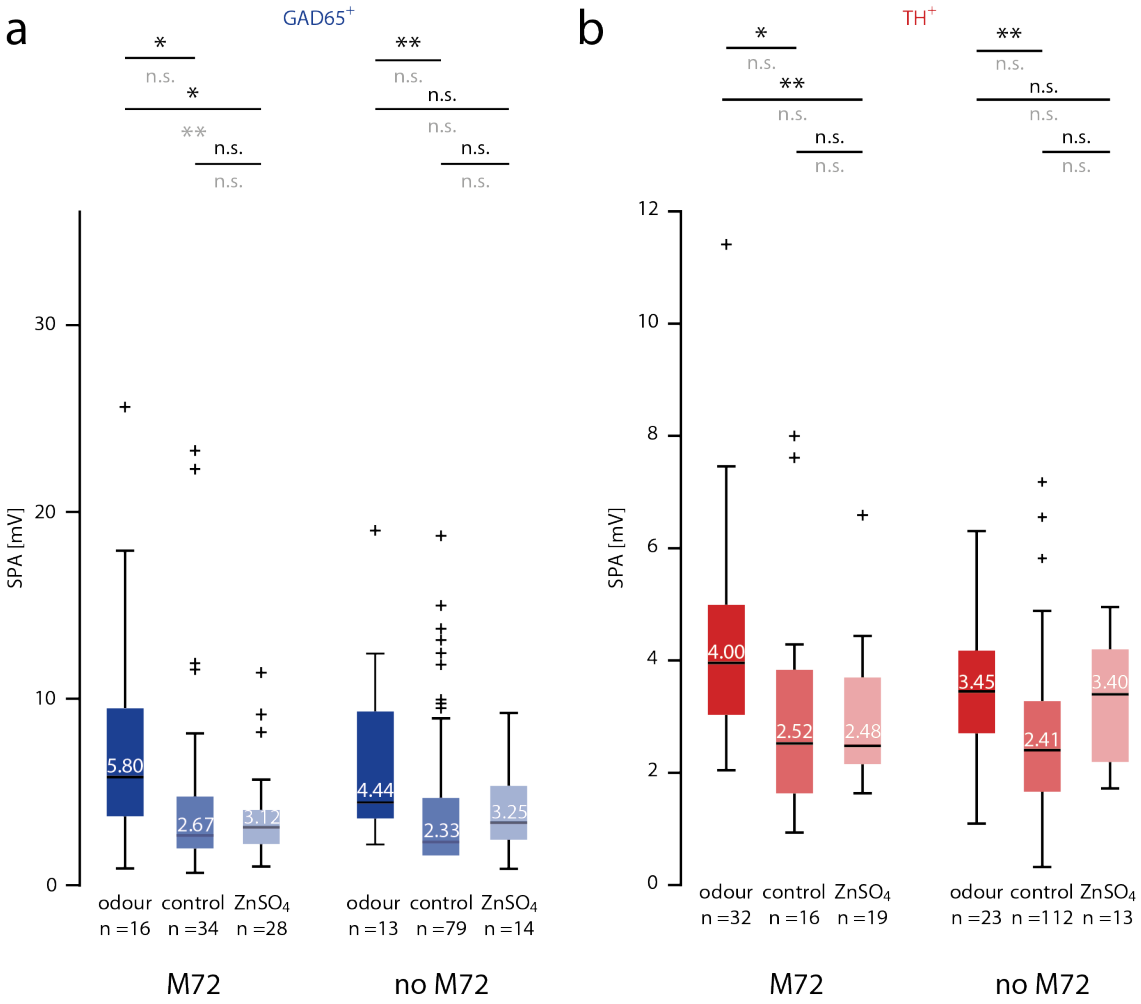

Figure 5.5 Long-Term Stimulation of the M72 Network with an Odour Ligand Increases the SPA in Interneurons Affiliated to M72

(a) *left:* Boxplot of GAD65$^+$ neurons affiliated to the M72 glomerulus divided in the three different conditions the cells were recorded in: Seven day exposure to 5 % 2-AHP, untreated control and treatment with $ZnSO_4$. *right:* Same boxplots for GAD65$^+$ neurons that did not innervate an M72 glomerulus. GAD65$^+$ population divided according to the same three experimental conditions.
(b) Boxplots as in (a) for TH$^+$ neurons either affiliated to the M72 glomerulus (*left*) or to other glomeruli (*right*) with recordings divided into the same three experimental conditions. Significance levels were determined by two-way ANOVA and post-hoc test (Wilcoxon rank sum test, Holm-Bonferroni corrected); n.s. = not significant, *: p-value < 0.05, **: p-value < 0.01, ***: p < 0.001.

the SPAs of control animals (p_{GAD65} = 0.750, p_{TH} = 0.631; Figure 5.5). Additionally, the SPAs of M72-affiliated GAD65$^+$ neurons in odour-exposed animals were significantly more diverse than the SPAs of M72-affiliated GAD65$^+$ neurons in odour-deprived animals (p = 0.009; Figure 5.5a, left).

Comparing non-M72-affiliated GAD65$^+$ and TH$^+$ neurons showed a significantly larger SPA in odour-exposed animals compared to control animals (p_{GAD65} = 0.007, p_{TH} = 0.008; Figure 5.5). However, no differences were seen in the SPAs of odour-treated and odour-deprived animals for either cell type (p_{GAD65} = 0.188, p_{TH} = 0.767; Figure 5.5). Furthermore, the SPA of TH$^+$ neurons in odour-deprived animals was significantly larger than the SPA in the TH$^+$ control group (p = 0.116). No significantly different variances in SPAs were observed between any of the non-M72-affiliated GAD65$^+$ or TH$^+$ populations.

5.2.3 Sag Potential Amplitude Diversity Within and Between the Two M72 Networks

Theoretically, all M72 glomeruli should receive a similar amount of odour-evoked input. Therefore, if SPA is regulated primarily due to direct sensory input (and is not primarily defined by lateral network interactions) it should be similar in neurons affiliated to these four local M72 networks. To investigate whether the location of the M72 glomerulus (medial or lateral) impacts on the SPA of a neuron affiliated to it, the SPAs measured in the medial and lateral M72 were compared for all three experimental conditions (odour-exposed, control, odour-deprived).

In both chemotypes, no significant differences in median SPA could be seen between the medial and lateral M72 glomerulus under odour-exposed (p_{GAD65} = 0.599, p_{TH} = 0.766), control (p_{GAD65} = 0.479, p_{TH} = 0.875) or odour-deprived condition (p_{GAD65} = 0.456, p_{TH} = 0.898; Figure 5.6a and b). Also the SPA variance was not significantly different between medial and lateral M72 in odour-exposed (p_{GAD65} = 0.850, p_{TH} = 0.653), control (p_{GAD65} = 0.324, p_{TH} = 0.310) or odour-deprived animals (p_{GAD65} = 0.726, p_{TH} = 0.992; Figure 5.6a and b).

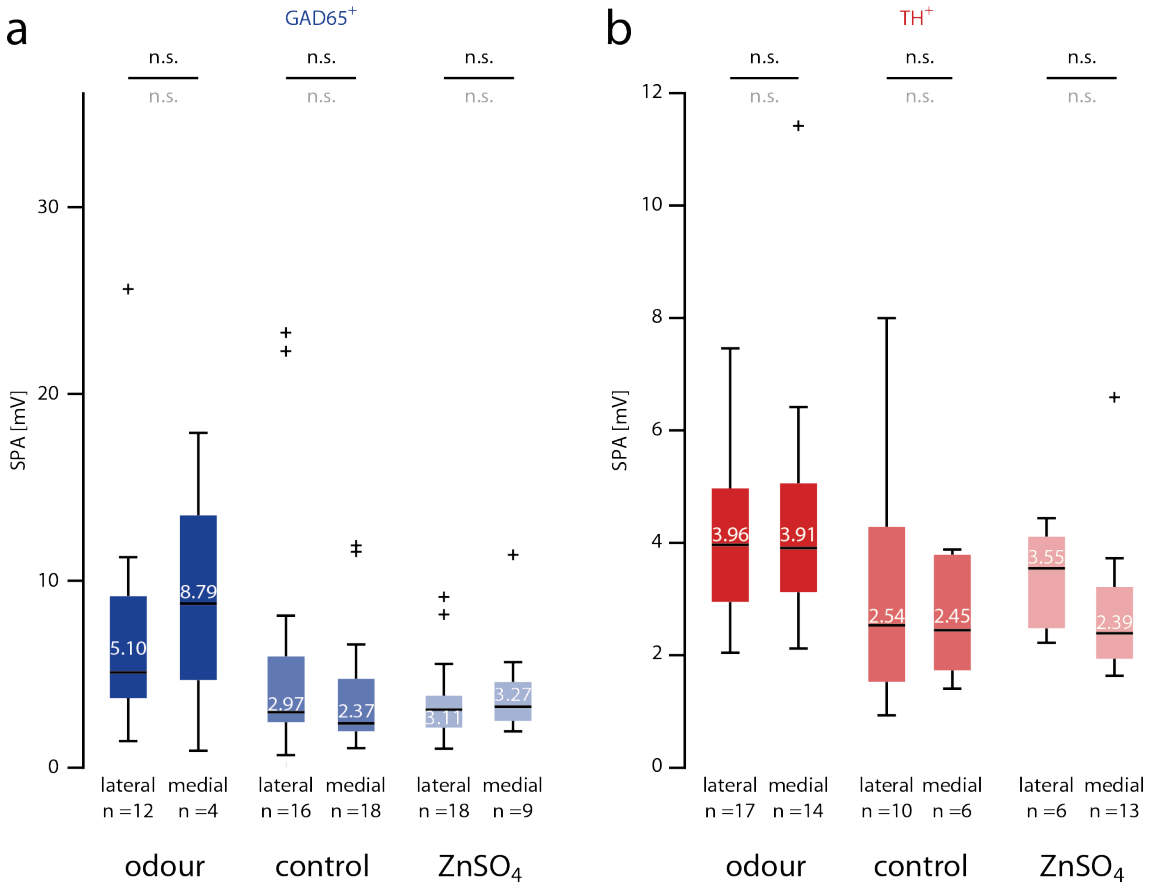

Figure 5.6 SPAs Do Not Depend on the Affiliation of GAD65$^+$ and TH$^+$ Neurons to the Lateral and Medial M72 Glomerulus

(a) Boxplot of GAD65$^+$ neurons receiving input from the lateral or medial M72 glomerulus, divided in the three different conditions the cells were recorded in: Seven day exposure to 5 % 2-AHP, untreated control and treatment with $ZnSO_4$. **(b)** Boxplot comparing the SPAs of TH$^+$ neurons innervating the lateral or medial M72 glomerulus in same three experimental conditions. Significance levels were determined by a Wilcoxon rank sum test for median *(black)* and a Brown–Forsythe test for variance *(grey)*; n.s.= not significant.

5.3 Discussion

The activity of a neuron can impact on HCN channel gating properties (Wang et al. 2002) as well as expression levels (Fan et al. 2005). I_h has in turn been shown to modulate neuronal excitability in various different cell types (Biel et al. 2009). Taken together, the activity-dependent plasticity of HCN channels can provide a feedback mechanism, regulating the input/output function of a neuron (McCormick and Pape 1990; Hutcheon and Yarom 2000; Giocomo and Hasselmo 2009; Wahl-Schott and Biel 2009). However, activity-dependent regulation of I_h has not been proposed to tune the output of a local network in any other brain area so far. The aim of this chapter was therefore to determine if there is evidence for a network-dependent, homotypic mechanism, regulating the SPA of interneurons within the glomerular network. The first step towards this was to explore whether the level of SPA is dependent on the activity history of the network and presumably the neuron.

To test this hypothesis, the genetically modified mouse line M72-IRES-ChR2-YFP (Smear et al. 2013) was used, which allowed the visualisation, targeted stimulation and recording from a specific glomerular network. One of the biggest challenges in using this system in slice physiology was to slice the OB in a way that ensured mostly intact, yet sufficiently superficial M72 glomeruli. During repeated experiments it became apparent that only light stimulation of an M72 glomerulus that was largely intact resulted in stable and reliable light-evoked responses in post-synaptically connected neurons throughout the duration of a whole-cell recording. After successful slice preparation, the activation of ChR2 in this mouse line provided a reliable way of testing the affiliation of individual neurons to a specific glomerular network, as several control experiments confirmed (Figure 5.2). By crossing Gad2-IRES-Cre-tdTomato or TH(9.0)tagRFP with the M72-IRES-ChR2-YFP mouse line it was possible to repeatedly target the same $GAD65^+$ and TH^+ interneuron population across different animals and experiments through light stimulation.

For data analysis, only neurons with a presumed monosynaptic connection to the M72 glomerulus were used, defined by reliable, short-latency post-synaptic responses to light stimulation of ChR2. Channelrhodopsin has an opening time around 2 ms (Nagel et al. 2005), but these opening kinetics can be slower, depending on the light intensity used,

as well as temperature and voltage (Chater et al. 2010). ChR2-induced depolarising currents can reach maximal rise within 2.3 ms in cultured neurons (Boyden et al. 2005; H134R might be slower) and elicit action potential firing in cultured hippocampal neurons with a latency of around 5 ms (Lin et al. 2009). It has also been shown that light activation can induce action potentials with similar latencies locally in axons (Schoenenberger et al. 2011). Taken together, a median response latency of 5.4 ms for $GAD65^+$ neurons and 5.9 ms for TH^+ neurons is consistent with the delay of previously reported channelrhodopsin-evoked responses and therefore likely the result of a monosynaptic connection between OSNs and interneurons. Varying numbers of stimulated axons and light-gated channels, and variable light penetration of the tissue might have cause the latency variance observed.

The high cross-correlation values measured in simultaneously recorded, M72-affiliated $GAD65^+$ neurons (Figure 5.3) further support the hypothesis that coincident events indicate synaptic input from the same local networks, as discussed in Chapter 4. The morphological reconstruction of the pair that exhibited the lowest cross-correlation value confirmed that even in this pair both neurons innervate the same M72 glomerulus (Figure 5.3a). These results suggest that while a high cross-correlation value indicates affiliation to a common glomerulus, a low cross-correlation value does not exclude it. Instead, a silent glomerular network, or neurons only receiving a small fraction of their input from the common network could cause the low cross-correlation values. Both hypotheses are possible for the presented low cross-correlation pair. Furthermore, these results suggest that the highly synchronised pairs might either receive common input from more than one network or receive the majority of their input from the shared source. Unfortunately, comparing only five $GAD65^+$ pairs with eight pseudo pairs did not provide the power necessary for a robust statistical analysis, but for future experiments, it would be interesting to see whether the SPA in these simultaneously recorded M72 pairs is more similar than the SPA from pseudo pairs.

To address whether there is evidence for SPA dependence on the history of network activity, changes in the activity of neurons participating in the M72 network were introduced by odour exposure or odour deprivation of animals.

Compared to the general OSN population, the OR160 OSNs converging onto the M72 glomerulus appear to be typical in their OR expression profile and innervation pattern (Zheng et al. 2000; Potter et al. 2001; Feinstein and Mombaerts 2004). In accordance with this, no significant differences between the SPAs measured in M72-affiliated and non-M72-affiliated neurons were observed in control conditions (Figure 5.4), showing that the M72 glomerulus is a valid model network to test our hypothesis and extrapolate findings to other glomerular networks. However, once a mouse line with ChR-YFP expression in another glomerulus becomes available it would be very interesting to repeat these recordings from neurons affiliated to a different glomerulus in order to generalise the results seen for neurons participating in the M72 network.

Also, odour deprivation was not selective for M72-affiliated OSNs, because the $ZnSO_4$-treatment non-specifically targets all OSNs. Therefore, no significant differences between the SPAs measured in M72-affiliated and non-M72-affiliated neurons were observed in the odour-deprived condition (Figure 5.4). It will be necessary to confirm these findings through control experiments using saline for nasal rinsing, as established with 0.9% w/v NaCl by Bracey et al. (2013).

It is perhaps not surprising to see an overall increase in SPA in all recordings from the odour-exposed group, even in neurons not affiliated to M72 (Figure 5.4). 2-HAP is not a specific ligand for M72, but likely an agonist for a range of different ORs, like OR151 which is expressed in OSNs converging onto M71 (Zhang et al. 2012). Furthermore, it has been shown that the exposure to an odour can increase the overall sensitivity to odours (Kass et al. 2016). However, a trend toward higher SPAs is observable in the M72 datasets for both odour-treated $GAD65^+$ and TH^+ populations and the lack of significance might be a result of too few data points.

The long-term exposure of animals to the M72 ligand 2-HAP caused an increase in SPA compared to control and $ZnSO_4$-treated animals in both M72-$GAD65^+$ and M72-TH^+ neurons (Figure 5.5). These results strongly suggest that odour-evoked activity can regulate SPA in these two types of interneurons.

When comparing the $ZnSO_4$-treatment group with the other two conditions, SPAs in the $ZnSO_4$-dataset consistently showed the lowest variability (Figure 5.5). Large SPA variability in the odour-treated and control groups was expected, because animals are continuously exposed to diverse range of complex odours in their normal environment.

However, this sensory input should be reduced in the anosmic $ZnSO_4$-treatment group, which in turn would be expected to reduce SPA variability and median SPA. Surprisingly, the odour-deprivation with $ZnSO_4$ did not cause a significant reduction in median SPA in either $GAD65^+$ or TH^+ neurons (and in one case even caused an increase compared to control conditions). This may be for several reasons. First, the median SPA recorded in control animals was rather small and potentially a large number of experiments would need to be conducted to show a significant reduction. Second, the $ZnSO_4$ might not have caused a full anosmia. Previous experiments demonstrated an anosmia in $ZnSO_4$-treated animals after one to four days (Ducray et al. 2002; McBride et al. 2003; Bracey et al. 2013). In the current experiments the electrophysiological recordings were conducted one day after the $ZnSO_4$ treatment, in order to preserve the ChR2-YFP expressing axons of the M72 glomerulus. One day might not be enough time to sufficiently down-regulate the activity of the glomerular networks, so the timing of these experiments might need to be adjusted accordingly. However, finding the balance between causing enough $ZnSO_4$-induced OSN degeneration and preserving ChR2-YFP expressing OSN axons may be challenging. In addition, the $ZnSO_4$-treatment might have affected the animals' behaviour. As shown by previous publications, OSN depletion by $ZnSO_4$ can result in altered performance of animals during behavioural tasks (Harding et al. 1978; Mayer and Rosenblatt 1993; McBride et al. 2003; Bracey et al. 2013), which might ultimately have global effect on the intrinsic properties of neurons participating in a highly plastic neuronal network, like the OB. Finally, the $ZnSO_4$-treatment might have had an additional unknown effect the intrinsic properties of the recorded neurons or other neurons participating in the same glomerular networks. It is conceivable that, if $ZnSO_4$ indeed induced a global depletion of OSNs, the dying OSNs could exhibit an altered firing pattern, inducing a temporal abnormal stimulation of local glomerular networks. Alternatively, the lack of OSN input might result in altered cell survival (although unlikely during such a short time period, see Harding et al. 1978; Mandairon et al. 2006a) or adapted intrinsic properties of neurons participating in glomerular circuits, as shown in naris occlusion experiments (Cummings and Brunjes 1997).

Next, a comparison between the SPA in the medial and lateral M72 was conducted (Figure 5.6) to address whether the SPA was at least partly dependent on the identity

and location of the glomerulus, which would suggest an additional component regulating the SPA. However, no systematic changes in SPA according to M72 identity could be observed in any of the three conditions in both chemotypes (Figure 5.6). This data strongly supports the hypothesis of a homotypic SPA regulation based on the history of sensory input in individual local networks, rather than lateral interglomerular interactions. Because all M72 glomeruli receive sensory information from clonally identical OR160 OSNs, if the SPA is predominately regulated by this sensory input, it should be similar in all four M72 networks.

However, to provide evidence for an odour-stimulation dependent activation of M72 affiliated neurons, the neuronal activation after odour stimulation would need to be demonstrated. A near future experiment that could provide such evidence would be the staining for immediate early genes, like c-fos, in animals that were stimulated with 2-HAP, as well as control animals. Repeated neuronal stimulation can lead to rapid and transient changes in gene transcription, such as the increase of immediate early gene transcription. Immediate early genes are transcribed only minutes after a cellular stimuli. So far around 40 of these genes have been identified as markers for neurons that have recently been activated (Flavell and Greenberg 2008). C-fos is one of the first immediate early genes that has been found suitable to track neuronal activation (Greenberg and Ziff 1984). Furthermore, it has been shown that c-fos, as well as the immediate early gene Egr1, are suitable to detect neuronal activation in the glomerular layer after odour stimulation (Bepari et al. 2012).

To summarise, these experiments demonstrate that I_h in glomerular networks is regulated based on glomerular affiliation and is activity-dependent. However, the experiments allow no conclusions regarding the molecular nature of the regulation. HCN channel plasticity has been shown to depend on conformational changes of the channel, as well as on changes in protein expression levels and intracellular relocation (Biel et al. 2009). To determine what mechanisms induce the SPA regulation in glomerular network, a temporally more precise change in network activity would be necessary, for example by repeated light activation of ChR2 in M72 OSNs. Unfortunately, the time for reliably measuring SPA in a whole-cell configuration is limited, making it difficult to follow light induced, activity-dependent changes in SPA during a single recording over a significant time period. However, introducing variable

durations of light-evoked activity by shining light onto the M72 glomerulus prior to whole-cell recording could help identify the time course of activity-dependent SPA regulation in these networks.

Chapter 6. Discussion

6.1 Summary of Results

This thesis investigates the diversity and activity-dependence of sag potential amplitude (SPA) in interneurons within the glomerular microcircuit of the olfactory bulb (OB). The major conclusions can be summarised as follows:

1. $GAD65^+$ and TH^+ transgenic mice are valid tools for targeting two populations of juxtaglomerular neurons that are different in their morphological (Figure 3.6, Figure 3.7) and physiological (Figure 3.9, Figure 3.13) properties.
2. Hyperpolarisation-activated current (I_h) can have a substantial impact on neuronal excitability in glomerular interneurons, as seen by the effect of its blockade in $GAD65^+$ cells (Figure 3.11), which exhibit substantial SPAs.
3. SPA correlates well with I_h amplitude in $GAD65^+$ and TH^+ neurons (Figure 3.10) and may be used as a proxy for I_h in interneuronal cell types.
4. The $GAD65^+$ interneuron population in the glomerular layer exhibits on average significantly larger and more heterogeneously distributed SPAs than the TH^+ population (Figure 3.13).
5. The degree of spontaneous sub-threshold synchrony observed for two simultaneously recorded neurons indicates affiliation to a common glomerulus (Figure 4.1, Figure 4.6 and Figure 5.3).
6. $GAD65^+$ and TH^+ neurons exhibit synchronised EPSPs with similar amplitudes, however $GAD65^+$ neurons appear to have more synchronised action potential firing than TH^+ neurons (Figure 4.4).
7. $GAD65^+$ neurons receiving input from a common network have significantly more similar SPAs than those belonging to different networks (Figure 4.6).
8. Neurons affiliated to the M72 glomerulus exhibit a distribution of SPA similar to the overall population (Figure 5.2 and Figure 5.4).

These conclusions will now be further discussed in the following sections.

6.2 GAD65$^+$ and TH$^+$ Neurons as Representative Examples for Glomerular Interneurons

In order to explore the potential physiological significance of SPA diversity in the glomerular layer, a method to reliably target the same juxtaglomerular subpopulation across animals and experiments was crucial. Using neurochemical markers to target distinct interneuron populations provided a reliable high-throughput method for performing recordings from neurons belonging to these populations. Also, in the densely populated glomerular layer, the genetic labelling of interneurons increased the success rate of simultaneous recordings from members of the same neuronal class.

GAD65$^+$ and TH$^+$ juxtaglomerular neurons were selected for two main reasons. Firstly, the two classes exhibit only moderate chemotopic overlap in the OB (Parrish-Aungst et al. 2007; Kiyokage et al. 2010; Figure 3.2). Secondly and most importantly, several previous publications established that GAD65$^+$ and TH$^+$ neurons morphologically resemble periglomerular (PG) cells (Aungst et al. 2003; Shao et al. 2009; Kiyokage et al. 2010) and short axon (SA) cells, respectively (Kiyokage et al. 2010; Liu et al. 2013). PG and SA cells are morphologically well-described classes of glomerular interneurons (section 1.4.1.3). While PG cells are believed to mediate intraglomerular inhibition, SA cells are thought to predominately mediate inhibition between glomeruli (section 1.4.2), which leads to the conclusion that these two classes of interneurons may be functionally distinct. By targeting these two classes, the aim was therefore to explore the diversity and regulation of I_h in the context of functionally different glomerular interneurons.

However, in order to interpret the result of the presented experiments one needs to first consider the limitations of defining neurons solely by their neurochemical expression profile. In the OB, the GAD65$^+$ and TH$^+$ interneuron population exhibit a small degree of overlap in the expression of their molecular markers, resulting in a small number of GAD65$^+$ neurons also being TH$^+$ and vice versa. When exploring an intrinsic biophysical property such as I_h in GAD65$^+$ and TH$^+$ interneurons, this overlap in molecular marker expression is likely to result in a small amount of cross-sampling in the data recorded from both chemotypes. Additionally, when working with developmentally plastic (Kosaka and Kosaka 2009; Akiba et al. 2010) and activity-dependent (Baker et al. 1983; Cigola et al. 1998; Parrish-Aungst et al. 2011; Banerjee et

al. 2013) marker molecules such as tyrosine hydroxylase, it is unlikely that the entire population of neurons will be fluorescently labelled. Moreover, a gradient in fluorescent labelling may introduce a bias in data sampling. However, the wide distribution of soma sizes and glomerular innervation patterns in the TH^+ dataset suggests that the sampling of TH^+ neurons was not restricted to a single subpopulation and therefore makes a selection bias less likely. In addition to $GAD65^+$ and TH^+ neurons exhibiting different chemical and morphological characteristics, each chemotype constitutes a diverse population of neurons (Halasz et al. 1981; McLean and Shipley 1988; Kosaka et al. 1998; Hayar et al. 2004a; Parrish-Aungst et al. 2007; Shao et al. 2009; Kiyokage et al. 2010; Banerjee et al. 2013; Chand et al. 2015). However, since the within-class distribution of morphological data was not found to be multimodal, no further sub-classification of $GAD65^+$ and TH^+ neurons was conducted so far, but may be considered for future analyses.

To that end, a cluster analysis performed on biophysical properties of these neurons, as carried out on OB principal and interneurons neurons by Kollo et al. (2014) (supplementary figure 2), could reveal physiologically distinct sub-populations of $GAD65^+$ and TH^+ neurons and therefore aid understanding the heterogeneity of these two populations. Additionally, morphological reconstruction of a larger number of neurons, and a principal component analysis of morphological and physiological parameters could provide a more comprehensive picture of the $GAD65^+$ and TH^+ populations and ultimately lead to reliable prediction of morphologically defined types without the need of laborious manual reconstructions. Increasing the number of morphological reconstructions from recorded neurons will be the next step in this project. Manual morphological reconstruction is an extremely laborious process, but will in future be aided by the use of partly automated tracing software (Neurolucida 360) that was recently made available in the lab.

Despite overlap in molecular, morphological and biophysical features, $GAD65^+$ and TH^+ neurons exhibit unique phenotypes regarding the distribution of SPA. The TH^+ population had, in general, very low and homogeneous levels of SPA, whereas the $GAD65^+$ population exhibited large diversity in their amplitudes of membrane potential sag.

6.3 Network-Dependent Regulation of Sag Potential Amplitude in Interneurons of the Glomerular Layer

Network-dependent regulation of SPA could be shown for neurons belonging to the $GAD65^+$ population. Membership of two neurons to the same local network was determined by quantifying the strength of synchrony in their sub-threshold activity. When simultaneously recording from two $GAD65^+$ neurons that were affiliated to the same local network, SPAs were significantly more similar than the SPAs of two randomly paired neurons from the same dataset. Interestingly, the TH^+ population only exhibited a trend towards more similar SPAs, despite sampling from twice as many pairs. One possible explanation might be that SPA in TH^+ neurons is not regulated in an activity-dependent manner. However, since both populations exhibited an increase in SPA in response to odour exposure (see Chapter 5), the regulation of I_h is likely to be subject to similar activity-dependent mechanisms in both cell types.

$GAD65^+$ neurons exhibited a much wider distribution of SPA than TH^+ neurons. It is therefore likely that uncovering any activity-dependent SPA regulation in TH^+ neurons requires a larger sample size, since the narrow distribution of SPAs results in a relatively small difference in SPA between any pair of TH^+ cells, independent of their network affiliation. This in turn means many more data points would be needed in the TH^+ population to observe a potential difference between pairs and pseudo-pairs compared to the $GAD65^+$ population.

Alternatively, activity-dependent regulation of SPA might have a larger impact on information processing in $GAD65^+$ neurons than in TH^+ neurons. In both chemotypes the temporal coincidence in their synaptic input correlates well with the degree of their dendritic overlap and thus potentially the location of their synaptic contacts.

However, as morphological reconstructions revealed, $GAD65^+$ neurons innervate on average significantly fewer glomeruli than TH^+ neurons (2 vs. 5 glomeruli), with a denser innervation pattern. Because of this local restriction of $GAD65^+$ dendrites, the majority of synchronised synaptic events in two simultaneously recorded $GAD65^+$ neurons must originate from the inputs of one, or possibly two glomeruli. On a functional level, the activity-dependent regulation of SPA together with innervation of few glomeruli could result in a strong relationship between I_h and the activity of

individual glomeruli. In contrast, in TH^+ neurons any activity-dependent regulation of SPA is likely the result of more diverse glomerular input and could be "averaged out", which would also explain the more homogeneous SPA distribution in this neuronal population.

6.4 Odour-Dependent Regulation of Sag Potential Amplitude in Interneurons of the Glomerular Layer

The experiments described in Chapter 5 demonstrate an increase in SPA in both $GAD65^+$ and TH^+ neurons after long-term exposure of animals to a monomolecular odour source. These results strongly suggest a dependence of SPA on the history of activation in $GAD65^+$ and TH^+ interneurons.

To support and extend the evidence for activity-dependent regulation of I_h in glomerular interneurons, experiments in which animals were deprived from sensory input were also conducted. If SPA linearly depended on a neuron's activity, the depletion of olfactory sensory neurons (OSN) by nasal irrigation with $ZnSO_4$ would be expected to reduce SPA. However, no such effect was seen when comparing SPAs in the $ZnSO_4$-treatment group with SPAs recorded in the control group. As discussed earlier (section 5.3), it might be difficult to demonstrate a significant reduction of SPA in $ZnSO_4$-treated animals, because the average SPA in untreated animals was already rather small. Also, $ZnSO_4$ is thought to induce anosmia after one to four days, therefore it could be possible that more than one day between treatment and slice preparation is necessary to drastically reduce the activity in glomerular networks. Furthermore, it is unclear whether nasal irrigation with $ZnSO_4$ destroys the entire olfactory epithelium (McBride et al. 2003). Given that OSN terminals exhibit a high release probability (Murphy et al. 2004), a less than total ablation might not significantly impact transmission onto postsynaptically connected glomerular neurons. In order to clarify the interpretation of these results, further $ZnSO_4$-induced sensory deprivation experiments, potentially with an extended time period between treatment and electrophysiological recordings should be conducted. If $ZnSO_4$-treatment fails to show an activity-dependent reduction in SPA, sensory deprivation could alternatively be achieved by naris occlusion (Cummings and Brunjes 1997; Mandairon et al. 2006a). However, naris occlusions have been shown to affect survival of adult-born glomerular interneurons (Mandairon et al. 2006a) and

therefore need to be timed appropriately. A genetically modified, anosmic mouse model (Brunet et al. 1996) could also provide the long-term sensory deprivation necessary for down-regulation of SPA. Crossing such a line with mice expressing an axonal marker under the control of the OR160 promoter would make it possible to identify the M72 fibres in an anosmic mouse (Zheng et al. 2000). However, it is not clear to what extend the action potential firing rate of OSNs is decreased in anosmic animals compared to control animals (Brunet et al. 1996). Moreover, the local glomerular network formation is heavily altered in these animals (Zheng et al. 2000), which might have additional impact on SPAs in local interneurons.

In order to investigate the activity-dependence of SPA in $GAD65^+$ and TH^+ neurons in more detail, I attempted to investigate SPA modulation in response to light stimulation of ChR2 in the M72 OSN terminals. However, during whole-cell recordings, SPA exhibits rundown after a few minutes and activity-induced changes of I_h have been reported to occur on a time scale of tens of minutes (van Welie et al. 2004; Fan et al. 2005). Therefore, reliable monitoring of SPA within such small neurons may not be achievable using whole-cell recordings. An alternative approach could be repeated light stimulation of ChR2 in M72 OSNs during brain slice incubation prior to recordings. On a timescale of 30 minutes, the increased activity of M72 OSN terminals should induce activity-dependent changes in the SPA of postsynaptically connected JG cells. Thus, it would be possible to compare the levels of SPA from neurons of the stimulated slices to neurons of non-stimulated slices.

If $ZnSO_4$-treatment or naris occlusion would be used for sensory deprivation, it could be possible to perform ChR2-based rescue experiments, in which the introduction of light-evoked activity is used to assess the reversibility of deprivation-induced SPA reduction.

If light-induced OSN activity is seen to modulate SPA in $GAD65^+$ and TH^+ neurons, pharmacological experiments, as conducted by Fan et al. (2005), could be performed on these JG cells to further address the mechanisms underlying activity dependence of I_h. Fan et al. (2005) have shown that postsynaptic action potential firing is necessary for upregulation of I_h in pyramidal neurons. In general, postsynaptic depolarisation causes Ca^{2+} influx into a neuron and cytoplasmic Ca^{2+} is known to perform various regulatory functions (Berridge 1998), including the modulation of ion channels by increasing the production of second messengers like cAMP (Cooper et al. 1995) or influencing gene

transcription (Berridge 1998). By using the calcium chelator BAPTA in intracellular solution (Fan et al. 2005) or BAPTA-AM in the bath (van Welie et al. 2004) it has been shown that the upregulation of I_h depends on the Ca^{2+} influx in the postsynaptic cell. The bath application of AP5 or CNQX further demonstrated a Ca^{2+} influx in these cells, primarily through NMDA receptors. Furthermore, the use of Ca^{2+}-dependent protein kinase (CAMKII) inhibitory peptide 281–309 revealed the dependence of I_h-regulation on CaMKII, a protein kinase that regulates transcription by phosphorylation of cAMP response element-binding protein (CREB; Sun et al. 1994). Lastly, the dependence of I_h-upregulation on *de novo* protein synthesis has been demonstrated by the use of anisomycin, a protein translational inhibitor (Fan et al. 2005). In accordance with these results, preliminary experiments described in this thesis indicated that synchronised synaptic input might result in more synchronised action potential firing in pairs of $GAD65^+$ neurons compared to pairs of TH^+ neurons. If action potential firing is indeed necessary for I_h-regulation in these interneurons, a high synchrony in postsynaptic action potential firing could be the mechanism underlying the homotypic regulation of SPA in $GAD65^+$ neurons.

6.5 I_h-Mediated Activity-Dependent Changes in Neuronal Excitability

As in mitral cells (MCs), $GAD65^+$ neurons exhibited diverse SPA, which not only originated from the affiliation of a neuron to a specific network, but also from the activity history of that network. Recorded SPAs were not significantly different between neurons affiliated to the medial or lateral M72 glomerulus, which indicates that SPA regulation could be mainly driven by sensory inputs through OSNs and is potentially neither pre-determined nor driven by interglomerular interactions with neighbouring glomeruli.

The aim of this thesis was to investigate the extent to which SPA in JG cells reflect local network activity, however the impact of the described regulatory effects on the integrative properties of cells remains to be explored.

When looking at previous work on the functional impact of I_h, the current has been shown to serve diverse functions in multiple neuronal classes (Robinson and Siegelbaum 2003). These functions include intrinsic oscillations and resonance (Pape

1996; Luthi and McCormick 1998; Dickson et al. 2000; Santoro et al. 2000; Liu and Shipley 2008b; Giocomo et al. 2011), synaptic integration (Williams and Stuart 2000; Berger et al. 2001; Angelo et al. 2007) and regulation of neuronal excitability (Poolos et al. 2002; van Welie et al. 2004; Fan et al. 2005; Nolan et al. 2007). No intrinsic oscillations or resonance has so far been shown for $GAD65^+$ and TH^+ JG neurons and exploring the dendritic integration of inputs or the distribution of ion channels on the dendritic arbour would be challenging due to the small size of these neurons.

Therefore, the focus of future experiments may be on how somatic HCN channel activity influences neuronal excitability by modulating the subthreshold voltage range.

As indicted by preliminary pharmacological experiments with the HCN channel blocker ZD7288 and analysis of synchronised action potential firing in paired recordings, I_h might have more impact on the excitability of $GAD65^+$ neurons. Upon specific blockade of HCN channels with ZD7288, $GAD65^+$ neurons exhibited a significant increase in their input resistance and a significant decrease in their probability of generating a rebound action potential. Both properties can influence the intrinsic excitability of neurons (Pape 1996; Robinson and Siegelbaum 2003; van Welie et al. 2004; Engbers et al. 2011; Gastrein et al. 2011). In contrast, no significant increase in input resistance was seen in TH^+ neurons and most TH^+ neurons did not exhibit rebound spiking under control conditions. More pharmacological experiments and experiments altering network activity need to be conducted in order to predict the impact of activity-dependent I_h regulation onto the integration of sensory stimuli in the glomerular layer.

HCN channels have been shown to alter passive properties, including membrane potential and input resistance (Pape 1996; Berger et al. 2003; Robinson and Siegelbaum 2003; van Welie et al. 2004; Aponte et al. 2006) as well as active properties, such as firing patterns (Nolan et al. 2007). However, whether an increase in I_h results in an increase or decrease of neuronal excitability depends on the interplay of I_h with other voltage-activated ion channels and the fine balance of passive membrane properties in each neuron. For example, in CA1 pyramidal cells I_h has been shown to reduce intrinsic excitability of both dendrites (Poolos et al. 2002) and soma (van Welie et al. 2004; Fan et al. 2005), but hippocampal interneurons and MCs show an increased excitability in the presence of I_h (Aponte et al. 2006; Angelo and Margrie 2011). It is known that depending on, for example neuromodulators (Marder 2012) or second messengers

(Siegelbaum et al. 1982), a given set of ion channels in a neuron can produce heterogeneous firing dynamics, but conversely different ion channel compositions can produce the same firing profile (Marder and Goaillard 2006). Consequently, the effect of I_h on neuronal excitability depends strongly on the balance of intrinsic properties, and can even change within a single neuron depending on the presence of neuromodulators (Pape and McCormick 1989). Therefore, the activity-dependent regulation of I_h is thought to be a homeostatic mechanism, scaling the output of neurons as an adaptive response to changes in synaptic input (van Welie et al. 2004). It would be of particular interest to investigate the impact of activity-dependent I_h regulation not only on a physiological level, but as a next step, also on a behavioural level. The regulation of integration of synaptic information through I_h has been suggested to play a role in learning and memory as well as synaptic plasticity in hippocampal CA1 pyramidal cells (Nolan et al. 2004). In the distal dendrites of these pyramidal neurons the activity of HCN1 channels is thought to counteract postsynaptic changes in membrane potential that would normally trigger synaptic plasticity. Furthermore, a recent modelling study suggested that a linear relationship between HCN channel plasticity and synaptic plasticity in hippocampal pyramidal neurons is necessary for firing rate homeostasis (Honnuraiah and Narayanan 2013). This study concludes that HCN channels are critical for a dynamic gain control mechanism that regulates synaptic learning in these neurons. In the olfactory system, MCs exhibit synaptic plasticity (Ennis et al. 1998; Delaney et al. 2009) and, similar to CA1 pyramidal cells, also exhibit larger I_h at the distal area of their apical dendrite (Angelo and Margrie 2011). Therefore it is conceivable that HCN1 channels might have a similar impact on olfactory learning and memory.

6.6 Implications of This Study

Within a glomerulus, JG interneurons are crucial for governing the strength and temporal structure of activity in principal neurons using feed-forward and recurrent inhibition (Aungst et al. 2003; Murphy et al. 2005; Shao et al. 2009). The results of the pharmacological block of HCN channels described in Chapter 3 suggest that I_h might increase the excitability of $GAD65^+$ neurons. If these results are confirmed in further experiments, it can be assumed that, on the level of local glomerular networks, I_h influences the balance of excitation and inhibition in principal neurons. The increase of

SPA upon increased sensory input might result in stronger feed-forward inhibition of principal neurons, reduction of their feed-forward excitation via inhibition of external tufted cells and recurrent inhibition of principal neurons via inhibition of OSN terminals. Interestingly, the inhibition of principal neurons mediated by $GAD65^+$ neurons appears to dominate at lower odour concentrations, whereas stimulation with high odour concentrations tends to result in a net excitation of principal neurons (Fukunaga et al. 2014). If a glomerulus has a history of strong activation, and I_h is therefore upregulated in affiliated $GAD65^+$ neurons, weak activation of this glomerular network might result in a stronger inhibition of principal neurons and therefore suppression of the output of previously active networks.

The network-dependence of SPA seems to play a minor role in TH^+ neurons, the type of glomerular interneuron that presumably transmits lateral, interglomerular inhibition. Therefore, a network- and activity-dependent regulation of I_h may serve as a form of gain control mechanism specifically on the level of local networks. Such a mechanism could tune the dynamic range of all neurons participating in the same glomerular network and shape their output across diverse levels of input activity. Since odour-induced changes of SPA persisted over several days, one could imagine an adaptive mechanism that decreases responsiveness of local glomerular networks underlying persistent stimulation. Such a mechanism could for example help scale the output of the olfactory system in the presence of background odours.

HCN channels show a rather ubiquitous expression and I_h has been demonstrated to shape the integrative properties of neurons throughout the brain (Robinson and Siegelbaum 2003; Wahl-Schott and Biel 2009). Furthermore, variations in I_h levels within the same cell type have been described in several brain regions (Giocomo and Hasselmo 2008; Hemond et al. 2009). However, the homeostatic impact of I_h plasticity on a neuron has been rather sparsely studied in principal neurons, like CA1 pyramidal neurons of the hippocampus (van Welie et al. 2004; Fan et al. 2005), but never in interneurons. Furthermore, these studies restricted their focus on a single-cell level and did not consider homeostatic regulation of networks through I_h. In addition, I_h was largely viewed as static, for instance the graded HCN channel expression in grid cells along the dorsal-ventral axis of the medial entorhinal cortex (Giocomo et al. 2011) or along the tonotopic axis of the nucleus laminaris (Yamada et al. 2005). In fact, a plastic,

network-wide regulatory mechanism through I_h was first suggested by Angelo et al. (2012). Therefore this thesis, together with previous publications of our lab (Angelo and Margrie 2011; Angelo et al. 2012), provides the first comprehensive and comparative analysis regarding the distribution, interplay and potential function of I_h in several neuronal types participating in the same local network. Once a more complete regulatory mechanism of I_h is established, the gained knowledge can likely be transferred and tested in other sensory areas, like the barrel cortex. In the barrel cortex sensory deprivation causes downregulation of HCN channel density in layer 5 pyramidal neurons, which results in an increased excitability, but also in a more likely discharge of action potential bursts (Breton and Stuart 2009). However, a potential function of I_h in interneurons of the same microcircuit is unknown.

Furthermore, the research of homeostatic I_h plasticity in interneurons of the OB could have implications for interneurons in other brain areas. For instance GABA-mediated inhibition is essential for synchronisation through local oscillations in neuronal populations of several brain areas (Buzsaki and Chrobak 1995; Singer 1996; Traub et al. 1998). Exploring the potential contribution of I_h to synchronisation of neuronal populations in the OB could contribute to a broader understanding of how GABAergic interneurons operate in local networks.

6.7 Future Directions

The findings presented in this thesis have raised new questions regarding the classification of glomerular interneurons and mechanisms behind network- and activity-based regulation of I_h, as well as the functional relevance of such regulatory mechanisms. In the following section, experiments proposed to target these questions are summarised:

1. The results presented in this thesis are based on a large set of electrophysiological recordings from $GAD65^+$ and TH^+ neurons. So far, no publication has presented a sub-classification of these interneurons using such a large dataset of intrinsic biophysical properties. Therefore, a systematic classification of $GAD65^+$ and TH^+ neurons based on intrinsic biophysical properties using a cluster analysis approach would help to further characterise these glomerular interneurons.

2. Obtaining a greater number of morphological reconstructions from recorded $GAD65^+$ and TH^+ neurons could refine our knowledge about morphological characteristics of these interneurons. Additionally, correlation between morphological and physiological characteristics of larger numbers of $GAD65^+$ and TH^+ neurons could establish a protocol for prediction of JG cell types purely based on electrophysiological measurements.

3. The results of this thesis strongly suggest an activity-dependent regulation of SPA in $GAD65^+$ and TH^+ neurons. To confirm and further establish the mechanisms behind such a homotypic mechanism of regulation, a protocol should be established for induction of SPA plasticity under temporally precise conditions using light stimulation of ChR2 in the M72 OSN terminals. Investigating the timing of SPA plasticity in more detail can help reveal the molecular mechanisms underlying the adaptive property of HCN channels (for example conformational changes of the channel vs. expressional changes).

4. Further experiments will be necessary to interpret the lack of SPA reduction observed after sensory deprivation by $ZnSO_4$-treatment. Additionally, control experiments with saline treatment will be necessary, as previously established by Bracey et al. (2013). If it is not possible to induce sufficient changes in glomerular network activity with $ZnSO_4$, nasal occlusion or genetically modified, anosmic animals could be used instead.

5. To address the impact of I_h on neuronal excitability in glomerular interneurons, a comparison of passive membrane properties (e.g. resting membrane potential, input resistance) and firing patterns in $GAD65^+$ and TH^+ neurons with and without pharmacological block of HCN channels should be conducted. It would also be interesting to investigate potential changes in neuronal excitability after odour stimulation, however it might be difficult to directly link these changes to the upregulation of I_h.

6. On a longer time-scale, pharmacological experiments, as conducted by Fan et al. 2005, should be considered to explore the molecular machinery underlying activity-dependent regulation of I_h in JG neurons.

7. Addressing the behavioural relevance of activity-dependent regulation of SPA in local glomerular networks could be a long-term goal of this research. Inducing SPA plasticity in behaving animals with light stimulation of the M72 glomerulus, is one possible way of investigating the significance of I_h modulation in olfactory performance.

To summarise, I have shown for the first time that I_h in glomerular interneurons is regulated by local network activity and sensory experience.

Together with the work of Angelo et al. (2012), these results indicate that HCN channels, which have a profound impact on network excitability, are regulated in both principal cells and interneurons as a result of odour processing. Given the simple anatomical structure of the OB and the fact it is possible to target, stimulate and record from specific glomerular circuits, the OB is an ideal structure to investigate the behavioural relevance of I_h regulation.

Chapter 7. Appendix

List of Reagents

2′-Hydroxyacetophenone ≥ 98 %	Sigma-Aldrich
4-Aminopyridine	Sigma-Aldrich
Adenosine 5′-triphosphate disodium salt hydrate (Na_2-ATP)	Sigma-Aldrich
Adenosine 5′-triphosphate magnesium salt (Mg-ATP)	Sigma-Aldrich
Alexa Fluor® 488 Hydrazide	Life Technologies
L-Ascorbic acid BioXtra, ≥ 99.0 %	Sigma-Aldrich
Certified™ Molecular Biology Agarose	Bio-Rad
Barium chloride dehydrate ($BaCl_2$)	Sigma-Aldrich
Biocytin hydrochloride ≥ 98 %	Sigma-Aldrich
Calcium chloride solution volumetric, 1.0 M ($CaCl_2$)	Sigma-Aldrich
Cobalt(II) chloride 97 % ($CoCl_2$)	Sigma-Aldrich
SIGMAFAST™ 3,3′-Diaminobenzidine tablets (DAB)	Sigma-Aldrich
D-(+)-Glucose BioXtra, ≥ 99.5 %	Sigma-Aldrich
D-2-amino-5-phosphonovalerate (D-AP5)	Tocris
Ethyleneglycol-bis(2-aminoethylether)-N,N,N′,N′-tetraacetic acid BioUltra, ≥ 99.0 % (EGTA)	Sigma-Aldrich
Ethanol, absolute ≥ 99.8 %	Fischer Scientific
Glycerol AnalaR	VWR
Guanosine 5′-triphosphate sodium salt hydrate (Na_2-GTP)	Sigma-Aldrich
Hydrogen peroxide solution 30 wt. % in H_2O	Sigma-Aldrich
HEPES BioXtra ≥ 99.5 %	Sigma-Aldrich
Magnesium chloride solution volumetric, 1.0 M ($MgCl_2$)	Sigma-Aldrich
Mineral oil	Sigma-Aldrich
MOWIOL® 4-88 Reagent	Calbiochem
Sodium chloride BioXtra, ≥ 99.5 % (NaCl)	Sigma-Aldrich
Sodium bicarbonate ≥ 99.5 % ($NaHCO_3$)	Sigma-Aldrich
Sodium phosphate monobasic BioXtra, ≥ 99.0 % (NaH_2PO_4)	Sigma-Aldrich
2,3-Dioxo-6-nitro-1,2,3,4-tetrahydrobenzo[*f*]quinoxaline-7-	Tocris

sulfonamide disodium salt (NBQX)	
Paraformaldehyde powder, 95 %	Sigma-Aldrich
Picrotoxin	Sigma-Aldrich
Potassium chloride EMSURE® (KCl)	Merck Millipore
Potassium methanesulfonate ≥ 98.0 % (CH_3KO_3S)	Sigma-Aldrich
Tetraethylammonium chloride hydrate (TEA-Cl)	Sigma-Aldrich
Triton™ X-100	Sigma-Aldrich
Tetrodotoxin (TTX)	Tocris
ZD7288 hydrate ≥ 98 %	Sigma-Aldrich
Zinc sulphate monohydrate ≥ 99 %	Sigma-Aldrich

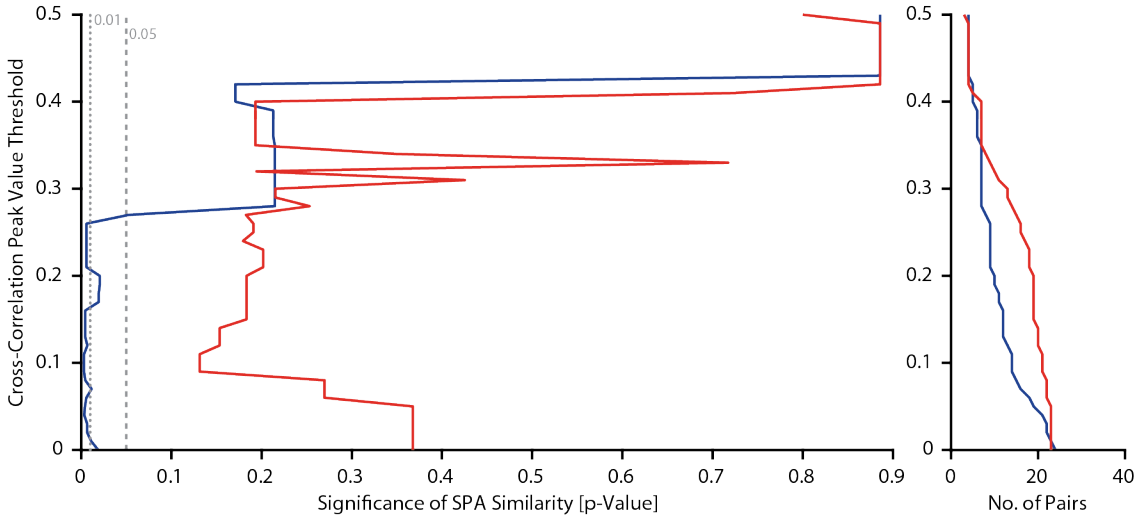

Figure 7.1 Significance of SPA Similarity in Pairs of GAD65$^+$ and TH$^+$ Neurons Depending on the Set Cross-Correlation Peak Value Threshold

Left: Graph illustrating the relationship between a chosen cross-correlation peak value threshold (0 – 0.5, corresponding to Figure 4.6) and the significance of SPA similarity in synchronised pairs of GAD65$^+$ *(blue)* and TH$^+$ *(red)* neurons compared to corresponding pseudo pairs using a Wilcoxon rank sum test (corresponding to the post-hoc analysis used with the ANOVA test in Figure 4.7). *Grey dashed line* indicating a significance level of $p = 0.05$ and *grey dotted line* indicating a significance level of $p = 0.01$.
Right: Number of GAD65$^+$ *(blue)* and TH$^+$ *(red)* pairs that exhibited a cross-correlation peak value above a set threshold and were used for the analysis displayed in the left graph.

Reference List

ABRAHAM, N. M., SPORS, H., CARLETON, A., MARGRIE, T. W., KUNER, T. & SCHAEFER, A. T. 2004. Maintaining accuracy at the expense of speed: stimulus similarity defines odor discrimination time in mice. *Neuron,* 44**,** 865-76.

ACHE, B. W. & YOUNG, J. M. 2005. Olfaction: diverse species, conserved principles. *Neuron,* 48**,** 417-30.

AKIBA, Y., CAVE, J. W., AKIBA, N., LANGLEY, B., RATAN, R. R. & BAKER, H. 2010. Histone deacetylase inhibitors de-repress tyrosine hydroxylase expression in the olfactory bulb and rostral migratory stream. *Biochem Biophys Res Commun,* 393**,** 673-7.

ALTMAN, J. 1969. Autoradiographic and histological studies of postnatal neurogenesis. IV. Cell proliferation and migration in the anterior forebrain, with special reference to persisting neurogenesis in the olfactory bulb. *J Comp Neurol,* 137**,** 433-57.

ALTOMARE, C., BUCCHI, A., CAMATINI, E., BARUSCOTTI, M., VISCOMI, C., MORONI, A. & DIFRANCESCO, D. 2001. Integrated allosteric model of voltage gating of HCN channels. *J Gen Physiol,* 117**,** 519-32.

ALTSCHULER, S. J. & WU, L. F. 2010. Cellular heterogeneity: do differences make a difference? *Cell,* 141**,** 559-63.

ANGELO, K., LONDON, M., CHRISTENSEN, S. R. & HAUSSER, M. 2007. Local and global effects of I(h) distribution in dendrites of mammalian neurons. *J Neurosci,* 27**,** 8643-53.

ANGELO, K. & MARGRIE, T. W. 2011. Population diversity and function of hyperpolarization-activated current in olfactory bulb mitral cells. *Sci Rep,* 1**,** 50.

ANGELO, K., RANCZ, E. A., PIMENTEL, D., HUNDAHL, C., HANNIBAL, J., FLEISCHMANN, A., PICHLER, B. & MARGRIE, T. W. 2012. A biophysical signature of network affiliation and sensory processing in mitral cells. *Nature,* 488**,** 375-8.

ANWYL, R. 1999. Metabotropic glutamate receptors: electrophysiological properties and role in plasticity. *Brain Res Brain Res Rev,* 29**,** 83-120.

APONTE, Y., LIEN, C. C., REISINGER, E. & JONAS, P. 2006. Hyperpolarization-activated cation channels in fast-spiking interneurons of rat hippocampus. *J Physiol,* 574**,** 229-43.

APTOWICZ, C. O., KUNKLER, P. E. & KRAIG, R. P. 2004. Homeostatic plasticity in hippocampal slice cultures involves changes in voltage-gated Na+ channel expression. *Brain Res,* 998**,** 155-63.

AREVIAN, A. C., KAPOOR, V. & URBAN, N. N. 2008. Activity-dependent gating of lateral inhibition in the mouse olfactory bulb. *Nat Neurosci,* 11**,** 80-7.

ARONIADOU-ANDERJASKA, V., ENNIS, M. & SHIPLEY, M. T. 1997. Glomerular synaptic responses to olfactory nerve input in rat olfactory bulb slices. *Neuroscience,* 79**,** 425-34.

ARONIADOU-ANDERJASKA, V., ENNIS, M. & SHIPLEY, M. T. 1999. Dendrodendritic recurrent excitation in mitral cells of the rat olfactory bulb. *J Neurophysiol,* 82**,** 489-94.

ARONIADOU-ANDERJASKA, V., ZHOU, F. M., PRIEST, C. A., ENNIS, M. & SHIPLEY, M. T. 2000. Tonic and synaptically evoked presynaptic inhibition of sensory input to the rat olfactory bulb via GABA(B) heteroreceptors. *J Neurophysiol,* 84**,** 1194-203.

AUNGST, J. L., HEYWARD, P. M., PUCHE, A. C., KARNUP, S. V., HAYAR, A., SZABO, G. & SHIPLEY, M. T. 2003. Centre-surround inhibition among olfactory bulb glomeruli. *Nature,* 426**,** 623-9.

AZDAD, K., CHAVEZ, M., DON BISCHOP, P., WETZELAER, P., MARESCAU, B., DE DEYN, P. P., GALL, D. & SCHIFFMANN, S. N. 2009. Homeostatic plasticity of striatal neurons intrinsic excitability following dopamine depletion. *PLoS One,* 4**,** e6908.

BADER, C. R., MACLEISH, P. R. & SCHWARTZ, E. A. 1979. A voltage-clamp study of the light response in solitary rods of the tiger salamander. *J Physiol,* 296**,** 1-26.

BAINES, R. A. 2003. Postsynaptic protein kinase A reduces neuronal excitability in response to increased synaptic excitation in the Drosophila CNS. *J Neurosci,* 23**,** 8664-72.

BAKER, H., KAWANO, T., MARGOLIS, F. L. & JOH, T. H. 1983. Transneuronal regulation of tyrosine hydroxylase expression in olfactory bulb of mouse and rat. *J Neurosci,* 3**,** 69-78.

BAKER, H., LIU, N., CHUN, H. S., SAINO, S., BERLIN, R., VOLPE, B. & SON, J. H. 2001. Phenotypic differentiation during migration of dopaminergic progenitor cells to the olfactory bulb. *J Neurosci,* 21**,** 8505-13.

BANERJEE, A., MARBACH, F., ANSELMI, F., KOH, M. S., DAVIS, M. B., GARCIA DA SILVA, P., DELEVICH, K., OYIBO, H. K., GUPTA, P., LI, B. & ALBEANU, D. F. 2015. An Interglomerular Circuit Gates Glomerular Output and Implements Gain Control in the Mouse Olfactory Bulb. *Neuron,* 87**,** 193-207.

BANERJEE, K., AKIBA, Y., BAKER, H. & CAVE, J. W. 2013. Epigenetic control of neurotransmitter expression in olfactory bulb interneurons. *Int J Dev Neurosci,* 31**,** 415-23.

BARROW, A. J. & WU, S. M. 2009. Low-conductance HCN1 ion channels augment the frequency response of rod and cone photoreceptors. *J Neurosci,* 29**,** 5841-53.

BARTLEY, A. F., HUANG, Z. J., HUBER, K. M. & GIBSON, J. R. 2008. Differential activity-dependent, homeostatic plasticity of two neocortical inhibitory circuits. *J Neurophysiol,* 100**,** 1983-94.

BASHIR, Z. I., BORTOLOTTO, Z. A., DAVIES, C. H., BERRETTA, N., IRVING, A. J., SEAL, A. J., HENLEY, J. M., JANE, D. E., WATKINS, J. C. & COLLINGRIDGE, G. L. 1993. Induction of LTP in the hippocampus needs synaptic activation of glutamate metabotropic receptors. *Nature,* 363**,** 347-50.

BEAUMONT, V. & ZUCKER, R. S. 2000. Enhancement of synaptic transmission by cyclic AMP modulation of presynaptic Ih channels. *Nat Neurosci,* 3**,** 133-41.

BELLUSCIO, L. & KATZ, L. C. 2001. Symmetry, stereotypy, and topography of odorant representations in mouse olfactory bulbs. *J Neurosci,* 21**,** 2113-22.

BELLUZZI, O., BENEDUSI, M., ACKMAN, J. & LOTURCO, J. J. 2003. Electrophysiological differentiation of new neurons in the olfactory bulb. *J Neurosci,* 23**,** 10411-8.

BENDER, K. J. & TRUSSELL, L. O. 2012. The physiology of the axon initial segment. *Annu Rev Neurosci,* 35**,** 249-65.

BENDER, R. A. & BARAM, T. Z. 2008. Hyperpolarization activated cyclic-nucleotide gated (HCN) channels in developing neuronal networks. *Prog Neurobiol,* 86**,** 129-40.

BENQUET, P., GEE, C. E. & GERBER, U. 2002. Two distinct signaling pathways upregulate NMDA receptor responses via two distinct metabotropic glutamate receptor subtypes. *J Neurosci,* 22**,** 9679-86.

BEPARI, A. K., WATANABE, K., YAMAGUCHI, M., TAMAMAKI, N. & TAKEBAYASHI, H. 2012. Visualization of odor-induced neuronal activity by immediate early gene expression. *BMC Neurosci,* 13**,** 140.

BERGER, T., LARKUM, M. E. & LUSCHER, H. R. 2001. High I(h) channel density in the distal apical dendrite of layer V pyramidal cells increases bidirectional attenuation of EPSPs. *J Neurophysiol,* 85**,** 855-68.

BERGER, T., SENN, W. & LUSCHER, H. R. 2003. Hyperpolarization-activated current Ih disconnects somatic and dendritic spike initiation zones in layer V pyramidal neurons. *J Neurophysiol,* 90**,** 2428-37.

BERKOWICZ, D. A., TROMBLEY, P. Q. & SHEPHERD, G. M. 1994. Evidence for glutamate as the olfactory receptor cell neurotransmitter. *J Neurophysiol,* 71**,** 2557-61.

BERRIDGE, M. J. 1998. Neuronal calcium signaling. *Neuron,* 21**,** 13-26.

BEST, A. R. & WILSON, D. A. 2004. Coordinate synaptic mechanisms contributing to olfactory cortical adaptation. *J Neurosci,* 24**,** 652-60.

BIEL, M., WAHL-SCHOTT, C., MICHALAKIS, S. & ZONG, X. 2009. Hyperpolarization-activated cation channels: from genes to function. *Physiol Rev,* 89**,** 847-85.

BITO, H., DEISSEROTH, K. & TSIEN, R. W. 1996. CREB phosphorylation and dephosphorylation: a Ca(2+)- and stimulus duration-dependent switch for hippocampal gene expression. *Cell,* 87**,** 1203-14.

BONINO, M., CANTINO, D. & SASSOE-POGNETTO, M. 1999. Cellular and subcellular localization of gamma-aminobutyric acidB receptors in the rat olfactory bulb. *Neurosci Lett,* 274**,** 195-8.

BONZANO, S., BOVETTI, S., FASOLO, A., PERETTO, P. & DE MARCHIS, S. 2014. Odour enrichment increases adult-born dopaminergic neurons in the mouse olfactory bulb. *Eur J Neurosci,* 40**,** 3450-7.

BOVETTI, S., VEYRAC, A., PERETTO, P., FASOLO, A. & DE MARCHIS, S. 2009. Olfactory enrichment influences adult neurogenesis modulating GAD67 and plasticity-related molecules expression in newborn cells of the olfactory bulb. *PLoS One,* 4**,** e6359.

BOYDEN, E. S., ZHANG, F., BAMBERG, E., NAGEL, G. & DEISSEROTH, K. 2005. Millisecond-timescale, genetically targeted optical control of neural activity. *Nat Neurosci,* 8**,** 1263-8.

BOZZA, T., MCGANN, J. P., MOMBAERTS, P. & WACHOWIAK, M. 2004. In vivo imaging of neuronal activity by targeted expression of a genetically encoded probe in the mouse. *Neuron,* 42**,** 9-21.

BRACEY, E. F., PICHLER, B., SCHAEFER, A. T., WALLACE, D. J. & MARGRIE, T. W. 2013. Perceptual judgements and chronic imaging of altered odour maps indicate comprehensive stimulus template matching in olfaction. *Nat Commun,* 4**,** 2100.

BRAGER, D. H. & JOHNSTON, D. 2007. Plasticity of intrinsic excitability during long-term depression is mediated through mGluR-dependent changes in I(h) in hippocampal CA1 pyramidal neurons. *J Neurosci,* 27**,** 13926-37.

BRENNAN, P. A. & KEVERNE, E. B. 1997. Neural mechanisms of mammalian olfactory learning. *Prog Neurobiol,* 51**,** 457-81.

BRENNAN, P. A., SCHELLINCK, H. M., DE LA RIVA, C., KENDRICK, K. M. & KEVERNE, E. B. 1998. Changes in neurotransmitter release in the main olfactory bulb following an olfactory conditioning procedure in mice. *Neuroscience,* 87**,** 583-90.

BRETON, J. D. & STUART, G. J. 2009. Loss of sensory input increases the intrinsic excitability of layer 5 pyramidal neurons in rat barrel cortex. *J Physiol,* 587**,** 5107-19.

BREWSTER, A. L., CHEN, Y., BENDER, R. A., YEH, A., SHIGEMOTO, R. & BARAM, T. Z. 2007a. Quantitative analysis and subcellular distribution of mRNA and protein expression of the hyperpolarization-activated cyclic nucleotide-gated channels throughout development in rat hippocampus. *Cereb Cortex,* 17**,** 702-12.

BREWSTER, A. L., CHEN, Y., BENDER, R. A., YEH, A., SHIGEMOTO, R. & BARAM, T. Z. 2007b. Quantitative analysis and subcellular distribution of mRNA and protein expression of the hyperpolarization-activated cyclic nucleotide-gated channels throughout development in rat hippocampus. *Cerebral Cortex,* 17**,** 702-712.

BRINON, J. G., ALONSO, J. R., AREVALO, R., GARCIA-OJEDA, E., LARA, J. & AIJON, J. 1992. Calbindin D-28k-positive neurons in the rat olfactory bulb. An immunohistochemical study. *Cell Tissue Res,* 269**,** 289-97.

BRINON, J. G., AREVALO, R., CRESPO, C., BRAVO, I. G., OKAZAKI, K., HIDAKA, H., AIJON, J. & ALONSO, J. R. 1998. Neurocalcin immunoreactivity in the rat main olfactory bulb. *Brain Res,* 795**,** 204-14.

BRINON, J. G., MARTINEZ-GUIJARRO, F. J., BRAVO, I. G., AREVALO, R., CRESPO, C., OKAZAKI, K., HIDAKA, H., AIJON, J. & ALONSO, J. R. 1999. Coexpression of neurocalcin with other calcium-binding proteins in the rat main olfactory bulb. *J Comp Neurol,* 407**,** 404-14.

BRUCE, H. M. & PARROTT, D. M. 1960. Role of olfactory sense in pregnancy block by strange males. *Science,* 131**,** 1526.

BRUNET, L. J., GOLD, G. H. & NGAI, J. 1996. General anosmia caused by a targeted disruption of the mouse olfactory cyclic nucleotide-gated cation channel. *Neuron,* 17**,** 681-93.

BULLIS, J. B., JONES, T. D. & POOLOS, N. P. 2007. Reversed somatodendritic I(h) gradient in a class of rat hippocampal neurons with pyramidal morphology. *J Physiol,* 579**,** 431-43.

BUONVISO, N., AMAT, C., LITAUDON, P., ROUX, S., ROYET, J. P., FARGET, V. & SICARD, G. 2003. Rhythm sequence through the olfactory bulb layers during the time window of a respiratory cycle. *Eur J Neurosci,* 17**,** 1811-9.

BURRONE, J., O'BYRNE, M. & MURTHY, V. N. 2002. Multiple forms of synaptic plasticity triggered by selective suppression of activity in individual neurons. *Nature,* 420**,** 414-8.

BUZSAKI, G. & CHROBAK, J. J. 1995. Temporal structure in spatially organized neuronal ensembles: a role for interneuronal networks. *Curr Opin Neurobiol,* 5**,** 504-10.

CADETTI, L. & BELLUZZI, O. 2001. Hyperpolarisation-activated current in glomerular cells of the rat olfactory bulb. *Neuroreport,* 12**,** 3117-20.

CADWELL, C. R., PALASANTZA, A., JIANG, X., BERENS, P., DENG, Q., YILMAZ, M., REIMER, J., SHEN, S., BETHGE, M., TOLIAS, K. F., SANDBERG, R. & TOLIAS, A. S. 2016. Electrophysiological, transcriptomic and morphologic profiling of single neurons using Patch-seq. *Nat Biotechnol,* 34**,** 199-203.

CAMPANAC, E., DAOUDAL, G., ANKRI, N. & DEBANNE, D. 2008. Downregulation of dendritic I(h) in CA1 pyramidal neurons after LTP. *J Neurosci,* 28**,** 8635-43.

CAMPANAC, E., GASSELIN, C., BAUDE, A., RAMA, S., ANKRI, N. & DEBANNE, D. 2013. Enhanced intrinsic excitability in basket cells maintains excitatory-inhibitory balance in hippocampal circuits. *Neuron,* 77**,** 712-22.

CANG, J. & ISAACSON, J. S. 2003. In vivo whole-cell recording of odor-evoked synaptic transmission in the rat olfactory bulb. *J Neurosci,* 23**,** 4108-16.

CARLETON, A., PETREANU, L. T., LANSFORD, R., ALVAREZ-BUYLLA, A. & LLEDO, P. M. 2003. Becoming a new neuron in the adult olfactory bulb. *Nat Neurosci,* 6**,** 507-18.

CARLSON, G. C., SHIPLEY, M. T. & KELLER, A. 2000. Long-lasting depolarizations in mitral cells of the rat olfactory bulb. *J Neurosci,* 20**,** 2011-21.

CHAND, A. N., GALLIANO, E., CHESTERS, R. A. & GRUBB, M. S. 2015. A distinct subtype of dopaminergic interneuron displays inverted structural plasticity at the axon initial segment. *J Neurosci,* 35**,** 1573-90.

CHATER, T. E., HENLEY, J. M., BROWN, J. T. & RANDALL, A. D. 2010. Voltage- and temperature-dependent gating of heterologously expressed channelrhodopsin-2. *J Neurosci Methods,* 193**,** 7-13.

CHATTERJEE, M., PEREZ DE LOS COBOS PALLARES, F., LOEBEL, A., LUKAS, M. & EGGER, V. 2016. Sniff-Like Patterned Input Results in Long-Term Plasticity at the Rat Olfactory Bulb Mitral and Tufted Cell to Granule Cell Synapse. *Neural Plast,* 2016**,** 9124986.

CHEN, S., WANG, J. & SIEGELBAUM, S. A. 2001. Properties of hyperpolarization-activated pacemaker current defined by coassembly of HCN1 and HCN2 subunits and basal modulation by cyclic nucleotide. *J Gen Physiol,* 117**,** 491-504.

CHRISTIE, J. M. & WESTBROOK, G. L. 2006. Lateral excitation within the olfactory bulb. *J Neurosci,* 26**,** 2269-77.

CIGOLA, E., VOLPE, B. T., LEE, J. W., FRANZEN, L. & BAKER, H. 1998. Tyrosine hydroxylase expression in primary cultures of olfactory bulb: role of L-type calcium channels. *J Neurosci,* 18**,** 7638-49.

CLELAND, T. A., JOHNSON, B. A., LEON, M. & LINSTER, C. 2007. Relational representation in the olfactory system. *Proc Natl Acad Sci U S A,* 104**,** 1953-8.

CLELAND, T. A. & LINSTER, C. 2012. On-Center/Inhibitory-Surround Decorrelation via Intraglomerular Inhibition in the Olfactory Bulb Glomerular Layer. *Front Integr Neurosci,* 6**,** 5.

CLELAND, T. A., MORSE, A., YUE, E. L. & LINSTER, C. 2002. Behavioral models of odor similarity. *Behav Neurosci,* 116**,** 222-31.

CLELAND, T. A. & SETHUPATHY, P. 2006. Non-topographical contrast enhancement in the olfactory bulb. *BMC Neurosci,* 7**,** 7.

COAN, E. J., SAYWOOD, W. & COLLINGRIDGE, G. L. 1987. MK-801 blocks NMDA receptor-mediated synaptic transmission and long term potentiation in rat hippocampal slices. *Neurosci Lett,* 80**,** 111-4.

COLLINGRIDGE, G. L. & BLISS, T. V. P. 1987. NMDA receptors - their role in long-term potentiation. *Trends in Neurosciences,* 10**,** 288-293.

COOPER, D. M., MONS, N. & KARPEN, J. W. 1995. Adenylyl cyclases and the interaction between calcium and cAMP signalling. *Nature,* 374**,** 421-4.

COSKUN, V. & LUSKIN, M. B. 2002. Intrinsic and extrinsic regulation of the proliferation and differentiation of cells in the rodent rostral migratory stream. *J Neurosci Res,* 69**,** 795-802.

CUMMINGS, D. M. & BRUNJES, P. C. 1997. The effects of variable periods of functional deprivation on olfactory bulb development in rats. *Exp Neurol,* 148**,** 360-6.

DAVIS, G. W. & BEZPROZVANNY, I. 2001. Maintaining the stability of neural function: a homeostatic hypothesis. *Annu Rev Physiol,* 63**,** 847-69.

DE MARCHIS, S., TEMONEY, S., ERDELYI, F., BOVETTI, S., BOVOLIN, P., SZABO, G. & PUCHE, A. C. 2004. GABAergic phenotypic differentiation of a subpopulation of subventricular derived migrating progenitors. *Eur J Neurosci,* 20**,** 1307-17.

DE SAINT JAN, D., HIRNET, D., WESTBROOK, G. L. & CHARPAK, S. 2009. External tufted cells drive the output of olfactory bulb glomeruli. *J Neurosci,* 29**,** 2043-52.

DELANEY, K. R., QNAIS, E. Y. & HARDY, A. B. 2009. Short-term synaptic plasticity at the main and vomeronasal olfactory receptor to mitral cell synapse in frog. *Eur J Neurosci,* 30**,** 2077-88.

DESAI, N. S. 2003. Homeostatic plasticity in the CNS: synaptic and intrinsic forms. *J Physiol Paris,* 97**,** 391-402.

DESAI, N. S., CUDMORE, R. H., NELSON, S. B. & TURRIGIANO, G. G. 2002. Critical periods for experience-dependent synaptic scaling in visual cortex. *Nat Neurosci,* 5**,** 783-9.

DESAI, N. S., RUTHERFORD, L. C. & TURRIGIANO, G. G. 1999. Plasticity in the intrinsic excitability of cortical pyramidal neurons. *Nat Neurosci,* 2**,** 515-20.

DHAWALE, A. K., HAGIWARA, A., BHALLA, U. S., MURTHY, V. N. & ALBEANU, D. F. 2010. Non-redundant odor coding by sister mitral cells revealed by light addressable glomeruli in the mouse. *Nat Neurosci,* 13**,** 1404-12.

DICKSON, C. T., MAGISTRETTI, J., SHALINSKY, M. H., FRANSEN, E., HASSELMO, M. E. & ALONSO, A. 2000. Properties and role of I(h) in the pacing of subthreshold oscillations in entorhinal cortex layer II neurons. *J Neurophysiol,* 83**,** 2562-79.

DIETZ, S. B. & MURTHY, V. N. 2005. Contrasting short-term plasticity at two sides of the mitral-granule reciprocal synapse in the mammalian olfactory bulb. *J Physiol,* 569**,** 475-88.

DIFRANCESCO, D., FERRONI, A., MAZZANTI, M. & TROMBA, C. 1986. Properties of the hyperpolarizing-activated current (if) in cells isolated from the rabbit sino-atrial node. *J Physiol,* 377**,** 61-88.

DIFRANCESCO, D. & TORTORA, P. 1991. Direct activation of cardiac pacemaker channels by intracellular cyclic AMP. *Nature,* 351**,** 145-7.

DUCHAMP-VIRET, P., CHAPUT, M. A. & DUCHAMP, A. 1999. Odor response properties of rat olfactory receptor neurons. *Science,* 284**,** 2171-4.

DUCRAY, A., BONDIER, J. R., MICHEL, G., BON, K., MILLOT, J. L., PROPPER, A. & KASTNER, A. 2002. Recovery following peripheral destruction of olfactory neurons in young and adult mice. *Eur J Neurosci,* 15**,** 1907-17.

DUGUE, G. P., DUMOULIN, A., TRILLER, A. & DIEUDONNE, S. 2005. Target-dependent use of co-released inhibitory transmitters at central synapses. *J Neurosci,* 25**,** 6490-8.

DYMECKI, S. M. & KIM, J. C. 2007. Molecular neuroanatomy's "Three Gs": a primer. *Neuron,* 54**,** 17-34.

ECONOMO, M. N., HANSEN, K. R. & WACHOWIAK, M. 2016. Control of Mitral/Tufted Cell Output by Selective Inhibition among Olfactory Bulb Glomeruli. *Neuron,* 91**,** 397-411.

ENGBERS, J. D., ANDERSON, D., TADAYONNEJAD, R., MEHAFFEY, W. H., MOLINEUX, M. L. & TURNER, R. W. 2011. Distinct roles for I(T) and I(H) in controlling the frequency and timing of rebound spike responses. *J Physiol,* 589**,** 5391-413.

ENNIS, M., LINSTER, C., ARONIADOU-ANDERJASKA, V., CIOMBOR, K. & SHIPLEY, M. T. 1998. Glutamate and synaptic plasticity at mammalian primary olfactory synapses. *Ann N Y Acad Sci,* 855**,** 457-66.

ENNIS, M., ZIMMER, L. A. & SHIPLEY, M. T. 1996. Olfactory nerve stimulation activates rat mitral cells via NMDA and non-NMDA receptors in vitro. *Neuroreport,* 7**,** 989-92.

FAN, Y., FRICKER, D., BRAGER, D. H., CHEN, X., LU, H. C., CHITWOOD, R. A. & JOHNSTON, D. 2005. Activity-dependent decrease of excitability in rat hippocampal neurons through increases in I(h). *Nat Neurosci,* 8**,** 1542-51.

FEINSTEIN, P., BOZZA, T., RODRIGUEZ, I., VASSALLI, A. & MOMBAERTS, P. 2004. Axon guidance of mouse olfactory sensory neurons by odorant receptors and the beta2 adrenergic receptor. *Cell,* 117**,** 833-46.

FEINSTEIN, P. & MOMBAERTS, P. 2004. A contextual model for axonal sorting into glomeruli in the mouse olfactory system. *Cell,* 117**,** 817-31.

FELDMAN, D. E. 2009. Synaptic mechanisms for plasticity in neocortex. *Annu Rev Neurosci,* 32**,** 33-55.

FISHELL, G. & HEINTZ, N. 2013. The neuron identity problem: form meets function. *Neuron,* 80**,** 602-12.

FLAVELL, S. W. & GREENBERG, M. E. 2008. Signaling mechanisms linking neuronal activity to gene expression and plasticity of the nervous system. *Annu Rev Neurosci,* 31**,** 563-90.

FRICK, A. & JOHNSTON, D. 2005. Plasticity of dendritic excitability. *J Neurobiol,* 64**,** 100-15.

FRICK, A., MAGEE, J. & JOHNSTON, D. 2004. LTP is accompanied by an enhanced local excitability of pyramidal neuron dendrites. *Nat Neurosci,* 7**,** 126-35.

FRIED, H. U., FUSS, S. H. & KORSCHING, S. I. 2002. Selective imaging of presynaptic activity in the mouse olfactory bulb shows concentration and structure dependence of odor responses in identified glomeruli. *Proc Natl Acad Sci U S A,* 99**,** 3222-7.

FRIEDMAN, D. & STROWBRIDGE, B. W. 2000. Functional role of NMDA autoreceptors in olfactory mitral cells. *J Neurophysiol,* 84**,** 39-50.

FUKUNAGA, I., BERNING, M., KOLLO, M., SCHMALTZ, A. & SCHAEFER, A. T. 2012. Two distinct channels of olfactory bulb output. *Neuron,* 75**,** 320-9.

FUKUNAGA, I., HERB, J. T., KOLLO, M., BOYDEN, E. S. & SCHAEFER, A. T. 2014. Independent control of gamma and theta activity by distinct interneuron networks in the olfactory bulb. *Nat Neurosci,* 17**,** 1208-16.

FUZIK, J., ZEISEL, A., MATE, Z., CALVIGIONI, D., YANAGAWA, Y., SZABO, G., LINNARSSON, S. & HARKANY, T. 2016. Integration of electrophysiological recordings with single-cell RNA-seq data identifies neuronal subtypes. *Nat Biotechnol,* 34**,** 175-83.

GASPARINI, S. & MAGEE, J. C. 2002. Phosphorylation-dependent differences in the activation properties of distal and proximal dendritic Na+ channels in rat CA1 hippocampal neurons. *J Physiol,* 541**,** 665-72.

GASTREIN, P., CAMPANAC, E., GASSELIN, C., CUDMORE, R. H., BIALOWAS, A., CARLIER, E., FRONZAROLI-MOLINIERES, L., ANKRI, N. & DEBANNE, D. 2011. The role of hyperpolarization-activated cationic current in spike-time precision and intrinsic resonance in cortical neurons in vitro. *J Physiol,* 589**,** 3753-73.

GEREAU, R. W. T. & CONN, P. J. 1995. Multiple presynaptic metabotropic glutamate receptors modulate excitatory and inhibitory synaptic transmission in hippocampal area CA1. *J Neurosci,* 15**,** 6879-89.

GERKIN, R. C., TRIPATHY, S. J. & URBAN, N. N. 2013. Origins of correlated spiking in the mammalian olfactory bulb. *Proc Natl Acad Sci U S A,* 110**,** 17083-8.

GIBSON, J. R., BARTLEY, A. F. & HUBER, K. M. 2006. Role for the subthreshold currents ILeak and IH in the homeostatic control of excitability in neocortical somatostatin-positive inhibitory neurons. *J Neurophysiol,* 96**,** 420-32.

GIOCOMO, L. M. & HASSELMO, M. E. 2007. Neuromodulation by glutamate and acetylcholine can change circuit dynamics by regulating the relative influence of afferent input and excitatory feedback. *Mol Neurobiol,* 36**,** 184-200.

GIOCOMO, L. M. & HASSELMO, M. E. 2008. Time constants of h current in layer ii stellate cells differ along the dorsal to ventral axis of medial entorhinal cortex. *J Neurosci,* 28**,** 9414-25.

GIOCOMO, L. M. & HASSELMO, M. E. 2009. Knock-out of HCN1 subunit flattens dorsal-ventral frequency gradient of medial entorhinal neurons in adult mice. *J Neurosci,* 29**,** 7625-30.

GIOCOMO, L. M., HUSSAINI, S. A., ZHENG, F., KANDEL, E. R., MOSER, M. B. & MOSER, E. I. 2011. Grid cells use HCN1 channels for spatial scaling. *Cell,* 147**,** 1159-70.

GIRE, D. H., FRANKS, K. M., ZAK, J. D., TANAKA, K. F., WHITESELL, J. D., MULLIGAN, A. A., HEN, R. & SCHOPPA, N. E. 2012. Mitral cells in the olfactory bulb are mainly excited through a multistep signaling path. *J Neurosci,* 32**,** 2964-75.

GOLGI, C. 1886. *Sulla fina anatomia degli organi centrali del sistema nervoso*, Ulrico Hoepli.

GREENBERG, M. E. & ZIFF, E. B. 1984. Stimulation of 3T3 cells induces transcription of the c-fos proto-oncogene. *Nature,* 311**,** 433-8.

GRUBB, M. S. & BURRONE, J. 2010. Activity-dependent relocation of the axon initial segment fine-tunes neuronal excitability. *Nature,* 465**,** 1070-4.

GUTHRIE, K. M. & GALL, C. M. 1995. Functional mapping of odor-activated neurons in the olfactory bulb. *Chem Senses,* 20**,** 271-82.

GUTHRIE, K. M., WILSON, D. A. & LEON, M. 1990. Early unilateral deprivation modifies olfactory bulb function. *J Neurosci,* 10**,** 3402-12.

HABERLY, L. B. & PRICE, J. L. 1977. The axonal projection patterns of the mitral and tufted cells of the olfactory bulb in the rat. *Brain Res,* 129**,** 152-7.

HALASZ, N., HOKFELT, T., NORMAN, A. W. & GOLDSTEIN, M. 1985. Tyrosine hydroxylase and 28K-vitamin D-dependent calcium binding protein are localized in different subpopulations of periglomerular cells of the rat olfactory bulb. *Neurosci Lett,* 61**,** 103-7.

HALASZ, N., JOHANSSON, O., HOKFELT, T., LJUNGDAHL, A. & GOLDSTEIN, M. 1981. Immunohistochemical identification of two types of dopamine neuron in the rat olfactory bulb as seen by serial sectioning. *J Neurocytol,* 10**,** 251-9.

HALLIWELL, J. V. & ADAMS, P. R. 1982. Voltage-clamp analysis of muscarinic excitation in hippocampal neurons. *Brain Res,* 250**,** 71-92.

HAMANA, H., HIRONO, J., KIZUMI, M. & SATO, T. 2003. Sensitivity-dependent hierarchical receptor codes for odors. *Chem Senses,* 28**,** 87-104.

HARDING, J. W., GETCHELL, T. V. & MARGOLIS, F. L. 1978. Denervation of the primary olfactory pathway in mice. V. Long-term effect of intranasal ZnSO4 irrigation on behavior, biochemistry and morphology. *Brain Res,* 140**,** 271-85.

HARRIS, N. C. & CONSTANTI, A. 1995. Mechanism of block by ZD 7288 of the hyperpolarization-activated inward rectifying current in guinea pig substantia nigra neurons in vitro. *J Neurophysiol,* 74**,** 2366-78.

HARTMAN, K. N., PAL, S. K., BURRONE, J. & MURTHY, V. N. 2006. Activity-dependent regulation of inhibitory synaptic transmission in hippocampal neurons. *Nat Neurosci,* 9**,** 642-9.

HAYAR, A., KARNUP, S., ENNIS, M. & SHIPLEY, M. T. 2004a. External tufted cells: a major excitatory element that coordinates glomerular activity. *J Neurosci,* 24**,** 6676-85.

HAYAR, A., KARNUP, S., SHIPLEY, M. T. & ENNIS, M. 2004b. Olfactory bulb glomeruli: external tufted cells intrinsically burst at theta frequency and are entrained by patterned olfactory input. *J Neurosci,* 24**,** 1190-9.

HAYAR, A., SHIPLEY, M. T. & ENNIS, M. 2005. Olfactory bulb external tufted cells are synchronized by multiple intraglomerular mechanisms. *J Neurosci,* 25**,** 8197-208.

HEMOND, P., MIGLIORE, M., ASCOLI, G. A. & JAFFE, D. B. 2009. The membrane response of hippocampal CA3b pyramidal neurons near rest: Heterogeneity of passive properties and the contribution of hyperpolarization-activated currents. *Neuroscience,* 160**,** 359-70.

HENDRY, S. H., HUNTSMAN, M. M., VINUELA, A., MOHLER, H., DE BLAS, A. L. & JONES, E. G. 1994. GABAA receptor subunit immunoreactivity in primate visual cortex: distribution in macaques and humans and regulation by visual input in adulthood. *J Neurosci,* 14**,** 2383-401.

HEYS, J. G. & HASSELMO, M. E. 2012. Neuromodulation of I(h) in layer II medial entorhinal cortex stellate cells: a voltage-clamp study. *J Neurosci,* 32**,** 9066-72.

HIGASHI, K., FUJITA, A., INANOBE, A., TANEMOTO, M., DOI, K., KUBO, T. & KURACHI, Y. 2001. An inwardly rectifying K(+) channel, Kir4.1, expressed in astrocytes surrounds synapses and blood vessels in brain. *Am J Physiol Cell Physiol,* 281**,** C922-31.

HILLE, B. 2001. *Ion channels of excitable membranes*, Sinauer Sunderland, MA.

HONNURAIAH, S. & NARAYANAN, R. 2013. A calcium-dependent plasticity rule for HCN channels maintains activity homeostasis and stable synaptic learning. *PLoS One,* 8**,** e55590.

HOU, Q., ZHANG, D., JARZYLO, L., HUGANIR, R. L. & MAN, H. Y. 2008. Homeostatic regulation of AMPA receptor expression at single hippocampal synapses. *Proc Natl Acad Sci U S A,* 105**,** 775-80.

HU, H., VERVAEKE, K. & STORM, J. F. 2002. Two forms of electrical resonance at theta frequencies, generated by M-current, h-current and persistent Na+ current in rat hippocampal pyramidal cells. *J Physiol,* 545**,** 783-805.

HUANG, Z., LI, G., AGUADO, C., LUJAN, R. & SHAH, M. M. 2017. HCN1 channels reduce the rate of exocytosis from a subset of cortical synaptic terminals. *Sci Rep,* 7**,** 40257.

HUTCHEON, B. & YAROM, Y. 2000. Resonance, oscillation and the intrinsic frequency preferences of neurons. *Trends Neurosci,* 23**,** 216-22.

IBATA, K., SUN, Q. & TURRIGIANO, G. G. 2008. Rapid synaptic scaling induced by changes in postsynaptic firing. *Neuron,* 57**,** 819-26.

IGARASHI, K. M., IEKI, N., AN, M., YAMAGUCHI, Y., NAGAYAMA, S., KOBAYAKAWA, K., KOBAYAKAWA, R., TANIFUJI, M., SAKANO, H., CHEN, W. R. & MORI, K. 2012. Parallel mitral and tufted cell pathways route distinct odor information to different targets in the olfactory cortex. *J Neurosci,* 32**,** 7970-85.

ISAACSON, J. S. & STROWBRIDGE, B. W. 1998. Olfactory reciprocal synapses: dendritic signaling in the CNS. *Neuron,* 20**,** 749-61.

JAFFE, E. H. & CUELLO, A. C. 1980. The distribution of catecholamines, glutamate decarboxylase and choline acetyltransferase in layers of the rat olfactory bulb. *Brain Res,* 186**,** 232-7.

JOHNSON, B. A. & LEON, M. 2000. Modular representations of odorants in the glomerular layer of the rat olfactory bulb and the effects of stimulus concentration. *J Comp Neurol,* 422**,** 496-509.

JOHNSON, B. A., WOO, C. C. & LEON, M. 1998. Spatial coding of odorant features in the glomerular layer of the rat olfactory bulb. *J Comp Neurol,* 393**,** 457-71.

JU, W., MORISHITA, W., TSUI, J., GAIETTA, G., DEERINCK, T. J., ADAMS, S. R., GARNER, C. C., TSIEN, R. Y., ELLISMAN, M. H. & MALENKA, R. C. 2004. Activity-dependent regulation of dendritic synthesis and trafficking of AMPA receptors. *Nat Neurosci,* 7**,** 244-53.

KASHIWADANI, H., SASAKI, Y. F., UCHIDA, N. & MORI, K. 1999. Synchronized oscillatory discharges of mitral/tufted cells with different molecular receptive ranges in the rabbit olfactory bulb. *J Neurophysiol,* 82**,** 1786-92.

KASOWSKI, H. J., KIM, H. & GREER, C. A. 1999. Compartmental organization of the olfactory bulb glomerulus. *J Comp Neurol,* 407**,** 261-74.

KASS, M. D., GUANG, S. A., MOBERLY, A. H. & MCGANN, J. P. 2016. Changes in Olfactory Sensory Neuron Physiology and Olfactory Perceptual Learning After Odorant Exposure in Adult Mice. *Chem Senses,* 41**,** 123-33.

KAUPP, U. B. & SEIFERT, R. 2001. Molecular diversity of pacemaker ion channels. *Annu Rev Physiol,* 63**,** 235-57.

KENDRICK, K. M., LEVY, F. & KEVERNE, E. B. 1992. Changes in the sensory processing of olfactory signals induced by birth in sheep. *Science,* 256**,** 833-6.

KEPECS, A., UCHIDA, N. & MAINEN, Z. F. 2006. The sniff as a unit of olfactory processing. *Chem Senses,* 31**,** 167-79.

KEPECS, A., UCHIDA, N. & MAINEN, Z. F. 2007. Rapid and precise control of sniffing during olfactory discrimination in rats. *J Neurophysiol,* 98**,** 205-13.

KIM, I. J., ZHANG, Y., YAMAGATA, M., MEISTER, M. & SANES, J. R. 2008. Molecular identification of a retinal cell type that responds to upward motion. *Nature,* 452**,** 478-82.

KIM, J., JUNG, S. C., CLEMENS, A. M., PETRALIA, R. S. & HOFFMAN, D. A. 2007. Regulation of dendritic excitability by activity-dependent trafficking of the A-type K+ channel subunit Kv4.2 in hippocampal neurons. *Neuron,* 54**,** 933-47.

KIM, J. A., SEKERKOVA, G., MUGNAINI, E. & MARTINA, M. 2012. Electrophysiological, morphological, and topological properties of two histochemically distinct subpopulations of cerebellar unipolar brush cells. *Cerebellum,* 11**,** 1012-25.

KIYOKAGE, E., PAN, Y. Z., SHAO, Z., KOBAYASHI, K., SZABO, G., YANAGAWA, Y., OBATA, K., OKANO, H., TOIDA, K., PUCHE, A. C. & SHIPLEY, M. T. 2010. Molecular identity of periglomerular and short axon cells. *J Neurosci,* 30**,** 1185-96.

KLENOFF, J. R. & GREER, C. A. 1998. Postnatal development of olfactory receptor cell axonal arbors. *J Comp Neurol,* 390**,** 256-67.

KOLLO, M., SCHMALTZ, A., ABDELHAMID, M., FUKUNAGA, I. & SCHAEFER, A. T. 2014. 'Silent' mitral cells dominate odor responses in the olfactory bulb of awake mice. *Nat Neurosci,* 17**,** 1313-5.

KOSAKA, K., AIKA, Y., TOIDA, K., HEIZMANN, C. W., HUNZIKER, W., JACOBOWITZ, D. M., NAGATSU, I., STREIT, P., VISSER, T. J. & KOSAKA, T. 1995. Chemically defined neuron groups and their subpopulations in the glomerular layer of the rat main olfactory bulb. *Neurosci Res,* 23**,** 73-88.

KOSAKA, K., HEIZMANN, C. W. & KOSAKA, T. 1994. Calcium-binding protein parvalbumin-immunoreactive neurons in the rat olfactory bulb. 1. Distribution and structural features in adult rat. *Exp Brain Res,* 99**,** 191-204.

KOSAKA, K., TOIDA, K., AIKA, Y. & KOSAKA, T. 1998. How simple is the organization of the olfactory glomerulus?: the heterogeneity of so-called periglomerular cells. *Neurosci Res,* 30**,** 101-10.

KOSAKA, T. & KOSAKA, K. 2008. Tyrosine hydroxylase-positive GABAergic juxtaglomerular neurons are the main source of the interglomerular connections in the mouse main olfactory bulb. *Neurosci Res,* 60**,** 349-54.

KOSAKA, T. & KOSAKA, K. 2009. Two types of tyrosine hydroxylase positive GABAergic juxtaglomerular neurons in the mouse main olfactory bulb are different in their time of origin. *Neurosci Res,* 64**,** 436-41.

KOSAKA, T. & KOSAKA, K. 2011. "Interneurons" in the olfactory bulb revisited. *Neurosci Res,* 69**,** 93-9.

KUBA, H., OICHI, Y. & OHMORI, H. 2010. Presynaptic activity regulates Na(+) channel distribution at the axon initial segment. *Nature,* 465**,** 1075-8.

KUMAR, P. & OHANA, O. 2008. Inter- and intralaminar subcircuits of excitatory and inhibitory neurons in layer 6a of the rat barrel cortex. *J Neurophysiol,* 100**,** 1909-22.

LAURIE, D. J., SEEBURG, P. H. & WISDEN, W. 1992. The distribution of 13 GABAA receptor subunit mRNAs in the rat brain. II. Olfactory bulb and cerebellum. *J Neurosci,* 12**,** 1063-76.

LEE, S. H., KWAN, A. C., ZHANG, S., PHOUMTHIPPHAVONG, V., FLANNERY, J. G., MASMANIDIS, S. C., TANIGUCHI, H., HUANG, Z. J., ZHANG, F., BOYDEN, E. S., DEISSEROTH, K. & DAN, Y. 2012. Activation of specific interneurons improves V1 feature selectivity and visual perception. *Nature,* 488**,** 379-83.

LEMASSON, G., MARDER, E. & ABBOTT, L. F. 1993. Activity-dependent regulation of conductances in model neurons. *Science,* 259**,** 1915-7.

LEON, M. 1998. Compensatory responses to early olfactory restriction. *Ann N Y Acad Sci,* 855**,** 104-8.

LEVY, F., GERVAIS, R., KINDERMANN, U., ORGEUR, P. & PIKETTY, V. 1990. Importance of beta-noradrenergic receptors in the olfactory bulb of sheep for recognition of lambs. *Behav Neurosci,* 104**,** 464-9.

LI, M., WEST, J. W., LAI, Y., SCHEUER, T. & CATTERALL, W. A. 1992. Functional modulation of brain sodium channels by cAMP-dependent phosphorylation. *Neuron,* 8**,** 1151-9.

LIN, J. Y., LIN, M. Z., STEINBACH, P. & TSIEN, R. Y. 2009. Characterization of engineered channelrhodopsin variants with improved properties and kinetics. *Biophys J,* 96**,** 1803-14.

LISSIN, D. V., GOMPERTS, S. N., CARROLL, R. C., CHRISTINE, C. W., KALMAN, D., KITAMURA, M., HARDY, S., NICOLL, R. A., MALENKA, R. C. & VON ZASTROW, M. 1998. Activity differentially regulates the surface expression of synaptic AMPA and NMDA glutamate receptors. *Proc Natl Acad Sci U S A,* 95**,** 7097-102.

LIU, A., SAVYA, S. & URBAN, N. N. 2016. Early Odorant Exposure Increases the Number of Mitral and Tufted Cells Associated with a Single Glomerulus. *J Neurosci,* 36**,** 11646-11653.

LIU, Q., MANIS, P. B. & DAVIS, R. L. 2014. I h and HCN channels in murine spiral ganglion neurons: tonotopic variation, local heterogeneity, and kinetic model. *J Assoc Res Otolaryngol,* 15**,** 585-99.

LIU, S., PLACHEZ, C., SHAO, Z., PUCHE, A. & SHIPLEY, M. T. 2013. Olfactory bulb short axon cell release of GABA and dopamine produces a temporally biphasic inhibition-excitation response in external tufted cells. *J Neurosci,* 33**,** 2916-26.

LIU, S. & SHIPLEY, M. T. 2008a. Intrinsic conductances actively shape excitatory and inhibitory postsynaptic responses in olfactory bulb external tufted cells. *J Neurosci,* 28**,** 10311-22.

LIU, S. & SHIPLEY, M. T. 2008b. Multiple conductances cooperatively regulate spontaneous bursting in mouse olfactory bulb external tufted cells. *J Neurosci,* 28**,** 1625-39.
LIU, Z., GOLOWASCH, J., MARDER, E. & ABBOTT, L. F. 1998. A model neuron with activity-dependent conductances regulated by multiple calcium sensors. *J Neurosci,* 18**,** 2309-20.
LIVNEH, Y., ADAM, Y. & MIZRAHI, A. 2014. Odor processing by adult-born neurons. *Neuron,* 81**,** 1097-110.
LLEDO, P. M., ALONSO, M. & GRUBB, M. S. 2006. Adult neurogenesis and functional plasticity in neuronal circuits. *Nat Rev Neurosci,* 7**,** 179-93.
LLEDO, P. M., MERKLE, F. T. & ALVAREZ-BUYLLA, A. 2008. Origin and function of olfactory bulb interneuron diversity. *Trends Neurosci,* 31**,** 392-400.
LLEDO, P. M. & VALLEY, M. 2016. Adult Olfactory Bulb Neurogenesis. *Cold Spring Harb Perspect Biol,* 8.
LORINCZ, A., NOTOMI, T., TAMAS, G., SHIGEMOTO, R. & NUSSER, Z. 2002. Polarized and compartment-dependent distribution of HCN1 in pyramidal cell dendrites. *Nat Neurosci,* 5**,** 1185-93.
LUDWIG, A., ZONG, X., JEGLITSCH, M., HOFMANN, F. & BIEL, M. 1998. A family of hyperpolarization-activated mammalian cation channels. *Nature,* 393**,** 587-91.
LUTHI, A. & MCCORMICK, D. A. 1998. H-current: properties of a neuronal and network pacemaker. *Neuron,* 21**,** 9-12.
MA, J. & LOWE, G. 2010. Correlated firing in tufted cells of mouse olfactory bulb. *Neuroscience,* 169**,** 1715-38.
MA, T. F., ZHAO, X. L., CAI, L., ZHANG, N., REN, S. Q., JI, F., TIAN, T. & LU, W. 2012. Regulation of spike timing-dependent plasticity of olfactory inputs in mitral cells in the rat olfactory bulb. *PLoS One,* 7**,** e35001.
MAGEE, J., HOFFMAN, D., COLBERT, C. & JOHNSTON, D. 1998. Electrical and calcium signaling in dendrites of hippocampal pyramidal neurons. *Annu Rev Physiol,* 60**,** 327-46.
MAGEE, J. C. 1999. Dendritic lh normalizes temporal summation in hippocampal CA1 neurons. *Nat Neurosci,* 2**,** 508-14.
MAHER, B. J. & WESTBROOK, G. L. 2008. Co-transmission of dopamine and GABA in periglomerular cells. *J Neurophysiol,* 99**,** 1559-64.
MALNIC, B., HIRONO, J., SATO, T. & BUCK, L. B. 1999. Combinatorial receptor codes for odors. *Cell,* 96**,** 713-23.
MANABE, H. & MORI, K. 2013. Sniff rhythm-paced fast and slow gamma-oscillations in the olfactory bulb: relation to tufted and mitral cells and behavioral states. *J Neurophysiol,* 110**,** 1593-9.
MANDAIRON, N., SACQUET, J., JOURDAN, F. & DIDIER, A. 2006a. Long-term fate and distribution of newborn cells in the adult mouse olfactory bulb: Influences of olfactory deprivation. *Neuroscience,* 141**,** 443-51.
MANDAIRON, N., STACK, C. & LINSTER, C. 2006b. Olfactory enrichment improves the recognition of individual components in mixtures. *Physiol Behav,* 89**,** 379-84.
MARDER, E. 2012. Neuromodulation of neuronal circuits: back to the future. *Neuron,* 76**,** 1-11.
MARDER, E. & GOAILLARD, J. M. 2006. Variability, compensation and homeostasis in neuron and network function. *Nat Rev Neurosci,* 7**,** 563-74.
MARGRIE, T. W., SAKMANN, B. & URBAN, N. N. 2001. Action potential propagation in mitral cell lateral dendrites is decremental and controls recurrent and lateral inhibition in the mammalian olfactory bulb. *Proc Natl Acad Sci U S A,* 98**,** 319-24.
MARGRIE, T. W. & SCHAEFER, A. T. 2003. Theta oscillation coupled spike latencies yield computational vigour in a mammalian sensory system. *J Physiol,* 546**,** 363-74.
MARKRAM, H., TOLEDO-RODRIGUEZ, M., WANG, Y., GUPTA, A., SILBERBERG, G. & WU, C. 2004. Interneurons of the neocortical inhibitory system. *Nat Rev Neurosci,* 5**,** 793-807.

MARSAT, G. & MALER, L. 2010. Neural heterogeneity and efficient population codes for communication signals. *J Neurophysiol,* 104**,** 2543-55.
MASLAND, R. H. 2012. The neuronal organization of the retina. *Neuron,* 76**,** 266-80.
MASON, A. & LARKMAN, A. 1990. Correlations between morphology and electrophysiology of pyramidal neurons in slices of rat visual cortex. II. Electrophysiology. *J Neurosci,* 10**,** 1415-28.
MAYER, A. D. & ROSENBLATT, J. S. 1993. Peripheral olfactory deafferentation of the primary olfactory system in rats using ZnSO4 nasal spray with special reference to maternal behavior. *Physiol Behav,* 53**,** 587-92.
MAYER, M. L. & WESTBROOK, G. L. 1983. A voltage-clamp analysis of inward (anomalous) rectification in mouse spinal sensory ganglion neurones. *J Physiol,* 340**,** 19-45.
MCBRIDE, K., SLOTNICK, B. & MARGOLIS, F. L. 2003. Does intranasal application of zinc sulfate produce anosmia in the mouse? An olfactometric and anatomical study. *Chem Senses,* 28**,** 659-70.
MCCORMICK, D. A. & PAPE, H. C. 1990. Properties of a hyperpolarization-activated cation current and its role in rhythmic oscillation in thalamic relay neurones. *J Physiol,* 431**,** 291-318.
MCGANN, J. P. 2013. Presynaptic inhibition of olfactory sensory neurons: new mechanisms and potential functions. *Chem Senses,* 38**,** 459-74.
MCLEAN, J. H. & SHIPLEY, M. T. 1988. Postmitotic, postmigrational expression of tyrosine hydroxylase in olfactory bulb dopaminergic neurons. *J Neurosci,* 8**,** 3658-69.
MCQUISTON, A. R. & KATZ, L. C. 2001. Electrophysiology of interneurons in the glomerular layer of the rat olfactory bulb. *J Neurophysiol,* 86**,** 1899-907.
MEISTER, M. & BONHOEFFER, T. 2001. Tuning and topography in an odor map on the rat olfactory bulb. *J Neurosci,* 21**,** 1351-60.
MELLOR, J., NICOLL, R. A. & SCHMITZ, D. 2002. Mediation of hippocampal mossy fiber long-term potentiation by presynaptic Ih channels. *Science,* 295**,** 143-7.
MERKLE, F. T., FUENTEALBA, L. C., SANDERS, T. A., MAGNO, L., KESSARIS, N. & ALVAREZ-BUYLLA, A. 2014. Adult neural stem cells in distinct microdomains generate previously unknown interneuron types. *Nat Neurosci,* 17**,** 207-14.
MIN, N., JOH, T. H., KIM, K. S., PENG, C. & SON, J. H. 1994. 5' upstream DNA sequence of the rat tyrosine hydroxylase gene directs high-level and tissue-specific expression to catecholaminergic neurons in the central nervous system of transgenic mice. *Brain Res Mol Brain Res,* 27**,** 281-9.
MING, G. L. & SONG, H. 2005. Adult neurogenesis in the mammalian central nervous system. *Annu Rev Neurosci,* 28**,** 223-50.
MISONOU, H., MOHAPATRA, D. P., PARK, E. W., LEUNG, V., ZHEN, D., MISONOU, K., ANDERSON, A. E. & TRIMMER, J. S. 2004. Regulation of ion channel localization and phosphorylation by neuronal activity. *Nat Neurosci,* 7**,** 711-8.
MOMBAERTS, P., WANG, F., DULAC, C., CHAO, S. K., NEMES, A., MENDELSOHN, M., EDMONDSON, J. & AXEL, R. 1996. Visualizing an olfactory sensory map. *Cell,* 87**,** 675-86.
MOORE, C. I., CARLEN, M., KNOBLICH, U. & CARDIN, J. A. 2010. Neocortical interneurons: from diversity, strength. *Cell,* 142**,** 189-93.
MOOSMANG, S., BIEL, M., HOFMANN, F. & LUDWIG, A. 1999. Differential distribution of four hyperpolarization-activated cation channels in mouse brain. *Biol Chem,* 380**,** 975-80.
MORI, K. 1987. Membrane and synaptic properties of identified neurons in the olfactory bulb. *Prog Neurobiol,* 29**,** 275-320.
MORI, K. & SAKANO, H. 2011. How is the olfactory map formed and interpreted in the mammalian brain? *Annu Rev Neurosci,* 34**,** 467-99.

MORI, K., TAKAHASHI, Y. K., IGARASHI, K. M. & YAMAGUCHI, M. 2006. Maps of odorant molecular features in the Mammalian olfactory bulb. *Physiol Rev,* 86**,** 409-33.

MOULDER, K. L., JIANG, X., TAYLOR, A. A., OLNEY, J. W. & MENNERICK, S. 2006. Physiological activity depresses synaptic function through an effect on vesicle priming. *J Neurosci,* 26**,** 6618-26.

MOULY, A.-M. & SULLIVAN, R. 2009. Memory and Plasticity in the Olfactory System. *The Neurobiology of Olfaction.* CRC Press.

MU, Y., OTSUKA, T., HORTON, A. C., SCOTT, D. B. & EHLERS, M. D. 2003. Activity-dependent mRNA splicing controls ER export and synaptic delivery of NMDA receptors. *Neuron,* 40**,** 581-94.

MUCH, B., WAHL-SCHOTT, C., ZONG, X., SCHNEIDER, A., BAUMANN, L., MOOSMANG, S., LUDWIG, A. & BIEL, M. 2003. Role of subunit heteromerization and N-linked glycosylation in the formation of functional hyperpolarization-activated cyclic nucleotide-gated channels. *J Biol Chem,* 278**,** 43781-6.

MULLER, F., SCHOLTEN, A., IVANOVA, E., HAVERKAMP, S., KREMMER, E. & KAUPP, U. B. 2003. HCN channels are expressed differentially in retinal bipolar cells and concentrated at synaptic terminals. *Eur J Neurosci,* 17**,** 2084-96.

MURPHY, G. J., DARCY, D. P. & ISAACSON, J. S. 2005. Intraglomerular inhibition: signaling mechanisms of an olfactory microcircuit. *Nat Neurosci,* 8**,** 354-64.

MURPHY, G. J., GLICKFELD, L. L., BALSEN, Z. & ISAACSON, J. S. 2004. Sensory neuron signaling to the brain: properties of transmitter release from olfactory nerve terminals. *J Neurosci,* 24**,** 3023-30.

MUTOH, H., YUAN, Q. & KNOPFEL, T. 2005. Long-term depression at olfactory nerve synapses. *J Neurosci,* 25**,** 4252-9.

NADI, N. S., HEAD, R., GRILLO, M., HEMPSTEAD, J., GRANNOT-REISFELD, N. & MARGOLIS, F. L. 1981. Chemical deafferentation of the olfactory bulb: plasticity of the levels of tyrosine hydroxylase, dopamine and norepinephrine. *Brain Res,* 213**,** 365-77.

NAGAYAMA, S., ENERVA, A., FLETCHER, M. L., MASURKAR, A. V., IGARASHI, K. M., MORI, K. & CHEN, W. R. 2010. Differential axonal projection of mitral and tufted cells in the mouse main olfactory system. *Front Neural Circuits,* 4.

NAGAYAMA, S., HOMMA, R. & IMAMURA, F. 2014. Neuronal organization of olfactory bulb circuits. *Front Neural Circuits,* 8**,** 98.

NAGEL, G., BRAUNER, M., LIEWALD, J. F., ADEISHVILI, N., BAMBERG, E. & GOTTSCHALK, A. 2005. Light activation of channelrhodopsin-2 in excitable cells of Caenorhabditis elegans triggers rapid behavioral responses. *Curr Biol,* 15**,** 2279-84.

NAJAC, M., DE SAINT JAN, D., REGUERO, L., GRANDES, P. & CHARPAK, S. 2011. Monosynaptic and polysynaptic feed-forward inputs to mitral cells from olfactory sensory neurons. *J Neurosci,* 31**,** 8722-9.

NELSON, A. B., KRISPEL, C. M., SEKIRNJAK, C. & DU LAC, S. 2003. Long-lasting increases in intrinsic excitability triggered by inhibition. *Neuron,* 40**,** 609-20.

NOLAN, M. F., DUDMAN, J. T., DODSON, P. D. & SANTORO, B. 2007. HCN1 channels control resting and active integrative properties of stellate cells from layer II of the entorhinal cortex. *J Neurosci,* 27**,** 12440-51.

NOLAN, M. F., MALLERET, G., DUDMAN, J. T., BUHL, D. L., SANTORO, B., GIBBS, E., VRONSKAYA, S., BUZSAKI, G., SIEGELBAUM, S. A., KANDEL, E. R. & MOROZOV, A. 2004. A behavioral role for dendritic integration: HCN1 channels constrain spatial memory and plasticity at inputs to distal dendrites of CA1 pyramidal neurons. *Cell,* 119**,** 719-32.

NOLAN, M. F., MALLERET, G., LEE, K. H., GIBBS, E., DUDMAN, J. T., SANTORO, B., YIN, D., THOMPSON, R. F., SIEGELBAUM, S. A., KANDEL, E. R. & MOROZOV, A. 2003. The hyperpolarization-activated HCN1 channel is important for motor learning and neuronal integration by cerebellar Purkinje cells. *Cell,* 115**,** 551-64.

NOTOMI, T. & SHIGEMOTO, R. 2004. Immunohistochemical localization of Ih channel subunits, HCN1-4, in the rat brain. *J Comp Neurol,* 471**,** 241-76.

NUSSER, Z. 2002. Release-independent short-term facilitation at GABAergic synapses in the olfactory bulb. *Neuropharmacology,* 43**,** 573-83.

NUSSER, Z. 2009. Variability in the subcellular distribution of ion channels increases neuronal diversity. *Trends Neurosci,* 32**,** 267-74.

O'BRIEN, R. J., KAMBOJ, S., EHLERS, M. D., ROSEN, K. R., FISCHBACH, G. D. & HUGANIR, R. L. 1998. Activity-dependent modulation of synaptic AMPA receptor accumulation. *Neuron,* 21**,** 1067-78.

O'LEARY, T., VAN ROSSUM, M. C. & WYLLIE, D. J. 2010. Homeostasis of intrinsic excitability in hippocampal neurones: dynamics and mechanism of the response to chronic depolarization. *J Physiol,* 588**,** 157-70.

ORONA, E., RAINER, E. C. & SCOTT, J. W. 1984. Dendritic and axonal organization of mitral and tufted cells in the rat olfactory bulb. *J Comp Neurol,* 226**,** 346-56.

PADMANABHAN, K. & URBAN, N. N. 2010. Intrinsic biophysical diversity decorrelates neuronal firing while increasing information content. *Nat Neurosci,* 13**,** 1276-82.

PANZANELLI, P., FRITSCHY, J. M., YANAGAWA, Y., OBATA, K. & SASSOE-POGNETTO, M. 2007. GABAergic phenotype of periglomerular cells in the rodent olfactory bulb. *J Comp Neurol,* 502**,** 990-1002.

PANZANELLI, P., LOPEZ-BENDITO, G., LUJAN, R. & SASSOE-POGNETTO, M. 2004. Localization and developmental expression of GABA(B) receptors in the rat olfactory bulb. *J Neurocytol,* 33**,** 87-99.

PAPE, H. C. 1996. Queer current and pacemaker: the hyperpolarization-activated cation current in neurons. *Annu Rev Physiol,* 58**,** 299-327.

PAPE, H. C. & MCCORMICK, D. A. 1989. Noradrenaline and serotonin selectively modulate thalamic burst firing by enhancing a hyperpolarization-activated cation current. *Nature,* 340**,** 715-8.

PARK, K. S., MOHAPATRA, D. P., MISONOU, H. & TRIMMER, J. S. 2006. Graded regulation of the Kv2.1 potassium channel by variable phosphorylation. *Science,* 313**,** 976-9.

PARRISH-AUNGST, S., KIYOKAGE, E., SZABO, G., YANAGAWA, Y., SHIPLEY, M. T. & PUCHE, A. C. 2011. Sensory experience selectively regulates transmitter synthesis enzymes in interglomerular circuits. *Brain Res,* 1382**,** 70-6.

PARRISH-AUNGST, S., SHIPLEY, M. T., ERDELYI, F., SZABO, G. & PUCHE, A. C. 2007. Quantitative analysis of neuronal diversity in the mouse olfactory bulb. *J Comp Neurol,* 501**,** 825-36.

PARSA, P. V., D'SOUZA, R. D. & VIJAYARAGHAVAN, S. 2015. Signaling between periglomerular cells reveals a bimodal role for GABA in modulating glomerular microcircuitry in the olfactory bulb. *Proc Natl Acad Sci U S A,* 112**,** 9478-83.

PASZEK, P., RYAN, S., ASHALL, L., SILLITOE, K., HARPER, C. V., SPILLER, D. G., RAND, D. A. & WHITE, M. R. 2010. Population robustness arising from cellular heterogeneity. *Proc Natl Acad Sci U S A,* 107**,** 11644-9.

PELKMANS, L. 2012. Cell Biology. Using cell-to-cell variability--a new era in molecular biology. *Science,* 336**,** 425-6.

PETERSEN, S. A., FETTER, R. D., NOORDERMEER, J. N., GOODMAN, C. S. & DIANTONIO, A. 1997. Genetic analysis of glutamate receptors in Drosophila reveals a retrograde signal regulating presynaptic transmitter release. *Neuron,* 19**,** 1237-48.

PETILLA INTERNEURON NOMENCLATURE, G., ASCOLI, G. A., ALONSO-NANCLARES, L., ANDERSON, S. A., BARRIONUEVO, G., BENAVIDES-PICCIONE, R., BURKHALTER, A., BUZSAKI, G., CAULI, B., DEFELIPE, J., FAIREN, A., FELDMEYER, D., FISHELL, G., FREGNAC, Y., FREUND, T. F., GARDNER, D., GARDNER, E. P., GOLDBERG, J. H., HELMSTAEDTER, M., HESTRIN, S., KARUBE, F., KISVARDAY, Z. F., LAMBOLEZ, B., LEWIS, D. A.,

MARIN, O., MARKRAM, H., MUNOZ, A., PACKER, A., PETERSEN, C. C., ROCKLAND, K. S., ROSSIER, J., RUDY, B., SOMOGYI, P., STAIGER, J. F., TAMAS, G., THOMSON, A. M., TOLEDO-RODRIGUEZ, M., WANG, Y., WEST, D. C. & YUSTE, R. 2008. Petilla terminology: nomenclature of features of GABAergic interneurons of the cerebral cortex. *Nat Rev Neurosci,* 9**,** 557-68.

PHILPOT, B. D., LIM, J. H. & BRUNJES, P. C. 1997. Activity-dependent regulation of calcium-binding proteins in the developing rat olfactory bulb. *J Comp Neurol,* 387**,** 12-26.

PIGNATELLI, A., BORIN, M., FOGLI ISEPPE, A., GAMBARDELLA, C. & BELLUZZI, O. 2013. The h-current in periglomerular dopaminergic neurons of the mouse olfactory bulb. *PLoS One,* 8**,** e56571.

PIMENTEL, D. O. & MARGRIE, T. W. 2008. Glutamatergic transmission and plasticity between olfactory bulb mitral cells. *J Physiol,* 586**,** 2107-19.

PIN, J. P. & DUVOISIN, R. 1995. The metabotropic glutamate receptors: structure and functions. *Neuropharmacology,* 34**,** 1-26.

PINCHING, A. J. & POWELL, T. P. 1971a. The neuron types of the glomerular layer of the olfactory bulb. *J Cell Sci,* 9**,** 305-45.

PINCHING, A. J. & POWELL, T. P. 1971b. The neuropil of the periglomerular region of the olfactory bulb. *J Cell Sci,* 9**,** 379-409.

PIREZ, N. & WACHOWIAK, M. 2008. In vivo modulation of sensory input to the olfactory bulb by tonic and activity-dependent presynaptic inhibition of receptor neurons. *J Neurosci,* 28**,** 6360-71.

POOLOS, N. P., MIGLIORE, M. & JOHNSTON, D. 2002. Pharmacological upregulation of h-channels reduces the excitability of pyramidal neuron dendrites. *Nat Neurosci,* 5**,** 767-74.

POTTER, S. M., ZHENG, C., KOOS, D. S., FEINSTEIN, P., FRASER, S. E. & MOMBAERTS, P. 2001. Structure and emergence of specific olfactory glomeruli in the mouse. *J Neurosci,* 21**,** 9713-23.

PUCHE, A. C. & SHIPLEY, M. T. 1999. Odor-induced, activity-dependent transneuronal gene induction in vitro: mediation by NMDA receptors. *J Neurosci,* 19**,** 1359-70.

PUOPOLO, M., BEAN, B. P. & RAVIOLA, E. 2005. Spontaneous activity of isolated dopaminergic periglomerular cells of the main olfactory bulb. *J Neurophysiol,* 94**,** 3618-27.

PUOPOLO, M. & BELLUZZI, O. 1998a. Functional heterogeneity of periglomerular cells in the rat olfactory bulb. *Eur J Neurosci,* 10**,** 1073-83.

PUOPOLO, M. & BELLUZZI, O. 1998b. Inhibitory synapses among interneurons in the glomerular layer of rat and frog olfactory bulbs. *J Neurophysiol,* 80**,** 344-9.

RABINOWITCH, I. & SEGEV, I. 2008. Two opposing plasticity mechanisms pulling a single synapse. *Trends Neurosci,* 31**,** 377-83.

RALL, W., SHEPHERD, G. M., REESE, T. S. & BRIGHTMAN, M. W. 1966. Dendrodendritic synaptic pathway for inhibition in the olfactory bulb. *Exp Neurol,* 14**,** 44-56.

RAMÓN Y CAJAL, S. 1909. *Histologie du système nerveux de l'homme & des vertébrés,* Paris :, Maloine.

RANNALS, M. D. & KAPUR, J. 2011. Homeostatic strengthening of inhibitory synapses is mediated by the accumulation of GABA(A) receptors. *J Neurosci,* 31**,** 17701-12.

RAO, A. & CRAIG, A. M. 1997. Activity regulates the synaptic localization of the NMDA receptor in hippocampal neurons. *Neuron,* 19**,** 801-12.

RESIBOIS, A. & ROGERS, J. H. 1992. Calretinin in rat brain: an immunohistochemical study. *Neuroscience,* 46**,** 101-34.

RIBAK, C. E., VAUGHN, J. E., SAITO, K., BARBER, R. & ROBERTS, E. 1977. Glutamate decarboxylase localization in neurons of the olfactory bulb. *Brain Res,* 126**,** 1-18.

ROBINSON, R. B. & SIEGELBAUM, S. A. 2003. Hyperpolarization-activated cation currents: from molecules to physiological function. *Annu Rev Physiol,* 65**,** 453-80.

ROGERS, J. H. & RESIBOIS, A. 1992. Calretinin and calbindin-D28k in rat brain: patterns of partial co-localization. *Neuroscience,* 51**,** 843-65.

ROSSER, A. E. & KEVERNE, E. B. 1985. The importance of central noradrenergic neurones in the formation of an olfactory memory in the prevention of pregnancy block. *Neuroscience,* 15**,** 1141-7.

ROYET, J. P., DISTEL, H., HUDSON, R. & GERVAIS, R. 1998. A re-estimation of the number of glomeruli and mitral cells in the olfactory bulb of rabbit. *Brain Res,* 788**,** 35-42.

RUBIN, B. D. & KATZ, L. C. 1999. Optical imaging of odorant representations in the mammalian olfactory bulb. *Neuron,* 23**,** 499-511.

RUTHERFORD, L. C., DEWAN, A., LAUER, H. M. & TURRIGIANO, G. G. 1997. Brain-derived neurotrophic factor mediates the activity-dependent regulation of inhibition in neocortical cultures. *J Neurosci,* 17**,** 4527-35.

SAAR, D., GROSSMAN, Y. & BARKAI, E. 2002. Learning-induced enhancement of postsynaptic potentials in pyramidal neurons. *J Neurophysiol,* 87**,** 2358-63.

SALIN, P. A., LLEDO, P. M., VINCENT, J. D. & CHARPAK, S. 2001. Dendritic glutamate autoreceptors modulate signal processing in rat mitral cells. *J Neurophysiol,* 85**,** 1275-82.

SAMMONS, R. P. & KECK, T. 2015. Adult plasticity and cortical reorganization after peripheral lesions. *Curr Opin Neurobiol,* 35**,** 136-41.

SANTORO, B., CHEN, S., LUTHI, A., PAVLIDIS, P., SHUMYATSKY, G. P., TIBBS, G. R. & SIEGELBAUM, S. A. 2000. Molecular and functional heterogeneity of hyperpolarization-activated pacemaker channels in the mouse CNS. *J Neurosci,* 20**,** 5264-75.

SANTORO, B., GRANT, S. G., BARTSCH, D. & KANDEL, E. R. 1997. Interactive cloning with the SH3 domain of N-src identifies a new brain specific ion channel protein, with homology to eag and cyclic nucleotide-gated channels. *Proc Natl Acad Sci U S A,* 94**,** 14815-20.

SANTORO, B., LIU, D. T., YAO, H., BARTSCH, D., KANDEL, E. R., SIEGELBAUM, S. A. & TIBBS, G. R. 1998. Identification of a gene encoding a hyperpolarization-activated pacemaker channel of brain. *Cell,* 93**,** 717-29.

SANTORO, B., PISKOROWSKI, R. A., PIAN, P., HU, L., LIU, H. & SIEGELBAUM, S. A. 2009. TRIP8b splice variants form a family of auxiliary subunits that regulate gating and trafficking of HCN channels in the brain. *Neuron,* 62**,** 802-13.

SANTORO, B., WAINGER, B. J. & SIEGELBAUM, S. A. 2004. Regulation of HCN channel surface expression by a novel C-terminal protein-protein interaction. *J Neurosci,* 24**,** 10750-62.

SATOU, M., ANZAI, S. & HURUNO, M. 2005. Long-term potentiation and olfactory memory formation in the carp (Cyprinus carpio L.) olfactory bulb. *J Comp Physiol A Neuroethol Sens Neural Behav Physiol,* 191**,** 421-34.

SAWADA, M., KANEKO, N., INADA, H., WAKE, H., KATO, Y., YANAGAWA, Y., KOBAYASHI, K., NEMOTO, T., NABEKURA, J. & SAWAMOTO, K. 2011. Sensory input regulates spatial and subtype-specific patterns of neuronal turnover in the adult olfactory bulb. *J Neurosci,* 31**,** 11587-96.

SCHAEFER, A. T. & MARGRIE, T. W. 2007. Spatiotemporal representations in the olfactory system. *Trends Neurosci,* 30**,** 92-100.

SCHOENENBERGER, P., SCHARER, Y. P. & OERTNER, T. G. 2011. Channelrhodopsin as a tool to investigate synaptic transmission and plasticity. *Exp Physiol,* 96**,** 34-9.

SCHOPPA, N. E. & WESTBROOK, G. L. 2002. AMPA autoreceptors drive correlated spiking in olfactory bulb glomeruli. *Nat Neurosci,* 5**,** 1194-202.

SCHULZ, D. J., GOAILLARD, J. M. & MARDER, E. 2006. Variable channel expression in identified single and electrically coupled neurons in different animals. *Nat Neurosci,* 9**,** 356-62.

SERIZAWA, S., ISHII, T., NAKATANI, H., TSUBOI, A., NAGAWA, F., ASANO, M., SUDO, K., SAKAGAMI, J., SAKANO, H., IJIRI, T., MATSUDA, Y., SUZUKI, M., YAMAMORI, T., IWAKURA, Y. & SAKANO, H. 2000. Mutually exclusive expression of odorant receptor transgenes. *Nat Neurosci,* 3**,** 687-93.

SHAO, Z., PUCHE, A. C., KIYOKAGE, E., SZABO, G. & SHIPLEY, M. T. 2009. Two GABAergic intraglomerular circuits differentially regulate tonic and phasic presynaptic inhibition of olfactory nerve terminals. *J Neurophysiol,* 101**,** 1988-2001.

SHAO, Z., PUCHE, A. C., LIU, S. & SHIPLEY, M. T. 2012. Intraglomerular inhibition shapes the strength and temporal structure of glomerular output. *J Neurophysiol,* 108**,** 782-93.

SHEPHERD, G. M. 2003. *The Synaptic Organization of the Brain*, Oxford University Press.

SHIN, K. S., ROTHBERG, B. S. & YELLEN, G. 2001. Blocker state dependence and trapping in hyperpolarization-activated cation channels: evidence for an intracellular activation gate. *J Gen Physiol,* 117**,** 91-101.

SHIN, M., BRAGER, D., JARAMILLO, T. C., JOHNSTON, D. & CHETKOVICH, D. M. 2008. Mislocalization of h channel subunits underlies h channelopathy in temporal lobe epilepsy. *Neurobiol Dis,* 32**,** 26-36.

SHIPLEY, M. T. & ENNIS, M. 1996. Functional organization of olfactory system. *J Neurobiol,* 30**,** 123-76.

SHIPLEY, M. T., ZIMMER, L. A., ENNIS, M. & MCLEAN, J. H. 1996. Chapter III The olfactory system. *In:* L.W. SWANSON, A. B. & HÖKFELT, T. (eds.) *Handbook of Chemical Neuroanatomy.* Elsevier.

SHU, Y., HASENSTAUB, A. & MCCORMICK, D. A. 2003. Turning on and off recurrent balanced cortical activity. *Nature,* 423**,** 288-93.

SHUSTERMAN, R., SMEAR, M. C., KOULAKOV, A. A. & RINBERG, D. 2011. Precise olfactory responses tile the sniff cycle. *Nat Neurosci,* 14**,** 1039-44.

SIEGELBAUM, S. A., CAMARDO, J. S. & KANDEL, E. R. 1982. Serotonin and cyclic AMP close single K+ channels in Aplysia sensory neurones. *Nature,* 299**,** 413-7.

SINGER, W. 1996. Neurophysiology: the changing face of inhibition. *Curr Biol,* 6**,** 395-7.

SLOTNICK, B. M. & KATZ, H. M. 1974. Olfactory learning-set formation in rats. *Science,* 185**,** 796-8.

SMEAR, M., RESULAJ, A., ZHANG, J., BOZZA, T. & RINBERG, D. 2013. Multiple perceptible signals from a single olfactory glomerulus. *Nat Neurosci,* 16**,** 1687-91.

SMITH, C. G. 1938. Changes in the Olfactory Mucosa and the Olfactory Nerves Following Intranasal Treatment with One Per Cent Zinc Sulphate. *Can Med Assoc J,* 39**,** 138-40.

SMITH, T. C. & JAHR, C. E. 2002. Self-inhibition of olfactory bulb neurons. *Nat Neurosci,* 5**,** 760-6.

SOGHOMONIAN, J. J. & MARTIN, D. L. 1998. Two isoforms of glutamate decarboxylase: why? *Trends Pharmacol Sci,* 19**,** 500-5.

SOUCY, E. R., ALBEANU, D. F., FANTANA, A. L., MURTHY, V. N. & MEISTER, M. 2009. Precision and diversity in an odor map on the olfactory bulb. *Nat Neurosci,* 12**,** 210-20.

SPAIN, W. J., SCHWINDT, P. C. & CRILL, W. E. 1987. Anomalous rectification in neurons from cat sensorimotor cortex in vitro. *J Neurophysiol,* 57**,** 1555-76.

SPORS, H. & GRINVALD, A. 2002. Spatio-temporal dynamics of odor representations in the mammalian olfactory bulb. *Neuron,* 34**,** 301-15.

STERNBERG, N. & HAMILTON, D. 1981. Bacteriophage P1 site-specific recombination. I. Recombination between loxP sites. *J Mol Biol,* 150**,** 467-86.

STIEBER, J., STOCKL, G., HERRMANN, S., HASSFURTH, B. & HOFMANN, F. 2005. Functional expression of the human HCN3 channel. *J Biol Chem,* 280**,** 34635-43.

SULLIVAN, R. M., STACKENWALT, G., NASR, F., LEMON, C. & WILSON, D. A. 2000. Association of an odor with activation of olfactory bulb noradrenergic beta-receptors or locus coeruleus stimulation is sufficient to produce learned approach responses to that odor in neonatal rats. *Behav Neurosci,* 114**,** 957-62.

SUN, P., ENSLEN, H., MYUNG, P. S. & MAURER, R. A. 1994. Differential activation of CREB by Ca2+/calmodulin-dependent protein kinases type II and type IV involves phosphorylation of a site that negatively regulates activity. *Genes Dev,* 8**,** 2527-39.

SUN, Q. Q. 2009. Experience-dependent intrinsic plasticity in interneurons of barrel cortex layer IV. *J Neurophysiol,* 102**,** 2955-73.

SUTTON, M. A., ITO, H. T., CRESSY, P., KEMPF, C., WOO, J. C. & SCHUMAN, E. M. 2006. Miniature neurotransmission stabilizes synaptic function via tonic suppression of local dendritic protein synthesis. *Cell,* 125**,** 785-99.

SWANWICK, C. C., MURTHY, N. R. & KAPUR, J. 2006. Activity-dependent scaling of GABAergic synapse strength is regulated by brain-derived neurotrophic factor. *Mol Cell Neurosci,* 31**,** 481-92.

TAKAHASHI, Y. K., KUROSAKI, M., HIRONO, S. & MORI, K. 2004. Topographic representation of odorant molecular features in the rat olfactory bulb. *J Neurophysiol,* 92**,** 2413-27.

TANIGUCHI, H., HE, M., WU, P., KIM, S., PAIK, R., SUGINO, K., KVITSIANI, D., FU, Y., LU, J., LIN, Y., MIYOSHI, G., SHIMA, Y., FISHELL, G., NELSON, S. B. & HUANG, Z. J. 2011. A resource of Cre driver lines for genetic targeting of GABAergic neurons in cerebral cortex. *Neuron,* 71**,** 995-1013.

TATTI, R., BHAUKAURALLY, K., GSCHWEND, O., SEAL, R. P., EDWARDS, R. H., RODRIGUEZ, I. & CARLETON, A. 2014. A population of glomerular glutamatergic neurons controls sensory information transfer in the mouse olfactory bulb. *Nat Commun,* 5**,** 3791.

THIAGARAJAN, T. C., LINDSKOG, M. & TSIEN, R. W. 2005. Adaptation to synaptic inactivity in hippocampal neurons. *Neuron,* 47**,** 725-37.

TOLEDO-RODRIGUEZ, M., BLUMENFELD, B., WU, C., LUO, J., ATTALI, B., GOODMAN, P. & MARKRAM, H. 2004. Correlation maps allow neuronal electrical properties to be predicted from single-cell gene expression profiles in rat neocortex. *Cereb Cortex,* 14**,** 1310-27.

TRAUB, R. D., SPRUSTON, N., SOLTESZ, I., KONNERTH, A., WHITTINGTON, M. A. & JEFFERYS, G. R. 1998. Gamma-frequency oscillations: a neuronal population phenomenon, regulated by synaptic and intrinsic cellular processes, and inducing synaptic plasticity. *Prog Neurobiol,* 55**,** 563-75.

TRIPATHY, S. J., PADMANABHAN, K., GERKIN, R. C. & URBAN, N. N. 2013. Intermediate intrinsic diversity enhances neural population coding. *Proc Natl Acad Sci U S A,* 110**,** 8248-53.

TSAY, D., DUDMAN, J. T. & SIEGELBAUM, S. A. 2007. HCN1 channels constrain synaptically evoked Ca2+ spikes in distal dendrites of CA1 pyramidal neurons. *Neuron,* 56**,** 1076-89.

TURRIGIANO, G. 2011. Too many cooks? Intrinsic and synaptic homeostatic mechanisms in cortical circuit refinement. *Annu Rev Neurosci,* 34**,** 89-103.

TURRIGIANO, G., ABBOTT, L. F. & MARDER, E. 1994. Activity-dependent changes in the intrinsic properties of cultured neurons. *Science,* 264**,** 974-7.

TURRIGIANO, G. G. 2008. The self-tuning neuron: synaptic scaling of excitatory synapses. *Cell,* 135**,** 422-35.

TURRIGIANO, G. G., LESLIE, K. R., DESAI, N. S., RUTHERFORD, L. C. & NELSON, S. B. 1998. Activity-dependent scaling of quantal amplitude in neocortical neurons. *Nature,* 391**,** 892-6.

TURRIGIANO, G. G. & NELSON, S. B. 2004. Homeostatic plasticity in the developing nervous system. *Nat Rev Neurosci,* 5**,** 97-107.

TYLER, W. J., PETZOLD, G. C., PAL, S. K. & MURTHY, V. N. 2007. Experience-dependent modification of primary sensory synapses in the mammalian olfactory bulb. *J Neurosci,* 27**,** 9427-38.

UCHIDA, N. & MAINEN, Z. F. 2003. Speed and accuracy of olfactory discrimination in the rat. *Nat Neurosci,* 6**,** 1224-9.

UCHIDA, N., TAKAHASHI, Y. K., TANIFUJI, M. & MORI, K. 2000. Odor maps in the mammalian olfactory bulb: domain organization and odorant structural features. *Nat Neurosci,* 3**,** 1035-43.

ULENS, C. & TYTGAT, J. 2001. Functional heteromerization of HCN1 and HCN2 pacemaker channels. *J Biol Chem,* 276**,** 6069-72.

ULRICH, D. 2002. Dendritic resonance in rat neocortical pyramidal cells. *J Neurophysiol,* 87**,** 2753-9.

URBAN, N. N. & SAKMANN, B. 2002. Reciprocal intraglomerular excitation and intra- and interglomerular lateral inhibition between mouse olfactory bulb mitral cells. *J Physiol,* 542**,** 355-67.

VAN WELIE, I., VAN HOOFT, J. A. & WADMAN, W. J. 2004. Homeostatic scaling of neuronal excitability by synaptic modulation of somatic hyperpolarization-activated Ih channels. *Proc Natl Acad Sci U S A,* 101**,** 5123-8.

VASSAR, R., NGAI, J. & AXEL, R. 1993. Spatial segregation of odorant receptor expression in the mammalian olfactory epithelium. *Cell,* 74**,** 309-18.

VINCENT, P. & MARTY, A. 1993. Neighboring cerebellar Purkinje cells communicate via retrograde inhibition of common presynaptic interneurons. *Neuron,* 11**,** 885-93.

VINCIS, R., GSCHWEND, O., BHAUKAURALLY, K., BEROUD, J. & CARLETON, A. 2012. Dense representation of natural odorants in the mouse olfactory bulb. *Nat Neurosci,* 15**,** 537-9.

WACHOWIAK, M. 2011. All in a sniff: olfaction as a model for active sensing. *Neuron,* 71**,** 962-73.

WACHOWIAK, M. & COHEN, L. B. 2001. Representation of odorants by receptor neuron input to the mouse olfactory bulb. *Neuron,* 32**,** 723-35.

WACHOWIAK, M. & COHEN, L. B. 2003. Correspondence between odorant-evoked patterns of receptor neuron input and intrinsic optical signals in the mouse olfactory bulb. *J Neurophysiol,* 89**,** 1623-39.

WACHOWIAK, M., DENK, W. & FRIEDRICH, R. W. 2004. Functional organization of sensory input to the olfactory bulb glomerulus analyzed by two-photon calcium imaging. *Proc Natl Acad Sci U S A,* 101**,** 9097-102.

WACHOWIAK, M., MCGANN, J. P., HEYWARD, P. M., SHAO, Z., PUCHE, A. C. & SHIPLEY, M. T. 2005. Inhibition [corrected] of olfactory receptor neuron input to olfactory bulb glomeruli mediated by suppression of presynaptic calcium influx. *J Neurophysiol,* 94**,** 2700-12.

WACHOWIAK, M. & SHIPLEY, M. T. 2006. Coding and synaptic processing of sensory information in the glomerular layer of the olfactory bulb. *Semin Cell Dev Biol,* 17**,** 411-23.

WAHL-SCHOTT, C., BAUMANN, L., ZONG, X. & BIEL, M. 2005. An arginine residue in the pore region is a key determinant of chloride dependence in cardiac pacemaker channels. *J Biol Chem,* 280**,** 13694-700.

WAHL-SCHOTT, C. & BIEL, M. 2009. HCN channels: structure, cellular regulation and physiological function. *Cell Mol Life Sci,* 66**,** 470-94.

WANG, J., CHEN, S., NOLAN, M. F. & SIEGELBAUM, S. A. 2002. Activity-dependent regulation of HCN pacemaker channels by cyclic AMP: signaling through dynamic allosteric coupling. *Neuron,* 36**,** 451-61.

WANG, M., RAMOS, B. P., PASPALAS, C. D., SHU, Y., SIMEN, A., DUQUE, A., VIJAYRAGHAVAN, S., BRENNAN, A., DUDLEY, A., NOU, E., MAZER, J. A., MCCORMICK, D. A. & ARNSTEN, A. F. 2007. Alpha2A-adrenoceptors strengthen working memory networks by inhibiting cAMP-HCN channel signaling in prefrontal cortex. *Cell,* 129**,** 397-410.

WANG, W. T., WAN, Y. H., ZHU, J. L., LEI, G. S., WANG, Y. Y., ZHANG, P. & HU, S. J. 2006. Theta-frequency membrane resonance and its ionic mechanisms in rat subicular pyramidal neurons. *Neuroscience,* 140**,** 45-55.

WATT, A. J., VAN ROSSUM, M. C., MACLEOD, K. M., NELSON, S. B. & TURRIGIANO, G. G. 2000. Activity coregulates quantal AMPA and NMDA currents at neocortical synapses. *Neuron,* 26**,** 659-70.

WATT, W. C., SAKANO, H., LEE, Z. Y., REUSCH, J. E., TRINH, K. & STORM, D. R. 2004. Odorant stimulation enhances survival of olfactory sensory neurons via MAPK and CREB. *Neuron,* 41**,** 955-67.

WEFELMEYER, W., PUHL, C. J. & BURRONE, J. 2016. Homeostatic Plasticity of Subcellular Neuronal Structures: From Inputs to Outputs. *Trends Neurosci,* 39**,** 656-667.

WELKER, W. I. 1964. Analysis of Sniffing of the Albino Rat 1). *Behaviour,* 22**,** 223-244.

WELLIS, D. P. & KAUER, J. S. 1993. GABAA and glutamate receptor involvement in dendrodendritic synaptic interactions from salamander olfactory bulb. *J Physiol,* 469**,** 315-39.

WHITESELL, J. D., SORENSEN, K. A., JARVIE, B. C., HENTGES, S. T. & SCHOPPA, N. E. 2013. Interglomerular lateral inhibition targeted on external tufted cells in the olfactory bulb. *J Neurosci,* 33**,** 1552-63.

WHITMAN, M. C. & GREER, C. A. 2007. Adult-generated neurons exhibit diverse developmental fates. *Dev Neurobiol,* 67**,** 1079-93.

WICK, S. D., WIECHERT, M. T., FRIEDRICH, R. W. & RIECKE, H. 2010. Pattern orthogonalization via channel decorrelation by adaptive networks. *J Comput Neurosci,* 28**,** 29-45.

WIECHERT, M. T., JUDKEWITZ, B., RIECKE, H. & FRIEDRICH, R. W. 2010. Mechanisms of pattern decorrelation by recurrent neuronal circuits. *Nat Neurosci,* 13**,** 1003-10.

WIERENGA, C. J., IBATA, K. & TURRIGIANO, G. G. 2005. Postsynaptic expression of homeostatic plasticity at neocortical synapses. *J Neurosci,* 25**,** 2895-905.

WILLIAMS, S. R. & STUART, G. J. 2000. Site independence of EPSP time course is mediated by dendritic I(h) in neocortical pyramidal neurons. *J Neurophysiol,* 83**,** 3177-82.

WILLIAMS, S. R. & STUART, G. J. 2003. Voltage- and site-dependent control of the somatic impact of dendritic IPSPs. *J Neurosci,* 23**,** 7358-67.

WILSON, D. A., BEST, A. R. & SULLIVAN, R. M. 2004. Plasticity in the olfactory system: lessons for the neurobiology of memory. *Neuroscientist,* 10**,** 513-24.

WILSON, D. A. & SULLIVAN, R. M. 1995. The D2 antagonist spiperone mimics the effects of olfactory deprivation on mitral/tufted cell odor response patterns. *J Neurosci,* 15**,** 5574-81.

WILSON, D. A., SULLIVAN, R. M. & LEON, M. 1985. Odor familiarity alters mitral cell response in the olfactory bulb of neonatal rats. *Brain Res,* 354**,** 314-7.

WILSON, N. R., RUNYAN, C. A., WANG, F. L. & SUR, M. 2012. Division and subtraction by distinct cortical inhibitory networks in vivo. *Nature,* 488**,** 343-8.

WYSOCKI, C. J. 1979. Neurobehavioral evidence for the involvement of the vomeronasal system in mammalian reproduction. *Neurosci Biobehav Rev,* 3**,** 301-41.

XUE, M., ATALLAH, B. V. & SCANZIANI, M. 2014. Equalizing excitation-inhibition ratios across visual cortical neurons. *Nature,* 511**,** 596-600.

YAKSI, E., JUDKEWITZ, B. & FRIEDRICH, R. W. 2007. Topological reorganization of odor representations in the olfactory bulb. *PLoS Biol,* 5**,** e178.

YAMADA, R., KUBA, H., ISHII, T. M. & OHMORI, H. 2005. Hyperpolarization-activated cyclic nucleotide-gated cation channels regulate auditory coincidence detection in nucleus laminaris of the chick. *J Neurosci,* 25**,** 8867-77.

YANAGIHARA, K. & IRISAWA, H. 1980. Inward current activated during hyperpolarization in the rabbit sinoatrial node cell. *Pflugers Arch,* 385**,** 11-9.

YU, L. M. & GODA, Y. 2009. Dendritic signalling and homeostatic adaptation. *Curr Opin Neurobiol,* 19**,** 327-35.

ZAGOTTA, W. N., OLIVIER, N. B., BLACK, K. D., YOUNG, E. C., OLSON, R. & GOUAUX, E. 2003. Structural basis for modulation and agonist specificity of HCN pacemaker channels. *Nature,* 425**,** 200-5.

ZHA, Q., BREWSTER, A. L., RICHICHI, C., BENDER, R. A. & BARAM, T. Z. 2008. Activity-dependent heteromerization of the hyperpolarization-activated, cyclic-nucleotide gated (HCN) channels: role of N-linked glycosylation. *J Neurochem,* 105**,** 68-77.

ZHANG, J., HUANG, G., DEWAN, A., FEINSTEIN, P. & BOZZA, T. 2012. Uncoupling stimulus specificity and glomerular position in the mouse olfactory system. *Mol Cell Neurosci,* 51**,** 79-88.

ZHANG, W. & LINDEN, D. J. 2003. The other side of the engram: experience-driven changes in neuronal intrinsic excitability. *Nat Rev Neurosci,* 4**,** 885-900.

ZHANG, X. & FIRESTEIN, S. 2002. The olfactory receptor gene superfamily of the mouse. *Nat Neurosci,* 5**,** 124-33.

ZHANG, X., RODRIGUEZ, I., MOMBAERTS, P. & FIRESTEIN, S. 2004. Odorant and vomeronasal receptor genes in two mouse genome assemblies. *Genomics,* 83**,** 802-11.

ZHENG, C., FEINSTEIN, P., BOZZA, T., RODRIGUEZ, I. & MOMBAERTS, P. 2000. Peripheral olfactory projections are differentially affected in mice deficient in a cyclic nucleotide-gated channel subunit. *Neuron,* 26**,** 81-91.

ZHU, P., FRANK, T. & FRIEDRICH, R. W. 2013. Equalization of odor representations by a network of electrically coupled inhibitory interneurons. *Nat Neurosci,* 16**,** 1678-86.

ZOLLES, G., KLOCKER, N., WENZEL, D., WEISSER-THOMAS, J., FLEISCHMANN, B. K., ROEPER, J. & FAKLER, B. 2006. Pacemaking by HCN channels requires interaction with phosphoinositides. *Neuron,* 52**,** 1027-36.

ZONG, X., ECKERT, C., YUAN, H., WAHL-SCHOTT, C., ABICHT, H., FANG, L., LI, R., MISTRIK, P., GERSTNER, A., MUCH, B., BAUMANN, L., MICHALAKIS, S., ZENG, R., CHEN, Z. & BIEL, M. 2005. A novel mechanism of modulation of hyperpolarization-activated cyclic nucleotide-gated channels by Src kinase. *J Biol Chem,* 280**,** 34224-32.

ZONG, X., STIEBER, J., LUDWIG, A., HOFMANN, F. & BIEL, M. 2001. A single histidine residue determines the pH sensitivity of the pacemaker channel HCN2. *J Biol Chem,* 276**,** 6313-9.